Catalysis in Flow: Chemoenzymatic Dynamic Kinetic Resolution of Chiral Amines

By

Matthew James Takle

Imperial College London

Department of Chemistry

2023

A Thesis Submitted in Partial Fulfilment of the

Requirements for the Degree of Doctor of Philosophy

Acknowledgements

Declaration of Originality

I declare that the work contained within this thesis was conducted by myself, Matthew Takle, and where appropriate all other work discussed was clearly and correctly referenced. All work was conducted in the Department of Chemistry at the Molecular Sciences Research Hub, Imperial College London. This work has not previously been submitted in attainment of any degree, at this or any other institution.

Matthew James Takle, 2023

Copyright Declaration

Abstract

An investigation of the Chemoenzymatic Dynamic Kinetic Resolution of racemic amines is reported using a dual transition metal-enzyme catalysed process, as a methodology for the synthesis of chiral amines. This work is comprised of 4 sections: a literature review of the existing synthetic methodologies for the synthesis of chiral amines; the discovery and development of a Flash Thermal Racemisation (FTR) procedure; the interrogation of enzymatic kinetic resolution in continuous flow; and finally, implementation and analysis of the first demonstration of a compartmentalised FTR-CE-DKR under flow conditions.

Previously, Chemoenzymatic Dynamic Kinetic Resolution has been reported to be an effective approach for the resolution of chiral amines but was greatly limited by its inability to be conducted on an industrially relevant scale. The key challenge faced by the process is the lack of compatibility of the two tandem catalysts required for the racemisation and enzyme-catalysed acylation steps. Despite much effort, this process has been plagued by the compromises made, which have led to the use of sub-optimal reaction conditions for each individual step. Deactivation of the transition metal or enzyme catalysts has also been a problem leading to overall limited productivity and lack of scalability, rendering the processes of limited application in a commercial setting.

The development of the FTR-CE-DKR methodology reported here has demonstrated how continuous flow can be applied to effectively compartmentalise each step of the processes, thus allowing optimal conditions to be applied to each step. This has enabled proof-of-concept studies to be carried out that demonstrate the ability of this approach to greatly increase the productivity of the process to synthesise chiral amines in a scalable manner.

Abbreviations

[S]	Initial Substrate Concentration
ΔG	Gibbs Free Energy
ΔH	Enthalpy
ΔS	Entropy
A	Pre-Exponential Factor
AD	Acyl Donor
Asp	Aspartic Acid
Bu	Butyl
C=C	Carbon-Carbon Double Bond
C=N	Carbon-Nitrogen Double Bond
Cat.	Catalyst
Cat.	Catalyst
C-C	Carbon-Carbon Single Bond
C-H	Carbon-Hydrogen Bond
C-N	Carbon-Nitrogen Single Bond
Conv.	Conversion
d	doublet
DMSO	Dimethyl sulfoxide
DCM	Dichloromethane
d_p	Depth of Penetration
e.e.	Enantiomeric Excess
E_a	Activation Energy
Et	Ethyl
EtOH	Ethanol
Et_3N	Triethylamine
GC	Gas Chromatography
His	Histidine

HPLC	High Performance Liquid Chromatography
ID	Internal Diameter
^{i}Pr	Isopropyl
IR	Infrared
K	Equilibrium Constant
k	Rate Constant
k_m	Substrate Binding Affinity
L*	Ligand
LC	Liquid Chromatography
m	multiplet
Me	Methyl
MeOH	Methanol
min	minute
MTBE	Methyl tert butyl ether
N	No
NaOH	Sodium hydroxide
NMR	Nuclear Magnetic Resonance
^{o}C	Degrees Celsius
OD	Outer Diameter
p	pentet
PFA	Perfluoroalkoxy Polymer
PhMe	Toluene
PLP	Pyridoxal phosphate
q	quartet
R	Universal Gas Constant
Rac.	Racemisation
s	singlet
Sel.	Selectivity
Ser	Serine

Sol. Conc.	Solution Concentration
SS	Stainless Steel
T	Temperature (Kelvin)
t	Retention Time
Temp.	Temperature
TM	Transition Metal
V_{max}	Maximum Rate of Enzymatic Reaction
V_o	Initial Rate of Enzymatic Reaction
wt%	Weight Percent
Y	Yes
τ	Residence Time

Table of Contents

Chapter 1: <u>Introduction to Chiral Amine Synthesis</u>

Chiral amines are an extremely prevalent function group in all chemical industries (Figure 1), particularly in the production of pharmaceuticals and agrochemicals.[1–12] Their importance is emphasised by their appearance in 40-45 % of API's and 20 – 30 % of agrochemicals products, which amounts to approximately € 3 billion of annual revenue, and 15 % of the total sales of these industries.[13–17] Chiral amines are also ubiquitous in biology because of their ability to form hydrogen bonds in specific orientations with chiral binding pockets. The 3 dimensional nature of chiral amine containing drugs/agrochemicals means they can bind more specifically to their biological targets, thus delivering higher levels of selectivity which can be key to preventing off target effects.
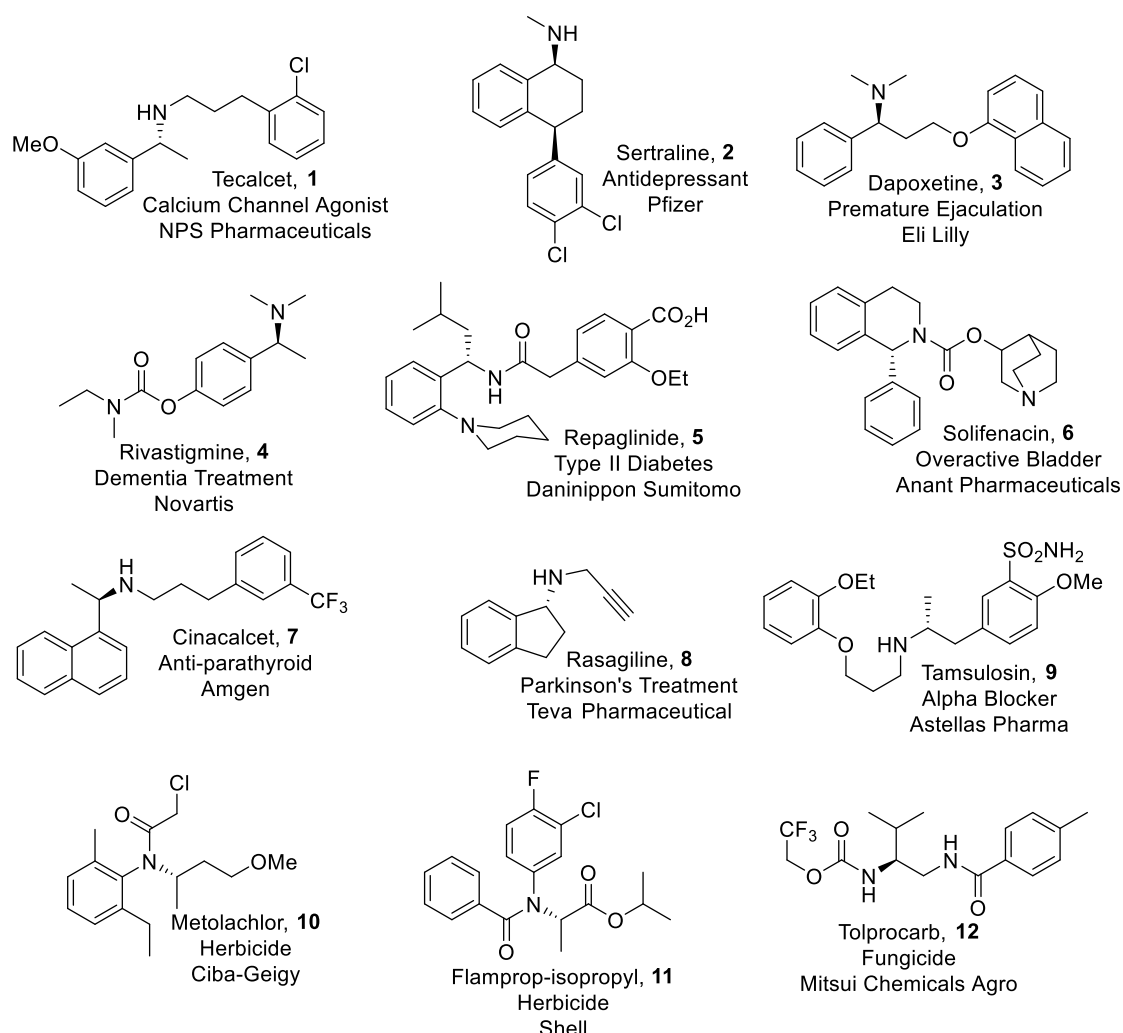
Figure 1 Examples of chiral C-N functionality in pharmaceuticals and agrochemicals.[1–12]

Sertraline, **2**, is a selective serotonin reuptake inhibitor (Figure 1) that is used to treat depression, obsessive compulsive disorder (OCD) and post-traumatic stress disorder (PTSD).[18] This class of compound was discovered

by Pfizer in the 1970's when developing a novel series of psychoactive compounds that also gave rise to tametraline (the enantiomer of **2**) and norepinephrine.[19] Due to a combination of the increasing prevalence of mental disorders and the effectiveness of Sertraline, global sales have been estimated to be over $1.3 billion as of 2022, making it a "Blockbuster drug".[20]

Cinacalcet, **7**, is a calcimimetic drug, mimicking the action of calcium in the body (Figure 1), that works to treat primary and secondary hyperparathyroidism, alongside calciphylaxis.[21] Primary hyperparathyroidism affects 25 in every 100,000 men, whereas this number jumps to 65 for women.[22] This reflects a not insignificant proportion of the population, with the potential to affect 360 million people worldwide. Following FDA approval in 2004, **7** was found to have huge success, also achieving "Blockbuster" status, with sales of over $200 million in the first quarter of 2013.

Metolachlor, **10**, is a member of the chloroacetanilide family of herbicides (Figure 1) discovered by Ciba-Geigy for the treatment of weeds through the inhibited growth of seedling shoots. **10** was first registered in the United States in 1976 where it is extensively used for the treatment of corn crops, of which the United States produces the most in the world.[23,24] Metolachlor's extensive use in the corn industry has led to its market being estimated at over $600 million in 2027.[25]

The industrial and economical significance of the aforementioned chiral amines is illustrative of all the compounds outlined in Figure 1, demonstrating that their synthesis must deliver high chemical and enantio selectivity while simultaneously being viable for large scale production. Although there are currently methodologies that can achieve the required chemical and enantio selectivity, the final obstacle is scalability. These processes need to be capable of delivering up to 1000 tons/year and 10,000 tons/year for the pharmaceutical and agrochemical industries respectively.[13]

There are 5 pillars of chiral amine synthesis: chiral pool, chiral auxiliaries, asymmetric catalysis, biocatalysis and resolution of racemic mixtures (chiral and dynamic kinetic). More broadly the chiral pool, i.e., amino acids, can be harnessed to provide chiral ligands for use in asymmetric catalysis, the creation of the chiral auxiliaries or the resolving agents in either kinetic resolutions (KR) or dynamic kinetic resolutions (DKR). Each methodology has been leveraged to deliver chiral amines on an industrial scale. In this chapter an example of each pillar will be selected and used to aid the discussion of the advantages and disadvantages that each process possesses. Thus, highlighting the need for constant progression in this space to expand the chemical toolbox and develop ever more cost effective and environmentally friendly ways to synthesise chiral amines on an industrial scale.

1.1. Chiral Pool

Before scientists had the ability to create chiral centres, they were only observed in enantiopure compounds which are readily available in nature and known as the Chiral Pool.[26] Therefore, early attempts at asymmetric synthesis began with these chirally pure, naturally occurring molecules, frequently amino acids. For the synthesis of chiral amines, a huge step forward was the discovery of the Pictet-Spengler reaction (Scheme 1) in 1911 to synthesise the tetrahydropyridoindole alkaloids, **17**, from the β-carboline family.[27]
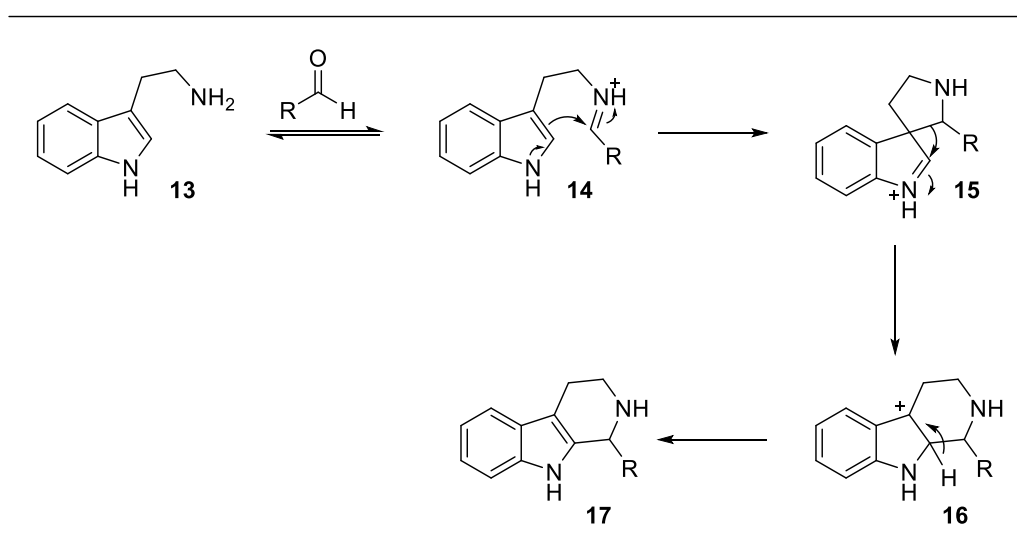
Scheme 1 The generic mechanism for the Pictet-Spengler reaction.

Alkaloids are secondary metabolites formed in nature, and the β-carboline family specifically has over 100 derivatives. Pinoline, **18**, is produced during the metabolism of melatonin (Scheme 2) and has been linked to antioxidant properties protecting brain function, alongside monoamine oxidase-A (MAO-A) inhibition which promotes neurogenesis and can be used to treat depression.[28] Harmaline, **19**, has been found to have central nervous system (CNS) stimulation and reversible MAO-A inhibition properties (Scheme 2).[29] Eudistomine C, **20**, has been linked extremely potent antiviral activity against both DNA and RNA viruses as well as antitumor and antimicrobial activity (Scheme 2).[30]
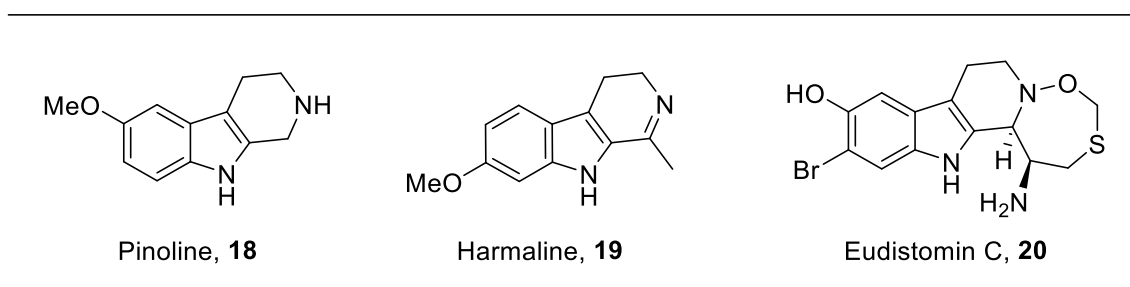
Scheme 2 Structures of β-carboline derivatives Pinoline, Harmaline and Eudistomin C.[28–30]

Cox and *Cook* discovered in 1995 that the Pictet-Spengler reaction could be applied to the amino acid tryptophan, **21**, (Scheme 3a) or its N-methylated derivative **22**.[31] It was discovered that the steric bulk of the carboxyl group caused the preferential formation of the trans diastereoisomer, the thermodynamic product.[32] When R^1 = H and R^2 = Ph, the *cis/trans* ratio moderately favours the *trans* configuration in a 40:60 ratio. The *trans* configuration (Scheme 3b) allows the clash between R^1 and the indole R^2 to be minimised by placing R^2 in the axial position, while the carboxyl can adopt the equatorial position. The *cis/trans* ratio can be shifted in favour of the trans product, through treatment of the reaction mixture with acid at reflux (Scheme 3c). This allows the kinetic *cis* diastereoisomer, to re-equilibrate to the lower energy *trans* configuration, through ring opening to give carbocation, *S* - **26**, and subsequent closing to deliver the lower energy product.

However, when R^1 = H, in **24**, the reduction in energy gained by minimising the clash with R^2 = Ph at the expense of putting R^2 = Ph axial is minimal (Scheme 3b), therefore *trans* is only moderately favoured in a 40:60 ratio. However, when R^1 is changed to a Me group, **25**, the R^2 = Ph clash is much more severe (Scheme b). Therefore, the greater stability of the *trans* configuration, outweighs the unfavourable axial positioning of the R^2=Ph group to a greater extent, reflected in **25** becoming diastereomerically pure (Scheme 3a).
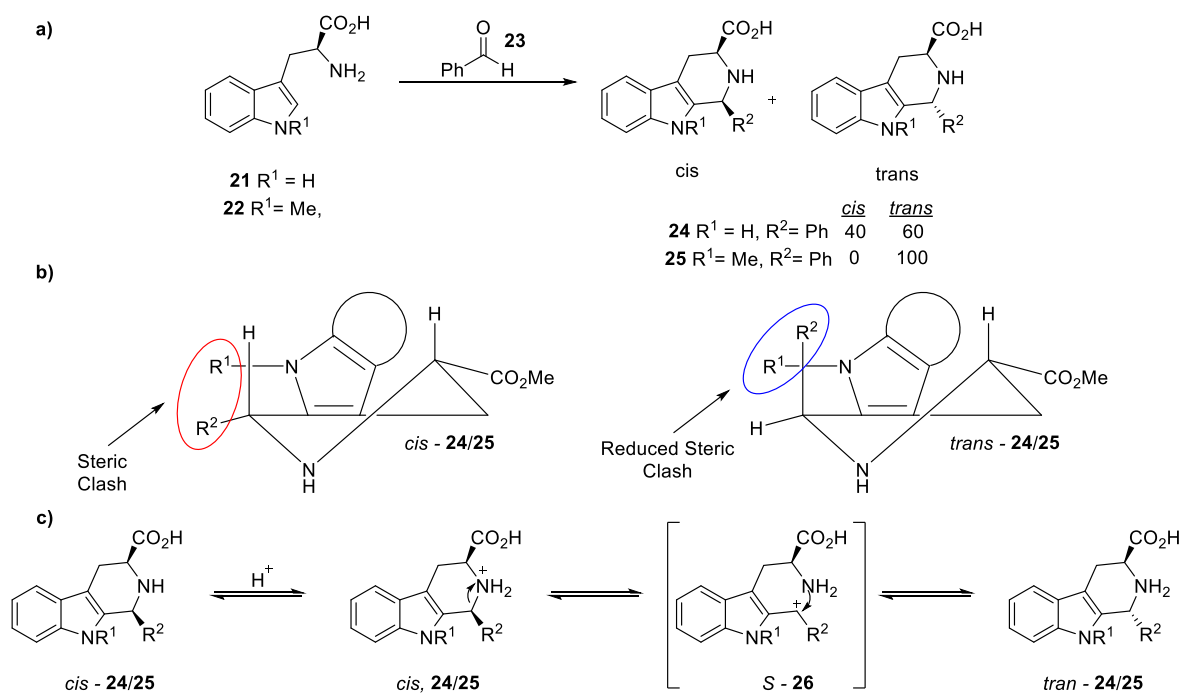
Scheme 3 The formation of chiral amines produced from Tryptophan derivatives undergoing a Pictet-Spengler reaction. a) The product distribution with respect to *cis/trans* configurations. b) The steric clash minimisation afforded by the *trans* diastereoisomer c) The mechanism for diastereomers interconversion from treatment with acid.[31]

This leads the way for the synthesis of a wide range of alkaloid derivatives (Scheme 4) with high diastereomeric purity. The Erectile Dysfunction (ED) drug, Tadalafil, **29**, was first discovered in 1991 and is synthesised from the methyl ester derivative of D-tryptophan, **27**, using the same key Pictet-Spengler reaction to install the second chiral centre.[33,34] In the synthesis by *Shi* et al., the kinetic *cis* product was successfully isolated with extremely high selectivity. This was achieved by exploiting the difference in solubility of the two isomers, whereby the kinetic, *cis*, product would precipitate out of solution once formed. Dissolving a diastereomerically pure sample of *cis* – **28** in a DMSO, where both configurations are soluble, led to spontaneous conversion to the thermodynamic *trans* product, confirming the driving force of the *cis* product formation is the difference in solubility.
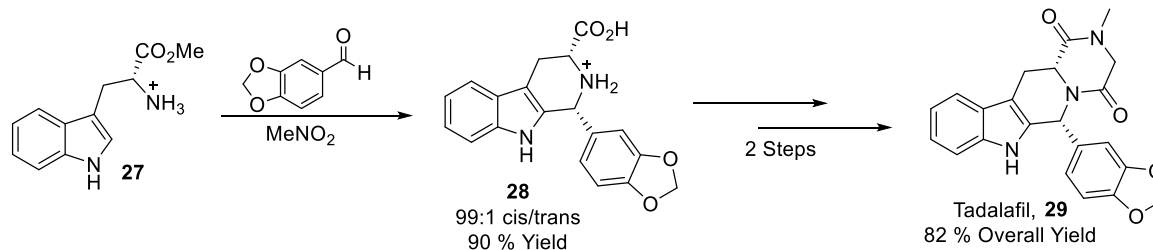
Scheme 4 The synthesis of Tadalafil from D-Tryptophan over 3 steps.[34]

Although the synthesis of **29** is relatively concise (Scheme 4), synthetic routes that start from the chiral pool are often extremely lengthy. A good example of this is the synthesis of Oseltamivir, **33**, an antiviral medication used to treat and prevent influenza A and B (Scheme 5), developed by Gilead Scientific in 1996.[35] The synthesis of **33** starts from naturally occurring Shikimic Acid, **30**, which is the biological starting point for the synthesis of multiple key metabolites, including L-tryptophan and L-phenylalanine amino acids. **30** is converted to **33** through an elongated 10 step synthesis proceeding (Scheme 5) *via* key intermediates **31** and **32**.[36] This synthesis is lengthy due to the need to add and removed protecting groups to protect the integrity of the chiral centres, as well as the need to add several new functionalities.

One of the main challenges that faces chiral pool synthetic strategies is the difficulty in securing sufficient feedstock to meet the demands of large chemical industries. Initially **30** that was used for the synthesis of **33** was extracted from plants, many of which are considered toxic.[36] This created a huge bottleneck in the synthesis as concentrations in these naturally occurring material was found to be low (1.6 – 3.7 % w/w), therefore large quantities are required to obtain sufficient starting substrate for the synthesis. For example, Chinese star anise can produce approximately 1 kg of **30** from 30 kg of plant material, whilst it still retains levels of neurotoxicity towards

infants.[37] These inefficiencies in the extraction process from natural sources led to the development of a modified

E.coli fermentation process being developed, capable of producing 69 g/L.[36]
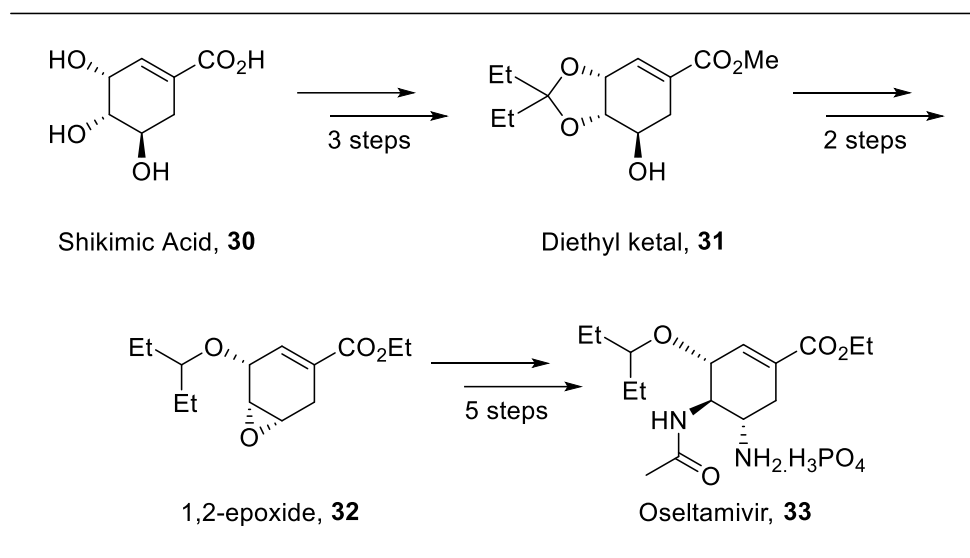
Scheme 5 The synthesis of Oseltamivir from Shikimic Acid.[36]

Overall, the synthesis of chiral amines from the chiral pool can yield highly enantiopure products without the need to create new chirality. However, there are many challenges that need to be overcome. The long synthetic routes that are often required can generate large amounts of waste and are extremely time inefficient. The limited structural diversity of the chiral pool makes shorter synthetic routes hard to achieve, as it a common requirement for numerous protection and de-protection steps to be used alongside multiple functional groups interconversions are required to achieve the desired structure. Furthermore, the naturally occurring stereocentres are created in only one configuration, i.e., L-amino acids and D- sugars, either limiting the chirality of the final product or requiring multiple additional synthetic steps to invert the natural stereochemistry. Finally, obtaining the stock material in sufficient quantities is often a barrier to making these strategies viable on an industrial scale.

1.2. Chiral Auxiliary

The use of chiral auxiliaries represents an alternative synthetic methodology capable of installing new chiral functionality into previously achiral molecules.[38] These auxiliaries work by temporarily incorporating a chiral group, *via* a covalent bond, to a prochiral substrate (Scheme 6a). This blocks attack of the electrophile from one of the two faces using steric bulk (Scheme 6b). Following the addition of the nucleophile in the enantioselective step, the auxiliary is then removed. In the case of chiral amines, Ellman's auxiliary is widely used to convert aldehyde or ketone containing compounds into chiral amines.[39,40]
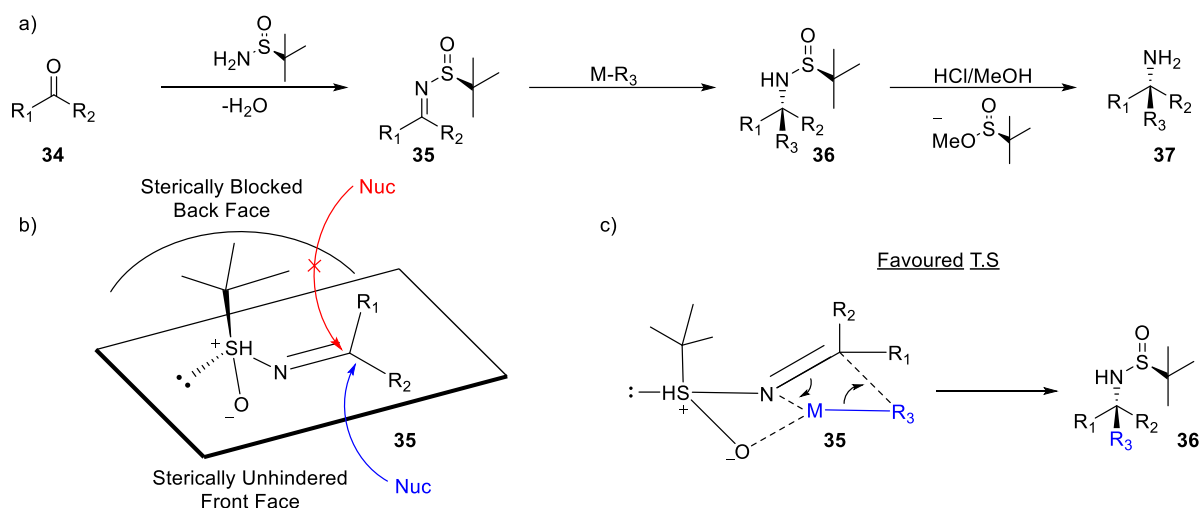
Scheme 6 a) Generic scheme for the asymmetric synthesis of a **37** using Ellman auxiliaries. b) Depiction of the tertbutyl group blocking the back face of **35**. c) The 6-membered transition state rational of **35** that delivers **36**.

During the condensation reaction with **34** (Scheme 6a) the E-isomer of **35** is exclusively formed. Once installed the bulky tertbutyl group blocks access to the prochiral C atom from the back face, **35** (Scheme 6b). This makes attack from the sterically hindered back face energetically disfavoured. Therefore, the chosen nucleophilic species inserts from the front face, creating the chiral centre. Due to the organometallic nature of the nucleophile, attack from the front face is further promoted by chelation of the O and N atoms to the metal ion (Scheme 6c). The stereochemistry can be rationalised through a 6 membered transition state. However, with excessive heat, attack from the undesirable face can be overcome. Therefore, low temperatures are important to protect the integrity of the stereogenic centres.

The Ellman auxiliary has been applied to the synthesis of Apremilast, **42** (Scheme 7), a drug patented by Amgen for the treatment of psoriasis.[41,42] In 2020 **42** made \$2 billion in sales, making it another blockbuster drug that contains a chiral amine motif. Although there have been several reported syntheses of **42**, the chiral auxiliary methodology is considered the most effective due to its simple, safe and economic nature.[41] The synthesis is derived from the prochiral ketone **38**, which undergoes several transformations to install the sulfonyl group. Key intermediate **39** can then undergo a condensation reaction with the desired *S* Ellman auxiliary which tautomerises to the more stable enamine, **40**. The C=C bond can then be reduced using a classical $NaBH_4$ reducing agent to deliver **41** with 99 % e.e. and 86 % yield.[41]
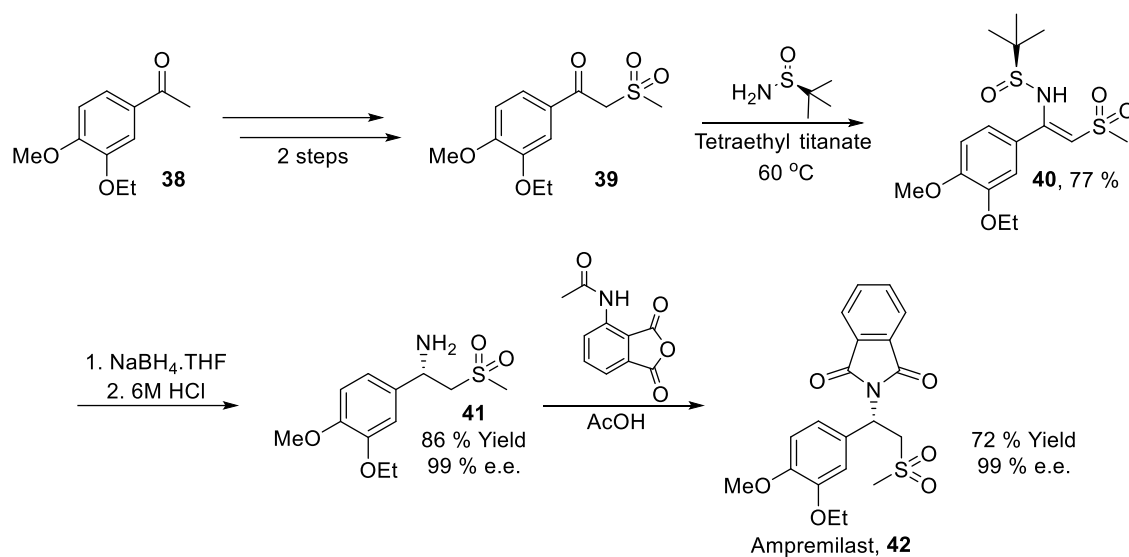
Scheme 7 The synthesis of **42** from **38** using Ellman's chiral auxiliary.[41]

Ellman auxiliaries have also been employed by Novartis in their synthesis of a novel DPP-4 Inhibitor, **46** (Scheme 8), used to treat glycemia.[43] This synthesis demonstrates how the auxiliary can be applied to an aldehyde **43** before treatment with a Grignard reagent to achieve midchain chiral amine, **45**. The initial dr of the product was lower than required despite optimisation. This may be due to the position of the midchain imine, where the difference in steric bulk between the adjacent C atoms is not significant. The energy difference between the two transition state confirmations is therefore likely relatively small, resulting in modest diastereoselectivity. It may be possible to have improved selectivity further through lowering the temperature, however, no attempts were reported below – 78 °C, likely due to the difficulty in scaling near cryogenic reactions.

A simple recrystallisation of **45** in MeOH was sufficient to increase the diastereopurity of the product to 99.8:0.2 (Scheme 8). This demonstrates the advantage of generating a diastereomeric intermediate where the physical properties of each diastereoisomer are different. This allows for simple purifications, such a recrystallisation, rather than expensive and time consuming chromatography or chiral purifications. Once installed, only simple deprotection and amide coupling reactions are required to deliver **46** with 99 % e.e.. The relative late stage introduction of the chiral centre reduces the chance of racemisation in subsequent step to obtain the final product.
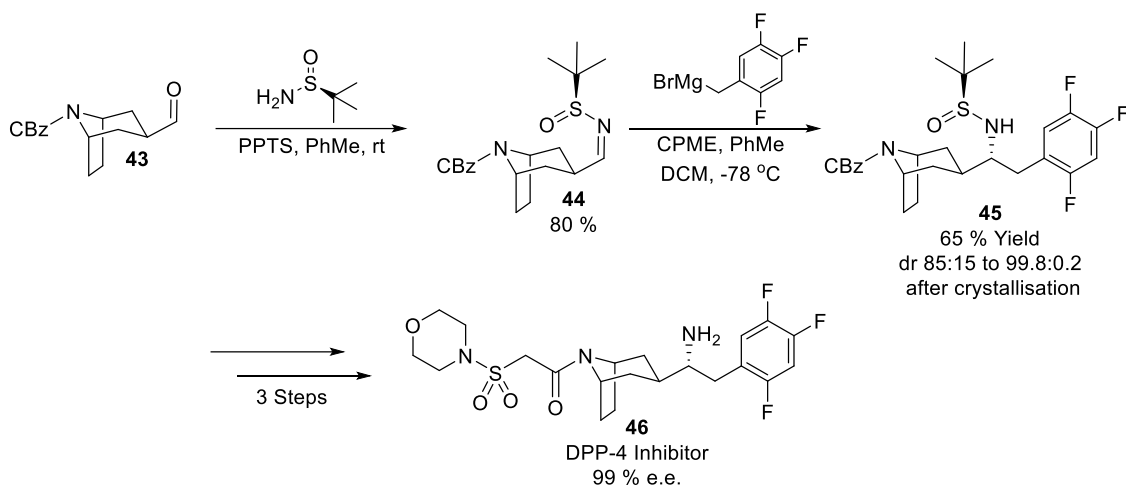
Scheme 8 The synthesis of **46** from **43** by Novartis through use of Ellman's chiral auxiliary.[43]

Chiral auxiliaries can be used to synthesise compounds over a wide chemical space, owing to the structural diversity of readily available prochiral carbonyl containing compounds and commercially available auxiliaries. However, the additional steps that are required to add and remove the chiral auxiliary drastically increases the overall process time for these synthetic approaches. Furthermore, the additional solvents and reagents that are used during the subsequent work-up makes these reactions less attractive from an environmental and economic standpoint, falling short of many Green Chemistry principles.[44] Use of alternative auxiliaries, such an Evans auxiliary, that can be recycled, can address some of these concerns, however the recovery process can in itself generate significant waste.

Another disadvantage to the use of chiral auxiliaries is the extremely low temperatures that are required during the imine reduction. These low temperatures are imperative to deliver high selectivity but, on a large industrial scale, it takes multiple hours to cool a reactor sufficiently, further elongating the overall reaction time. Cooling large reactors to such low temperature is also extremely energy intensive and therefore expensive. Furthermore, to protect the integrity of the batch, extremely good reaction monitoring is required and reactor system capable of responding to spikes in temperature.

Finally, perhaps the biggest criticism of the use of chiral auxiliaries, especially for commercially available ones such as Ellman auxiliaries, is that the chirality is essentially being bought rather than generating new chirality. Also given that auxiliaries are employed stoichiometrically, this is akin to a synthesis starting from chiral substrate, such as the chiral pool.

1.3. Asymmetric Catalysis

Asymmetric catalysis is a class of reactions in which a chiral catalyst directs the preferential formation of a single stereoisomer as the product. Asymmetric hydrogenation of imines and enamines is currently used extensively throughout research laboratories and industrial processes to install new chiral amine centres. It is an attractive methodology because appropriate development can deliver processes that can have relatively high functional group tolerance, allowing for chirality to be installed later in synthetic routes, therefore reducing the risk of loss in e.e. in subsequent reactions. In these reactions a transition metal catalyst, typically Rh or Ir, is combined with a chiral ligand to create a catalyst with a chiral binding pocket. [45–47] This catalyst is then capable of selectively delivering H_2 to the prochiral C=N or C=C bond (Scheme 9).

The ratio of the two potential enantiomeric products of the hydrogenation can be rationalised using the Curtin-Hammet Principle (Figure 2). The imine substrate can bind to the catalyst in two different orientations, thus creating two different diastereomeric intermediates, S or R – **51**. The difference in energy between these two intermediates, is given by ΔG^o. Due to the chiral nature of the ligands bound to the catalyst, the transition state energies required to form the respective products are different for S and R – **51**. The activations energies taken to reach S and R - **51** are denoted by $\Delta G_S^{\ddagger}$ and $\Delta G_R^{\ddagger}$ respectively. $\Delta G_S^{\ddagger}$ and $\Delta G_R^{\ddagger}$ do not govern the product ratios as this does not consider ΔG^o. The ratio of the S and R enantiomers in the product is determined by the difference in energy between the S and R – **51** transition state energies, $\Delta\Delta G^{\ddagger}$ (Equation 1). The greater $\Delta\Delta G^{\ddagger}$ is the higher the enantioselectivity of the reaction and it becomes easier to discriminate between the two enantiomers. Using the rate equations for this reaction, the product distribution can be described by Equation 2.
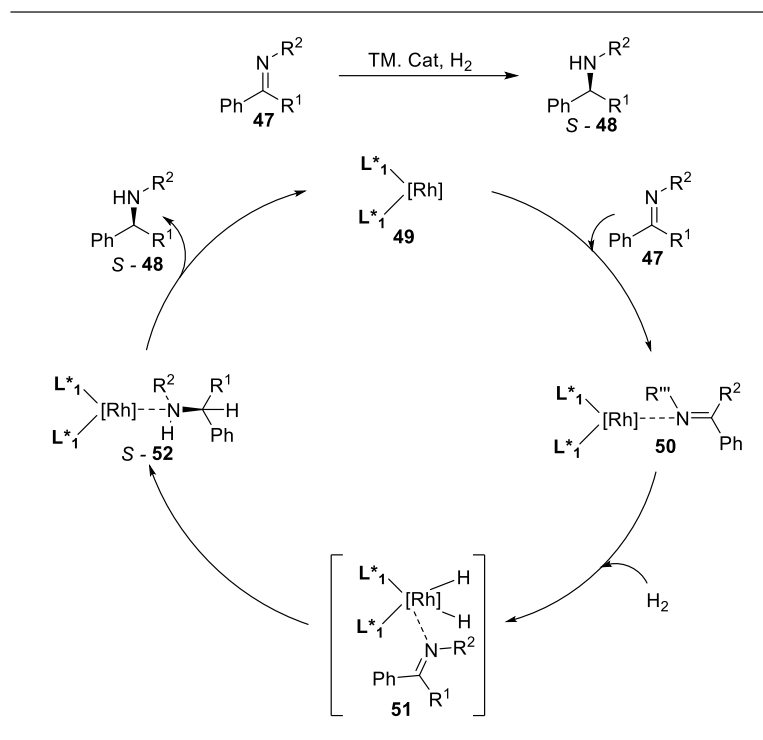
Scheme 9 Generic scheme for the asymmetric hydrogenation of prochiral benzylic imines using a Rh based catalyst.
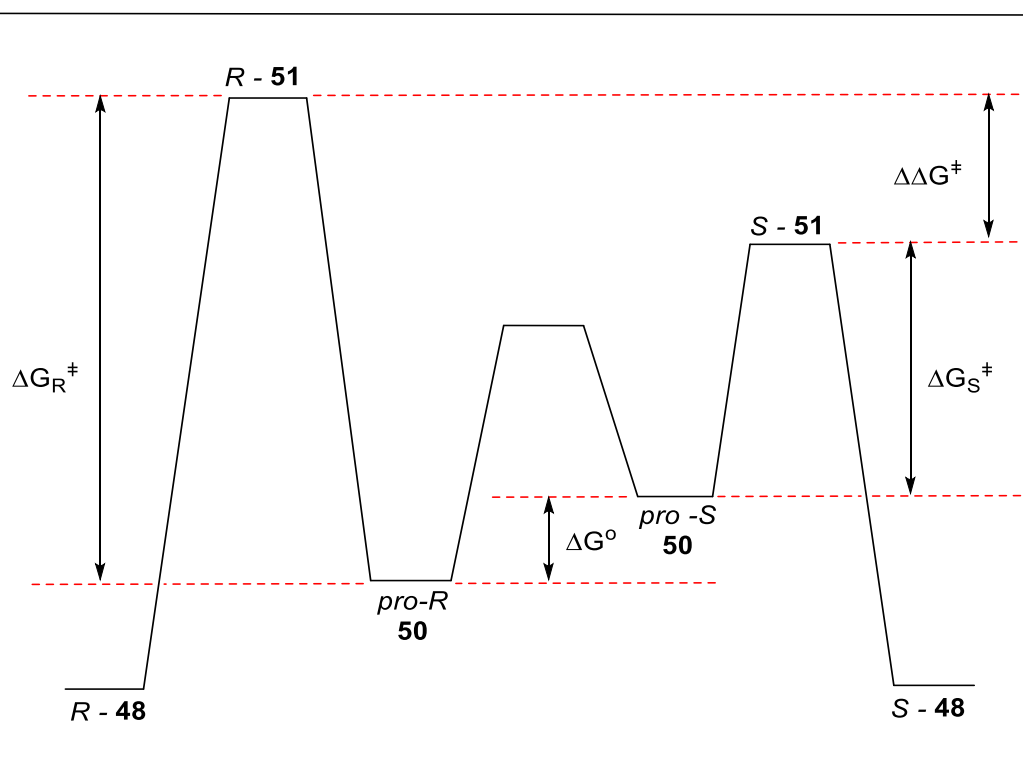
Figure 2 Generic Curtain-Hammett plot demonstrating how enantioselectivity is driven by chiral catalysts.

$$\Delta\Delta G^{\ddagger} = \Delta G^{o} + \left(\Delta G_R^{\ddagger} - \Delta G_S^{\ddagger}\right) \quad \text{Equation 1}$$

$$\frac{[R]}{[S]} = e^{-\Delta\Delta G^{\ddagger}/RT} \quad \text{Equation 2}$$

22

Asymmetric hydrogenation of an enamine was employed by Merck in their synthesis of Sitagliptin, **55**, another DPP-4 inhibitor used for the treatment of Type II diabetes (Scheme 10).[48] **55** generated $5.3 billion in 2021 alone and ranked as Merck's third bestselling drug.[49] Previously **55** was synthesised through the asymmetric hydrogenation of a ketone at the very start of the synthetic route followed by 7 subsequent synthetic steps to deliver the desired product.[48] Merck scientists set about investigating the potential of employing an asymmetric hydrogenation of an N-unprotected enamine, **53** (Scheme 10), *via* the imine resonance form, **54**, on a late stage intermediate. Usually, the amine is required to be functionalised with a sterically large group to increase $\Delta\Delta G^{\ddagger}$ and subsequently drive higher enantioselectivity of the hydrogenation step. However, in this work this step was avoided, **54**, to give a more direct synthetic route. This was possible due to the intramolecular chelation of the substrate to the catalyst and the advanced nature of the intermediate, meaning sufficient steric bulk was present from the existing desired functionality of the molecule.
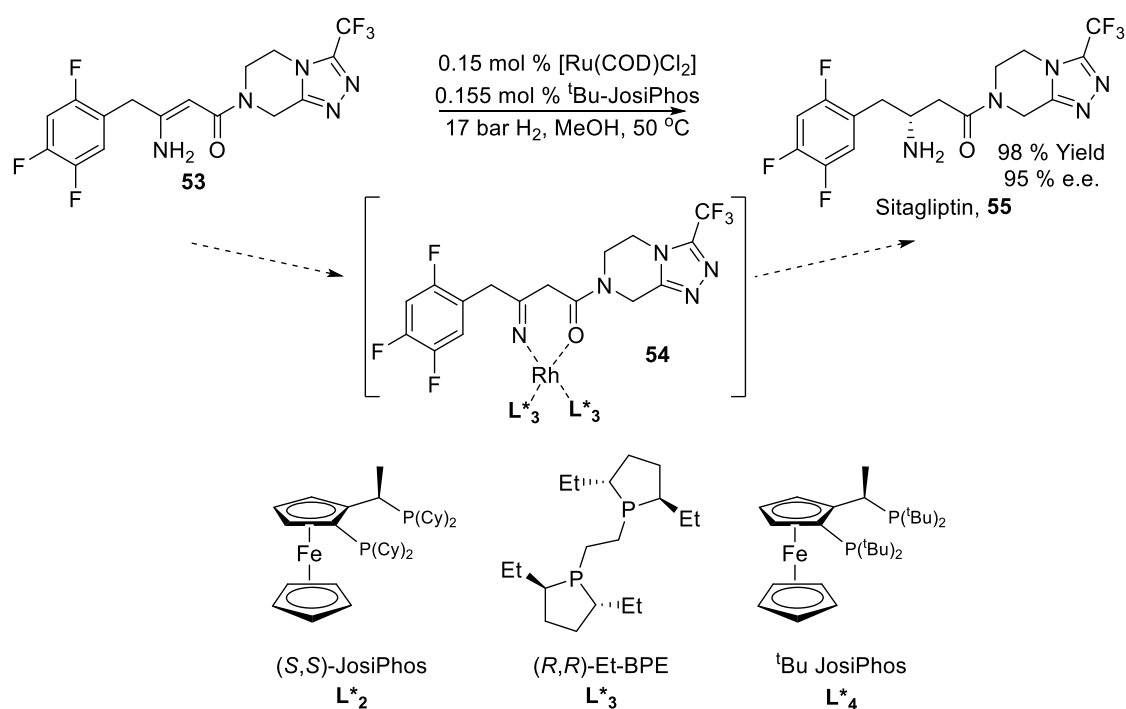
Scheme 10 Merck's asymmetric hydrogenation of an N-unprotected enamine to synthesise **55**.[48]

Initial work focused on the screening of Rh, Ir and Ru metal precursors with a variety of proprietary ligands, **L*₂**, **L*₃** and **L*₄** (Table 1 and Scheme 10). It was found that the Ru catalysts showed little to no activity (Entries 1 and 2), while Ir catalyst show moderate conversion with almost no enantioselectivity (Entries 3 and 4). This highlighted the challenge of this transformation without protecting groups and such a late stage intermediate. However, it was found that Rh catalysts displayed excellent conversion (Entries 5 – 7) with moderate to extremely

high enantioselectivity. Buchwald's ^{t}Bu-Josiphos ligand, **L*₄**, proved to be the best suited, delivering > 99 % conversion and 95 % selectivity.

Additional developments of the reaction conditions were performed. It was noted that the reaction was becoming mass transfer limited, due to the availability of H_2 in solution. This led to the pressure of the reaction being increased from 6.2 bar to 17.2 bar, enabling the reaction to proceed uninhibited. The increase in pressure allowed the catalyst loading of the metal precursor and ligand to be reduced from 5 and 10 mol % to 0.15 and 0.155 mol % respectively. These, amongst other, developmental steps allowed the reaction to achieve 98 % yield and 95 % e.e. on a 400 g (1 mol) scale.

Table 1 Extracts from the results of the catalyst screen for the asymmetric hydrogenation of N-unprotected enamine. [48]

Entry	Catalyst	Conv. (%)	e.e. (%)
1	Ru-L^*_2	6	-
2	Ru-L^*_3	1	-
3	Ir-L^*_2	35	8
4	Ir-L^*_3	33	4
5	Rh-L^*_2	> 99	86
6	Rh-L^*_3	40	38
7	Rh-L^*_4	> 99	95

Reaction Conditions: 5 mol % metal precursor, 10 mol % ligand, 6.2 bar H_2, MeOH, 50 °C

The synthesis of **55** by Merck represents the culmination of a vast amount of work across a huge industrial company. During the development of this novel chemistry, Merck were able to reduce the synthetic route from 8-steps to 5-steps, in doing so they managed to sidestep many of the pitfalls of asymmetric hydrogenation. Firstly, the lack of protecting group to add greater steric bulk to **53** meant that key steps to add and remove such groups was negated, greatly decreasing the Process Mass Intensity (PMI) and increasing Atom Economy (AE) of the reaction.[44] The more direct route and reduction in catalyst loading, alongside other optimisations, allowed the total waste per kg of **55** to be reduced from 250 kg to just 50 kg, while completely eliminating water waste leading to the awarding of both the Presidential Green Chemistry Award and the ICHEME Astra-Zeneca Award for Sustainability.[48]

Aside from increasing the Green Chemistry Metrics for the process, the reduction in catalyst loading was hugely beneficial to the economic viability of the process (Figure 3). Rh is one of the most expensive transition metals, however unfortunately it was demonstrated to be integral for the key hydrogenation of **53** (Table 1). With Rh costing around € 300,000 kg^{-1} in 2023, the 33-fold reduction in catalyst loading could result in significant savings of € 36,000 per ton of **54** reduced, this could add up to enormous savings given the scale that Sitagliptin is

produced on each year. The Merck scientists also established an effective procedure for the recovery of the catalyst, enabling it to be reused which can also increase the cost efficiency of the process.
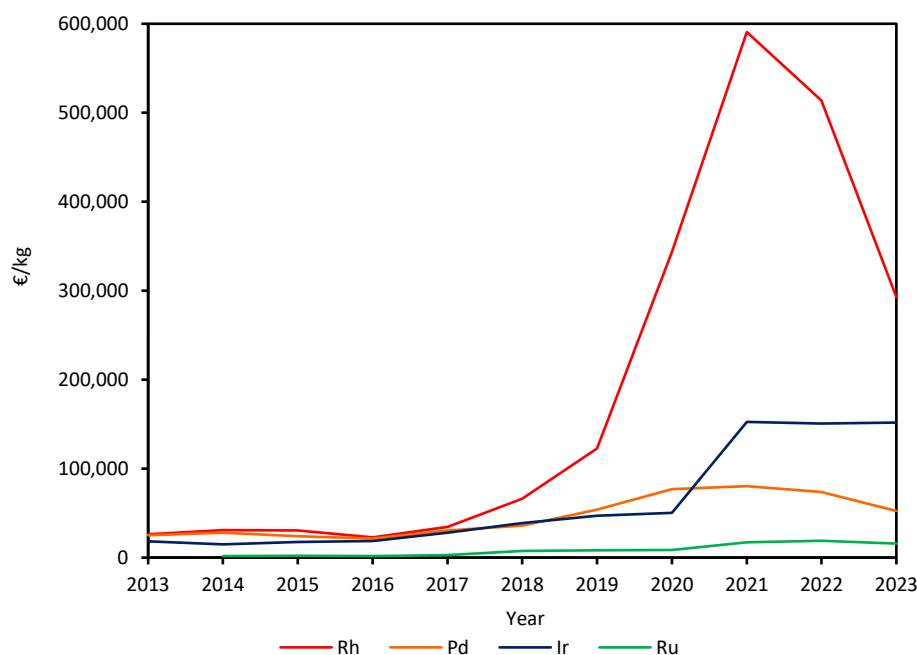
Figure 3 Price of transition metals (per kg) from 2013 to 2023.[50]

1.4. <u>Biocatalysis</u>

Biocatalytic transformations can be an extremely attractive approach for large industries, leading to the global industrial enzyme market reaching $7 billion in 2022.[51] One such advance is that biochemical transformations can be highly enantioselective, offering a direct synthesis of chiral amines from prochiral ketones using simple nitrogen sources, such as amino acids or isopropylamine.[52] For the synthesis of chiral amines ω-transaminase (TA) enzymes are commonly utilised (Scheme 11), working in tandem with a PLP co-factor, **56**, to transfer amino groups from an amine donor, **58**, to prochiral ketone, **63**, to ultimately deliver chiral amines, **66**.[17,53,54]

A high profile example of a biocatalytic synthesis was provided by a collaboration between Merck and Codexis (Scheme 12) for a third generation synthesis of **55**.[55] This work was motivated by the extremely high price of Rh (Figure 3), as well as the need for an additional crystallisation step following the asymmetric hydrogenation to increase the e.e. of **55** from 95 % to the required 98 % (Scheme 10). Furthermore, the use of transition metals requires the need for intensive work up steps to remove Rh from the final product due to strict regulations, and this requires expensive specialist equipment.
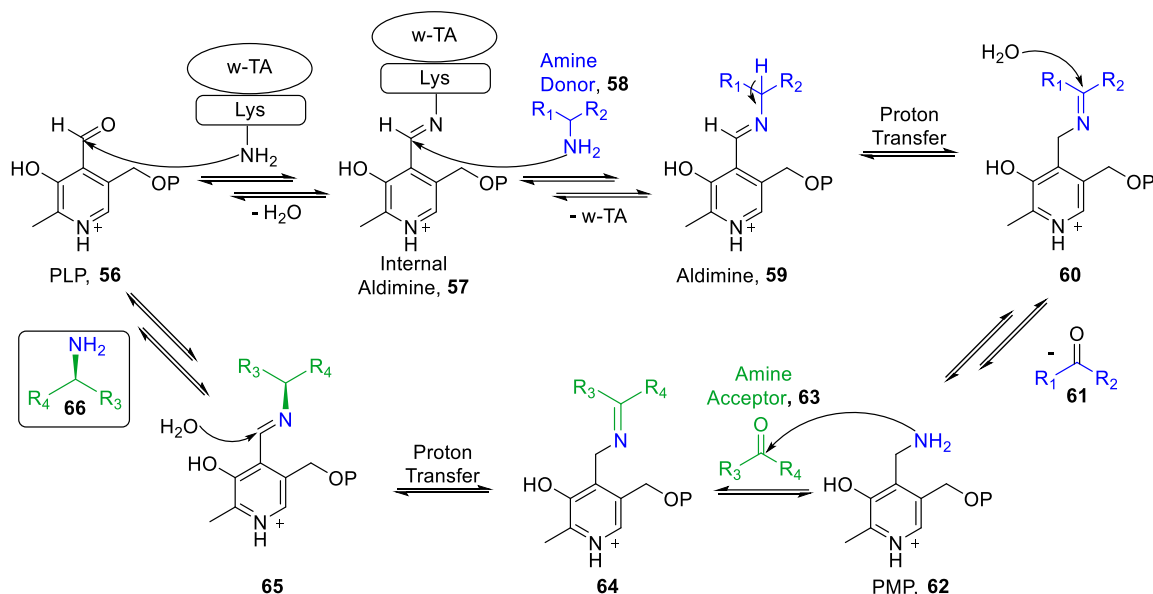
Scheme 11. The mechanism for transaminase biocatalysis of chiral amines.[53]
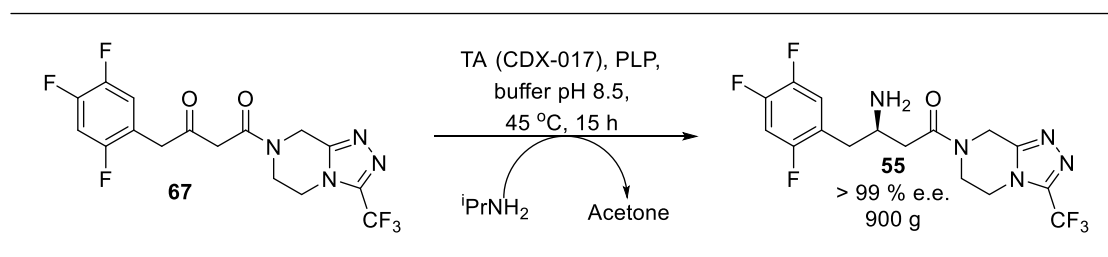
Scheme 12. Transaminase synthesis of Sitagliptin developed through the Merck/Codexis collboration.[55,56]

In order to meet industrial demands many challenges surrounding transaminase enzymes had to be addressed. Firstly, transaminase enzymes have very narrow substrate scope due to their extremely specific role in nature.[57,58] In its natural form the two key binding pockets of the transaminase, large and small, can only accommodate substrates approximately the size of a phenyl group and a methyl group respectively (Figure 4a).[55] Furthermore, enzymes suffer from low stability to high substrate concentrations alongside low turnover numbers, which greatly limits their productivity, and makes meeting the demands of industry extremely difficult.

The industrial collaborators set about combatting these challenges through a directed evolution approach in tandem with *in silico* modelling.[55] Firstly, the limitations surrounding capacity of the substrate binding pockets was addressed through a modification technique known as substrate walking (Figure 4). This strategy incrementally increases the size of the substrate in each binding pocket, and once mutations begin to accommodate the new size it can be further increased until the desired substrate is accepted.

Initially an ATA-117 *R*-selective transaminase was subject to a simplified scaffold (Figure 4b), **69**. The *in silico* model suggested it would be unable to bind effectively because of steric clashes in the large pocket. As predicted by the modelling, only 4 % conversion was observed. The large binding pocket was then subjected to site saturation mutagenesis, where 3 amino acid units were exchanged with all possible amino acids. The expansion of the large pocket to accommodate **69** (Figure 4c), yielded an 11-fold increase in activity.
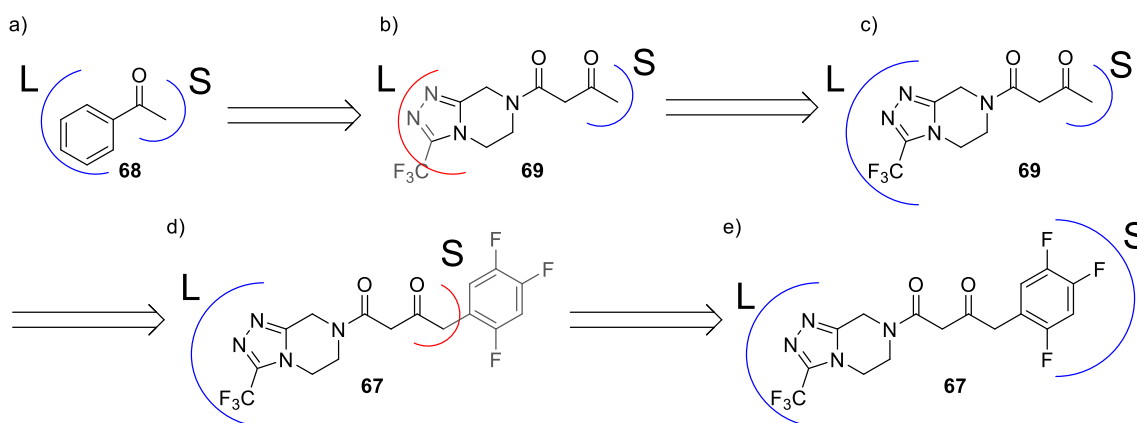
Figure 4 Expanding of both the large and small binding pocket of transaminase ATA-117 through substrate walking to accommodate Sitagliptin ketone.

With the large pocket sufficiently expanded (Figure 4c), 217 new strains of the enzyme were derived from the mutant strain. The substrate was switched to the desired substrate, **67**, to increase the size of the small binding pocket (Figure 4d). Initially, as expected, these results were poor, retuning just 0.7 % conversion. Subsequent site saturation mutagenesis, to accept the right hand side of **67** (Figure 4e), resulted in a 75-fold increase in activity. Despite the great increase in activity the enzyme was still not practically useful and further modifications were required to increase its stability under the reaction conditions. As transaminase reactions are equilibrium controlled the enzyme would need to be stable up to ~ 50 °C to evaporate the acetone by-product from the isopropyl amine donor to drive the reaction to completion. The elevated temperature, and tolerance of organic solvents, were also necessary to offset the low solubility of the substrate. Greater solubility allowed higher concentrations of both the substrate and amine donor to be reached, which were needed to achieve the required productivity. These constraints also demanded a greater stability of the enzyme under these harsher conditions.

In total 11 rounds of direct evolution were required to identify the final CDX-017 transaminase enzyme, followed by reaction optimisation. The result of this mammoth effort is the creation of a new enzyme which can convert up to 200 g/L of **67** with > 99.95 % e.e. with a 92 % yield over a 32 hour processing time (8 hours of addition followed by a 24 hour reaction).

These impressive results compared extremely favourably to the Rh catalysed asymmetric hydrogenation route previously discussed in Section 1.3. Specifically, CDX-017 was able to increase the overall yield of the synthesis of Sitagliptin by 10-13 %, with a 53 % increase in productivity (kg/L/day). Furthermore, it was able to reduce the total amount of waste by 19 % and completely eliminate the need for Rh or any other heavy metals, leading to huge environmental and economic benefits. Furthermore, this reaction could be carried out in multipurpose vessels which negate the need for investment into highly specialised high pressure hydrogenation reactors. Due to the significant improvement of the Green Chemistry characteristics of such a huge industrial operation, Merck and Codexis were awarded the 2010 Green Chemistry Challenge Award for Greener Reaction Conditions by the United States Environmental Protection Agency.[44,59]
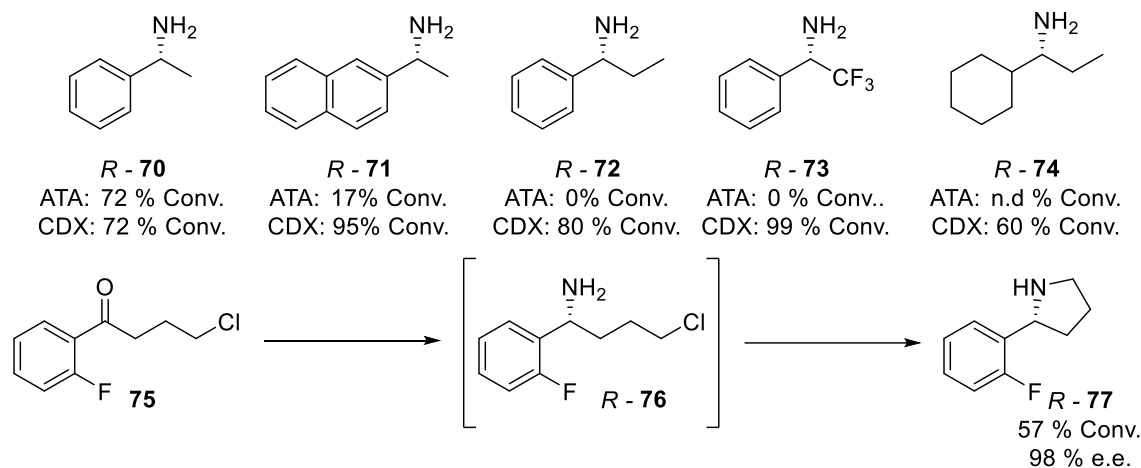
Scheme 13 Examples of the increased substate scope that CDX-017 affords compared to the original ATA-117 transaminase.[55]

Due to the expansion of the binding pockets this enzyme was able to be applied to a much wider range of substrates (Scheme 13). CDX-017 showed improved conversion of nearly all substates compared to the original ATA-117 enzyme and was shown to have a tolerance for bulkier substrates, **71**, electron deficient substrates, **73**, and aliphatic substrates, **74**. This work reflects a hugely successful collaboration between Merck and Codexis, demonstrating what can be achieved with biocatalytic approaches to chiral amine production, overcoming many of the challenges previously thought to prevent them being an industrially viable.

1.5. Chiral Resolution of Racemic Mixtures

1.5.1. Kinetic Resolution

Kinetic resolution (KR) has been a cornerstone for the delivery of compounds with high chiral purity on an industrial scale, appearing in the synthesis of > 50 % of enantio-enriched drugs in the early 2000's.[60] In the KR process (Figure 5), a racemic mixture is treated with an optically pure resolving agent or enantioselective catalyst which preferentially forms a derivative with of one of the enantiomers faster than it does with the other.[61] The optically pure derivative can be separated from the unreacted remaining enantiomer of the starting material using conventional achiral separation techniques.
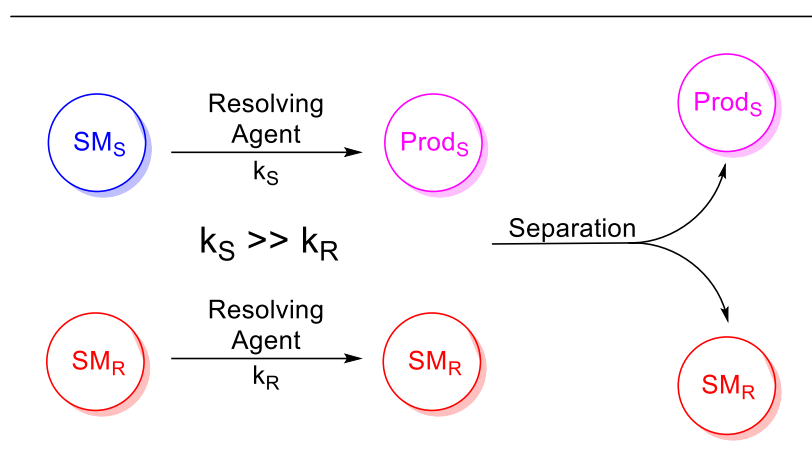
Figure 5 The general graphic for the kinetic resolution of a racemic mixture of chiral amines.

An example of KR is the enantioselective separation of **78** (Scheme 14), an isoquinoline alkaloid related to the Norrecticuline natural product family, previous investigated for its local anaesthetic properties.[62–64] A KR catalyst, **80**, was used in combination with acyl donor **79** to selectively form an amide derivative, $S - $**82**, of just one of the enantiomers of the starting material before being regenerated through the use of co-catalysts. Similarly, to asymmetric hydrogenation reactions, there the ratio of the KR's products is also dictated by the Curtin-Hammett Principle, however this system has some key differences (Figure 6). This reaction was able to deliver 50 % conversion, to provide the derivative, $S - $**82**, with 92 % e.e., leaving the unresolved amine, $R - $**78**, with an e.e. of 90 %.

Both starting enantiomers, S and R - **78**, have the same energy (Figure 6), however due to the chiral nature of the resolving agent the transition state energies each of the enantiomers are different, S and $R - $**81**. As the starting materials are enantiomers of each other, interconversion between them is energetically extremely unfavourable under these conditions, denoted by ΔG_{Rac}. In fact, ΔG_{Rac} is greater than the activation energy for the S and $R - $**81**,

$\Delta G_S{}^\ddagger$ and $\Delta G_R{}^\ddagger$. As ΔG_{Rac} is so much greater than $\Delta G_S{}^\ddagger$ and $\Delta G_R{}^\ddagger$ it can be discounted from the equation. This means the ratio of the product formation is solely down to the difference between $\Delta G_S{}^\ddagger$ and $\Delta G_R{}^\ddagger$.
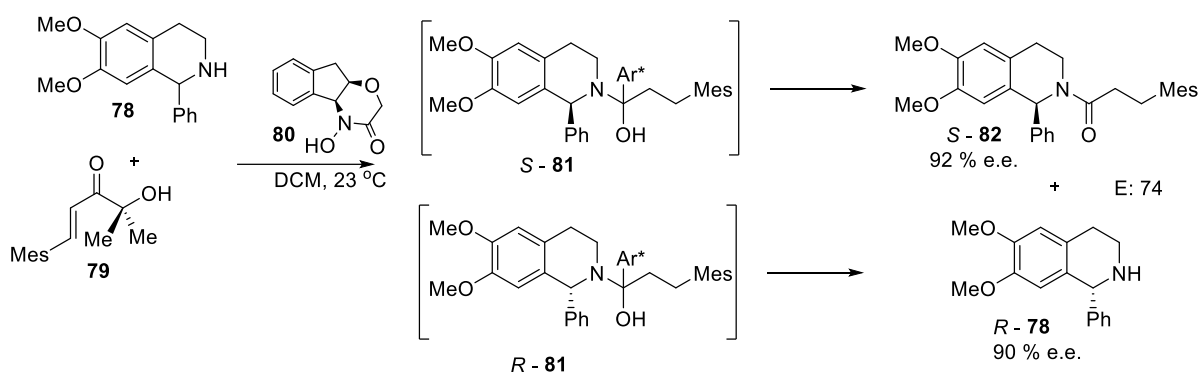
Scheme 14 The kinetic resolution of **78** using kinetic resolution catalyst **80**.[62]

In KR's the product distribution is quantified by Selectivity Factor (E) (Equation 3), that is calculated from the e.e. of the substrate and product. A rule of thumb dictates that a E of > 10 is required to be synthetically useful, and a E of > 50 should allow for both enantiomers to be recovered in their chirally pure form.[61] As the reaction progresses, and the concentration of the desired reacting enantiomer drops, the selectivity factor becomes increasingly important. If the selectivity factor is relatively low then the reagent/catalyst is more likely to react competitively with the undesirable enantiomer due to its increasing relative concentration. .

$$E = \frac{K_S}{K_R} = e^{\Delta\Delta G^\ddagger / RT} = \frac{Ln[(1 - C)(1 - ee_s)]}{Ln[(1 - C)(1 + ee_R)]} , C = \frac{e.e._s}{e.e._s + e.e._P} \quad \text{Equation 3}$$
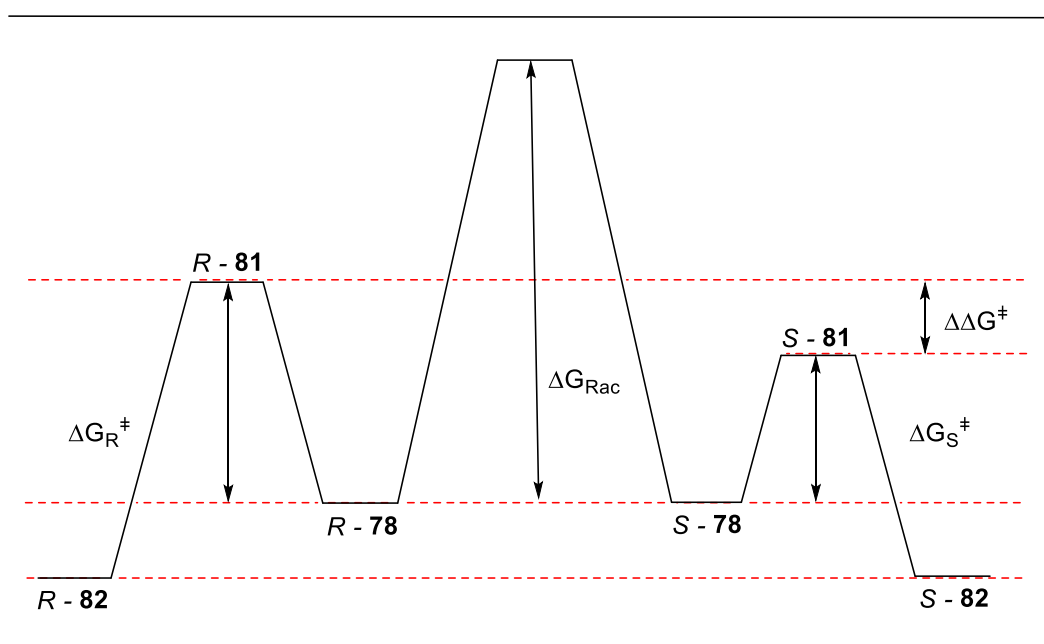
Figure 6 Curtin-Hammet plot demonstrating the relative activation energies in the kinetic resolution process.

1.5.2. Chiral Resolution

Alternatively, racemic mixtures can be resolved through chiral resolution, whereby both enantiomers of the starting material interact with the resolving agent to form derivatives that have different physical properties (Figure 7), which allows them to be separated.[65] This can be achieved through use of chiral salts in a process called diastereomeric crystallisation, whereby the diastereomeric derivatives have different solubilities that can be separated *via* a simple filtration. Alternatively, chiral resolution can be performed using a high performance liquid chromatography in combination with a chiral stationary phase, such a Cyclodextrin. Each enantiomer forms a transient diastereomeric complex with the chiral stationary phase, therefore giving each of them having different retention times, allowing them to be separated.
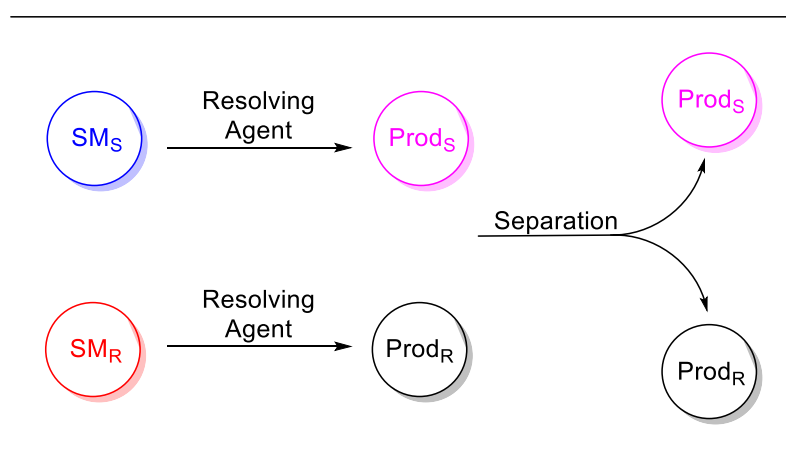
Figure 7 The general graphic for the chiral resolution of a racemic mixture of chiral amines.

Chiral resolutions, particularly diastereomeric crystallisation is scalable, cheap and only requires simple purification processes and is therefore widely used on a production scale.[65–67] This is exemplified by the blockbuster drug, *Clopidogrel*, **85**, an anti-platelet drug used to treat heart disease and stroke.[68] Before its patent expired, **85** was the second bestselling drug in the world, grossing $ 9 billion in 2010. The production of *Clopidogrel* involves a diastereomeric crystallisation process (Scheme 15) which makes use of treating **83** with **84**, to preferentially precipitate **85** out of solution with 47 % yield and 99 % e.e. on a 100 mmol scale.[66,69]
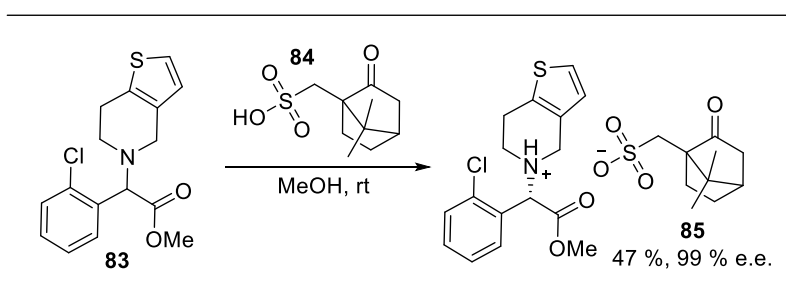
Scheme 15 Chiral resolution for the synthesis of **84**.[66,67]

The use of both kinetic and chiral resolutions is common practice in the pharmaceutical industry.[65] However, the main disadvantage of both of these processes is that the theoretical yield is limited to 50 %. This creates a large amount of waste in the form of the unwanted enantiomer and can make these processes undesirable, particularly for high value compounds.

1.5.3. Dynamic Kinetic Resolution

Dynamic kinetic resolution (DKR) is an alternative resolution approach, combining KR methodologies, described above, in tandem with a racemisation catalyst. The most common form of DKR for the resolution of amines is known as Chemoenzymatic Dynamic Kinetic Resolution (CE-DKR) (Scheme 16), where the combination of a transition metal catalyst and an enzyme, typically *candida antarctica* lipase B (CALB), is employed.[70,71]
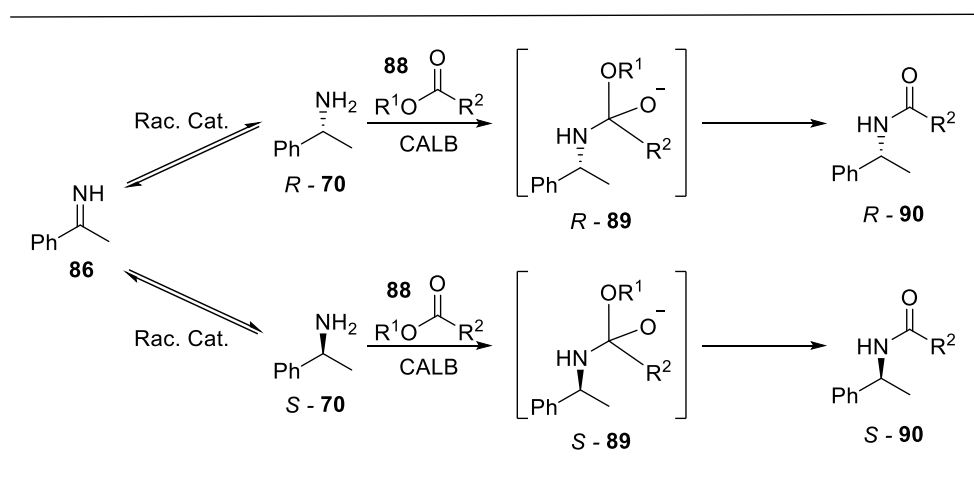
Scheme 16 A generic scheme for the CE-DKR of **70**.

Interconversion between the starting material occurs by abstraction of hydrogen from either *S* or *R* -**70**, removing the sp^3 character and converting it to a sp^2 hybridised imine intermediate, **86** (Figure 8) before restoring the sp^3 character to complete the racemisation process. **70** can then combine with the acyl donor, **88**, and the CALB enzyme to form the tetrahedral intermediate *S* or *R* – **89**, which have different transition state energies denoted by $\Delta G_S^{\ddagger}$ and $\Delta G_R^{\ddagger}$, before the alcohol leaving group in the *R* – **89** transition state is released to form the final product *R* - **90**. This creates a system akin to that in asymmetric hydrogenation where ΔG_{Rac} must be taken into consideration therefore the product distribution of this reaction is also described by Equation 2. This, in turn, creates a system where a theoretical 100 % yield is possible as the desired enantiomers feedstock can be replenished from the undesirable enantiomer through racemisation.

The enantioselective acylation of the *R – 70* is catalysed through a Ser-His-Asp catalytic triad (Scheme 17) in the CALB binding pocket. The acyl donor, **88**, is activated by the Ser[105] residue before *R - 70* attacks to form the enantioselective transition state, **89**, that ends with the liberation of product *R - 90*.
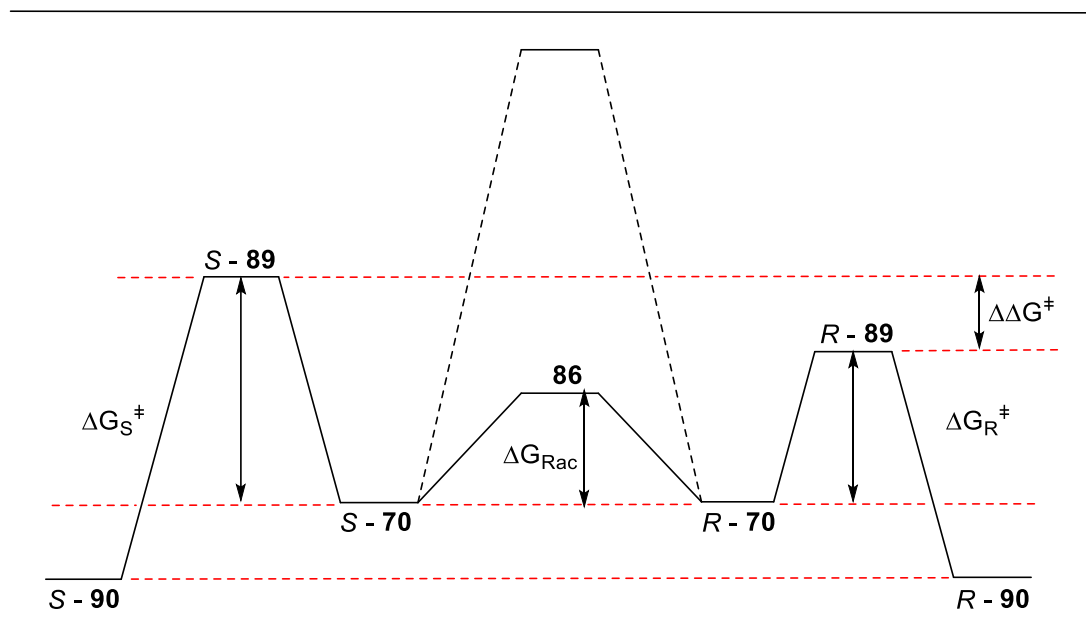
Figure 8 Curtin-Hammet plot demonstrating the relative activation energies in the dynamic kinetic resolution process.
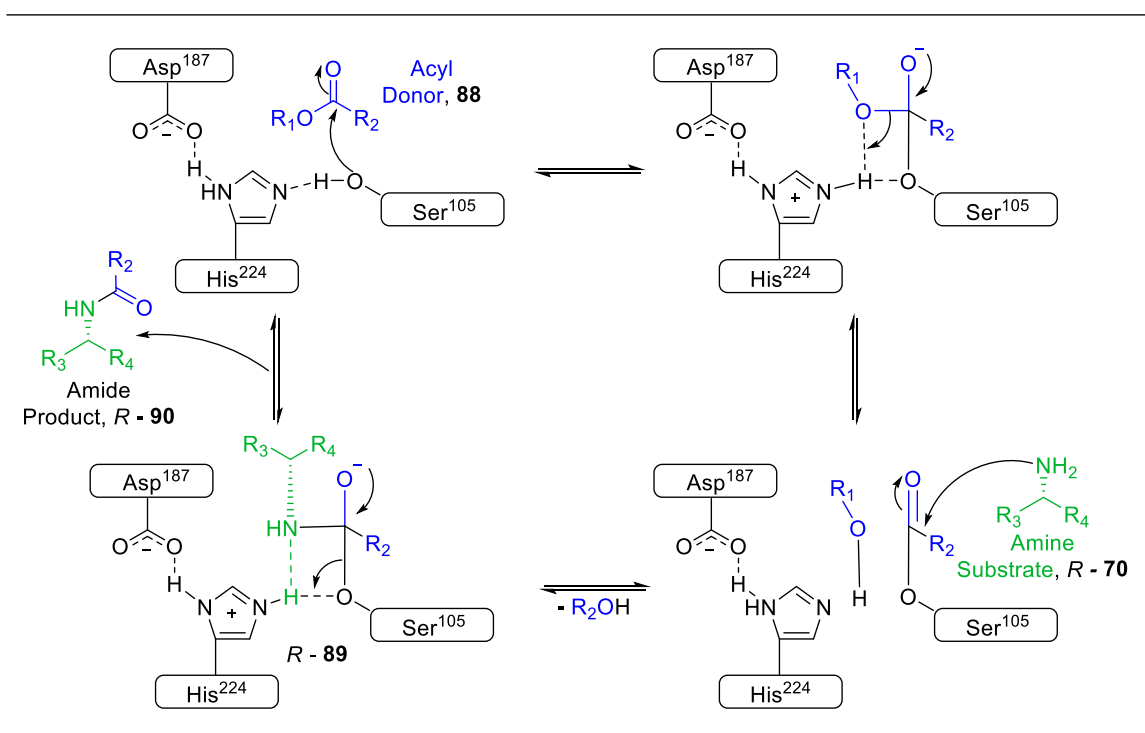
Scheme 17 CALB mechanism for the stereoselective acylation of prochiral amines.[72]

33

The DKR process can be challenging to optimise due to the two processes occurring at the same time. *Bäckvall et al.* developed a list of 4 criteria that are essential for a DKR process to be successful.[73]

1. The KR must have a E $\geq$ 20.

2. The two reagents, often catalysts, must be compatible with each other. This prevents deactivation or competing reactions from occurring.

3. The rate of racemisation must be $\geq$ 10 times faster than the KR of the slowest reacting enantiomer.

4. The reagent/catalyst being use for the racemisation event must not interact with the product of the KR.

Currently, CE-DKR are more commonly applied to alcohols rather than amines. This is largely due to the greater challenge in racemising chiral amines compared to chiral alcohols, due to their propensity for low selectivity. This means that harsher conditions are required to racemise chiral amines, which are less compatible with the KR enzyme. The reason the racemisation of chiral amines is so challenging is two-fold (Scheme 18). Primarily it is due to the imine intermediate **86** that forms, which is more likely to react with the initial substrate, **70**, which is more nucleophilic than the analogous alcohol. Attack of **70** into **86** forms a chiral imine intermediate, **91**, which can then be reduced to form a family of diastereoisomers, **92**, or liberate ethyl benzene, **93**. This results in poor selectivity, which is defined as the amount of the initial amine that is present in solution at the end of the reaction (Equation 4).
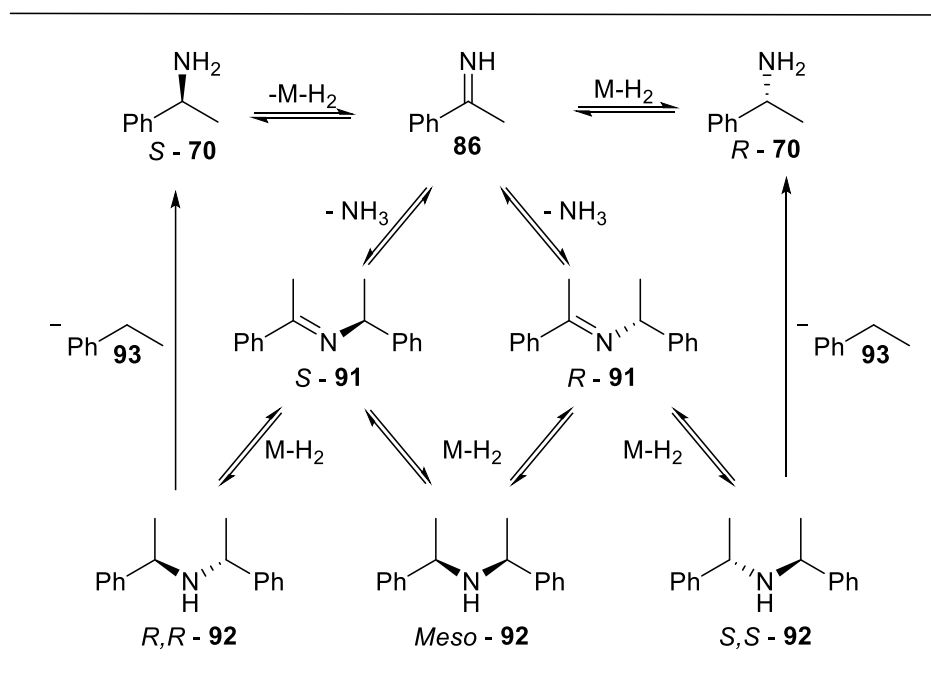
Scheme 18. The mechanism for the various undesirable by-product's formation from the racemisation of *S-***70**.[74–80]

$$\text{Selectivity of Racemisaiton (\%)} = \frac{[\text{Amine}]_{\text{Final}}}{[\text{Amine}]_{\text{Intial}}} \times 100 \quad \text{Equation 4}$$

Over the years significant effort has been made to achieve selective racemisation of primary amines, such as **70**, under milder conditions to increase compatibility with the CALB enzyme. [74,75,80–90] Although there has been steady progress in this field a set of conditions that are feasible for industrial application have not been achieved. The racemisation step continues to be rate limiting, due to the lack of compatibility of the faster racemisation conditions with the CALB enzyme. This has led to predominately small scale (< 1 mmol) reactions being run over reactions times of 1 – 8 days, although extremely high e.e.'s and selectivity's have been achieved for these processes.

An excellent demonstration of the potential of the CE-DKR was published in OPRD in 2014 whereby *Jia* et al. reported the most significant scale up of a CE-DKR synthesis to date.[91] They were successfully able to resolve 73.2 g of **94** (Scheme 19), an important building block for the Parkinson's drug Rasagiline, using a Pd/AlO(OH) racemisation catalyst alongside CALB and acyl donor **i** to achieve 88 % conversion (Equation 5), and 97 % e.e. in 12 hours.[82,83]
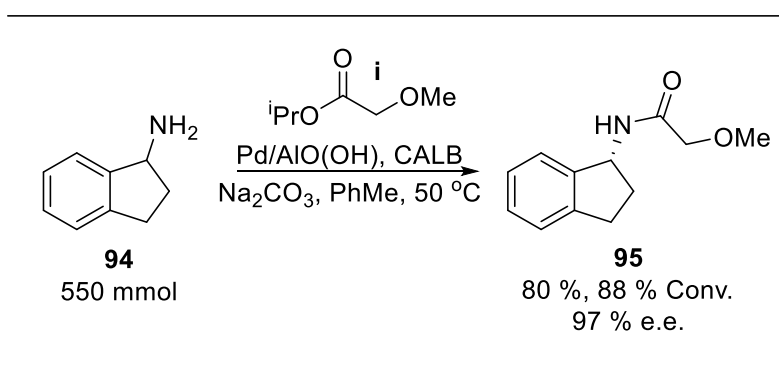
Scheme 19. Large scale DKR of **94** by Jia et al.. 550 mmol amine, 825 mmol **a**, CALB (18.3 g), Na2CO3 (18.3 g), Pd/AlO(OH) (2.35 mol %), PhMe (336 mL), 50 oC, 12 h.[91]

$$\text{Conversion (\%)} = \frac{[\text{Amine}]_{\text{Initial}} - [\text{Amine}]_{\text{Final}}}{[\text{Amine}]_{\text{Initial}}} \times 100 \quad \text{Equation 5}$$

To carry out such a large scale reaction, the compatibility between the Pd/AlO(OH) and CALB catalysts needed to be high. Initially, the racemisation and KR conditions must be established that are compatible for both the racemisation catalyst and the enzyme. This was done through optimising each step individually (Tables 2 and 3) and identified that both performed sufficiently well at 50 °C. Furthermore, Na$_2$CO$_3$ was added to the reaction to maintain a basic environment that decreased the likelihood of by-product formation that may lead to catalyst

deactivation. *Jia* et al. also avoided the use of other additives commonly used in CE-DKR process, such as the H_2

substitute NH_4CO_2 which has been suspected of deactivating CALB.[89]
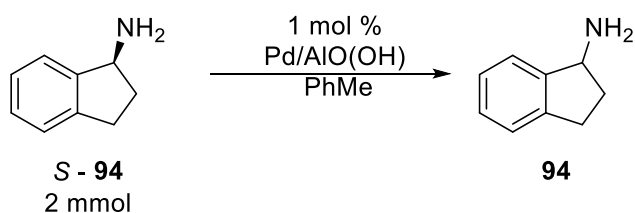
Table 2 The effect of temperature on the racemisation of **94**. [91]

Entry	Temp. (ºC)	Time (h)	e.e. (%)
1	50	6	35
2	60	6	12
3	70	3	3

2 mmol amine, 1 mol % Pd/AlO(OH), PhMe (2 mL).
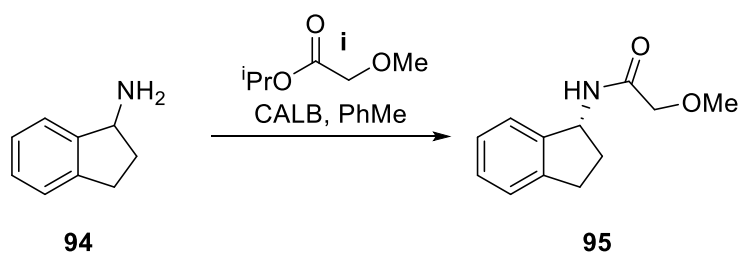
Table 3 The effect on temperature on the selectivity ratio during the kinetic resolution of **94**. [91]

Entry	Temp. (ºC)	Conv. (%)	e.e. (%)	E
1	50	15.7	99.5	375
2	60	20.1	97.9	226
3	70	43.4	97.5	173
4	80	48.7	94.8	116

Reaction Conditions: 2 mmol amime, 2.4 mmol acyl donor, PhMe (2 mL), 6 hours.

The result of these efforts was the establishment of an extremely stable reaction system. *Jia* demonstrated that the

reaction conditions were able to use the same dual catalysts for up to 6 repeated reaction cycles (Figure 9) before

a significant drop in conversion or e.e. was observed. This stability was integral to permit a large scale reaction to

proceed with high conversion because a long reaction time was unavoidable.

Despite the success of this reaction this work did highlight the compromise that is struck between the racemisation

and KR during the CE-DKR process.[91] The racemisation of **94** was found to increase nearly 12- fold (Table 2) in

half the reaction time when increasing the temperature from 50 to 70 ºC (Entries 1 and 3). As the racemisation is

the known rate determining step, such increases in rate could greatly improve the productivity of the reaction.

However, the increase in temperature causes a > 2-fold decrease in the selectivity factor for the KR process (Table 3, Entries 1 and 3). The compromise between the efficiency of the racemisation, and therefore the productivity of the whole reaction, and the enantioselectivity of the acylation must be struck. Ultimately, the integrity of **95**'s e.e. was more important than the throughput of the process, therefore a working temperature of 50 °C was chosen.
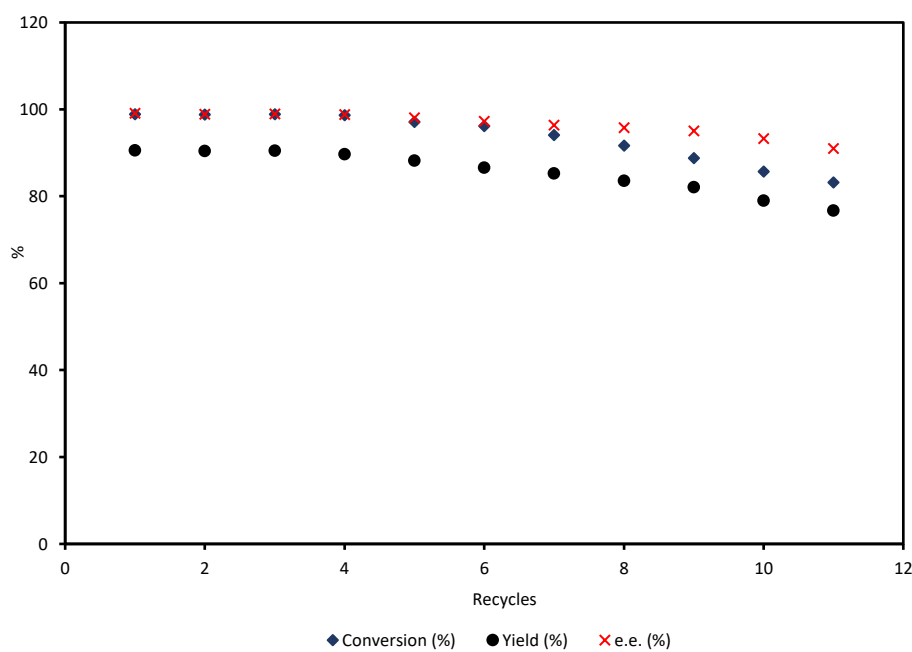
Figure 9 The stability of Pd/AlO(OH) and CALB over multiple recycles.[86]

1.6. <u>Conclusion</u>

There are multiple chemical transformations capable of delivering chiral amines in high enantioselectivity, each of which has different advantages/disadvantages that must be considered, particularly on an industrial scale. This highlights the importance of having a diverse "synthetic toolbox" at the disposal of organic chemist, to combat the range of challenging substrates that are required by research and industry. Currently, CE-DKR is not a viable synthetic strategy for the synthesis of chiral amines on an industrial scale due to the challenge in scaling up the reactions and their poor productivity. However, it is one of the newest and least researched strategies in the field. Despite this, the research carried out in this area has demonstrated that relatively cheap transition metal catalysts and environmentally friendly enzymes can be brought together to deliver highly enantioselective transformations with high levels of conversion. It is hoped that further development of the CE-DKR strategy using modern synthetic strategies, reaction engineering and data-led optimiastion can allow the challenges surrounding catalyst compatibility, productivity, and scalability to be solved and allow it to become a complimentary methodology to the more established asymmetric synthetic strategies and thus be employed on an industrial scale.

1.7. <u>Objectives</u>

The aim of this work is to use flow chemistry to enhance the productivity of the CE-DKR process, particularly of amines, and demonstrate that this approach is viable on an industrially relevant scale. This work plans to compartmentalise each step of the CE-DKR process to permit individual optimisation before bringing them together again in a continuous flow system. In subjecting each step to its own unique set of conditions it is hoped to increase the efficiency of the processes a whole. It is planned to achieve this goal with a 4 step approach, each of which will be addressed with its own chapters.

Objective 1 – To identify a suitable heterogeneous racemisation catalyst that can achieve high rates of racemisation while delivering high selectivity using High Throughput Screening

Objective 2 – To transition the racemisation process into continuous flow to further increase the efficiency of racemisation using key flow chemistry principles

Objective 3 – To establish a complimentary step of KR conditions in flow that is able to deliver rapid resolution of racemic amines with high enantioselectivity

Objective 4 – To bring the racemisation and KR flow systems together in a telescoped CE-DKR system, capable of resolving racemic mixtures of amines in a highly efficient manner.

This work will use **70** as a phenotype substrate as it exemplifies the most challenging substrate to racemise due to the challenging selectivity previously discussed in Section 1.5.3. Furthermore, **70** is widely used in other CE-DKR process which will allow the results of this work to be directly comparable to the work previously published by peers. Finally, benzylic chiral amines are an extremely prevalent functional group in chemical industries, as is **70** itself, therefore it is directly relevant to the end use of this work.

It is anticipated that High Throughput Screening (HTS) will be employed to identify a suitable heterogeneous racemisation catalyst for easy transition into a flow reactor. The screening will hope to replicate literature precedent while including novel catalyst for direct comparison within the same reactor. There will be a particular aim to identify a cheap, commercially available catalyst to lower the cost of the process while also reducing the barrier of uptake to other researchers. Reactions will be monitored through a combination of a chiral Gas Chromatography (GC) to measure selectivity, while chiral HPLC will be used to measure e.e..

The optimisation of each of the racemisation and KR process is anticipated to be achieved using a data-led Design of Experiments (DoE) approach. This is hoped to allow for rapid determination of the key reaction parameters and allow them to be exploited to optimise the reaction in an efficient manner.

Chapter 2: <u>Racemisation of Chiral Amines</u>

2.1. <u>Introduction</u>

Initial work on the challenging racemisation of chiral amines began in 1982 with a serendipitous discovery by *Murahashi* et al..[92] During the investigation of alkyl exchange reactions, they discovered the ability of Pd/C to racemise $S – \mathbf{70}$ between $50 – 100$ °C. Due to the original nature of the research, the attack of the highly reactive imine **86** by the starting amine, **70**, (Scheme 18) to form a family of by-products, as discussed in Section 1.5.3., was characterised and understood for the first time. This mechanism dictates that for every mol of by-product formed, two mols of substrate must be lost and has subsequently been supported by numerous publications.[74–80,83] This potential for loss of material during racemisation reactions made selectivity a key challenge in the field, where selectivity is defined as the amount of the starting amine remaining at the end of the reaction, (Section 1.5.3., Equation 4).

During a DKR reaction, racemisation reactions are constantly occurring to maintain a steady supply of the desired enantiomer to be resolved. This means that selectivity during the racemisation step is paramount, otherwise exponential loss of the amine can occur due to the 2:1 ratio of amine to by-product formation resulting in low yields of **70**. This effect can be exacerbated in batch reactions as they are plagued by long reaction times.

By-product formation can be supressed through the inclusion of an external H_2 source to increase the rate of the imine reduction, thus decreasing the effective concentration of the reactive intermediate, **86**, therefore reducing the probability of nucleophilic attack by **70**. H_2 sources can be introduced either through H_2 gas, the thermal decomposition of NH_4HCO_2 or through a H-transfer reagent, such an alcohol (i.e., isopropyl alcohol or diisopropylmethyl alcohol). When using H_2 (gas) or NH_4HCO_2 (solid) good mass transfer is required to keep sufficient H_2 in solution to have the desired effect.

This first CE-DKR was demonstrated by *Reetz* and *Schimossek* in 1996, who identified the ability of Pd/C to effectively racemise of S - **70** at 50 °C, which is compatible with the high thermal stability of CALB enzymes.[81,93] The combination of Pd/C and CALB in a one-pot reaction, was able to convert **70** into $R – \mathbf{96}$ with 99 % e.e. (Scheme 20), marking the first CE-DKR. In this reaction Et_3N was employed as a solvent, to maintain a basic environment to help prevent acid catalysis of the attack of **86**, leading to by-product formation. Although this was a significant milestone, the reaction required 8 days to reach 76 % conversion.
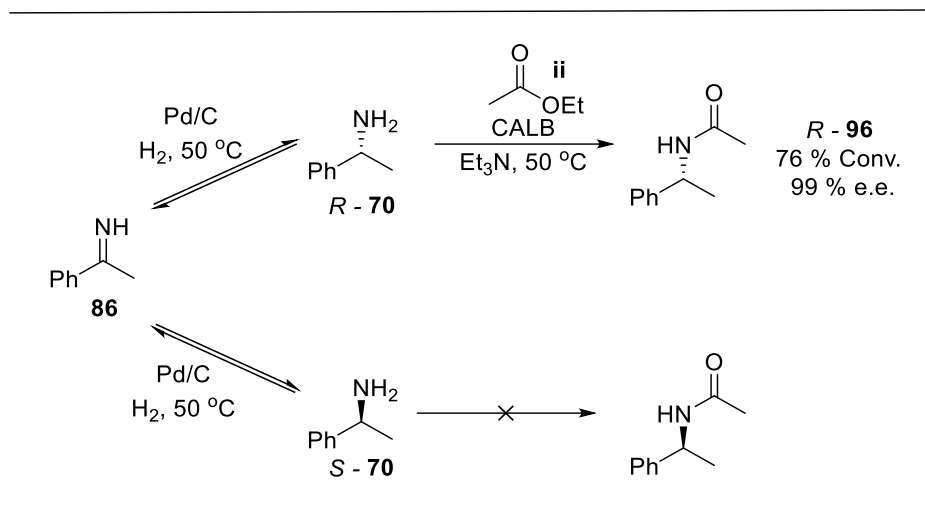
Pd/C was also employed as a 'bifunctional' catalyst by *Kim* et al. in 2001, simultaneously reducing prochiral ketoximes, **97**, as well as acting as a racemisation catalyst (Scheme 21) to interconvert between both enantiomer of the resulting amine, **70**, to facilitate a CE-DKR reaction.[12] This work made significant contributions to the field, by demonstrating that CE-DKR could be applied to a range of racemic amine substrates. Despite the increased diversity in the functionalisation of the aromatic rings, all the substrates contained benzylic amines. This is likely due to the relative ease by which benzylic functionalities can be oxidised, thus instigating racemisation.

Compared to the earlier publication by Reetz et al., the reaction conditions were modified in several ways.[84] Firstly, the reaction was diluted 2-fold through use of toluene as a solvent. This could prevent over saturation of the catalyst and decrease the likelihood of by-product formation. Secondly, a bulkier base was employed, diisopropylethylamine (DIPEA), thus reducing the nucleophilicity to prevent attack of the imine intermediate and prevent competitive binding to the catalyst. Both of these changes would enable higher levels of conversion to be reached. Thirdly, the catalyst loading was increased from 0.5 mol % to 4 mol %, leading to a higher rate of reaction.

Despite now performing 3 transformations in a single flask (Scheme 21), these conditions yielded similarly high e.e. (98 %) to that of *Reetz*, however an increase in conversion to > 98 % over a 5 day reaction was achieved.[81,84]
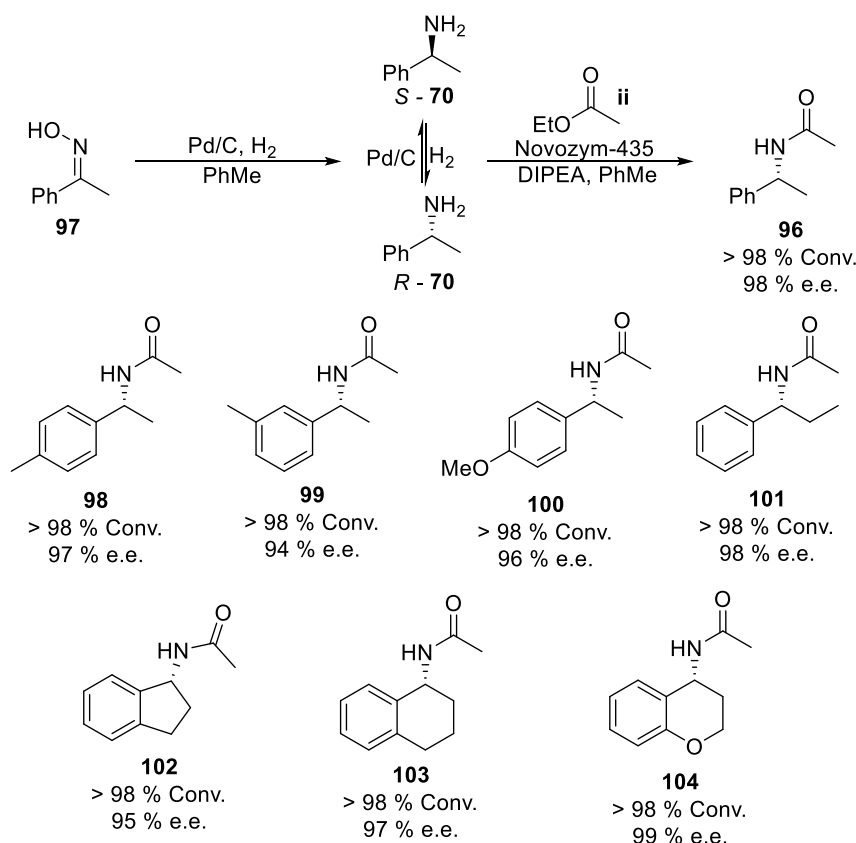
Scheme 21 Kim et al.'s DKR from prochiral ketoximes. Reaction conditions: 0.37 mmol ketoxime, 0.74 mmol ethyl acetate, 1.11 mmol DIPEA, Novozym-435 (100 mg), 5 % Pd/C (33 mg), PhMe (3.7 mL), H_2 (1 atm), 5 days.[84]

Although this appears to mark a significant increase in productivity of the reaction, the Space-Time Yield (STY) of the two reactions are very similar (Table 4). STY evaluates the productivity of reactions though the amount of material converted, normalised by the time taken and volume of the reactor, which in batch reaction is deemed to be the volume of solvent used (Equation 6). The lower concentrations employed by *Kim* compared to the work by *Reetz* prevented a higher throughput of material resulting in only a modest increase in STY, despite the shorter reaction time. [81,84]

Table 4 A comparison of e.e., conversion and STY for the CE-DKR of **70**.

Entry	e.e. (%)	Conv. (%)	STY (μmol mL^{-1} h^{-1})	Reference
1	99	76	0.802	[Reetz 1996] [81]
2	98	> 98	0.816	[Kim 2001][84]

$$STY\ (\mu mol\ mL^{-1}\ h^{-1}) = \frac{Conversion\ (\%)\ x\ Amine\ (\mu mol)}{Volume\ (mL)\ x\ Time\ (h)} \quad \text{Equation 6}$$

Comparing these STY to previous work by *Reetz* in 1994 where the standalone KR of **70** was investigated (Scheme 22), it can be demonstrated the resolution of the amine could be achieved more quickly than the racemisation.[94] The KR of 2 mmol of **70** could be achieved with 43 % conversion to *R* - **96** in just 60 hours with a high selectivity factor of > 200. This equated to a STY of 2.87 µmol mL^{-1} h^{-1} which represents a far greater rate of reaction than was achieved for either of CE-DKR process (Table 4), using the same acyl donor.[81,84] This suggests that the racemisation of *S* – **70** is the rate determining step of the CE-DRK process, thus greatly limiting the productivity of the reaction leading to long reaction times.
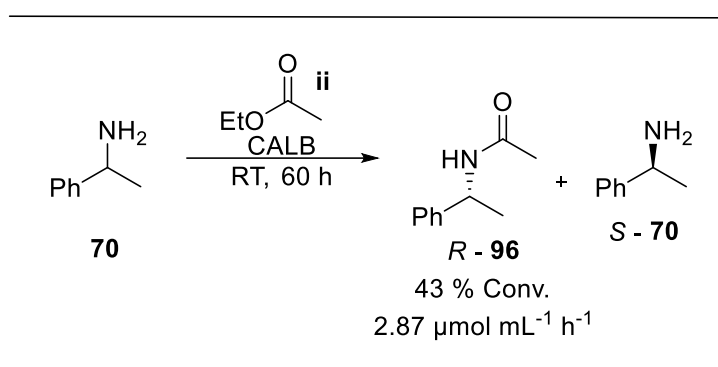
Scheme 22 The kinetic resolution of **70** by *Reetz* et al..
Reaction conditions: 2.5 mmol amine, 2.5 equiv. acyl donor, CALB (300 mg), dioxane (20 mL), RT.[94]

This prompted more extensive research into the racemisation of chiral amine substrates, in order to identify highly selective and fast racemisation under mild conditions, compatible with CALB enzymes. To date, research in this area has predominately focused on *S* – **70** as a model substrate, due to its ubiquitous nature in pharmaceuticals and agrochemicals making it a good substrate for benchmarking progresses in this field.

Both homogeneous and heterogeneous catalysts have been reported for the racemisation of chiral amines, however the remit of this thesis is focused on heterogeneous catalysts due to their compatibility with continuous flow reactors. Specifically, their application for the racemisation of primary amines, represented by *S* – **70**. The ability to racemise primary amine substrates, that have a high propensity for competitive by-product formation, should enable translation of these conditions to more amenable secondary and tertiary amines in the future.

Homogeneous catalysis for amine racemisation has been effectively used in a number of prominent publications without the use of external H$_2$ sources (Table 5).[78–80,86,95,96] *Bäckvall* and *Turner* focused on a Shvo-type catalyst **105** (Entries 1 and 2), which yielded high selectivity of > 97 %, but were hampered by low turnover frequencies (TOF).[78,80] The TOF of the racemisation catalysts are calculated by Equation 7, where the amount of racemisation achieved by a catalyst was normalised by the total number of mols of the transition metal per unit time, serving a metric to quantitatively compare catalysts.[97] Subsequently, *Blacker* et al. was able to achieve a significantly greater TOF for the racemisation of *S* – **70** using Ir SCRAM catalyst **106** (Entry 3), employing milder temperatures that

would be more compatible with the CALB enzyme.[79] However, this coincided with much lower selectivity of 30 %. Last but not least, *De Vries* employed a derivative of the Ir SCRAM catalyst, **107**, which showed rapid by-product formation leaving insufficient material to establish the e.e. of the process after just 6 hour (Entry 4).

R= *p*-MeO-C$_6$H$_4$
105

106

107

Table 5 A summary of the homogeneous racemisation of *S*-**70**. [78–80,95]

Entry	Catalyst	Reaction Time (h)	Temp. (°C)	H (Y/N)	e.e. (%)	Rac. TOF (h^{-1})	Sel. (%)	Reference
1	**105**	24	90	N	55	0.47	> 98	[Bäckvall 2005][80]
2	**105**	24	100	N	28	0.30	97	[Turner 2014][78]
3	**106**	16	80	N	0	6.25	30	[Blacker 2007][79]
4	**107**	6	100	N	-	-	< 40	[de Vries 2009][95]

$$\text{Batch TOF of Rac. (h}^{-1}) = \frac{\text{Frac. Racemised x Amine (mmol) x 60}}{\text{Cat. (mmol) x Reaction Time (min)}} \quad \text{Equation 7}$$

Although *Bäckvall* and *Turner* were able to achieve the highest selectivity (Table 5, Entries 1 and 2), the reactions were also performed on the smallest scale, 0.5 and 0.13 mmol of *S* - **70** respectively. Furthermore, they were also performed at the lowest concentration of 62.5 and 656 mM, which may have aided in their high levels of selectively. Comparatively *Blacker* et al. performed their racemisation on a much larger scale and higher concentration, 1 mmol of *S* – **70** at 500 mM. Similarly, *de Vries* work used 0.75 mmol of *S* – **70** and used concentration of 250 mM. The much higher concentrations employed for **106** and **107** would have made maintaining high levels of selectivity significantly harder, due to the increased probability of the amine, **70**, attacking the reactive imine, **86**.

The Ru and Ir catalysts were proposed to proceed *via* different mechanisms (Scheme 23 and Scheme 24). The Ru-Shvo catalysts, **105**, was shown to proceed *via* the "inner sphere" mechanism (Scheme 23), where the catalytic dimer first dissociates to form the active species **109**.[80,85,98] From here, the oxidation of the substrate is facilitated

by the formation of a H-bond to the ketone functionality of the Cp* ligand, **110**. Association of the imine **86** to the catalyst, **112**, followed by re-addition of the abstracted H_2, completes the redox cycle and delivers the racemised product, **70**, in the turnover step.

In comparison, the proposed mechanism for the Ir catalyst, **106** undergoes an initial dissociation of the dimeric species to the active form for the catalyst (Scheme 24). [99] Interestingly, from this point the mechanism differs from the Ru mechanism, whereby the Ir catalyst proceeds through abstraction of a single hydride anion to form an ion pair with the resulting imine, **114** and **86**, before a hydride reduction takes place, **115**. This differs from the usual transfer hydrogenation mechanism when two hydrogen atoms would be extracted from the amine to form an uncharged imine species. This charged imine intermediate drives the low selectivity as this further increases the susceptibility of the already reactive imine species to nucleophilic attack.
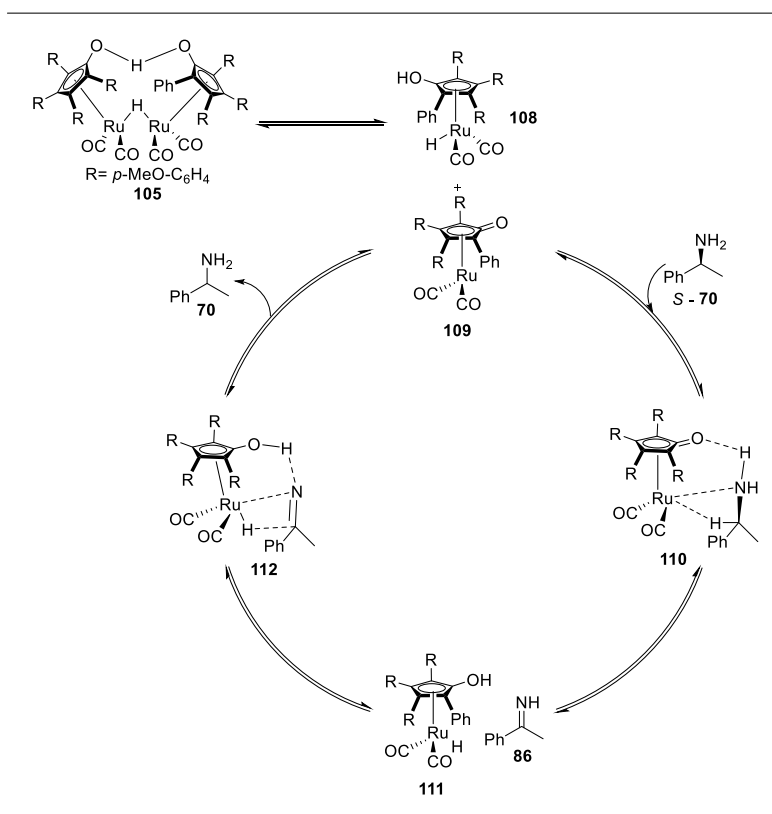
Scheme 23 Inner sphere mechanism for the racemisation of *S*-**70** with catalyst **105**.[80,85,98]
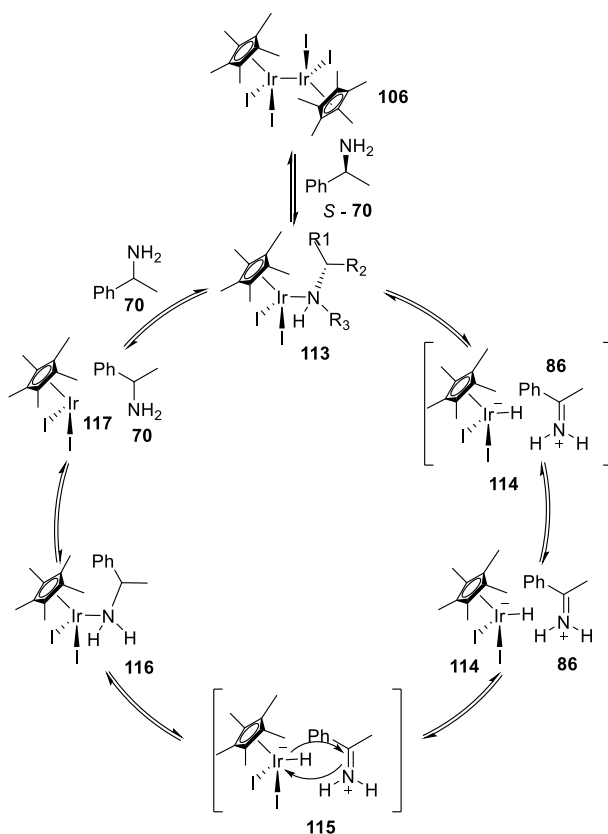
Scheme 24 The proposed racemisation mechanism for the Ir SCRAM catalyst.[99]

2.1.1. Heterogeneous Racemisation Catalyst

Heterogeneous catalysis for the racemisation of amines was extensively explored by *De Vos* et al., with important contributions also being made by *Kim* and *de Siqueira* (Table 6).[75,83,100] To date predominately the use of group 8, 9 and 10 transition metal catalysts have been explored with a range of results being reported. Key differences between heterogenous and homogeneous racemisations can be observed. Notably, the heterogeneous reactions are typically performed at a more moderate temperature range (70 - 80 °C), with the use of external H_2 sources. These conditions are largely observed to result in slower reactions over 1 – 3 days and returning lower TOF than the homogeneous catalysts. However, heterogeneous catalysts are generally observed to have much higher selectivity, likely due to the presence of H_2.

Overall heterogeneous Pd catalysts can be seen to be return the highest TOFs (Table 6, Entries 6 – 10) alongside some of the highest selectivities, highlighting their suitability for the racemisation of chiral amines. The data appears to show that the choice of support has a significant influence over the TOF and selectivity of the catalyst. This prompted *De Vos* and *Kim* to pursue in-depth evaluation of the effect of the support and the size of the Pd particles on the catalyst.[75,82,88,101]
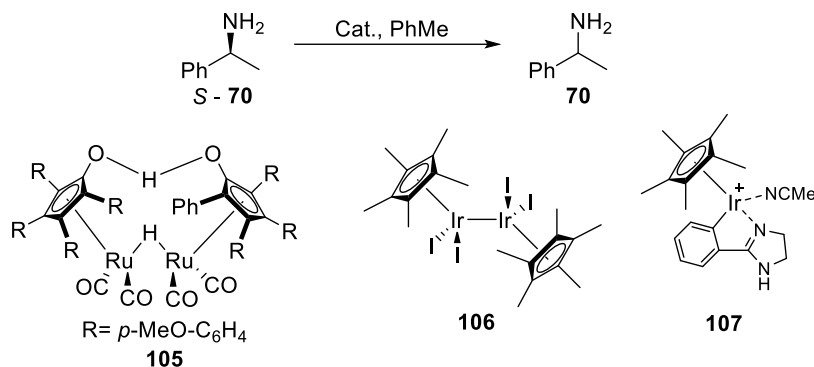
Table 6 A summary of heterogeneous racemisation of *S*-**70**.

Entry	Catalyst	Reaction Time (h)	Temp. (ºC)	H (Y/N)	e.e. (%)	Rac. TOF (h⁻¹)	Sel. (%)	Reference
1	Ru/C	72	70	Y	70	0.080	9	[De Vos 2007][75]
2	Raney Co	72	70	Y	7	0.003	98	[De Vos 2008][87]
3	Rh/C	72	70	Y	N/A[a]	N/A[a]	0	[De Vos 2007][75]
4	Ir/C	72	70	Y	98	0.010	33	[De Vos 2007][75]
5	Raney Ni	24	70	Y	0	0.020	92	[De Vos 2008][87]
6	Pd/AlO(OH)	24	70	N	2	5.92	82	[Kim 2007][83]
7	Pd/AlO(OH)	3	70	N	4	32.0	-[b]	[Kim 2010][82]
8	Pd/BaSO₄	5	70	Y	25	3.00	91	[De Vos 2007][75]
9	Pd/CaCO₃	24	70	Y	2	0.82	80	[De Vos 2007][75]
10	Pd/MgCO₃	24	80	Y	1	0.83	76	[de Siqueira 2018][100]
11	Pd/C	24	70	Y	60	0.33	11	[De Vos 2009] [88]
12	Pt/C	24	70	Y	100	0	0	[De Vos 2007][75]

[a]Insufficient amine remaining to determine e.e.. [b]Selectivity data not provided.

De Vos parameterised the number of basic sites per gram of catalyst for 6 out of the 9 catalysts, using bromothymol titrations.[88] Analysis of this data appears to show that the greater number of basic sites found on a catalyst, the greater the selectivity (Figure 10). This strongly suggests that an acidic support may be catalysing the attack of the imine intermediate, **86**, by **70** to form by-products. However, the method used to parameterise the basicity for the other supports was not applicable to Pd/SiO₂ and Pd/C catalysts, notably more acidic supports. Pd/SiO₂ and Pd/C were shown to have significantly lower selectivity than the basic supported catalysts. This further suggests that the support must be acid catalysing the undesirable by-product formation, and therefore not occurring in the bulk solution. If the support is catalysing the by-product formation, then by-product formation will occur faster in heterogeneous reactions than in homogeneous reactions where this effect is not observed. Therefore, heterogeneous reactions require the reduction of the imine to occur more rapidly than in than homogeneous reactions, hence the inclusion of external H₂ in all bar 2 examples (Table 6, Entry 6 and 7).
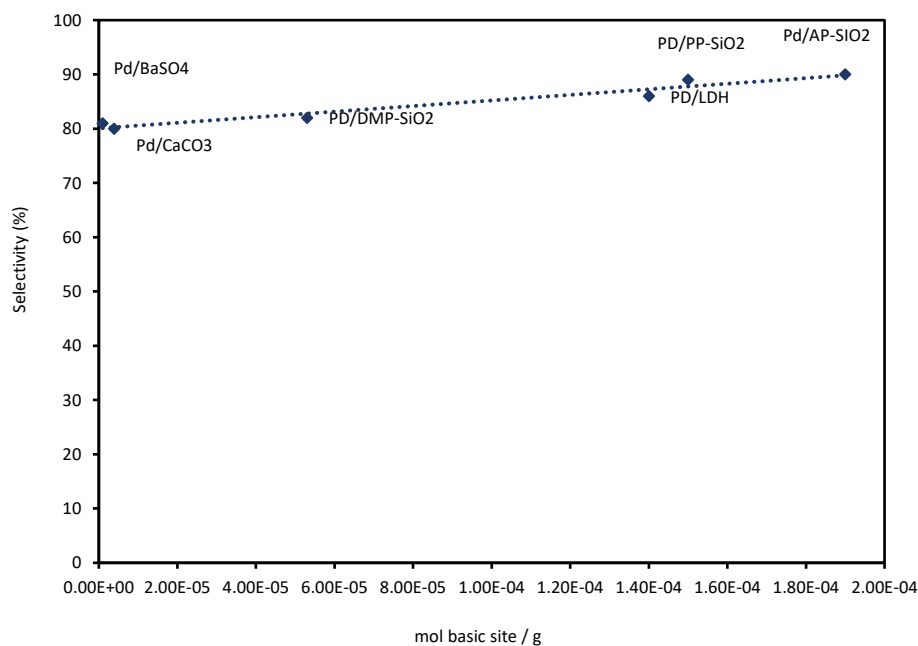
Figure 10 The relationship between mol basic site/g and selectivity.[88]

The analysis of the number of basic sites of the catalysts was followed by calculating the TOF of each catalyst and quantification of the number of mols of CO absorbed by a catalyst per mol of Pd. [88] The TOF were calculated based of the initial rates of the reactions, < 10 % conversion. The assumption was made, by *De Vos*, that under these conditions, racemisation is the only reaction present, and that attack of **86** by **70** is not occurring. The assumption that the concentration of **86** remained constant, and the rate of reduction of **86** was sufficiently fast compared to the oxidation of **70** that it could be disregarded. Therefore, the TOF is directly proportional to the oxidation of **70**.

The number of mols of CO absorbed by a catalyst was calculated through CO chemisorption measurements to determine the number of available Pd atoms and their dispersion. This was then plotted against the TOF of the respective catalyst (Figure 11), and it was suggested that there may be a directly proportional relationship between number of available Pd atoms and the TOF. This was unsurprisingly since the greater number of available Pd atoms reflects a greater the number of active sites for substrates to interact, thus a higher effective catalyst loading. It is difficult to tell if the difference in porosity of the supports is either a result of the inherent property of the support material, or from the different methodologies used to prepared them.
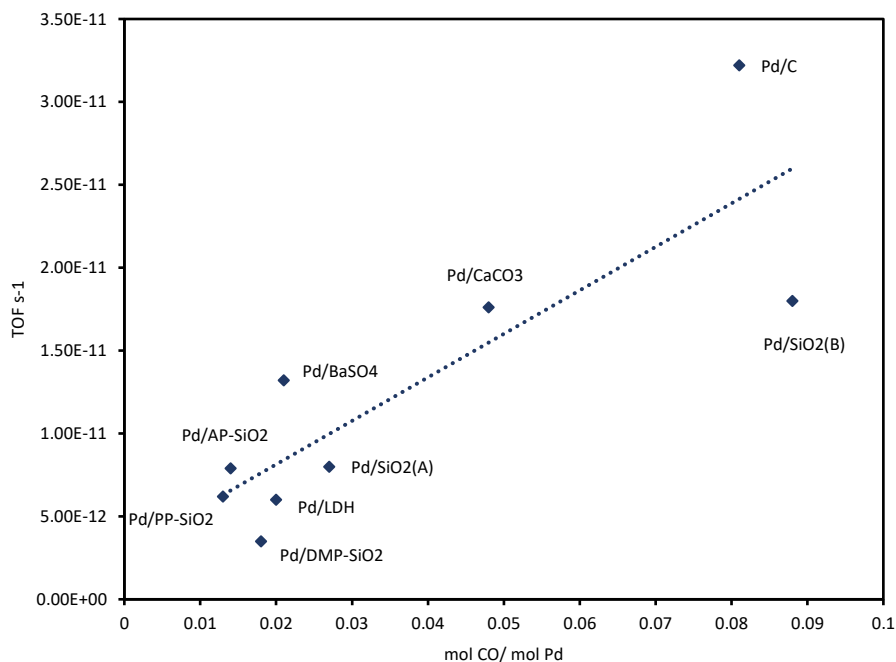
Figure 11 The relationship between TOF and mol CO/mol Pd.[88]

De Vos found no relationship between the size of the Pd nanoparticles of the catalyst and the e.e., TOF or selectivity over a 5 – 12 nm range.[75,88] However, *Kim* et al. found a significant increase in TOF using Pd/AlO(OH) with a reduction in Pd nanoparticle size (Table 7). When the particle size was reduced from 2.34 nm (Entry 1) to 1.73 nm (Entry 2) under the same conditions, an almost 8-fold increase in TOF was observed due to the increase in surface area. The TOF of the larger nanoparticle size at 70 ºC (Entry 1) was replicated at 40 ºC (Entry 4) by the smaller catalyst nanoparticles. *De Vos* may not have observed the same trend if the increased surface area of the particles did not translate into an increased number of active sites. This could be due to poor catalyst preparation methodology.
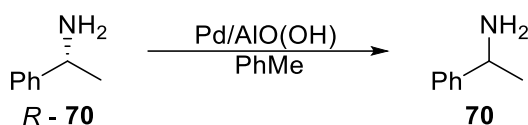
Table 7 A comparison of rate of reactions of different particle sizes of Pd/AlO(OH). [88]

Entry	Particle Size (nm)	Loading (mol %)	Temp (ºC)	Time (h)	e.e. (%)	Rac. TOF (h^{-1})
1	2.34	1	70	24	2	4.08
2	1.73	1	70	3	4	32.0
3	1.73	1	50	12	7	7.75
4	1.73	1	40	24	8	3.83

Reaction conditions: 0.1 mmol amine, Pd/AlO(OH), PhMe (1 mL).

49

Kim et al. built on their early contributions to the field by expanding their efforts into the pursuit of Pd nanoparticles in the form of Pd/AlO(OH).[82,83] This work marked the only instance of a heterogeneous catalyst where no external H_2 source was employed, instead proceeding through a purely H-transfer mechanism (Scheme 25). This approach was able to yield the highest TOF noted for any racemisation catalyst to date (Table 7, Entry 2), reducing the e.e. to just 4 % over a 3 hour reaction to achieve a TOF of 32.0 h^{-1}.
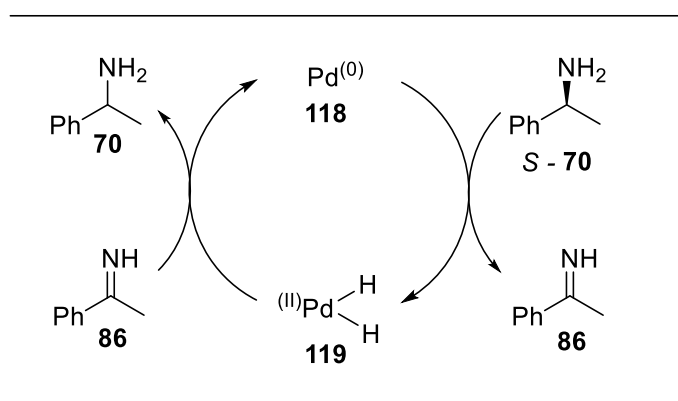
Scheme 25 Transfer hydrogenation mechanism for the racemisation of *S*-**70**.

The catalyst activities of commercially available Pd/Al$_2$O$_3$ and the in-house prepared Pd/AlO(OH) were also compared by *Kim* et al. (Table 8), where the former was found to be significantly less active than the latter. This resulted in the max TOF of Pd/AlO(OH) (Entry 1) being almost 6-fold greater than that of commercial Pd/Al$_2$O$_3$ (Entry 4). However, the selectivity of the commercial catalyst was found to be better over longer reaction times. The greater activity of the in-house Pd/AlO(OH) may be due to the preparative methodology, rather than the morphology of the alumina. The in-house catalyst may be prepared with smaller particle sizes, shown to increase activity (Table 7). Alternatively, the methodology developed by *Kim* may be leading to greater porosity in the Pd/AlO(OH) leading to a greater number of available active sites, which is shown to increase TOF by *De Vos* (Figure 11). The greater selectivity of the commercial catalyst is likely to be due to the be due to the Al$_2$O$_3$ morphology of the alumina having fewer pendant OH residues capable of acting as acid catalysts.

Table 8 The disparity between commercial Pd/Al$_2$O$_3$ and in-house prepared Pd/AlO(OH).

Entry	Catalyst	Time (h)	e.e. (%)	Rac. TOF (h^{-1})	Sel. (%)
1	Pd/AlO(OH)	12	29	5.92	99
2		24	2	4.08	82
3	Pd/Al$_2$O$_3$	12	94	0.25	99
4		24	88	1	99

Reaction conditions: 0.2 mmol amine, 1 mol % Cat., PhMe (2 mL), 70 ºC.

The elimination of H_2 from the reaction, alongside the high levels of selectivity for these reactions is extremely impressive. Elimination of H_2 creates a simplified reaction media, from tri-phasic to bi-phasic, thus negating potential mass transfer limitations. It also negates the need for costly specialist equipment and creates a safer reaction to perform at larger scale. Finally, the ability to remove extraneous reagents from the reaction increases the green characteristics of the reaction, while simultaneously decreasing the likelihood of deactivating the enzyme during the CE-DKR process.[44]

2.2. Results and Discussion

This work aims to develop the first High Throughput Screening (HTS) protocol for the identification of the most suitable heterogeneous racemisation catalyst for S – **70**. HTS allows the collection of a large dataset in a more efficient manner than the repetition of single experiments. The ability to directly compare data between catalysts will be greatly increased as the reactions will be run in multi-well plates which are subjected to the same reaction conditions. Furthermore, the use of automation will decrease the human error both within and between runs. This will yield a larger amount of higher accuracy data in a reduced time frame.

The following discussion will be divided into two parts. Firstly, the development of the HTS will be discussed, wherein identification of the reaction conditions and the equipment used for this process will be presented. This will also include the evaluation and subsequent improvement of reproducibility of the screening protocol. Secondly, the outcomes of the HTS will be discussed with the novel results highlighted and the trends elucidated from the screen rationalised.

2.2.1. Development of High Throughput Screening Protocol

2.2.1.1. Pd/γ-Al$_2$O$_3$ vs Pd/AlOOH (Microwave Vials)

The work by *De Vos* and *Kim* highlighted that heterogeneous Pd catalysts were well suited catalysts for the racemisation of primary chiral amines, delivering good levels of racemisation with high selectivity.[75,82–84,88,101] The prior literature suggests that Pd/AlO(OH) was the best performing catalyst with a TOF of 32.0 h^{-1} being achieved.[82] As this is not commercially avaiable, the intial work began with commercially avaiable Pd/γ-Al$_2$O$_3$ as a racemisation catalyst. Although it had previously been disregarded by *Kim* due to its low levels of activity over 24 hours, retuning a TOF of just 1 h^{-1}, it was envisaged that by manipulating the reaction conditions using temperature, external H_2 and catalyst loading, we could sufficiently improve the performance of the commercially available catalyst.

Initially, the catalytic performance of Pd/γ-Al$_2$O$_3$ was compared against the data reported by *Kim* et al. using Pd/AlOOH and Pd/Al$_2$O$_3$ (Table 9). The results obtained by *Kim* suggested that in-house prepared Pd/AlO(OH) (Entry 1) was highly effective at racemising *S* – **70** at 70 °C under an inert atmosphere, whereas commercially available Pd/Al$_2$O$_3$ (Entry 2) was much less reactive.[82,83] The following reaction conditions were initially chosen: a concentration of 82.5 mM and reaction temperature of 70 °C, falling in-line with many of the heterogenous reaction conditions previously reported by *De Vos*.[75,88,101] Catalyst loadings of 3, 6 and 12 mol % were chosen to counter the anticipated slow rate of reaction.[83] Finally, the reaction was performed under H$_2$, where the atmosphere was exchanged using backflushing with a vacuum and H$_2$ balloon.

It was decided to include H$_2$ in the reaction for three reasons. Firstly, the presence of external H$_2$ in the system would aid in higher levels of selectivity being achieved due to the more facile rate of reduction of imine intermediate, **86**. Secondly, it was suspected that the poor activity with commercial Pd/Al$_2$O$_3$ observed by *De Vos* due to the Pd itself being in the PdO form, as a result of oxidation with air. This would put the Pd in the + II oxidation state and therefore unable to perform the initial oxidation of *S* – **70** to start the racemisation process. The addition of H$_2$ in the reaction would therefore facilitate the reduction of the PdO(+II) back to Pd(0), allowing the racemisation to occur. Thirdly, given that Pd/AlO(OH) was the only heterogeneous catalyst reported to work without the need for external H$_2$, including H$_2$ would increase the generality of the screen.

Table 9. The effect of catalyst loading and temperature on racemisation of *S* –**70**.
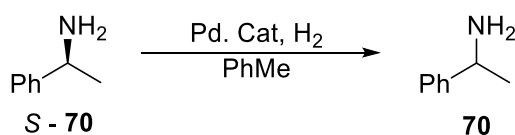
Entry	Catalyst	H$_2$ (Y/N)	Catalyst Loading (mol %)	Time (h)	Temp (°C)	e.e. (%)	Rac. TOF (h^{-1})	Reference
1	Pd/AlO(OH)	N	1	3	70	4	31.0	[Kim 2007][83]
2	Pd/Al$_2$O$_3$	N	1	12	70	94	0.25	[Kim 2007][83]
3	Pd/γ-Al$_2$O$_3$	Y	3	1	70	68	10.7	[This Work]
4	Pd/γ-Al$_2$O$_3$	Y	6	1	70	39	10.2	[This Work]
5	Pd/γ-Al$_2$O$_3$	Y	12	1	70	19	6.75	[This Work]

Reaction Conditions: Entries 1 – 2: 0.2 mmol amine, H$_2$, PhMe (2 mL), 70 °C, RBF. Entries 3 - 5: 0.33 mmol amine, H$_2$ (atm), PhMe (4 mL), microwave vial.[83]

Increasing the catalyst loading to 3 mol % (Table 9, Entry 3) and the presence of H$_2$ was shown to increase the TOF for Pd/Al$_2$O$_3$ by > 40-fold compared to literature (Entry 2). The preliminary results suggest a pseudo 1st order relationship with respect to Pd loading and the rate of racemisation emerged, when doubling the catalyst loading to 6 (Entry 4) and then 12 mol % (Entry 5). At 12 mol % racemisation of *S* – **70** occurred to significant enough extent, to allow the identification of other active catalysts on a sufficiently short timescale to allow rapid

generation of results. Therefore, these conditions (Entry 5) were taken forward into the development of a HTS protocol in a multi-well plate.

2.2.1.2. High-throughput Screening Reaction Platform

Next, we proceeded to develop a HTS Protocol for screening a larger number of catalysts in multi-well plates using automated solid and liquid handlers. The development of a HTS Protocol is split into 4 key steps (Figure 12): Pre-reaction, Reaction, Sample Preparation and Analysis. It is important to optimise each of these procedures to maximise productivity while minimising uncertainty. Therefore, automation is extensively used through HTS methodologies. We aimed to identify the key areas of the protocol where automation could be applied to mitigate unknown or uncontrollable levels of uncertainty.
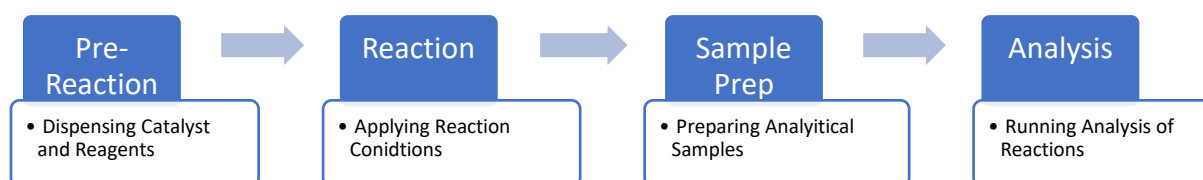
Figure 12 HTS Protocol workflow.

Firstly, the dispensation of catalysts and reagents is a common area where automation can effectively be applied. For this operation an Unchained Labs "Junior" Powder Dispensing Robot (Figure 13a) was chosen to automate the weighing of the desired catalyst. This robot was able to weigh the desired catalyst directly into the reaction vials, thus minimising the loss of material through multiple transfer steps. A similar Unchained Labs "Junior" Liquid Handling Robot (Figure 13b) was employed to dispense the stock solution of the $S - 70$ into each of the catalyst containing vials using automatically dispensing air displacement needle.

Figure 13 Pictures of a) Unchained Labs "Junior" Power Dispensing Robot (left) and b) Unchained Lab "Junior" Liquid Handler and Reactor.[102]

Following the preparation of the reaction mixture the reactions were performed in a Deck Screening Pressure Reactor (DSPR) (Figure 14) on the associated Unchained Labs Reactor (Figure 13b) which allowed for precise control over the reaction parameters such as temperature, pressure, stirring and reaction time. The DSPR is a 48-well plate constructed of two aluminium blocks that are bolted together to create a sealed reactor (112 mm x 282 mm x 112 mm) . Within the top aluminium block is a thermocouple that measures the internal temperature of the reactor. The top block contains stainless steel pressure release valves and a pressure gauge fitted, allowing the pressure inside the reactor to be controlled.

The DSPR allows reactions to be performed under different atmospheres. Positive pressure of an inert gas, such as N_2, can be applied with the outlet closer to build pressure before allowing it to be purged. This process can be repeated to effectively displace atmospheric air to an inert atmosphere. If desired, this can subsequently be repeated with a reactive gas of choice to displace the inert N_2 environment. This functionality is extremely important for identifying racemisation catalysts as it has been shown that the composition of the atmosphere under which racemisation reactions occur can be extremely influential. [75,87,88,95] Furthermore, the inlet gas can be applied above atmospheric pressure. This allows for super-ambient conditions, above the boiling point of the solvent, to be applied to the reaction mixture and allows the HTS to effectively mimic the capabilities of continuous flow which can use an increased operating window to increase the rate of reaction.

Figure 14 A 48 well Deck Screen Pressure Reactor (DSPR).

The stirring and heating of the reaction can then be controlled through the Unchained Labs "Junior" Reactor. This is a specialised reactor for the DSPR, which applies heating and stirring uniformly across the plate. It also operates a feedback loop with the internal thermocouple maintaining the desired temperature within the reactor as opposed to monitoring the heating plate's temperature. Post-reaction a recirculatory chiller, connected to the Unchained Labs "Junior" Reactor stirrer hotplate, is used to cool the DSPR down to 15 ºC. This creates more standardised,

faster, cooling of the reaction that is independent of the airflow or temperature of the room to create a more well-defined end of the reaction. Once cooled, the pressure of the reaction can be released and the DSPR opened.

The third unit of operation is the preparation of the analytical sample for analysis using chiral liquid and gas chromatography (LC and GC). This involves taking an aliquot of the reaction and diluting it with a solvent containing an internal standard, that is compatible with the analytical methods. In this case 100 µL of the reaction mixture is taken and diluted with 400 µL of a 10 mM solution of anisole in MeOH. This process can be automated through the use of the Unchained Labs "Junior" Liquid Handler, previously used to dispense the stock reaction solution.

The final unit of operation is the running of the analytical sample and is performed in a fully automated manner by the respective analytical instrument. The analytical sample is run through a chiral LC to determine the e.e. of **70** by direct comparison on the relative peak areas of the two enantiomers, recovered over a 3 minute method. The sample can then be moved to an achiral GC instrument where the selectivity of the racemisation of **70** can be determined using a 6.5 minute method. In this case the area of the peak related to **70** is normalised against the area of the internal standard and subsequently this can be converted into concentration using a calibration curve. Selectivity can then be compared to concentration of the stock solution, calculated in the same manner using Equation 4.

2.2.1.3. Reproducibility Screen

To assess the reproducibility of HTS Protocol 1 (Figure 15) across the DSPR plate, an experiment was performed to check that the variation between each well inside the DSPR was within an acceptable range of uncertainty. This was done by carrying out 46 identical Pd/Al$_2$O$_3$ mediated racemisation reactions of S – **70** alongside 2 control reactions.

A wide range of e.e.'s were observed with values ranging between 20 and 89 %, giving an uncertainty of 35 % (+/- half the range). Plotting this data as a Normal Distribution (ND) illustrates how broadly the data is spread around the mean of 54 % e.e. (Figure 16). This can also be visualised in the heatmap that shows that the variation in e.e.'s is not randomised across the plate (Figure 17). Worryingly there appears to be a trend whereby e.e.'s at the top end of the range is found in the top left of the plate and e.e.'s at the lower end of the range is found in the bottom right of the plate indicating a systematic error in the HTS Protocol 1.
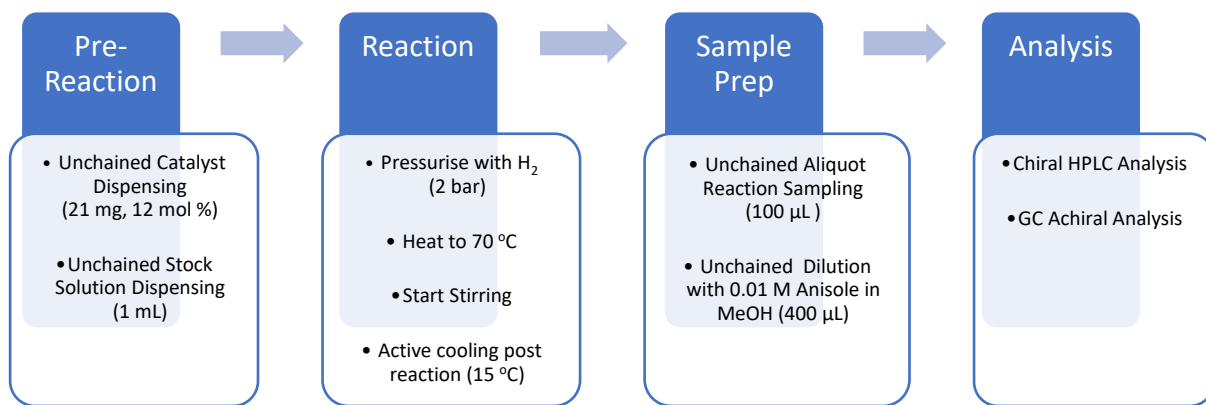
Figure 15 HTS Protocol 1.
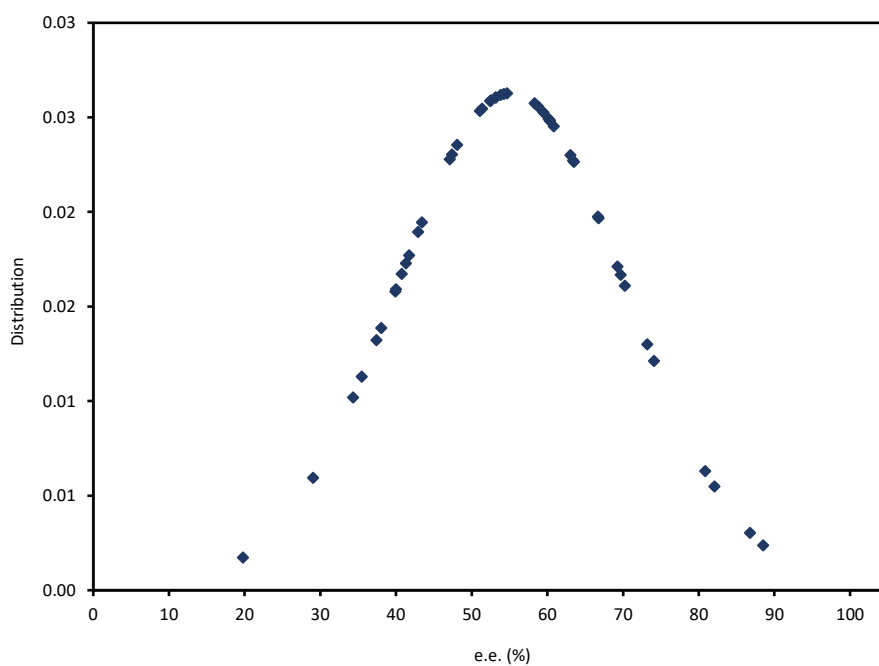
Figure 16 The ND for HTS Protocol 1.
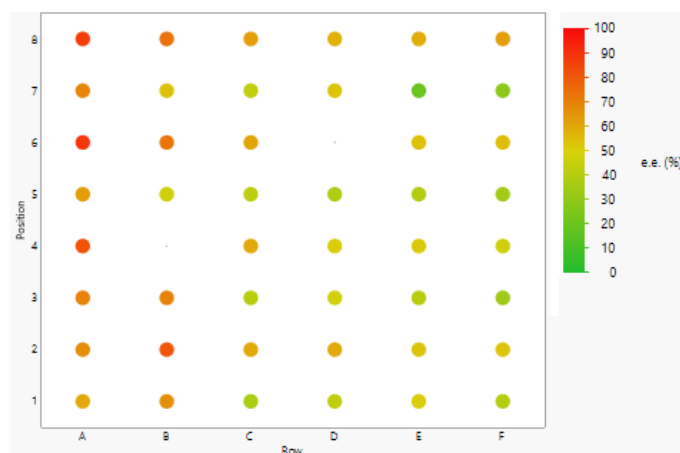
Figure 17 Heatmap of DSPR reproducibility screen for HTS Protocol 1. Two missing data points represent control experiments.

To identify the sources of error in the protocol, HTS Protocol 1 was systematically analysed to quantify each source of error (Table 10). This could then be compared against the known total uncertainty in the results (35 %) to calculate the unaccounted for uncertainty. Firstly, the automated catalyst weighing was investigated (Entry 1) to check for any differences in catalyst loading. Data obtained from the Unchained Labs Powder Dispensing Robot conclusively proved that the weighing was accurate to within +/- 0.4 mg, representing only 2 % uncertainty.

Secondly, the Unchained Labs Liquid Handling Robot was investigated regarding the accuracy of dispensation of various volumes of solutions, this determined by Unchained Labs documentation. It was found that dispensing larger volumes contained a lower degree of relative error, compared to smaller volumes. Therefore, the relative error in the dispensation of 1 mL of stock solution into each reaction vial (Table 10, Entry 2) was estimated to be 1 %. The extraction of a 100 μL aliquot of the reaction for analytical sample preparation (Entry 3) was estimated to be 5 %. Whilst dilution of the reaction aliquot with 400 μL of 0.01 M anisole in MeOH (Entry 4) was estimated to be 3 %.

Thirdly, the chiral LC analysis of the analytical samples was investigated (Table 10, Entry 5). Two of the analytical samples prepared during HTS Protocol 1 were selected at random. Each of these samples was subjected to chiral LC analysis 10 times consecutively, and the e.e. of each run was calculated. The results showed that the two sample had a combined uncertainty for the measurement of the e.e. of 4 %.

Table 10 Quantified sources of error for HTS Protocols 1.

Entry	Source of Error	HTS Protocol 1 Error (%)
1	Catalyst Weighing	2
2	Stock Solution Dispensing	1
3	Reaction Aliquot Sampling	5
4	Dilution of Analytical Sample	3
5	Chiral LCMS	4
6	Total Estimated Error	15
7	Observed Error	35
8	Unaccounted For Error	20

The analysis of the units of operation within HTS Protocol 1 gave a total estimated error of 15 % (Table 10, Entry 6), whereas the estimated error within the reproducibility screen was 35 % (Table 10, Entry 7). This leaves 20 % error within the reproducibility screen unaccounted for (Entry 8). Therefore, we set out to identify where the additional sources of error had been introduced in HTS Protocol 1.

Upon further reflection, it transpired that some of the analytical samples generated during HTS Protocol 1 contained small amounts of Pd/Al_2O_3, from the sampling of the reaction aliquot. Subsequently, these samples had then been manually filtered to prevent blockage of the LC system. This not only introduced human error due to the manual filtration but raised questions surrounding the accuracy of the analytical sample preparation, although the reactions were left for the same amount of time to allow the catalyst to settle to the bottom of the vial before the aliquot of the reaction was taken. However, the presence of catalyst in a random selection of the analytical samples suggested that either the depth of the needle extracting the sample was varying from vial to vial, or the volume of the aliquot being taken was varying between vials. It was concluded that if the extraction of the reaction aliquot is inconsistent, then the dispensation of the stock solution and analytical sample dilution may also not be performing within the assumed level of accuracy. Therefore, the 20 % unaccounted for error was presumed to be a combination of inconsistent liquid handling due to poor configuration of the Unchain Labs Liquid Handling Robot and the human error introduced through manual filtration. With this in mind, a revised strategy was devised to counter the introduction of error from these operations.

To prevent catalyst uptake during sampling of the reaction aliquot, it was decided to reduce the catalyst loading in the reaction (Table 11). This required redevelopment of the reaction conditions in microwave vials as previously conducted in Section 2.2.1.2. where the initial 12 mol % loading for HTS Protocol 1 was selected, (Entry 1). In the earlier study it had been found that at lower catalyst loadings of 6 and 3 mol % (Entries 2 and 3) the e.e. of *S* – **70** was not reduced sufficiently to be confident of detecting activity in less active catalysts. To compensate for this, the reaction temperature could be increased. To conduct HTS reactions at elevated temperatures, the H_2 pressure of the DSPR was increased to 5 bar to ensure evaporation of the samples did not occur. By lowering the loading to 3 mol % and increasing the temperature to 100 °C (Entry 4) a 3-fold increase in TOF and a > 10-fold increase in rate was observed. This pleasingly falls in line with the Arrhenius Equation (Equation 8) "rule of thumb" that the reaction rate doubles for every 10 °C, in this case predicts an 8-fold increase in reaction rate.

$$k = Ae^{\frac{-E_a}{RT}} \qquad \text{Equation 8}$$

Given the high levels of racemisation observed at 3 mol % and 100 ºC, further reduction in loading was investigated. It transpired that further reducing the loading to 2 and 1 mol % (Table 11, Entries 5 and 6) did not show considerable change in e.e. but did result in an overall 3-fold increase in the TOF to 91.0 h^{-1}, the highest record for the racemisation of S – **70**.
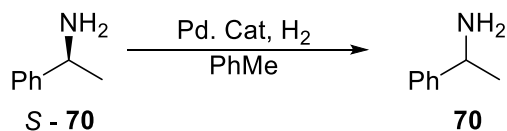
Table 11 The effect of catalyst loading and temperature on racemisation of S-**70**.

Entry	Catalyst Loading (mol %)	Temp (ºC)	e.e. (%)	Rac. TOF (h^{-1})
1	12	70	19	6.75
2	6	70	39	10.2
3	3	70	68	10.7
4	3	100	5	31.2
5	2	100	6	47.0
6	1	100	9	91.0

Reaction Conditions: 0.33 mmol amine, H$_2$ (atm), PhMe (4 mL), microwave vial, 1 hour

At this stage of the project we also started to explore the use of other more accessible liquid handlers, including the use of a Handystep Repetitive Pipette (Figure 18a) for the dispensing of the stock solution and an Opentron OT-2 Pipetting Robot (Figure 18b) for the preparation of the analytical samples.[103,104] The Handystep Repetitive Pipette allows volumes of between 1 – 50 mL of a solution to be dispensed across multiple steps with a high degree of accuracy within a single uptake. This increases the efficiency of dispensing a large volume of solution compared to a traditional adjustable pipette. It also reduces the error compared to traditional adjustable pipettes as it avoids the need to repeatedly draw the solution when further error can be introduced. On the other hand, the Opentron OT-2 Pipetting Robot is a low-cost benchtop pipetting robot, primarily designed for biological sciences, but has been repurposed for dispensing small volumes of liquids in the improved HTS Protocol.
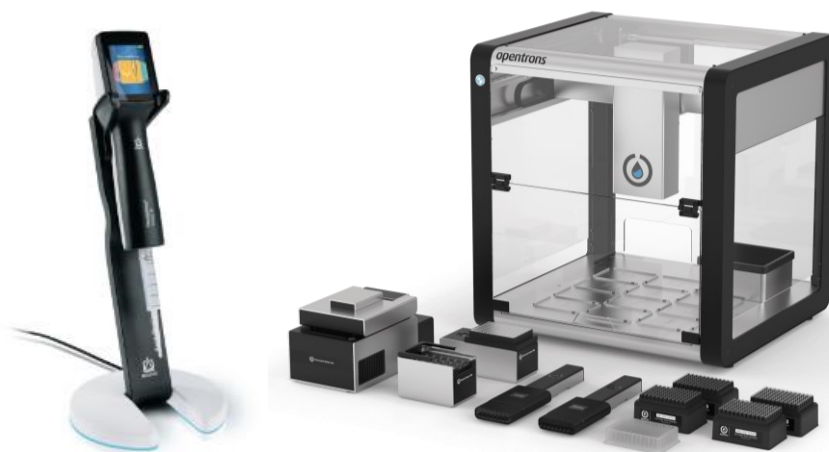
Lastly, the preparation of the analytical samples was also modified . Rather than taking a 100 μL aliquot of the reaction mixture this was decreased to 20 μL which would help avoid uptake of the catalyst from the reaction mixture. The dilution of the reaction aliquot was increased to 1 mL as this was found to have a smaller source of error compared to the 400 μL previously used. All these changes to HTS Protocol 1 were brought together to generate HTS Protocol 2 (Figure 19).

Pre-Reaction	Reaction	Sample Prep	Analysis
• Unchained Catalyst Dispensing (1.8 mg, 1 mol %) • Handystep Pipette Stock Solution Dispensing (1 mL)	• Pressurise with H_2 (5 bar) • Heat to 100 °C • Start Stirring • Active cooling post reaction (15 °C)	• Opentron OT-2 Aliquot Reaction Sampling (20 μL) • Opentron OT-2 Dilution with 0.01 M Anisole in MeOH (1 mL)	• Chiral HPLC Analysis • GC Achiral Analysis

Figure 19 HTS Protocol 2.

Pleasingly, the changes made to HTS Protocol 2 returned much more consistent results in the reproducibility screen. The heatmap shows a visual representation of the lack of systematic error shown across the DSPR (Figure 20), with a much smaller range of 29 % in e.e.'s reported, giving an uncertainty of 15 %. The same ND and visual evaluation were performed on the HTS Protocol 2 results, where it can be seen that there is a much tighter distribution of the data around the 49 % e.e. mean (Figure 20), while the variation in racemisation across the plate appears much more randomised (Figure 21).
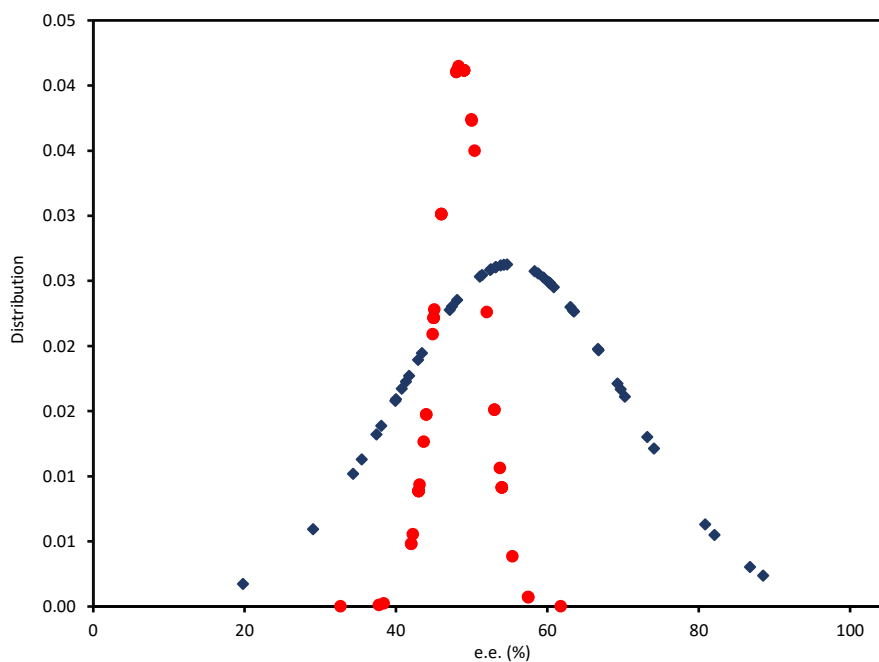
Figure 20 Comparison of the Standard Distributions of the HTS Protocol 1 (Blue) v's the HTS Protocol 2 (Red).
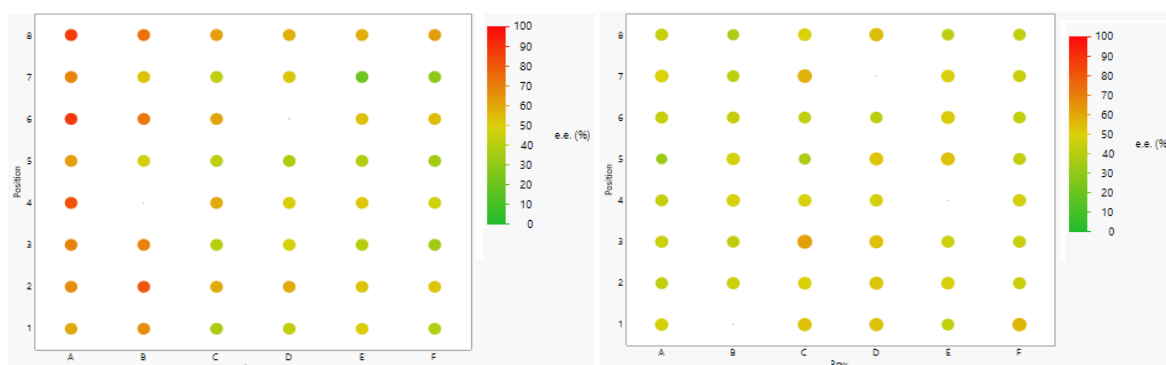
Figure 21 A comparison of the results from the HTS Protocol 1 (left) and HTS Protocol 2 (right) reproducibility screens.

The units of operation with HTS Protocol 2 were again quantitatively analysed (Table 12) to account for the total uncertainty in the reproducibility screen. The catalyst weighing remained consistent with 2 % uncertainty, (Entry 1). The uncertainty in the dispensation of the stock solution, removal of an aliquot of reaction mixture (Entry 2) and the dilution of the reaction aliquot (Entry 4) were established from the Handystep and Opentron OT-2 documentation. Finally, the uncertainty in the LC analysis also remained the same (Entry 5). Overall, the total estimated error found in HTS Protocol 2 was 12 % (Entry 6), compared to the observed error of 15 % (Entry 7). This left just 3 % error unaccounted for during HTS Protocol 2 (Entry 8), which was deemed acceptable considering the number of operations carried out.

61

Table 12 Quantified sources of uncertainty for HTS Protocols 1 and 2.

Entry	Source of Error	HTS Protocol 1 Error (%)	HTS Protocol 2 Error (%)
1	Catalyst Weighing	2	2
2	Stock Solution Dispensing	1	3
3	Reaction Aliquot Sampling	5	2
4	Dilution of Analytical Sample	3	1
5	Chiral LCMS	4	4
6	Total Estimated Error	15	12
7	Observed Error	35	15
8	Unaccounted For Error	20	3

Although the calculated error between HTS Protocol 1 and HTS Protocol 2 was only reduced by 3 %, the unaccounted for error dropped by 17 %. (Table 12, Entries 6 and 8). It was postulated that the change in liquid handling equipment had the greatest reduction in the unaccounted for uncertainty. It is thought that the Unchained Labs Liquid Handler was not operating within the anticipated level of error, likely be due to incorrect calibration of the robot prior to use. To further reduce variability between reactions run in different wells it was decided that each reaction would be run in duplicate, so an average of the two reactions could be taken. Each of the two repeats would be placed in a randomised position across the plate, using this approach on the HTS Protocol 2

Furthermore, a tiered approach would be taken for screening catalysts at different temperatures (Figure 22), to maximise the chance of assessing a catalyst within its ideal reaction space. An initial screen would be carried out at 100 °C. If a catalyst was found to display high racemisation but poor selectivity, it would subsequently be included a screen at a lower temperature (70 °C) to see if selectivity could be improved. Conversely, if a catalyst showed high selectivity but little to no racemisation, it would be included in a higher temperature screen (145 °C) to see if catalytic activity could be achieved. Finally, a screen would be carried out with all catalysts at 145 °C under a N_2 atmosphere to see which catalysts were capable of a similar "thermal-only" racemisation as described by *Kim* et al. and how this would affect the racemisation and selectivity profiles of the catalysts.[83] The super-ambient 145 °C screening would be possible due to the elevated 5 bar of pressure introduced in the HTS Protocol 2. The combination of these final changes to the protocol gave rise to HTS Protocol 3 (Figure 23).
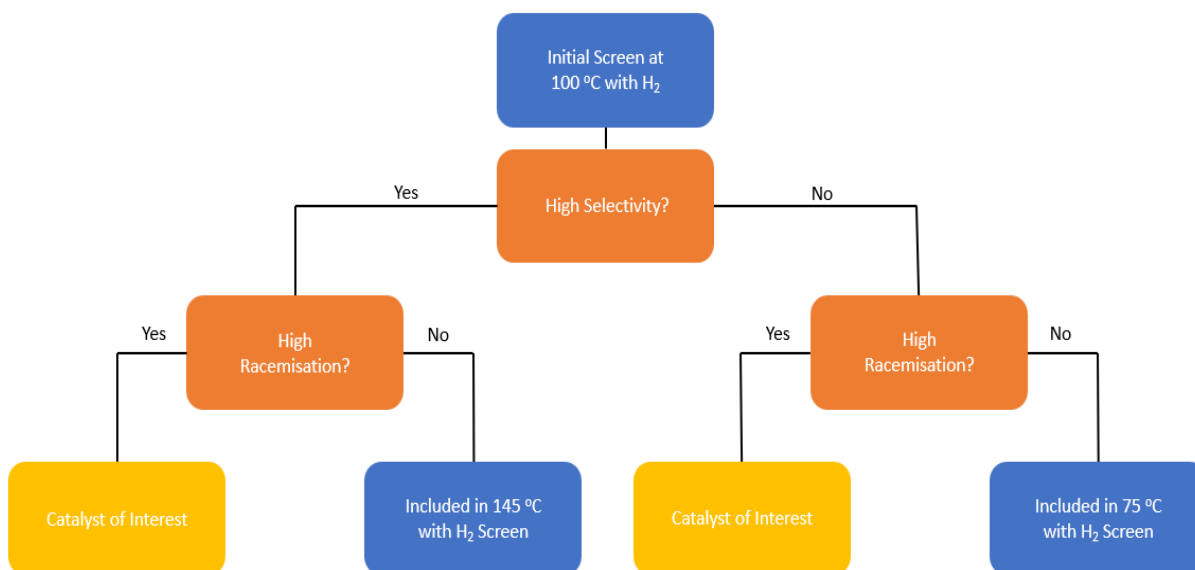
Figure 22 A flow diagram to represent the tiered screening system used in HTS Protocol 3.
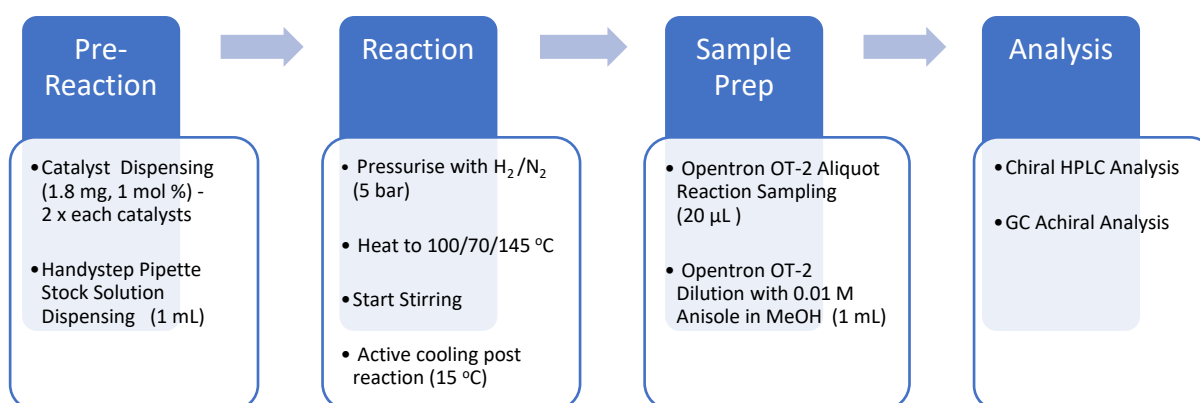
Figure 23 HTS Protocol 3.

2.2.2. High Throughput Catalyst Screening Results

2.2.2.1. Catalyst Selection

A range of heterogeneous transition metal catalysts were selected for the HTS based on a variety of criteria (Table 13), chosen from commercial catalogues, and a series of TiO_2 catalysts prepared by a previous member of the research group, Dr Luka Hare neé Tallon. [105] Beginning with Group 8, Ru catalysts have been extensively used in homogeneous racemisation of amines, and Ru/C was also explored by *De Vos* as a heterogeneous catalyst.[75,78,80] Therefore, Ru/C was included in this screen alongside Ru/γ-Al_2O_3 as Al_2O_3 had proven to be an extremely effective support in the case of Pd/γ-Al_2O_3 during the HTS development.[83] The HTS also included Fe/TiO_2 as a

representative first row group 8 transition metal catalyst. Fe is one of the cheapest and most earth-abundant metals, and Fe catalysts have been known to reduce imines in other types of reactions.[106]

A series of Group 9 catalysts were selected, inspired by the use of Ir in both homogeneous and heterogenous chiral amine racemisation.[75,79,95,97] Ir/C and Ir/CaCO$_3$ were reported by *De Vos*, however they displayed low selectivity. This led to the inclusion of Ir/TiO$_2$ in the screen. Although Rh is an extremely expensive transition metal it was previously explored by *De Vos* and has significant track record in the field of imine hydrogenation reactions.[45,107] With this in mind, Rh/γ-Al$_2$O$_3$ and Rh/TiO$_2$ were included to serve as a suitable benchmark that could be compared to cheaper catalysts. The first row transition metal Co has previously been investigated in the form of Raney Co, serving as a lower cost alternative to both Rh and Ir therefore Co/TiO$_2$ was also included in the screen.[87]

Table 13 Summary of catalysts included in the HTS.

Transition Metal Group

	8		9			10				11	
	Fe	Ru	Co	Rh	Ir	Ni	Pd	Pd(OH)$_2$	Pt	Cu	Au
Al$_2$O$_3$		C		C			C		C		
TiO$_2$	I		I	I	I	I	I		I	I	I
C		C					C	C	C		C

(Support)

Green: Literature Precedent, Orange: Novel, C: Commercial Supplier, I: In-house Preparation[105]

Group 10 metals have been the most intensely investigated of the transition metals for the racemisation of chiral amines.[75,87,88,90,100] Various different heterogeneous Pd catalyst have been explored, therefore the previously reported γ-Al$_2$O$_3$ and C supported Pd catalysts were included alongside the novel Pd/TiO$_2$ and Pd(OH)$_2$/C. Similarly, commercially available Pt/C was included as it was found by *De Vos* to show extremely high activity, with very little selectivity.[88] Subsequently, Pt/ γ-Al$_2$O$_3$ and Pt/TiO$_2$ were included in the hope that the support effect also noted by *De Vos* could increase the selectivity of the Pt catalysts.[88] Raney Ni was used by *De Vos* as a cheaper Group 10 alternative, therefore Ni/TiO$_2$ was included in this study.[87]

Group 11 transition metals have never been explored for the racemisation of chiral amines. However, Cu has been reported to catalyse the reduction of imines as well as other C=N bonds.[108,109] This prompted the inclusion of the low cost Cu/TiO$_2$ in the HTS. Finally, Au has been shown to be able to both oxidise amines to form imines as well

as reduce imines to amines.[110,111] This gives it great potential to have the required redox capabilities for the racemisation of chiral amines, therefore Au/TiO_2 and Au/C were both included in the study.

2.2.2.2. <u>Results of the 100 ºC H_2 Screen</u>

The first HTS was performed at 100 ºC under 5 bar of H_2, and the results were presented in Table 14. Group 8 metals gave mixed results, with the Ru catalysts (Entries 1-3) showing less activity than expected, despite their presence in a number of homogeneous racemisation catalysts.[78,80,85] Only Ru/C (Entry 3) was shown to slightly reduce the e.e. of the substrate (97 %), with a TOF of 3 h^{-1} which compared favourably to the 0.08 h^{-1} reported in literature.[75] However, both in this work and reported in literature, Ru/C delivered poor selectivity with 74 and 9 % being achieved respectively. Fe/TiO_2 and Ru/Al_2O_3 (Entries 1 and 2) showed no reduction in e.e. but were not completely unreactive as the selectivity was seen to drop in both instances. The formation of by-products implies that the initial oxidation of the amine has occurred, however under these conditions reduction of the intermediate imine **86** was unsuccessful and was attacked by $S – $ **70** instead. This suggested that racemisation may still be possible under different conditions if the rate of reduction of the imine was increased.

The Group 9 metals also returned mixed results. Disappointingly, Co/TiO_2 appeared to be completely unreactive under these conditions (Table 14, Entry 4). Whereas the Rh catalysts showed a range of activity, with the TiO_2 supported catalyst (Entry 6) displaying considerably greater activity than the Al_2O_3 version (Entry 5) with TOF's of 24 and 2 h^{-1} respectively. The mild to moderate selectivity of the Rh catalysts was surprising given the extensive use of Rh to reduce imines, although poor selectivity with heterogeneous Rh catalysts had been previously observed by *De Vos* with Rh/C completely consuming **70**. The 56 and 80 % selectivity observed for TiO_2 and Al_2O_3 respectively, therefore shows a considerable improvement.[75]

Ir/TiO_2 had been expected to be highly active, as it had been widely used as a homogeneous racemisation catalyst (Table 14, Entry 7), however, under these conditions no racemisation was achieved, with only 82 % of the **70** being present at the end of the reaction. The lack of selectivity has been a consistent feature of Ir catalysts in the racemisation of primary amines. Homogeneous Ir catalysts achieved < 40 % selectivity in the hands of both *Blacker* and *de Vries*, while the previous example of the use of Ir/C by *De Vos* returned 33 % selectivity.[75,79,95]

Table 14 Summary of the HTS at 100 °C

Entry	Group	Catalyst	e.e. (%)	Rac. TOF (h^{-1})	Sel. (%)	Entry	Group	Catalyst	e.e. (%)	Rac. TOF (h^{-1})	Sel. (%)
1		Fe/TiO_2	100	0	86	10		Pd/TiO_2	25	75	63
2	8	Ru/Al_2O_3	100	0	89	11		Pd/C	39	61	5
3		Ru/C	97	3	74	12	10	$Pd(OH)_2/C$	N/A[a]	-	1
4		Co/TiO_2	100	0	100	13		Pt/Al_2O_3	100	0	82
5	9	Rh/Al_2O_3	98	2	80	14		Pt/TiO_2	97	3	69
6		Rh/TiO_2	76	24	56	15		Pt/C	15	85	9
7		Ir/TiO_2	100	0	82	16		Cu/TiO_2	100	0	92
8	10	Ni/TiO_2	100	0	100	17	11	Au/TiO_2	100	0	100
9		Pd/Al_2O_3	51	49	87	18		Au/C	100	0	98

Reaction Conditions: 0.0825 mmol amine, 1 mol % Cat., PhMe (1 mL), H$_2$ (5 bar), 100 °C, 1 h.

[a]Insufficient amine remaining to determine and e.e..

In contrast, the Group 10 metal catalysts returned the highest levels of activity at 100 °C. Although the low cost Ni/TiO_2 appeared to be completely inert (Table 14, Entry 8) both Pd and Pt were, in the main, found to be highly active (Entries 9 – 15). The activity of Pd was not unexpected given its frequent occurrence in racemisation literature, and particularly that of Pd/Al_2O_3 (Entry 9). [75,81–84,88,90,92] The high levels of activity returned by Pd/TiO_2 (Entry 10) and $Pd(OH)_2/C$ (Entry 12) however were extremely interesting as they have not previously been reported. The complete consumption of the amine by $Pd(OH)_2/C$ is likely due to the electron withdrawing ligand promoting the oxidative power while simultaneously reducing the reductive power of the catalyst. Under these conditions the TOF of Pd/C (Entry 11) was also observed to be increased from values reported in the literature by > 180-fold from 0.33 h^{-1} to 61 h^{-1}.[88] The low levels of selectivity observed with Pd/TiO_2, Pd/C and $Pd(OH)_2/C$ will be subject to further study at lower temperatures. The wide-ranging results also support findings by *De Vos* that the nature of the support has significant effect on the selectivity of the catalyst, but also potentially its racemisation potential.[75,88]

The Pt catalysts were of greater interest as there had only been one previous attempt to use a Pt, as a racemisation catalyst, in the form of Pt/C which resulted in no racemisation and complete consumption of the amine.[75] In this work, while using Pt/C (Table 14, Entry 15) low levels of selectivity were also observed (9 %), however the highest TOF of the screen was also observed with a value of 85 h^{-1}. Once again, the support appeared to have a significant effect on the selectivity of the process. Vastly improved preservation of the amine was observed when using Pt/Al_2O_3 and Pt/TiO_2 (Entry 13 and 14) however little to no racemisation was elicited.

Finally, no catalytic activity was achieved with Cu or Au (Table 14, Entries 16 – 18). The lack of racemisation was coupled with very high selectivity; therefore, these catalysts were subjected to a higher temperature screen at 145 °C in the hope this would elicit greater racemisation activity.

2.2.2.3. <u>Results of the 145 °C H$_2$ Screen</u>

As outlined previously, catalysts with high selectivity but low racemisation activity were included in a higher temperature 145 °C screen with H$_2$ (Table 15). Although many of the catalysts persisted with low levels of activity, improved performance was observed with, Ru/Al$_2$O$_3$, Ir/TiO$_2$ and Pt/Al$_2$O$_3$ (Entries 2, 6 and 8), which did not previously show any catalyst activity at 100 ^{0}C. At 145 °C, these catalysts were able to display modest racemisation of the primary amine with only minor further decreases in selectivity. This shows promise for these catalyst during future investigations. In comparison, Ru/C and Pt/TiO$_2$ (Entries 3 and 9) were able to further improve their racemisation capabilities at 145 °C. Ru/C was able to increase its TOF by > 9-fold with only a mild 17 % drop in selectivity. Pt/TiO$_2$ was also able to achieve a > 9-fold increase in TOF, however a more considerable 29 % drop in selectivity occurred. These results are also extremely promising as the change in activity observed shows extremely encouraging signs that, with bespoke optimisation, they could mark a step forward in the racemisation of chiral amines.

Table 15 Summary of the HTS at 145 °C.

Entry	Group	Catalyst	e.e. (%)	Rac. TOF (h^{-1})	Sel. (%)	Entry	Group	Catalyst	e.e. (%)	Rac. TOF (h^{-1})	Sel. (%)
1		Fe/TiO$_2$	100	0	100	7		Ni/TiO$_2$	100	0	97
2	8	Ru/Al$_2$O$_3$	89	11	86	8	10	Pt/Al$_2$O$_3$	94	6	78
3		Ru/C	72	28	57	9		Pt/TiO$_2$	73	27	40
4		Co/TiO$_2$	100	0	100	10		Cu/TiO$_2$	100	0	100
5	9	Rh/Al$_2$O$_3$	100	0	96	11	11	Au/TiO$_2$	100	0	100
6		Ir/TiO$_2$	95	5	78	12		Au/C	100	0	93

Reaction conditions: 0.0825 mmol amine, 1 mol % Cat., PhMe (1 mL), H$_2$ (5 bar), 145 °C, 1 h

2.2.2.4. <u>Results of the 70 ºC H$_2$ Screen</u>

The catalysts that were shown to have low selectivity but high racemisation potential at 100 ºC were included in another round of screening at 70 ºC with H$_2$ (Table 16) with the hope the selectivity of the catalyst could be increased while still maintaining the ability of the catalyst to racemise *S* - **70**.

Rh/TiO$_2$ had been shown to be highly active with a TOF of 24 h^{-1} at 100 ºC (Table 14, Entry 6); however, only 56 % selectivity was observed. Lowering the temperature to 70 ºC led to a 6-fold drop in TOF to just 4 h^{-1}(Table 16, Entry 1). Disappointingly, the anticipated increase in selectivity was not observed, with only a modest increase of 10 %. However, it did demonstrate the selectivity could be influenced by temperature.

The highly active Group 10 catalysts, Pd and Pt, were shown to be influenced to a much greater degree by lowering the temperature (Table 16, Entries 2 – 5). Pd/C and Pd(OH)$_2$/C (Entries 3 and 4) in particular were shown to have a > 17-fold and 88-fold increase in selectivity respectively . In the case of Pd(OH)$_2$/C the increase in selectivity allowed for total racemisation to be observed, achieving a TOF of 13 h^{-1}. Notably Pt/C, became completely inactive at 70 ºC after previously returning just 9 % selectivity. This shows particular susceptibility to the influence of temperature over the reaction which bodes well for future optimisation.

Table 16 Summary of the HTS at 70 ºC.

Entry	Group	Catalyst	e.e. (%)	Rac. TOF (h^{-1})	Sel. (%)
1	9	Rh/TiO$_2$	96	4	66
2		Pd/TiO$_2$	82	18	97
3		Pd/C	88	12	88
4	10	Pd(OH)$_2$/C	87	13	87
5		Pt/C	100	0	100

Reaction Conditions: 0.0825 mmol amine, 1 mol % Cat., PhMe (1 mL), H2 (5 bar), 70 ºC, 1 h

2.2.2.5. <u>The Effect of the Support During the HTS under H$_2$</u>

It has been reported by *De Vos* that the basicity of the support influences the selectivity of heterogeneous catalysts, as discussed in Section 2.1.1.[88] With the more basic support, (i.e., BaSO$_4$ or CaCO$_3$) the selectivity of the catalyst was observed to increase. The hypothesis is that the acidic nature of supports can catalyse the competitive by-product formation. *De Vos* observed the worst selectivity was Pd/C, the most acidic support tested. In this HTS, at 100 ºC we can explore similar trends through the 2 complete series of Pd and Pt catalysts supported on Al$_2$O$_3$,

TiO$_2$ and C (Table 14). Within these series the trend of Al$_2$O$_3$ > TiO$_2$ > C emerges with respect to selectivity, supporting *De Vos's* findings that C supported catalysts are the least selective (Entries 9 – 15).

However, when looking to apply *De Vos's* basicity/acidity theory, this becomes harder to rationalise with Al$_2$O$_3$ and TiO$_2$ as both are amphoteric; meaning that they are capable of displaying both acidic and basic characteristics depending on the conditions. However, this observation may be rationalised under a similar theory using the strength of Lewis Acidity. Ti in the TiO$_2$ is in a +IV oxidation state, as opposed to the +III oxidation state of Al in Al$_2$O$_3$. Therefore, TiO$_2$ is a more effective Lewis acid, which could promote nucleophilic attack of the imine species to a higher degree than the Al$_2$O$_3$ species. This would align the observed trend in the data. Similar trends can be observed in the incomplete Ru and Rh catalysts. Where the Ru/γ-Al$_2$O$_3$ is found to be more selective than Ru/C (Table 14, Entries 2 and 3), and Rh/γ-Al$_2$O$_3$ is seen to be more selective than its TiO$_2$ counterpart (Entries 5 and 6).

De Vos assumes, in the kinetic model, that the support material does not affect the rate of racemisation, and the rate of reduction is kept constant across all the supports.[88] However, it appears in our data series that this is not the case. Once again, looking at the Pd and Pt data sets, a trend of TiO$_2$ > C > Al$_2$O$_3$ emerges across both series (Table 14, Entries 9 – 15) with TOF's of 75 (TiO$_2$), 61 (C) and 49 (Al$_2$O$_3$) h^{-1} reported for Pd catalysts and 85 (TiO$_2$), 3 (C) and 0 (Al$_2$O$_3$) h^{-1} for Pt catalysts. This is further supported by the Ru and Rh partial series, where Ru/C has a greater TOF than Ru/Al$_2$O$_3$ (3 v 0 h^{-1}) (Entries 2 and 3) and Rh/TiO$_2$ has a greater TOF than Rh/Al$_2$O$_3$ (24 v 2 h^{-1}) (Entries 5 and 6).

It may also be possible that the redox properties of the support can also affect the catalytic activity, for example through strong metal-support interactions (SMSI). A stronger oxidiser would be expected to increase the potential for racemisation. The oxidative strength of a catalyst could be increased by a stronger Lewis Acid through pulling a greater amount of electron density from a metal centre. It can be hypothesized then that TiO$_2$ would show higher levels of racemisation than Al$_2$O$_3$ if this were true. Indeed, this is what was observed when comparing the same sets of catalysts as previous, in the Pd, Pt and Rh cases, TiO$_2$ displays a higher degree of racemisation than Al$_2$O$_3$.

2.2.2.6. Results of the 145 °C Thermal-Only Screen

A final HTS of all catalysts was performed at 145 °C without the presence of H_2 (Table 17). *Kim* et al. had described the ability of Pd/AlO(OH) to deliver high levels of racemisation with high selectivity under thermal-only conditions.[83] This screen served to explore if this phenomenon could be achieved by other heterogeneous catalyst and if so, how this affects the racemisation and selectivity of the catalyst compared to presence of H_2.

While most of the catalysts appeared completely inert, a small number displayed activity under the thermal-only conditions, This was rather surprising as the absence of H_2 was expected to increase the rate of oxidation, whilst slowing the rate of reduction. Therefore, little racemisation and low selectivity were expected. Of the 8 catalysts found to have the potential for racemisation under the inert atmosphere (Rh/Al$_2$O$_3$, Rh/TiO$_2$, Pd/ γ-Al$_2$O$_3$, Pd/TiO$_2$, Pd/C, Pd(OH)$_2$/C, Pt/ γ-Al$_2$O$_3$, Pt/TiO$_2$ and Pt/C), 7 had not previously been reported to racemise chiral amines without H_2 present; Pd/γ-Al$_2$O$_3$ being the only previously known catalyst.

Table 17 Results of the HTS at 145 °C without H_2.

Entry	Group	Catalyst	e.e. (%)	Rac. TOF (h^{-1})	Sel. (%)	Entry	Group	Catalyst	e.e. (%)	Rac. TOF (h^{-1})	Sel. (%)
1		Fe/TiO$_2$	100	0	100	10		Pd/TiO$_2$	7	93	15
2	8	Ru/Al$_2$O$_3$	100	0	95	11		Pd/C	1	99	9
3		Ru/C	100	0	98	12	10	Pd(OH)$_2$/C	31	69	38
4		Co/TiO$_2$	100	0	100	13		Pt/Al$_2$O$_3$	28	72	68
5	9	Rh/Al$_2$O$_3$	99	1	99	14		Pt/TiO$_2$	100	0	76
6		Rh/TiO$_2$	90	10	95	15		Pt/C	14	86	30
7		Ir/TiO$_2$	100	0	92	16		Cu/TiO$_2$	100	0	100
8	10	Ni/TiO$_2$	100	0	95	17	11	Au/TiO$_2$	100	0	94
9		Pd/Al$_2$O$_3$	5	95	23	18		Au/C	100	0	90

Reaction Conditions: 0.0825 mmol, 1 mol % Cat., PhMe (1 mL), N$_2$ (5 bar), 145 °C, 1 h

All of the thermal-only racemisation catalysts showed interesting differences in their performance in the absence or in the presence of H_2. The Rh catalysts were both found to have reduced TOF's compared to reaction under a H_2 atmosphere but showed marked improvements with respect to selectivity in spite of the higher temperature (Table 17, Entries 5 and 6). Rh/TiO$_2$ especially showed extremely encouraging potential with a TOF of 10 h^{-1} and a selectivity of 95 % (Entry 6), which is a 39 % increase in selectivity to compared to the 100 °C screen with H_2 (Table 14, Entry 6)

The remaining active catalysts were all found in Group 10 (Table 17, Entries 8 -15). Commercially available Pd/γ-Al$_2$O$_3$ was deemed very weakly active by *Kim* with a TOF of 1 h^{-1}, whereas the in-house Pd/AlO(OH) was found to have a TOF of 32.0 h^{-1}, (Table 9, Entries 1 and 2).[82,83] This contrasts significantly with our results, where Pd/γ-Al$_2$O$_3$ was found to be highly active, with a TOF of 95 h^{-1} returning a near 3-fold increase compared to the in-house Pd/AlO(OH) reported by *Kim*, and a 95-fold increase compare to the previously reported value for commercial Pd/γ-Al$_2$O$_3$, (Table 17, Entry 9). Proving Pd/γ-Al$_2$O$_3$ to be a considerably better racemising catalyst than previously reported.

In fact, the remaining Pd catalysts all showed greater levels of activity in the absence of H$_2$ compared to the corresponding results obtained with the presence of H$_2$ with Pd/TiO$_2$ and Pd/C (Table 17, Entries 10 – 12) achieving complete racemisation in just 1 hour. Another surprising result is the fact that Pd/C and Pd(OH)$_2$/C both achieved higher levels of selectivity without H$_2$ than they did with H$_2$. Similarly, Pt/C also responded extremely well to the thermal-only reaction conditions. At 100 °C with H$_2$, Pt/C was able to achieve a TOF of 85 h^{-1} and just 9 % selectivity (Table 14, Entry 15), whereas at 145 °C without H$_2$, it was able to maintain the same TOF while improving its selectivity to 30 %.

Pt/γ-Al$_2$O$_3$ had previously been found to be only mildly active at 145 °C with H$_2$, with a TOF of 6 h^{-1} and 78 % selectivity (Table 15, Entry 8). At the same temperature, under an inert atmosphere the TOF was increased 12-fold with a very similar 68 % selectivity (Table 17, Entry 13). In contrast, Pt/TiO$_2$ displayed good activity at 145 °C under H$_2$, with a TOF of 27 h^{-1} and selectivity of 40 % (Table 15, Entry 9), but was found to be completely inactive in the absence of H$_2$ (Table 17, Entry 14).

These results demonstrate that the effect of thermal-only racemisation could be found in a wider range of heterogeneous catalysts, under the right reaction conditions. Furthermore, temperature alone could be found to be extremely beneficial to the performance of some catalysts, maintaining or even improving activity whilst improving selectivity in some cases.

The discovery of the thermal-only racemisation catalysts serves to be an extremely exciting route for further investigation for the racemisation of chiral amines. The elimination of H$_2$ from reactions greatly simplifies the reaction system, from a tri-phasic (solid-liquid-gas) to bi-phasic (solid-liquid) system, bypassing complex mass transfer limitations of multiphasic reactions. Furthermore, the catalysts were shown to return the highest TOF achieved by a transition metal racemisation catalyst for the racemisation of *S* – **70** (Tables 5 and 6). In-part the key to these extremely high levels of racemisation were the super-ambient temperatures explored within inert

atmosphere screens, exploring a wider reaction space, which has not previously been explored in the field. This is in part due to lack of compatibility between these conditions and the enzymes employed in CE-DKR processes which is the general application of chiral amine racemisation.

2.3. <u>Conclusion</u>

This work represents the first time that HTS methodologies have been applied to screening amine racemisation catalysts. This has allowed direct comparisons to be draw between results in a reliable and accurate way, compared to the running of multiple individual experiments which can have poor control over variables between experiments. A HTS Protocol was develop that afforded good reproducibility across the plate and allowed a much greater degree of confidence to be placed in each result. The initial difficulty in developing this screen highlights the challenges that can be involved in controlling reaction parameters which may appear trivial. The HTS protocol allowed the efficient running of 108 reactions over 3 different temperatures in just 4 hours.

The culmination of these efforts has led to the identification of 12 racemisation catalysts under a H_2 atmosphere, 9 of which have not previously been reported (Ru/γ-Al$_2$O$_3$, Rh/TiO$_2$, Rh/ γ-Al$_2$O$_3$, Ir/TiO$_2$, Pd/TiO$_2$, Pd(OH)$_2$/C, Pt/ γ-Al$_2$O$_3$, Pt/TiO$_2$ and Pt/C) and demonstrated increased selectivity for 2 more that allowed for their racemisation potential to be observed (Ru/C and Pt/C). The observation of some of these catalysts' potential for the racemisation was only possible due to the ability to screen multiple reaction temperatures. During the screening without the presence of H_2 a further 7 novel catalysts were found to be active amine racemisation catalysts under these conditions (Rh/γ-Al$_2$O$_3$, Rh/TiO$_2$, Pd/TiO$_2$, Pd/C, Pd(OH)$_2$/C, Pt/γ-Al$_2$O$_3$ and Pt/C).

Under both the H_2 and N_2 atmospheres, the results reported during the HTS achieved TOF's that are unprecedented in batch reaction conditions. This enabled a new avenue of research into utilising these thermal-only racemisation catalyst in continuous flow reactors, to create an effective racemisation flow system.

Chapter 3: <u>Flash Thermal Racemisation of Chiral Amines</u>

The outcome of the HTS (Chapter 2, Section 2.2.4.), allowed for the identification of a family of transfer hydrogenation catalysts (Rh/Al$_2$O$_3$, Rh/TiO$_2$, Pd/γ-Al$_2$O$_3$, Pd/TiO$_2$, Pd/C, Pd(OH)$_2$/C, Pt/γ-Al$_2$O$_3$ and Pt/C), many of which were not previously known for the racemisation of chiral amines. It was hoped that these catalysts could be transitioned into a flow system where their full capabilities could be realized.

The super-ambient conditions used during the HTS in Section 2.2.3.6. returned extremely high TOF's, therefore it was decided to continue to explore this increased operating window, made more accessible by continuous flow. These high temperatures can also be more precisely controlled owing to the high surface area to volume ratio available for efficient heat transfer offered by a continuous reactor.

The use of external H$_2$ sources have been shown to be superfluous for a high degree of amine racemisation during the HTS (Section 2.2.3.6). Although the selectivity of these catalysts was generally observed to be poor, we postulated that it will be possible to dispense with the use of H$_2$ to act as a by-product suppressant, by capitalising on of the exquisite residence time (τ) control to discriminate between the desirable redox racemisation pathway and the undesirable by-product formation. It was hypothesised that applying these super-ambient temperatures over short residence times could result in high TOF's with high selectivity. Combining these two pillars of "Flash Chemistry" pioneered by Professor *J. Yoshida* to create a novel approach to chiral amine racemisation, which we term "Flash Thermal Racemisation" (FTR). [112]

In this chapter previous attempts to harness super-ambient conditions for the racemisation of amines will be discussed alongside the early forays into continuous flow amine racemisation. The innovative steps taken during these key publications and their shortcomings that inspired our work will be highlighted. The insights provided by these previous works were integral to paving the way for pioneering the FRT approach.

3.1. <u>Introduction</u>

3.1.1. <u>Super-ambient Racemisation of Chiral Amines</u>

Previously *De Vos* had reported encouraging results for the racemisation of *S* - **70** with Pd/CaCO$_3$ under traditional batch conditions (Table 18, Entry 1).[75,88] Unfortunately, despite the high degree of racemisation and selectivity, a long reaction time of 24 hours were required, resulting in extremely low TOF of 0.82 h^{-1} . This led to *De Vos* exploring, for the first time, the potential for super-ambient reaction conditions to exponentially increase the rate

of racemisation.[74] Initially, a stainless steel autoclave was used to reach temperatures of 120 °C under an atmosphere of H$_2$. After just 15 minutes, a 69 % reduction in e.e. was observed (Entry 2), resulting in a near 60-fold increase in TOF whilst increasing selectivity to 99 %. This early experiment shows how powerful this approach could be, combining super-ambient to temperatures to drive the rate of reaction, with short reaction times that prevented by-product formation.
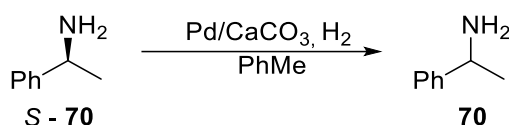
Table 18 Exploration into super-ambient conditions to increase the rate of racemisation of *S* – **70**.[74,75,88]

Entry	Heating	Temp. (°C)	H$_2$ (bar)	Time (min)	e.e. (%)	Rac. TOF (h^{-1})	Sel. (%)
1	Standard	70	0.1	1440	2	0.82	80
2	Standard	120	0.05	15	31	48.5	99
3	Microwave	120	0.05	15	11	62.5	100

Reaction conditions: 0.33 mmol amine, 40 mg 5 % Pd/CaCO$_3$, H$_2$, PhMe (4 mL)

Further attempts were made to increase the rate of reaction through the use of microwave irradiation (Table 18, Entry 3). This was found to prompt a further increase in TOF to 62.5 h^{-1} while maintaining complete selectivity. This represents a combined > 75-fold increase in TOF compared to the traditional 70 °C reaction temperatures usually deployed in heterogeneous racemisation reactions, to achieve the highest TOF reported in the field (Table 18, Entries 1 and 3).[71,75,83,88]

The authors attributed the increase in racemisation rate and selectivity to a superheated metal centre achieved using microwave irradiation.[74] It was thought that by increasing the rate of reactions occurring on the metal centre (racemisation) competitive reactions occurring on the support or bulk solution (by-product formation) can be suppressed. Although high TOF and selectivity have been observed using this approach (Table 18, Entries 2 and 3), the source of these impressive results does not appear to lie with microwave irradiation. Rather, it is more likely that these experiments are delivering these high TOF and selectivity through more classical chemistry principles. The high rate of reaction appears to stem from the exploitation of super-ambient conditions delivering high TOFs, while the short reaction times are driving selectivity through discriminating between the faster racemisation reaction pathway, and the slow by-product forming pathway.

The higher TOF achieved by the microwave reaction compared to the original thermal reaction(Table 18, Entries 1 and 3) is easily explained by the Arrhenius equation (Equation 8). The traditional racemisation reaction (Entry 1) was found to reduce the e.e. of *S* – **70** by 98 % over a 1440 minute reactions, giving an overall rate of 0.0681

Δe.e. min^{-1} (Equation 9). The Arrhenius equation (Equation 8) predicts that increasing the temperature to 120 °C would increase the rate by 32-fold, doubling with every 10 °C increase. If this is applied to the rate derived by Equation 9, we can predict that this should be increased to 2.1778 Δe.e. min^{-1} given by Equation 10. If this rate was maintained over the course of the microwave irradiated reaction (Entry 3), it would predict that the 89 % reduction in e.e. observed in this reaction would be achieved in just 41 minutes (Equation 11). The rate established in Equation 9 will be an underestimation of the initial rate of the reaction due to the inherent reduction in rate over the course of a reaction and the catalyst deactivation that is likely to occur over the 24 hour period (Entry 1). Therefore, it can be postulated that the increase in rate achieved by the microwave irradiation can be accounted for by the increase in reaction temperature rather than a microwave effect.

$$\text{rate} = \frac{98}{1440} = 0.0681\ \Delta\text{e.e. min}^{-1} \quad \text{Equation 9}$$

$$0.0681\ \Delta\text{e.e. min}^{-1}\ x\ 32 = \ 2.1778\ \Delta\text{e.e. min}^{-1} \quad \text{Equation 10}$$

$$\frac{89\ \Delta\text{e.e}}{2.1778\ \Delta\text{e.e. min}^{-1}} = 40.9\ \text{mins} \quad \text{Equation 11}$$

However, there continues to be a disparity between the microwave irradiated and the thermally activation reactions with respect to TOF (Table 18, Entries 2 and 3). This too can be explained by the more efficient heating experience in the microwave vial reactor compared to the stainless steel autoclave reactor. Microwave irradiation has the advantage over thermal activation in that it can more rapidly heat solvents to the desired temperature. Therefore, over a given time, a microwave reaction can spend longer at the desired temperature than a thermal reaction, as the thermal reaction will spend a larger portion of the time reaching the set temperature. The slower heating of the thermal reaction may be exaggerated in this work by the thick stainless steel walls of the autoclave. This could act as an insulator during the initial part of the reaction before reaching the appropriate temperature. These effects could artificially elongate the relative reaction time of the microwave reaction, causing a higher degree of racemisation. The discrepancy between the heating rates of reactions would be particularly pronounced over the short 15 minute reaction times used in this work.

The results achieved by *De Vos* are extremely significant to the field as they represent the highest TOF's published in literature for the transition metal racemisation of *S* – **70**, combined with extremely high selectivity which is vital in CE-DKR processes.[74] However it is felt that the underlying cause of these results may have been misinterpreted. They have been assigned to the properties of microwave irradiation, rather than the innovative approach that was taken to apply the reactions to short, sharp, high temperature conditions. However, the

difference between the mechanism that brings about the results and the underlying reaction parameters can be easily conflated. For many synthetic organic chemists, microwave reactors are the most convenient way to deliver short pulses of high temperatures to a reaction. However, the flow chemistry community is acutely aware that such rapid high temperature pulses can be recreated in a more efficient way in flow. Furthermore, flow chemistry has the additional advantage or scalability compared to microwave irradiated reactions.

Microware reactions are hampered by lack of scalability due to the drop-off in penetration of microwaves with distance (Equation 12).[113] It is believed that microwaves can only penetrate into the reaction solution over distances on the order of a few cm. Therefore, if the scale of the reaction is increased the irradiation of only the outer edge of the reaction is possible, thus creating temperature gradients across the reaction where only the outer portion of the reaction is performing as expected. This may be why *De Vos* subsequently moved away from this method of activation and only performed these reaction on a 0.33 mmol (40 mg) scale. To overcome the lack of scalability, microwave irradiated reactions have been performed in continuous flow where the small cross section of the flow reactor tubing negates the lack of penetration of radiation, while the continuous processes permit easy scalability.[114] However, these approaches continue to be hampered by the limited materials and solvents that are compatible with microwave irradiation. Materials that are highly absorbing of microwaves (i.e., stainless steel tubing) cannot be used as they will greatly reduce the intensity of the irradiation reaching the desired species in solution, while the solvents are limited to polar solvents due to their permanent dipole moment. Alternatively, flow chemistry can be used to recreate the short, high temperature reactions with traditional thermal activation, due to the combination of high surface area to volume ratios, allowing the reaction medium to be heated to high temperature over very short time periods, and precise residence time control achieved by flow rate manipulation.

$$d_p = \frac{1}{2\alpha}, \alpha = \text{attenuation constant} \quad \text{Equation 12}$$

3.1.2. Racemisation in Continuous Flow

Flow chemistry can provide an alternative approach to perform reactions at high-temperatures in a more convenient, precise and scalable manner. Super-ambient temperatures can be reached by simply applying a Back Pressure Regular (BPR) of the desired pressure at the end of the system before heating to the desired temperature. These elevated temperatures can be more rapidly achieved and controlled with a higher degree of accuracy due to the excellent heat transfer afforded by the flow reactor. This means that flow systems have a superior ability to discriminate between activation energies of competing reactions, increasing selectivity (Figure 24). Furthermore,

76

a specific sections of the reactor can be heated, e.g., only the Packed Bed Reactor (PBR) containing the heterogeneous catalyst. This creates a more defined reaction time since when the solution leaves the PBR it is no longer exposed to the catalyst and will also rapidly cool to room temperature.
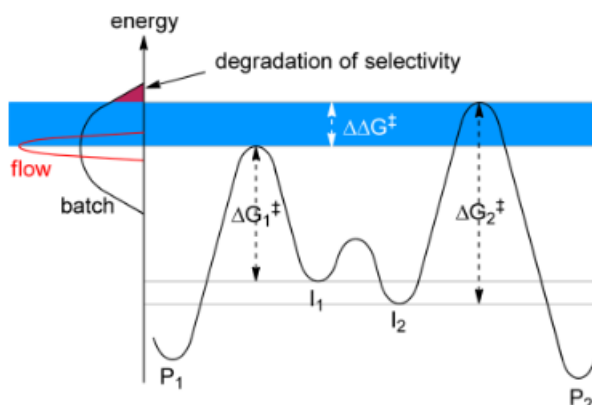
Figure 24 The greater control of temperature in flow compared to batch. Taken from *Seeberger* et al..[115]

The residence time distribution (RTD) for each molecule in a flow system is also much narrower compared to a batch system (Figure 25). Therefore, the time in which the reaction solution is exposed to the catalyst inside the PBR, and in contact with the catalyst, is much more defined in flow. Consequently, more consistent results can be obtained within a reaction and between repeated reactions. Additionally, the residence times can be more precisely controlled through manipulation of the flow rate.
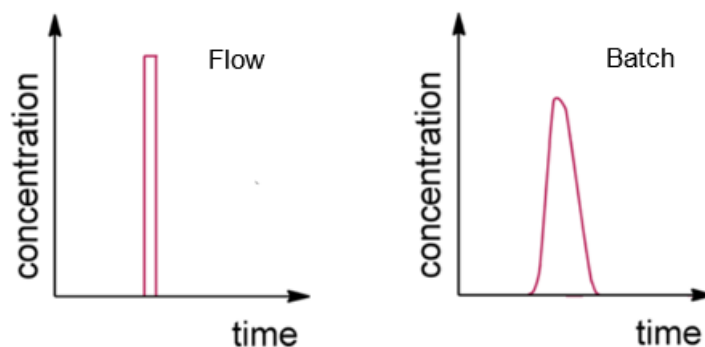
Figure 25 The greater precision of RTD afforded by flow compared to batch. Adapted from *Seeberger* et al..[115]

Finally, the PBR containing a heterogeneous catalyst can have a very small void volume therefore only a small proportion of the stock solution is subject to the entirety of the catalyst at a given time. This increases the effective substrate:catalyst ratio at the time of the reaction. Therefore, this can also further increase the rate of reaction, alongside the higher temperatures.

The TOF of racemisation reactions conducted in continuous flow is calculated using Equation 13, first proposed by *Blacker* et al., which represents a modification of Equation 8.[97] Equation 13 was further modified in this work

77

to be normalised relative to the volume of the reactor, rather than the total stock solution, in much the same was a *Kappe* defined STY calculations in flow.[116] STY was defined as being standardised by the volume of the reactor, that being in batch the amount of solvent used and in flow the volume of the tubing where the reaction occurs, i.e. the void volume in the PBR. Therefore, when calculating TOF of flow reactions the amount of amine being converted will be calculated relative to the number of mols of amine in the PBR at any given time. This figure will once again be normalised by the total number of mols of the transition metal per unit time, giving rise to the refined TOF equation (Equation 13). If this was not considered then the TOF of a flow reaction could be inflated through running of the reaction for longer periods of time, something not possible in batch reactions. This therefore treats flow as multiple, discrete reactions giving a fairer comparison between batch and flow.

$$\text{Flow TOF of Rac.} (\text{h}^{-1}) = \frac{\text{Frac. Racemised x Volume of Reactor (mL) x } [\text{Amine}]_{\text{Initial}} \text{ x } 60}{\text{Cat. (mmol) x } \tau \text{ (min)}} \qquad \text{Equation 13}$$

Previously, there have only been 2 examples where racemisation of amines has been achieved in continuous flow.[90,97] This was first achieved by *Poppe* et al. in 2018, and subsequently by *Blacker* et al. in 2021. *Poppe* employed a mixed PBR, containing both the racemisation catalyst and the CALB enzyme as part of a CE-DKR system (Figure 26). Whereas, *Blacker* used a standalone racemisation PBR to decouple the racemisation step of a diastereomeric crystallisation DKR process (Figure 27). *Poppe* employed NH_4HCO_2 as a source of H_2 while *Blacker* employed DIPMA as a H-donor, to aid selectivity.
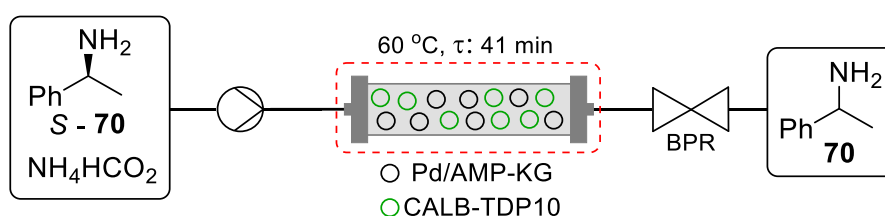
Figure 26 The continuous flow racemisation system developed by *Poppe* et al..[90]
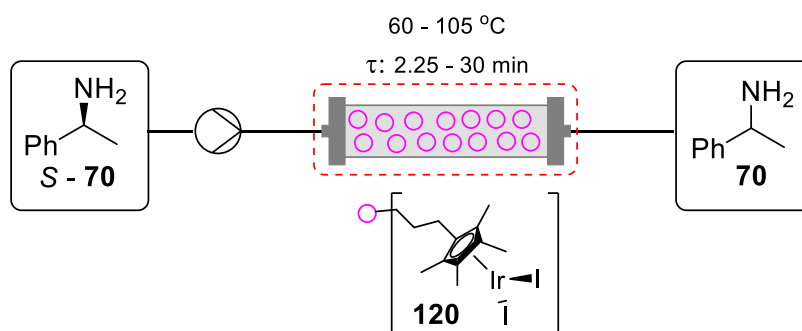
Figure 27 The continuous flow racemisation system developed by *Blacker* et al..[97]

78

The Pd based catalysts used by *Poppe* were shown to be highly effective (Table 19). Pd/AlO(OH) continued to return extremely impressive results in flow (Entries 3 and 4), boasting the highest TOF of the catalysts in this study with 6.0 h^{-1}, alongside high levels of racemisation across both temperatures. Surprisingly, Pd/C was shown to elicit no racemisation (Entries 1 and 2) despite extensive activity found in batch.[75,81,84,88] While Pd/BaSO$_4$ also displayed a reduced TOF, and selectivity compared to batch (Entry 9); TOF 0.3 h^{-1} and 68 % selectivity in flow compared to TOF 3.00 h^{-1} and 91 % selectivity in batch.

In comparison, the heterogeneous Ir SCRAM catalyst, **123**, performed significantly worse in flow than the homogeneous analogue in batch (Table 19, Entry 13), where the TOF dropped from 6.25 h^{-1} to 0.3 h^{-1}.[97] Despite this, it was found to have greater activity than Pd/C (Entries 1 and 2), Pd/AEAP-D (Entries 5 and 6) and Pd/BaCO$_3$ (Entries 7 and 8). However, the Ir catalyst suffers from poor selectivity in the racemisation of primary amines as did its homogeneous analogue. Despite the inclusion of a H-donor, by-product formation could not be eliminated entirely, and it was suspected that NH$_3$ liberation was causing catalyst deactivation.

Table 19 Catalyst screening results using the continuous flow racemisation system at 90 °C.

Entry	Catalyst	τ (min)	Temp. (°C)	e.e. (%)	Rac. TOF (h^{-1})	Sel. (%)	Reference
1	Pd/C	41	90	> 99	N/A	2	[Poppe 2018][90]
2			60	> 99	N/A	13	
3	Pd/AlO(OH)	41	90	4	6.0	98	
4			60	57	2.7	99	
5	Pd/AEAP-D	41	90	2	0.2	74	
6			60	36	0.2	95	
7	Pd/BaCO$_3$	41	90	13	0.2	41	
8			60	6	0.2	66	
9	Pd/BaSO$_4$	41	60	1	0.3	68	
10	Pd/AMP-D	41	90	< 1	0.9	9	
11			60	5	0.8	90	
12	Pd/AMP-KG	41	60	2	0.6	94	
13	Ir SCRAM	16	105	94	0.3	-[b,C]	[Blacker 2021][97]

[a]Insufficient amine remaining to determine and e.e.. [b]Selectivity data not provided. [c]Author states "most amine decomposed". Reaction Conditions: *Poppe*: Amine (69 mM), NH$_4$HCO$_2$ (69 mM), 2-methyl-2-butanol, 60 °C, 0.02 mL min^{-1}. *Blacker*: Amine (100 mM), DIPMA (H-donor), PhMe, 0.1 mL min^{-1}.[90,97]

Although there may be inconsistencies in the performance of the catalysts used by *Poppe* in batch and flow, there was good translation of the trends observed by *De Vos* and *Kim* with respect to the nature of the support and particle size of the Pd (Table 19). [75,82,83,88,90] *De Vos* observed a correlation between the basicity of the catalyst support and selectivity of the catalyst. *Poppe* also found that BaCO$_3$ (Entries 7 and 8) and BaSO$_4$ (Entries 9) basic support had much greater selectivity than the C support (Entry 1 and 2). Furthermore, the extremely high

selectivity observed by *Kim* for Pd/AlO(OH) was confirmed by *Poppe* (Entries 3 and 4), undoubtedly aided by the presence of H_2 where it had not previously been used.

SiO_2 supports were also found to be poorly selective by *De Vos*, however functionalisation of the support with basic groups was found to significantly increase their selectivity.[88] *De Vos* used AMP (3-aminopropylfunctionalized silica) and PP (3-(1-piperazino)propyl functionalized silica) to achieve much higher selectivity by neutralising the acidic Si-OH residues. Similarly, *Poppe* found that modifying SiO_2 with AMP (Entry 10, 11 and 12) and ADEAP (Entries 5 and 6) (3-(2-aminoethylamino)propyl-modified silica) returned comparable selectivity to the alkaline earth supports.[90] ADEAP, which contained more amine groups, was found to be more selective than AMP.

Poppe also found that the particle size of the catalyst support influences the activity of the catalyst (Table 19), as previously reported by Kim.[82,90] AMK-KG supports had particle sizes of 63 – 100 μm (Entry 12) whereas AMP-D had 40 – 63 μm particles (Entries 10 and 11). At 60 °C AMP-D has a TOF of 0.8 h^{-1} whereas AMP-KG returned a TOF of 0.6 h^{-1}. This suggests that the reaction is diffusion limited, thus the smaller particle size of the Pd provided an increased surface area for substrate to bind, thus increasing the rate of reaction.

The presence of the CALB in the mixed PBR, with a thermal decomposition at > 70 °C, restricted the author to operate the CE-DKR at 60 °C.[90] Previously, Pd/AlO(OH) had appeared the most attractive catalyst at 90 °C with complete racemisation and selectivity (Table 19, Entry 3). However, at 60 °C (Entry 4), only a moderate racemisation was observed. Whereas Pd/AMP-KG (Entry 12) was able to return complete racemisation and high selectivity at the lower temperature and was therefore selected to be taken forward. However, comparison using e.e. and selectivity in this way is unfair due to the inconsistency observed in the catalyst loading within each PBR (Table 20). When the quantity of Pd in each PBR was considered, there is 10-fold greater Pd content in the AMP-KG PBR than the AlO(OH) PBR (Table 20, Entries 2 and 7). To account for this the TOF should be used to more fairly compare the productivity of the catalyst (Table 19), this clearly demonstrate the superior racemisation potential of Pd/AlO(OH) over AMP-KG (Entries 4 and 12).

Entry	Catalyst	Mass of Cat. (mg)	wt % Loading	mmol of Pd
1	Pd/C	248	4.7	0.110
2	Pd/AlO(OH)	142	1.0	0.013
3	Pd/AEAP-D	260	13.6	0.332
4	Pd/BaCO₃	766	6.0	0.432
5	Pd/BaSO₄	922	3.2	0.277
6	Pd/AMP-D	246	4.2	0.097
7	Pd/AMP-KG	251	5.5	0.130

It was felt that although both of the initial forays into racemisation in flow by *Poppe* and *Blacker* had been successful, learnings from each system could be taken and combined to deliver a more efficient next generation racemisation system.[90,97] Although *Poppe*'s work had found a more effective catalyst for the racemisation of *S* – **70**, use of the mixed PBR greatly limited the reaction space that could be used. This was in contrast to the excellent use of compartmentalisation employed by *Blacker* where each operation within a flow system can be effectively decoupled from each other, allowing the racemisation and diastereomeric crystallisation steps to be performed under independent reaction conditions (Figure 28). This permits optimal performance of each unit of operation. Furthermore, *Poppe* opted to use a mixed PBR as part of a single pass flow system (Figure 29) where full conversion is required to be complete before the end of the pass. Whereas *Blacker* et al. used the racemisation PBR as part of a recycle loop, dynamic diastereomeric crystallisation system (Figure 28) which means that full conversion in a single pass in not required and material can iteratively increase towards full racemisation with each pass. This can greatly increase the productivity of a reaction but using multiple shorter residence times to achieve full conversion.
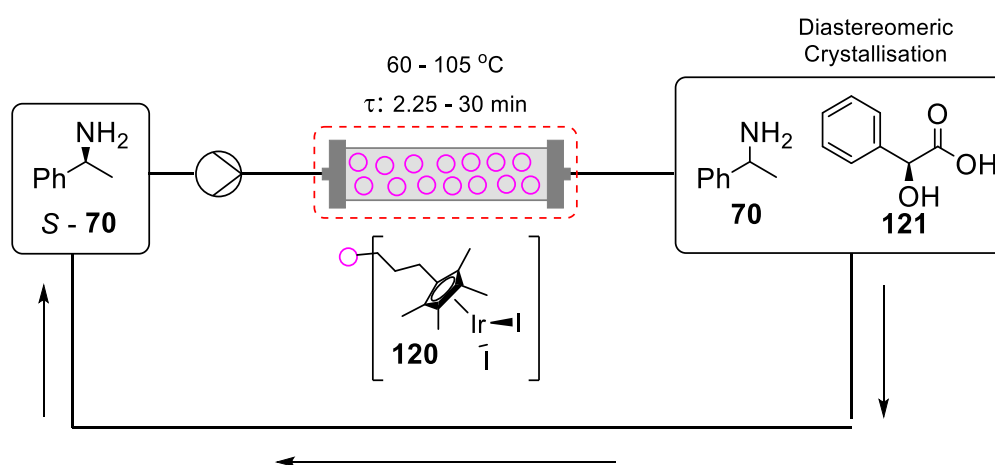
Figure 28 The full DKR flow system developed by *Blacker* et al..[97]
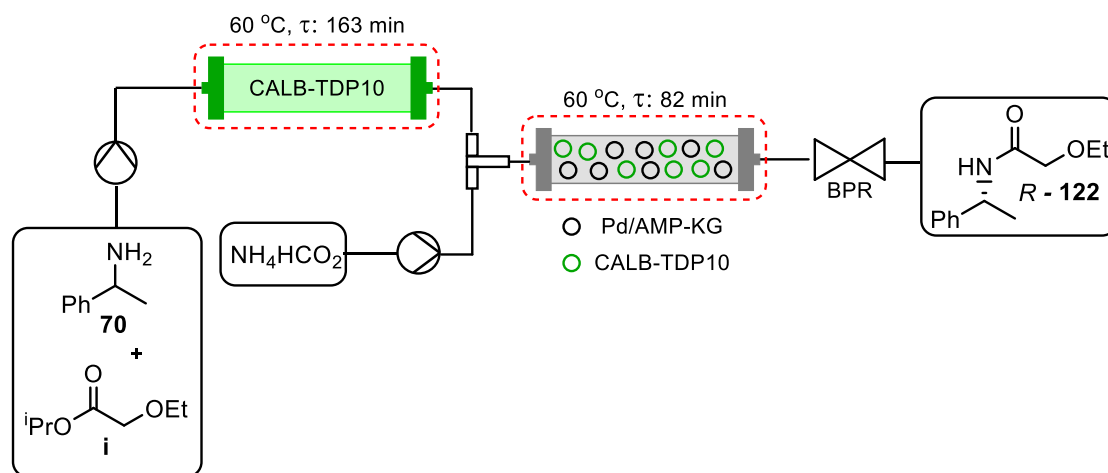
Figure 29 The full CE-DKR system developed by *Poppe* et al..[90]

Decoupling the racemisation and enzymatic KR in *Poppe*'s system (Figure 29) would have allowed a greater operating window to be explored. The complete racemisation and selectivity achieved by Pd/AlO(OH) at 90 °C (Table 19, Entry 4), displaying the best TOF, could have been further built on by increasing the flow rate. This would have increased the TOF and increased the throughput of the system. If a drop in racemisation had occurred during the shorter residence times, the temperature could be easily increased to establish full racemisation as the super-ambient range of the 2-methyl-2-butanol solvent (b.p 105 °C) was not explored. This aside, the Pd/AMP-KG catalyst achieved full racemisation and selectivity at 60 °C, therefore this suggests that an increase in flow rate could be employed to reduce the residence time and increase the TOF. However, the mixed PBR nature meant that a higher flow rate could not be used without sacrificing incomplete KR.

Blacker reported low selectivity for the racemisation of *S*-**70** (Table 19, Entry 13).[97] However, this occurred at a residence time of 16 minutes, whereas for other substrates in the scope, 2.25 minute residence time was used. It would have been interesting to see how manipulating the flow rate affected both the selectivity and racemisation. The moderate racemisation also observed by *Blacker* may be due to consumption of the racemised material into undesirable by-products. Therefore, the true activity of the catalyst may be missed by observing the optical activity of **70** alone.

Poppe and *Blacker*'s innovative approach to amine racemisation using flow chemistry signified the greatest advance in the field for some time.[90,97] Providing a new perspective on the challenge where previously efforts had appeared stagnated. Many key learnings can be taken from both works, as many positives were achieved in both. However, it is extremely exciting that these encouraging results were achieved with so many potential areas to build upon. Combining the decoupled recycling loop system described by *Blacker* with the highly effective racemisation catalysts identified by *Poppe* could create an extremely powerful flow system. Furthermore,

application of the high temperature, short reaction time conditions identified by *De Vos* in the microwave racemisation work could also be explored to provide an extremely efficient system for the racemisation of chiral amines.[74]

3.2. <u>Results & Discussion</u>

Inspired by *Poppe*, *Blacker*, *De Vos* and *Yoshida,* our "Flash Thermal Racemisation" FTR approach was developed. [74,90,97,112,117]In this design, a specific racemisation PBR would be used, containing only the racemisation catalyst, whereby the $S - $ **70** is exposed to a super-ambient PBR for short period of time could be applied to replicate *De Vos*'s findings. Within this, the goal was to achieve maximum racemisation and TOF whilst ensuring high selectivity of the amine. These conditions could be applied to a recycle loop system, and consequently full conversion would not be required with a single pass.

Although a range of catalysts capable of transfer hydrogenation racemisation had been identified in the HTS (Section 2.2.4.) with promising activity, it was decided to take Pd/Al_2O_3 forwards to prove the concept of FTR. This was decided through a process of elimination. The Rh based Al_2O_3 and TiO_2 catalysts were not the most active, whilst also utilising an unattractive, expensive transition metal centre. The C supported Pd, $Pd(OH)_2$ and Pt catalysts were difficult to implement in the flow system due to their extremely small particle size, and would therefore require further preparation, such as pelletisation to avoid a large pressure drop in the flow system. This left Pd/Al_2O_3, Pd/TiO_2 and Pt/Al_2O_3 as potential candidates. Due to its commercial availability, $Pd/\gamma\text{-}Al_2O_3$ represents the ideal candidate in the preliminary study, in order to validate the FTR strategy.

3.2.1. <u>The Development of the Flash Thermal Racemisation System</u>

A flow system was designed and custom-built for the purposes of this project to meet the requirements of an FTR reactor (Figure 30).[118] A HPLC pump was used to pump the reaction mixture, or toluene, through a PBR containing Pd/Al_2O_3 dispersed in chemically inert silicon carbide (SiC). The PBR was housed in an aluminium heating block controlled by a PID allowing heating in excess of 200 ºC, while a BPR pressurised this portion of the system to 8 bar to maintain the liquid phase when super-ambient temperatures are reached. Following this part of the system a thermoelectric, Peltier, heat exchanger was installed to actively cool the reaction mixture. This would act as a thermal quench for the reaction, helping to further increase the precision with which the reaction time is defined.
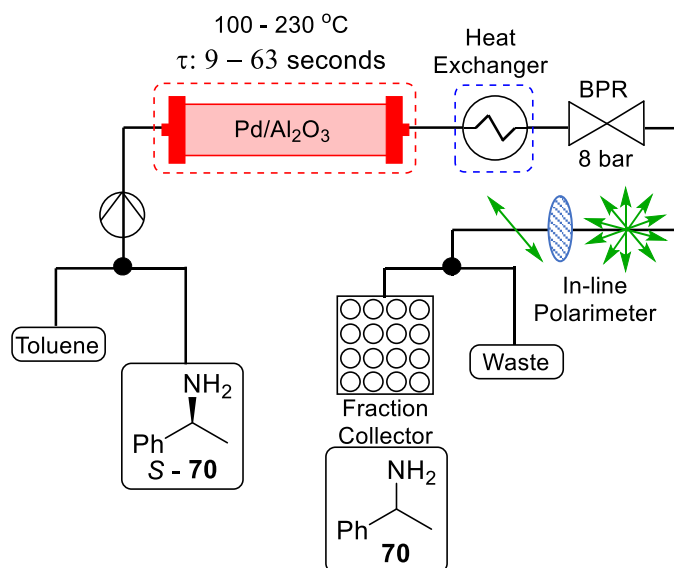
Figure 30 The flow system designed for FTR.[118]

The reaction mixture was then passed through an in-line polarimeter to assess the optical rotation of the product mixture in real-time. This would allow concurrent determination of the point when the flow system has achieved steady state, whilst also monitoring catalyst deactivation. Due to the potential presence of the by-products this could not be used to determine the e.e. (extent of racemisation) of the chiral amine in real time. Since optical rotation is temperature dependent, inconsistent or varying temperature of the solution entering the polarimeter can give noisy, fluctuating readings. This was prevented by the use of Peltier heat exchanger. Lastly, the reaction mixture was diverted either to waste or, once steady state was reached, to a fraction collector. The resulting samples could then be analysed by chiral HPLC and GC to determine the amines e.e. and selectivity respectively.

3.2.2. Scoping of Reaction Space

Once the FTR system had been constructed, preliminary experiments were conducted to explore the reaction space using the new flow system (Table 21). *S* –**70** was chosen as a model substrate due to its extensive presence in related literature and relevant industries, as well as the challenges it presents in terms of selectivity. The scoping of the reaction space started with relatively mild reaction conditions, with low temperatures (100 °C) and relatively long residence times (τ: 63 seconds), resulting in no detectable racemisation (Entry 1). Subsequently, the temperature was increased by increments of 50 °C (Entries 2 - 4), and racemisation began to be observed. When the reaction was conducted at 250 °C (Entry 4) the starting amine was completely consumed, however incrementally increasing the flow rate from 1 to 7 mL min^{-1} (τ: 63 to 9 seconds), improved the selectivity (Entries 5 – 7). These results showed that super-ambient temperatures were for racemisation to occur on these time scales and that selectivity could be manipulated through a change in flow rate.

84

Table 21 The results of initial scoping experiments in the FTR system.

Entry	Flow Rate (mL min^{-1})	τ (s)	Temp (^{o}C)	e.e. (%)	Sel. (%)
1	1	63	100	100	100
2	1	63	150	31	66
3	1	63	200	9	8
4	1	63	250	-^{a}	0
5	3	21	250	17	9
6	5	13	250	33	27
7	7	9	250	67	41

^{a}Insufficient amine remaining to determine e.e..
Reaction conditions: 82.5 mM amine, 200 mg Pd/Al$_2$O$_3$, anhydrous PhMe

Unfortunately, higher flow rates (> 7 mL min^{-1}) could not be explored due to the pressure limit of the polarimeter flow cell (12 bar), established without a BPR present. Furthermore, when performing reactions at 250 ^{o}C and 7 mL min^{-1} it was found that the heating elements struggled to provide sufficient heating power to maintain the high temperatures due to the high turnover of solvent which requires heating, representing an upper limit of the reactor. From these results a working temperature range of 100 – 230 ^{o}C and a flow rate range of 1 – 7 mL min^{-1} was established for the prototype reactor. The results obtained (Table 21) also highlights the need for precise residence times control as the difference of just 4 seconds can produce a 14 % drop in selectivity (Entries 6 and 7).

Although good results were obtained at the same 82.5 mM concentration that was used in Section 2.2. for the HTS it was decided to also investigate the change in substrate concentration as a proxy for substrate:catalyst ratio. Changing the solution concentration and maintaining the same catalyst loading within the PBR alters the effective catalyst loading within the PBR. At lower solution concentrations there is a lower ratio of substrate:catalyst, mimicking higher catalyst loading, whereas at higher concentrations there is a larger ratio of substrate:catalyst, mimicking a lower catalyst loading. Furthermore, changing the solution concentration would allow a more efficient workflow, as it removed the need to stop the reactor to replace the PBR. Instead, the inlet solution could be changed without interruption. 82.5 mM was deemed the top end of the concentration range and 20.6 mM was chosen as a lower limit as it represents a quarter of the original concentration.

3.2.3. Design of Experiments Optimisation – Round 1

Further investigation of FTR of chiral amines was conducted through a data-led Design of Experiments (DoE) based approach. [119,120] DoE is a method of statistically developing a set of experiments to investigate a reaction system. A key feature of DoE's is that they are factorial approach, i.e., multiple factors are changed between each experiment. In contrast, in the traditional scientific method of one-factor-at-a-time (OFAT) optimisation, where

changes are made to a single variable per experiment (Figure 31). Generally, when OFAT analysis is employed only 1 dimension of the reaction space is explored, making it extremely challenging to elucidate the interactions between the variables themselves in multi-dimensional space. Whereas DoE enables multiple reaction variables to be changed between experimental runs thus exploring the reaction space in multiple dimensions and allowing for facile understanding of how the reaction parameters interact with each other. The model created by DoE can then be used to plot a Response Surface Model (RSM) where the outcome of reactions to be predicted or help identify the global optima of the reaction depending on the desired outcome by interpolating between datapoints. OFAT analysis can identify reaction optima, although it can be difficult to tell if this is a local optima as opposed to the global optima. Therefore, DoE can deliver a much more detailed understanding of the reaction space while performing fewer experiments to achieve this objective
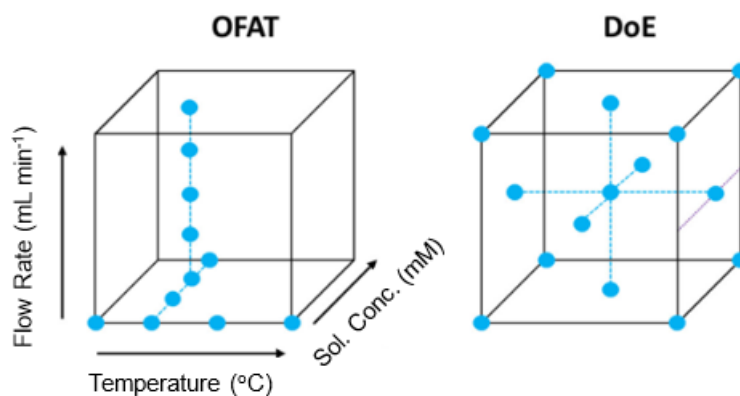
Figure 31 A comparison of OFAT against DoE. Adapted from *Bourne* et al..[120]

DoE must be carefully developed to realise these benefits over OFAT. Lack of understanding of a reaction space before designing a DoE can waste experimental runs on design points that may not add usable information to the model. The three results that appear to show no activity, 100 % e.e., can be difficult to differentiate from each other as this is a limitation of the sensitivity of the analytical equipment. These values may actually by different but appear the same because the difference between them is indistinguishable by the instrument being used as it is below the level of error. Therefore, these results add less information to the system compared to data points that can be properly quantified. Conversely, reactions that show high degree of activity, i.e., 0 % e.e., are also difficult to derive meaning from. Although the time in which the measurement is taken makes the reaction conditions appear to provide the same response, the route to that same value may be completely different (Figure 32).

It can be a matter of making sure the measurement is taken so that a cross section of the reaction is seen where the difference between the reactions can be observed. For example, in Figure 32, observing the three reactions at

time Observation 1 will make all the reactions seem the same, 0 % e.e. Whereas if a measurement was taken at time Observation 2 then it can be seen that the different experiments are all eliciting a different response. Therefore, it is important to understand the reaction space before carrying out a DoE to make sure as many experiments as possible are adding usable information to the model. Although this can also be an issue for OFAT analysis, as each reaction is dependent on the previous one, the direction of the experiments can be changed in response to the lack of activity or over activity. Whereas the DoE can be completed, involving extensive experimental effort, before it is found that many of the results do not add useable information to the model and significant time can be wasted.
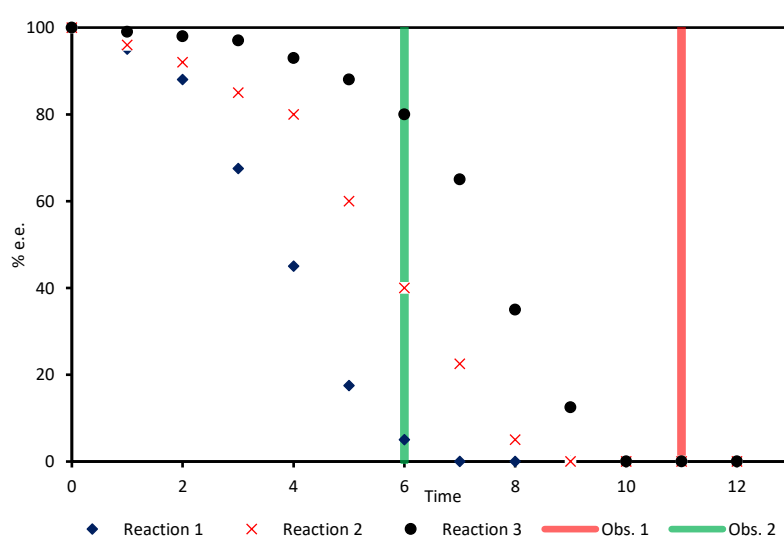
Figure 32 A general graphic to show demonstrate the challenge in differentiating between three low end (0 %) results.

In this DoE three reaction variables, reaction temperature ($100 - 230\ ^{\circ}C$), flow rate ($1 - 7$ mL min^{-1}) and solution concentration ($20.6 - 82.5$ mM) were investigated with respect to their influence on e.e. and selectivity.[118] In this work, JMP software was used to construct an I-optimal split plot response surface design, comprised of 18 experiments. This protocol was used to screen the defined reaction space for main effects, quadratic effects and second order interactions between the input variables. From here the influence of the reaction parameters on the reaction outcomes can be analysed using Analysis of Variance (ANOVA) and linear regression to identify the parameters that are statistically significant.

The I-optimal split-plot design was divided into whole plots, whereby solution concentration was kept the same throughout each whole plot. Solution concentration was deemed a hard to change variable due to the need to completely flush the system at each changeover of feedstock solutions. This would have been a barrier to complete randomisation of the run order and therefore the split-plot method was selected to reduce the number of times this

variable would need to be changed. Using the split-plot method allows the variation between the whole plots to be estimated, acting as a check for potential drift in the system performance over time (i.e., due to catalyst deactivation). At the end of each whole plot the first reaction within that plot with a result that is either at the upper or lower limit would be repeated. This also allowed for catalyst performance to be monitored throughout the DoE by comparison between whole plots.

DoE and flow chemistry work well together as complimentary tools as the data can be collected in a timely manner due to the short reaction times synonymous with flow chemistry. While the ease in which reaction parameters can be changed between runs can reduce deadtime between reactions. This was heightened, in this work, by the particularly short reaction times of 9 – 63 seconds under investigation permitting data to be rapidly generated.

The I-optimal design's 18 experiments were completed within 8 hours. Firstly, ANOVA analysis primarily focusing of a combination of P-values and F-ratio's was used to identify the statistically significant reaction parameters. Following this, a model was created using a Standard Least Squares and Restricted Maximum Likelihood (REML) to construct the model, exploring all primary and secondary interactions of all inputs with respect to e.e. and selectivity. The model was then checked for obvious shortcomings using actual by predicted plots, residuals by rows and studentised residuals.

P-values are a statistical parameter used to either prove or disprove the null hypothesis. The null hypothesis states that "changing the factor setting (reaction parameter) has no effect on the response". The P-value is the probability that the observed response could be due to the natural run-by-run variation present in the system. For example, a P-value of under 0.05 represents a > 95 % chance of the null hypothesis being disproved. Whether or not the P-value is considered to have proven or disproven the null hypothesis, i.e., if it is statistically significant or not, is governed by the α-value. The α-value is the significance threshold, whereby a P-value below that threshold defines that reaction parameter as statistically significant. Commonly an α-value of 0.05 is used but this can be reduced to 0.10, to prevent elimination of reaction parameters that may become significant with additional data. Any parameters P-values above this threshold were discounted from the model, unless appearing as part of lower P-value secondary interactions.

If the null hypothesis is successfully disproven with > 95 % confidence, i.e., the α-value is < 0.05, then the reaction input variable can be deemed statistically significant in the reaction. This analysis was performed on the I-optimal design results and determined that temperature and temperature*temperature were statistically significant with

respect to e.e., while temperature, flow rate and temperature*flow rate were statistically significant with respect to selectivity (Table 22 and 23).

Table 22 I-optimal design screen effects summary for Pd/Al$_2$O$_3$ for e.e..

Entry	Reaction Parameter	P-value	F-Ratio
1	Temp.	< 0.00001	363
2	Temp.*Temp	< 0.00001	96

Despite the predictability of temperatures significance in both outcomes, these results can provide interesting insights into the reaction. With respect to e.e., the lack of significance of flow rate suggests that the speed of the racemisation reaction is extremely fast, occurring on a time scale far quicker than the 9 seconds – the shortest residence times explored in this screen (Table 22). Furthermore, the lack of significance of solution concentration tells us that there is extremely effective diffusion of molecules to and from the active sites of the catalyst, preventing oversaturation at the higher concentration ranges investigated. There is also an interesting temperature*temperature, quadratic term with respect to e.e., meaning there is a parabolic relationship (Entry 2). This suggests that after a certain temperature, further increase in temperature becomes detrimental to decreasing e.e.. This effect may be caused by the rate of by-product formation being sufficiently increased whereby all racemised *S*-**70** material is seconded into the by-product formation pathway. Thus, measuring the e.e. of **70** does not permit the full extent of the racemisation that had occurred to be detected. Rather, this would be more evident by analysing the diastereoisomeric ratio of the by-products.

Table 23 I-optimal design screen effects summary for Pd/A$_2$O$_3$ selectivity.

Entry	Reaction Parameter	P-value	F-Ratio
1	Temp.	0.00001	237
2	Flow Rate	0.00241	15
3	Temp*Flow Rate	0.01910	7

Similar insights can be made with respect to selectivity (Table 23). Temperature once again is the most significant parameter; however, it affects selectivity in a directly proportional, linear fashion (Entry 1). Flow rate is statistically significant with respect to selectivity (Entry 2), which suggests nucleophilic attack of the intermediate imine species occurs on a time scale relevant to the 9 – 63 seconds investigated in this screen. The fact that flow rate only appears to be significant with respect to selectivity, and not to e.e., gives a good indication that we can use flow rate to tune the selectivity of a reaction without sacrificing e.e.. There is a temperature*flow rate quadratic

term (Entry 3), indicates that these parameters are interacting therefore changing one of them will change how the other effects the outcome of the reaction. The lack of solution concentration significance once again suggests that there is effective diffusion to and from the by-product catalysing sites on the support. Furthermore, if by-product formation was occurring in the bulk solution it would be expected that increasing the concentration, especially at high temperature, would decrease the selectivity. However, this was not observed in this screen.

F-ratio analysis is the ratio of "between group variance" and "within group variance", or "explained variation" to "unexplained variation". If the null hypothesis is true, then the variation between and within groups will be very similar, therefore the closer the F-ratio is to 1, the less likely it is to disprove the hypothesis. Conversely, the larger the F-ratio the more confident you can be that the null hypothesis is disproven, and the reaction parameter is statistically significant to the reaction outcome. This can be used to determine the magnitude that the statistically significant effect has on the reaction outcome (Table 22 and 23). In the analysis of e.e. and selectivity it can be seen that temperature is overwhelmingly dominant.

The ANOVA analysis of the model can be visually presented through an actual vs predicted plot (Figures 33a and 33b). This is where a linear regression is plotted showing the difference in the models predicted outcomes against the actual experimental outcomes. R^2 analysis comments on how well the experimental data fits to the model, a value of 1 being a perfect fit. Whereas root mean squared error (RMSE) measures the average of all the residuals, where the residuals are difference between the predicted values and the actual values. A smaller RMSE shows a better fit to the model.
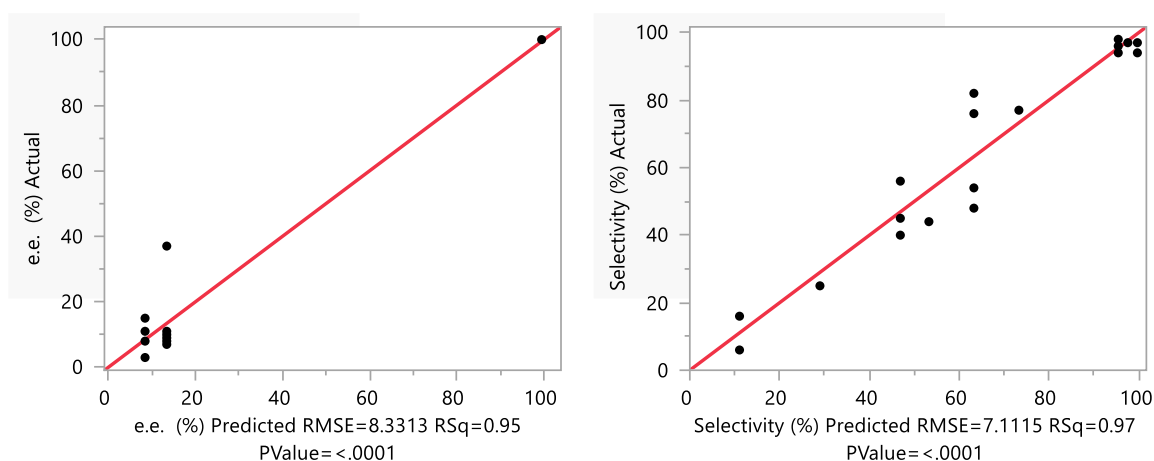

Figure 33 Actual by Predicted plots for the I-optimal design for Pd/Al$_2$O$_3$ with respect to a) e.e. (left) and b) selectivity (right).

The actual by predicted plot for e.e. has a good R^2 values of 0.95 (Figure 33a)., showing the experimental data lies extremely closely to the linear regression, however the RMSE is higher than typically desirable. Unfortunately, the experimental data is largely clustered around 0 – 20 % and 100 % e.e. which is undesirable as it gives a weaker description of the reaction space across the range of e.e.'s. Ideally, more data would be obtained between 20 – 80 % e.e.. Conversely, the selectivity data is spread much more evenly along the linear regression (Figure 33b). This gives a much better description of the overall reaction space. This data also largely lies closely along the regression line with a R^2 of 0.97, however once again the RMSE is larger than desired.

The residuals, the difference between the actual and predicted values, can also be determined from the actual by predicted plots (Figure 33a and 33b). However, multiple data points can sit on top of each other making it hard to visualise. Alternatively, the residuals can be plotted by row, allowing easier analysis across the dataset. This also allows us to compare results between whole plots and any drift in results across the dataset which may be caused by background effects in the DoE such as inaccurate solution preparation or catalyst deactivation. The residuals can be normalised by the standard deviation to give a studentised residual, this can help identify outliers (Figure 34a and 34b). A datapoint is considered to have minimal variation between the actual by predicted value if the studentised residual is between +/- 3. If there is no systematic error in the DoE then the studentised residuals will be randomly distributed around the centre point, 0. This random distribution can be observed in the e.e. and selectivity models (Figure 34a and 34b), however experiment 10 of the analysis of the e.e. response appears to be an outlier.

Figure 34 I-optimal design results for studentised residuals for Pd/Al$_2$O$_3$ with respect to a) e.e. (top) and b) selectivity (bottom).

The Prediction Profiler function in JMP (Figure 35) plots the profile traces for each variable that can be interacted with in real-time. The plots for variables that have secondary interactions are linked, therefore the Prediction Profiler recalculates the profile trace of a given variable if its related variable is changed. This is an extremely effective way to visualise the model and identify key regions of interest.

To increase the predictive power of the model, a greater number of data points for e.e. in the 20 – 90 % region would be desirable. To achieve these e.e. values, the prediction profiler indicated that temperature between 100 and 165 °C would be required, as would flow rates from 1 – 7 mL min^{-1}. Therefore, it was decided to increase the data density in this area of the model by performing an augmented space filling screen, where 6 additional data points were implemented. As part of these experiments, the solution concentration was set to the mid-point, 51.5 mM, as it was deemed statistically insignificant in the I-optimal screen while the temperatures and flow rates were generated by the JMP software within the desired ranges.
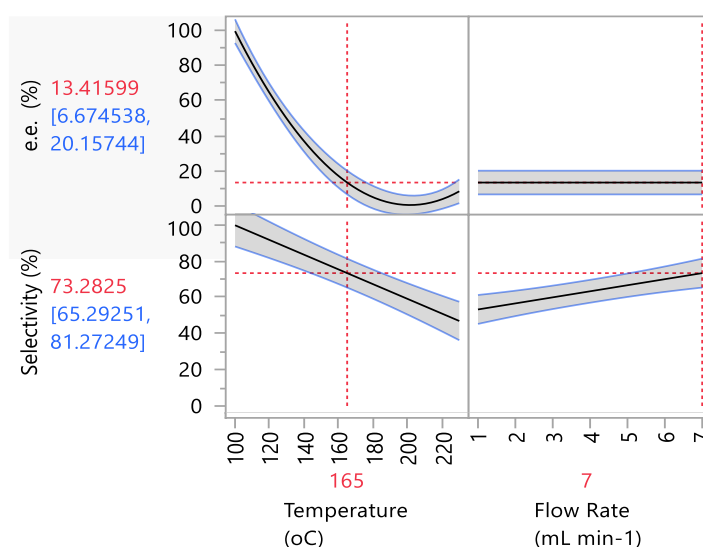
Figure 35 I-optimal design Prediction Profiler for Pd/Al$_2$O$_3$.

3.2.4. DoE Model Validation and Implementation

With this additional data, a new model was created. A similar process of identification of the statistically significant parameters from P-values and F ratios was used (Tables 24 and 25). However, the presence of the temperature*flow rate term for e.e. and the temperature*solution concentration term for selectivity increased the R^2 and decreased RMSE values for both models (Figures 36a and 36b). Therefore, a more lenient α-value of 0.1 was employed for this model, still giving a 90 % confidence in disproving the null hypothesis.

92

Table 24 Augmented design screen effects summary for e.e..

Entry	Reaction Parameter	P-value	F-Ratio
1	Temp.	0.00001	66.5
2	Temp.*Temp	0.00001	43.5
3	Flow Rate	0.04913	4.70
4	Temp.*Flow Rate	0.08189	3.51

Table 25 Augmented design screen effects summary for selectivity.

Entry	Reaction Parameter	P-value	F-Ratio
1	Temp.	0.00001	434
2	Flow Rate	0.00022	50.4
3	Temp.*Flow Rate	0.05205	5.36
4	Temp.*Sol. Conc.	0.09362	3.888
5	Sol. Conc.	0.15924[a]	2.45

[a]Included as it is part of a secondary interaction where α value is < 0.1.

Pleasingly, it can be seen from the actual by predicted plots for e.e. that the 6 additional experiments all fell within the 20 – 90 % range targeted by the augmented design (Figure 36a). Despite this, the R^2 and RMSE were increased from the additional datapoints, however, the additional data allows the model to better describe the full range of reaction space. The additional datapoints further improved the R^2 and RMSE with respect to selectivity, meaning the model is now highly predictive for selectivity across the whole reaction space.
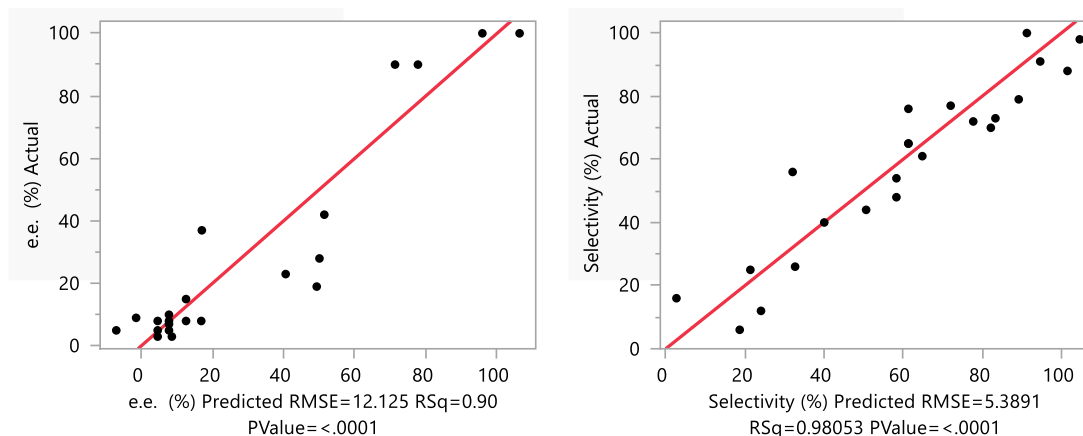
Figure 36 Actual by Predicted plots for the augmented design for Pd/Al$_2$O$_3$ with respect to a) e.e. (left) and b) selectivity (right).

The additional data decreased the R^2 and increased the RMSE for the e.e. model, whereas the selectivity model saw an increase in R^2 and a decrease in RMSE. This suggests there is either a greater degree of error in collecting the e.e. data, or the racemisation reaction is much more sensitive to its reaction parameters therefore any error is magnified in these results. As discussed in Section 2.2.1.3. the uncertainty in the chiral LC method appeared to be +/- 4 %, demonstrating that the error stems from the reaction parameters rather than the analytical method. It may

be that another reaction parameter is affecting the e.e. that was not controlled during the DoE and was therefore unaccounted for. The augmented design model was also deemed to have no systematic error and no outliers from the studentised residuals (Figure 37a and 37b).
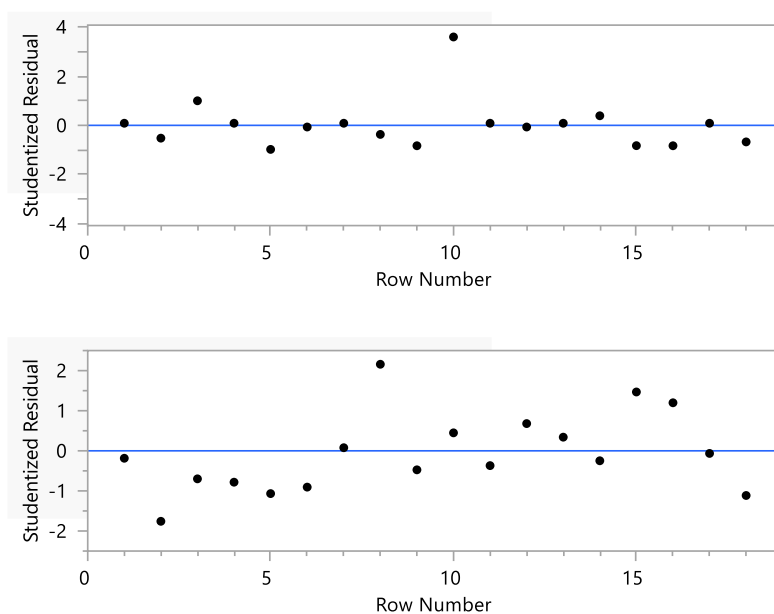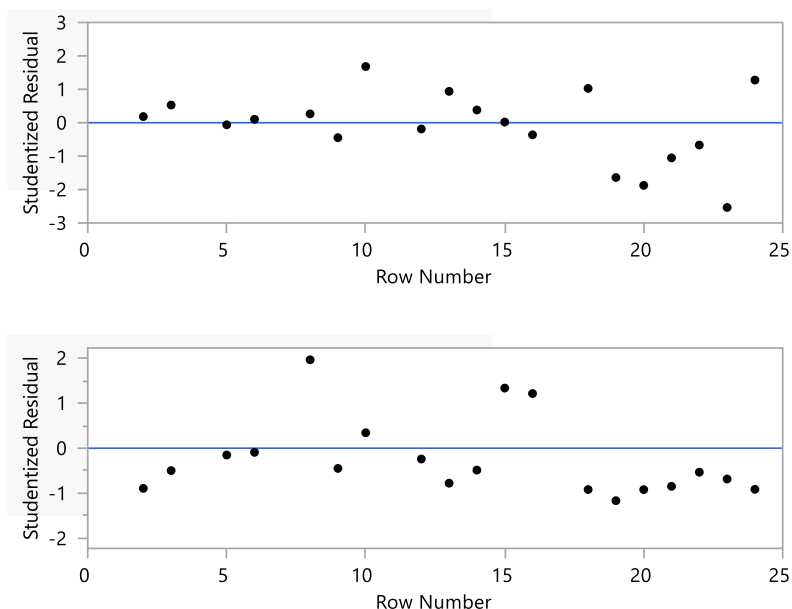

Figure 37 Augmented design results for studentised residuals for Pd/AlO$_3$ with respect to a) e.e. (top) and b) selectivity (bottom).

As the result of the additional data, a more complete model had now been created that can describe the reaction space with respect to e.e. and selectivity through Equations 14 and 15. With this model in hand, validation was required to determine if it was capable of predicting the outcome of the reaction. It was decided to randomly generate 3 sets of reaction conditions and use the model to predict the outcome of these conditions (Table 26, Entries 1 – 3). Subsequently the reaction would be performed experimentally and the alignment between the two values could be investigated. It was expected that the model would be able to predict each value to within +/- 20%, which was considered tolerable for such a relatively limited data set.

$$\text{e. e. } (\%) = 7.82 - 54.8\left(\frac{\text{Temp.} - 165}{65}\right) + 9.23\left(\frac{\text{Flow Rate} - 4}{3}\right) \qquad \text{Equation 14}$$

$$+ 55.7\left(\frac{\text{Temp.} - 165}{65}\right)\left(\frac{\text{Temp.} - 165}{65}\right) - 13.2\left(\frac{\text{Temp.} - 165}{65}\right)\left(\frac{\text{Flow Rate} - 4}{3}\right)$$

$$\text{Sel. } (\%) = 61.3 - 40.0\left(\frac{\text{Temp.} - 165}{65}\right) + 10.7\left(\frac{\text{Flow Rate} - 4}{3}\right) \qquad \text{Equation 15}$$

$$+ 3.03\left(\frac{\text{Sol. Conc.} - 51.6}{31}\right) - 11.0\left(\frac{\text{Temp.} - 165}{65}\right)\left(\frac{\text{Sol. Conc.} - 51.6}{31}\right)$$

94

The predictive power of the model appeared to be much more accurate than originally thought, with all predicted parameters, with the exception of e.e. in entry 2, were predicted to within < 20 %. On average both e.e. and selectivity were able to be predicted within 9 %. Due to the good predictive power of the model, it was decided that it could be used to predict the optimal reaction conditions. To do this the desirability function was employed where a set of desirability criteria were inputted (Table 27). The desirability criteria were chosen to try and maximise racemisation while maintaining > 90 % selectivity. This can be visualised through the Prediction Profiler (Figure 38).

Table 26 Augmented design model prediction of reaction outcomes[a]

Entry	Temp. (°C)	Flow Rate (mL min⁻¹)	Sol. Conc. (mM)	Pred. e.e. (%)[b]	Exp. e.e. (%)[b]	Pred. Sel. (%)[c]	Exp. Sel. (%)[c]
1	165	4	51.6	8	5	63	65
2	125	5.5	51.6	70	90	88	100
3	200	2	51.6	0	< 5	36	26
4	140	7	82.5	-	42	-	91

[a]All experiments started with a solution of optically pure *S* – **70** in anhydrous PhMe. [b] Determined by chiral HPLC. [c]Determined by GC. [d] Values in parentheses predicted by the DoE model

Table 27 Desirability criteria for the optimal racemisation conditions.

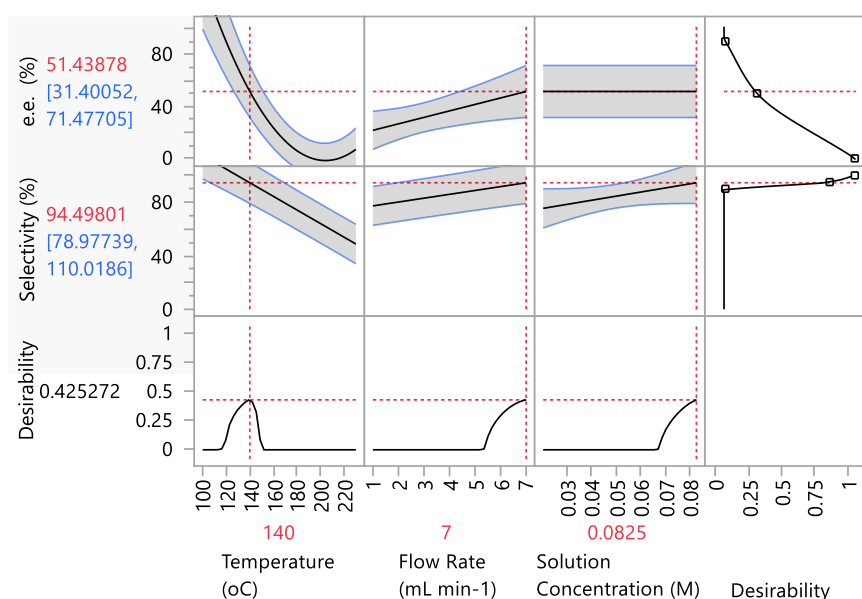| Entry	e.e. (%)	Value	Desirability	Sel. (%)	Value	Desirability
1	High	90	0.01	High	100	0.99
2	Middle	50	0.25	Middle	95	0.8
3	Low	0	0.99	Low	90	0.01

Figure 38 Prediction profiler based on the augment design data with the predicted optimal reaction conditions shown by dotted red lines based on the desirability criteria.

The culmination of this novel approach to the racemisation of chiral amines resulted in the ability to reduce the optical activity of chirally pure S - **70** to 41 % e.e. with 91 % selectivity, in 9 seconds (Table 28, Entry 1). This exponential increase in rate of reaction is evident in the TOF of 218 h^{-1} achieved using FTR. This compares extremely favourably to the previous highest TOF achieved reported by *De Vos* of 62.5 h^{-1}, by 3.5-fold, (Entry 2).[74] Furthermore, this marks a > 36-fold increase compared to the highest TOF achieved in flow using Pd/AlO(OH) of 6 h^{-1} by *Poppe* (Entry 3) both of which require H$_2$ atmospheres to achieve these results. [90]

Transfer hydrogenation mediated heterogeneous amine racemisation has only previously been explored by *Kim* et al. (Entries 4 – 6).[82,83] Wherein, in-house Pd/AlO(OH) was preferred to commercial Pd/Al$_2$O$_3$ as it was found to display greater activity. However, in this work we have not only been able to demonstrate a near 7-fold increase in TOF compared to Pd/AlO(OH) with comparable selectivity, but this was also accomplished with the seemingly less active version of the catalyst (Entries 1 and 4 – 6).

Table 28 A comparison of the best results for the racemisation of S – **70**.

Entry	Catalyst	Reactor	H$_2$ (Y/N)	e.e. (%)	Rac. TOF (h^{-1})	Sel. (%)	Reference
1	Pd/Al$_2$O$_3$	Flow	N	41	218	91	This Work[118]
2	Pd/CaCO$_3$	Microwave	Y	11	62.5	100	[De Vos 2008][74]
3	Pd/AlO(OH)	Flow	Y	4	6.00	98	[Poppe 2018][90]
4	Pd/AlO(OH)	Batch	N	4	32.0	-[a]	[Kim 2010][82]
5	Pd/AlO(OH)	Batch	N	29	5.92	99	[Kim 2007][83]
6	Pd/Al$_2$O$_3$	Batch	N	88	1.00	99	[Kim 2007][83]

[a]Not reported by author.
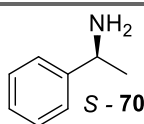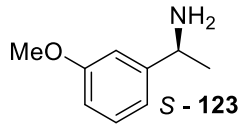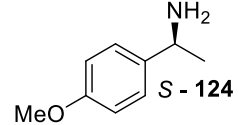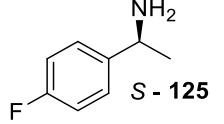
The newly developed FTR strategy allows for extremely fast, selective racemisation in extremely short reaction times. Also, although full racemisation has not been achieved in a single pass, recycling of the reaction mixture through the system is feasible. This marks a hugely important step forward in the field of CE-DKR, and other DKR strategies that requires separate redox racemisations steps. Previously the slow amine racemisation reaction has been the limiting factor that prevents CE-DKR methodologies from being more widely accepted, particularly on an industrial scale. In this proof-of-concept work, we will investigate whether FTR can provide a viable approach to mitigate these drawbacks.
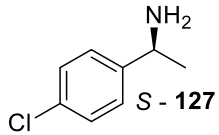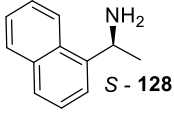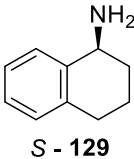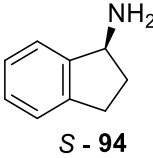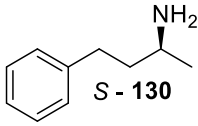
3.2.5. Substrate Scope

With optimised conditions for the racemisation of $S - $ **70** in hand, efforts were made to expand the substrate scope for the Pd/Al$_2$O$_3$ FTR. This would focus on building blocks of relevance to pharmaceutical and agrochemical products (Table 29). It was decided to employ a traditional substrate scope approach and apply the optimal conditions identified for $S - $ **70** to all the substrates, whilst recognising these highly specific reaction conditions may provide false negatives. Therefore, it was decided if no activity was observed then the substrate could be repeated with incremental 45 ℃ increases in temperature. It was hoped that this approach would ascertain catalyst activity for different substrates whilst mitigating the investment of time taken to perform full DoE optimisations for each substrate.

Lack of activity in this substrate scope does not necessarily make FTR unsuited for such a substrate, rather that the given substrate shows poor activity with Pd/Al$_2$O$_3$ FTR under these specific conditions. A repeat of the DoE optimisation strategy could be performed with a new substrate to identify more suitable conditions. Alternatively, substrates of interest could be screened against the catalysts identified in the HTS (Section 2.2.4.) capable of transfer hydrogenation in order to find a more suitable catalyst for the given substrate before subsequent DoE optimisation. However, there will undoubtedly be some substrates that are not capable of undergoing racemisation within the 9 – 63 second time window.
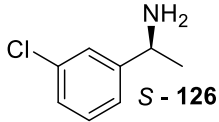
Table 29 Primary amine substrate scope for FTR with Pd/Al$_2$O$_3$.

Entry	Substrate	Temp. (℃)	e.e. (%)	Rac. TOF (h^{-1})	Sel. (%)	Reference
1	(NH$_2$ structure) S - **70**	140	41	218	91	This Work[118]
2		120[a]	11	62.5	100	[De Vos 2008][74]
3	MeO (NH$_2$ structure) S - **123**	185	40	221	83	This Work
4	(NH$_2$ structure) S - **124**	140	85	55.3	97	This Work
5	MeO	120[a]	30	49.2	100	[De Vos 2008][74]
6	(NH$_2$ structure) S - **125**	230	78	81.1	90	This Work
7	F	110	2	0.82	95	[Bäckvall 2002][85]

Entry	Structure					
8	Cl-substituted α-methylbenzylamine, *S* - **126**	230	100	-	97	This Work
9	Cl-substituted α-methylbenzylamine, *S* - **127**	140	100	-	96	This Work
10	naphthyl ethylamine, *S* - **128**	185	94	22.1	97	This Work
11		70	50	0.55	91	[De Vos 2009][88]
12	tetrahydronaphthylamine, *S* - **129**	140	45	203	80	This Work
13		120[a]	44	39.3	100	[De Vos 2008][74]
14	indanamine, *S* - **94**	140	20	295	96	This Work
15		70	3	32.3	N/A[b]	[Jia 2014][91]
16	4-phenylbutan-2-amine, *S* - **130**	230	100	0	87	This Work
17		70	10	0.02	62	[De Vos 2007][75]

[a]Microwave Irradiated Reaction. [b]Selectivity not provided.

Reaction Conditions: 82.5 mM, 140 °C, 7 mL min^{-1}, 200 mg 5 % Pd/Al$_2$O$_3$, PhMe.

As previously discussed, the model substrate *S* – **70** compared favourably to the microwave irradiated method developed by *De Vos* (Table 29, Entries 1 and 2).[74] The development of FTR enables a 3.5-fold increase in the TOF of the reaction while delivering only a slight reduction in selectivity. The expansion of the substrate scope began with the inclusion of electron donating groups (EDG) substituent MeO- in the 3- and 4- positions of the aromatic ring (Entries 3 and 4). Both substrates responded well to the FTR conditions. The racemisation of the 3-MeO, *S* – **123**, showed excellent selectivity, allowing the temperature to be raised to 185 °C to afford 40 % e.e. and 97 % selectivity (Entry 3). This represents a TOF of 221 h^{-1}, higher than that of the model substrate and with improved selectivity. This was a particularly impressive result as racemisation of a 3-MeO substrate has not previously been reported and **123** is a key building block in the synthesis of Tecalcet, a Calcium Channel Agonist (Figure 39).[12] In comparison, the 4-MeO derivative, *S* – **124**, racemises at 140 °C, with 85 % e.e. and 97 % selectivity (Entry 4). This corresponds to a TOF of 55.3 h^{-1} which was a modest increase on the microwave irradiated methodology develop by *De Vos* with comparable selectivity (Entry 5).[74]
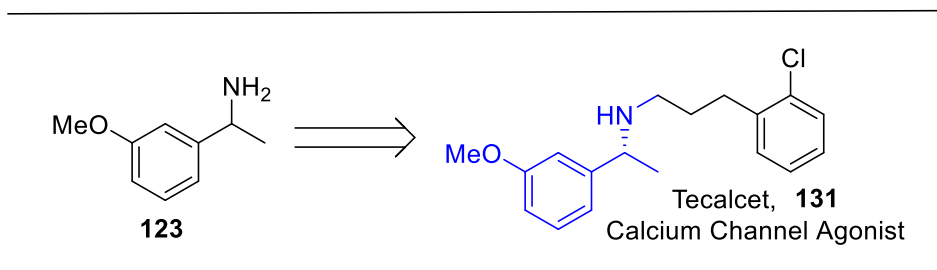
The racemisation of halogen functionalised substrates is rarely reported in literature. To counter this, we attempted to racemise a 4-F analogue, *S* – **125** (Table 29, Entry 6), along with 3- and 4-Cl substrates, *S* – **126** and **127** (Entries 8 and 9). The racemisation of *S* – **125** had only ever been reported twice before, with the best result reported by *Bäckvall* (Entry 7) where 2 % e.e. and 95 % selectivity were reported.[85] Although *Bäckvall* achieved full racemisation, the TOF of the FTR process was nearly 10 fold greater, with a TOF of 81.1 h^{-1} (Entry 6), however temperatures of 230 °C were required to achieve this and the selectivity was slightly lower.

The Cl substituted analogues, *S* – **126** and **127**, were found to be essentially unreactive under the reaction conditions tested (Entries 8 and 9). These would be ideal substrates for resubmission to the HTS to find a better catalyst which can be further developed using DoE. Racemisation of such halogenated substrates would be highly desirable due to their prevalence in medicinal chemistry. The halides can also be further elaborated through cross-coupling chemistry, for example Suzuki, Negishi, Kumada, Buchwald and Sonogashira Couplings. The difficulty in racemising these substrates is supported by the lack of previous literature precedent for the racemisation of amine adjacent to electron deficient aromatic rings. The electron withdrawing groups (EWG) will lead to the benzylic position becoming more electron deficient, making the abstraction of H$_2$ during the initial oxidative step of the racemisation process more challenging, as reflected in the lack of reactivity seen in these results (Entries 8 and 9). Furthermore, the ability of the halogen function to act as a point of derivatisation could also lead to deactivation or by-product formation pathways with cross coupling or dehalogenations reactions beginning to compete with the desired racemisation pathway.

The naphthyl substrate, *S* – **128**, is a building block of the antiparathyroid drug Cinacalcet,**7** (Section 1.) and was shown to be mildly active under the FTR conditions.[21] At 185 °C the e.e. was successfully reduced to 94 %, giving a TOF of 22.1 h^{-1} with 97 % selectivity, although the drop in activity from **70** was surprisingly due to the structural similarity. This result compares favourably to the literature precedent reported by *De Vos* where a drop of 50 % was achieved over 24 hours to yield a TOF of just 0.55 h^{-1} with 91 % selectivity, representing a 40-fold increase in rate using FTR.[88]

The tetrahydronaphthylamine substrate, $S - $ **129** (Table 29, Entry 12), is a widely investigated substrate in the field of amine racemisation and CE-DKR, due to its similarity to the blockbuster drug Sertraline, **1** (Section 1.). Under FTR conditions, this substrate underwent facile racemisation at 140 °C to afford 45 % e.e. and 80 % selectivity (Entry 12). This once again outperformed *De Vos*'s microwave irradiation by > 5-fold (Entry 13), however the selectivity was markedly lower.[74] Due to the reduction in selectivity, re-optimisation of the substrate in a DoE would be preferable but should be possible within the same reaction space explored previously.
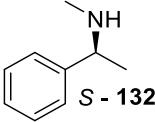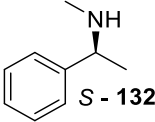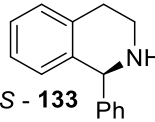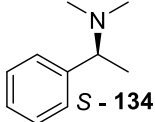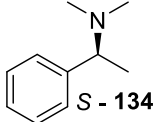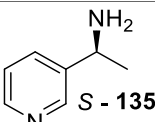
1-aminoindan, *S* - **94**, was also of industrial interest owing to its position as a key intermediate in the synthesis of Rasagiline, **8**, a drug used to treat Parkinson's disease (Section 1).[5] Due to its prevalence in medicinal chemistry, the racemisation of $S - $ **94** has been reported previously, most notably by *Jia* et al., who were able to completely racemise the chirally pure substrate (3 % e.e.) in just 3 hours to give a TOF of 32.3 h^{-1}.[91] Subjecting $S - $ **94** to the FTR conditions at 140 °C yielded and e.e. of 20 % and 96 % selectivity to give a TOF of 295 h^{-1}, which represented a 9-fold increase compared to previous literature.

Racemisation of aliphatic substrates is much less well exemplified in the literature compared to benzylic substrates. However, 4-phenylbutan-2-amine, $S - $ **134** (Table 29, Entry 16), is often used as an example of an aliphatic substrate, owing to its similarity to amphetamine, a common component of psychoactive drugs, or other drugs such a as Tamsulosin.[6] *De Vos* has reported several successful attempts to racemise $S - $ **134** under a H$_2$ atmosphere, the highest TOF of which was 0.02 h^{-1} using Pd/BaSO$_4$ (Entry 17).[75] However, this approach was met with only 63 % selectivity. Alternatively, Raney Ni was shown to complete full racemisation with 100 % selectivity in just 48 hours, however much higher catalyst loadings were used.[87] In this work it was found that no racemisation occurred under the standard reaction conditions. This is postulated to be due to the more challenging reduction of the imine intermediate when it is not in the benzylic position. *Kim* et al., also using transfer hydrogenation with Pd/AlO(OH), noted that their CE-DKR with aliphatic substrates only worked when external H$_2$ was employed.[83] Therefore, a different transfer hydrogenation catalyst identified in the HTS with greater reductive power may be more suitable.

Secondary amines are generally seen to represent easier targets for racemisation as they are less prone to selectivity challenges. A group of secondary and tertiary amines were explored due to their structural similarities to API's: Sertraline*, 2* , Dapoxetine, **3**, Rivastigmine, **4**, and Solifenacin*, 6* (Chapter 1).[1,3,10,11,121] The N-Me derivative, $S - $ **132** (Table 30, Entry 1), was first to be investigated and showed extremely high levels of racemisation. Almost complete racemisation was achieved in just 9 seconds, leading to a TOF of 347 h^{-1}. Although the selectivity was

lower than desired, this is nevertheless an extremely impressive result, outperforming the long standing previous best reported by *Bäckvall* by > 3-fold (Entry 17) in some of the earliest work in the field.[85] *Bäckvall*' s work did pose significantly superior 100 % selectivity, potentially making it still the most desirable approach.

Table 30 Secondary, tertiary and heterocyclic amine substrates for FTR with Pd/Al$_2$O$_3$.

Entry	Structure	Temp. (°C)	e.e. (%)	Rac. TOF (h^{-1})	Sel. (%)	Reference
1	*S* - **132**	140	6	347	83	This Work
2		110	30	105	100	[Bäckvall 2002][85]
3	*S* - **133**	140	30	258	100	This Work
4	*S* - **134**	140	85	55.3	95	This Work
5		90	0	4.80	- [b]	[Blacker 2007][79]
6	*S* - **135**	185	84	59	81	This Work

[a]Microwave Irradiated Reaction. [b] Selectivity not provided.

Reaction Conditions: 82.5 mM, 140 °C, 7 mL min^{-1}, 200 mg 5 % Pd/Al$_2$O$_3$, PhMe

The Solifenacin building block (Section 1.), *S* – **133** (Table 30, Entry 3), returned an extremely impressive result with only 30 % e.e. remaining after a single pass, corresponding to a TOF of 258 h^{-1} with complete selectivity. Racemisation of this substrate has not previously been reported. These extremely encouraging results indicate that an extremely effective CE-DKR process for the synthesis of Solifenacin could be developed.

The N,N-dimethyl derivative *S* – **134** (Table 30, Entry 4), a building block of Dapoxetine, is the only tertiary amine that has been previously reported in literature to have been racemised.[10] It provides an interesting substrate as the assumed mechanism of racemisation using heterogeneous catalysts is initiated through abstraction of a proton from the chiral centre (Scheme 26) to form the imine **136**. However, this is not feasible in the case of *S* - **134** , thus and alternative mechanism must be occurring *via* the enamine, **137**. In this work, the racemisation of the tertiary amine delivers a TOF of 55.3 h^{-1} and selectivity of 95 % (Entry 4), compare this to the N-Me substrate where the TOF is 347 h^{-1} and selectivity is 83 % (Entry 1). It is clear that racemisation is occurring at a slower rate for the tertiary amine than the secondary amine, as the imine product is more stable and therefore more likely to form than the less stable enamine. However, selectivity was observed to be higher for the tertiary amine. The

FTR of $S - 134$ (TOF: 55.3 h^{-1} and 95 % selectivity) (Entry 4) compared favourably to the best recorded case in literature performed by *Blacker*, where a TOF of 4.80 h^{-1} was achieved (Entry 5).[79]

-PdH$_2$ +PdH$_2$

Ph   Ph   Ph

S - 131   136 R - 131

-PdH$_2$

Ph

S - 133

-PdH$_2$ +PdH$_2$

Ph   Ph   Ph

S - 133   137 R - 133
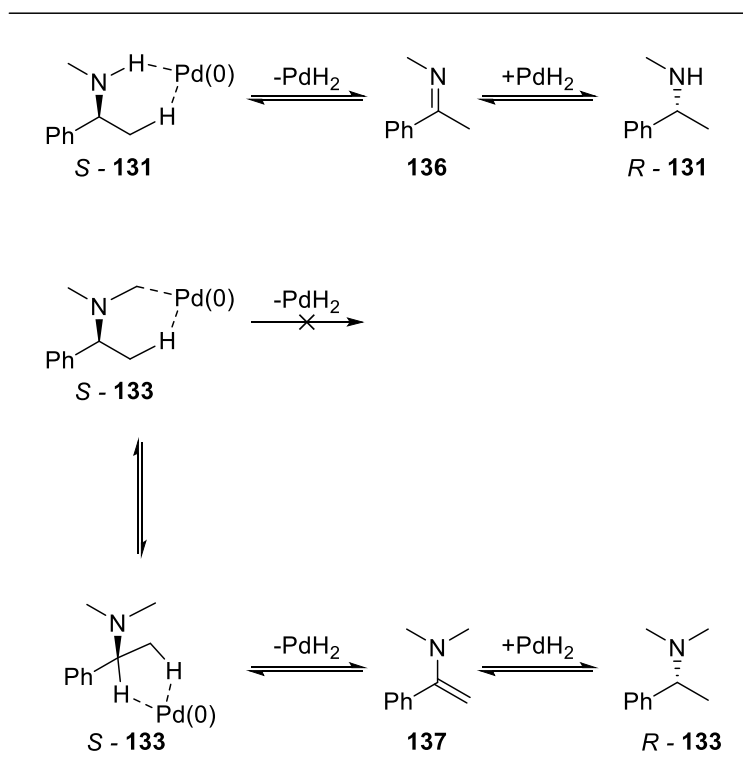
Scheme 26 The mechanism for the racemisation of $S - 131$ and $S - 133$.

The racemisation of heteroaromatic substrates such as, $S - 135$ (Table 30, Entry 6) is of great interest as they are ubiquitous across pharmaceutical and agrochemical industries. However, the only recorded effort to racemise a heteroaromatic substrate (nicotine) was unsuccessful.[79] Initial efforts at 140 °C showed no activity, however raising the temperature to 185 °C gave an e.e. of 84 %, equating to a TOF of 59 h^{-1} which was extremely encouraging. However, the selectivity was reduced to a greater extent than the e.e., 81 %, therefore, re-optimisation of the reaction conditions, or the use of an alternative catalyst may be required for this substrate.

3.3. <u>Conclusion</u>

This work has demonstrated the viability of Pd/Al$_2$O$_3$ as a FTR catalyst in a PBR, and in turn validated FTR as a strategy for the effective racemisation of chiral amines. The Pd/γ-Al$_2$O$_3$ catalysed FTR of S – **70** was investigated using DoE methodology to better understand the reaction parameters and their effects on the outcome of the reaction with respect to e.e. and selectivity. This approach created an accurate model of the reaction space that was capable of both predicting the outcome of reactions as well as generating optimal reaction conditions in line with set desirable criteria. The combination of these approaches enables the efficiency of the racemisation of S-**70** to be increased by 3.5-fold, whilst further advancing the field in its ability to scale up the processes effectively.

FTR with Pd/Al$_2$O$_3$ was also shown to not be limited to S – **70**. The optimised conditions were applied to a variety of substrates with different functionalities, including key intermediates of API's. Many different functionalities were shown to be tolerated under these conditions, with higher TOF achieved by FTR compared to literature precedent. although the selectivity data may be lower than desirable in some cases. Further development of the reaction conditions or an alternative catalyst may be required for these substrates.

The ability of FTR to greatly increase the speed of racemisation of amines has huge implications in the CE-DKR field. Previously amine racemisation has been hugely rate limiting at moderate reaction temperatures, and the constraint this has put on the productivity of CE-DKR has prevented its application as an industrially relevant methodology. In this work we have been able to use super-ambient reaction conditions to speed up the racemisation of amines in continuous flow, using flow rate to drive the selectivity of the reaction, thus negating the need for any external by-product supressing additives to be included in the reaction. This approach was optimised using a DoE strategy that identified reaction conditions capable of achieving the highest TOF for multiple amine substrates. With the rate of racemisation suitably increased it is hoped that this strategy can be employed alongside a complimentary, decoupled enzymatic KR strategy to enable its full potential to be realised. The two independently functioning processes would be allowed to proceed under their own optimal reaction conditions, much like the racemisation and diastereomeric KR adopted by *Blacker*, in order to improve the productivity of the overall process.[97]

Chapter 4: <u>Kinetic Resolution of Racemic Amines</u>

The development of the FTR methodology (Chapter 3) has vastly increased the rate of amine racemisation compared to previous transition metal racemisation strategies employed in both batch and flow. Ultimately, a continuous flow system will be designed and constructed that combines FTR and KR to form a CE-KR process that is scalable (Chapter 5).

In this Chapter we will investigate the use of Novozym-435 as a chiral amine resolving agent. The immobilised lipase is the commercially available form of the CALB enzyme, that has been widely reported for the KR of amines, making it an excellent candidate for our preliminary work. [93,122] The high thermal and chemical stability of Novozym-435 will allow a wide reaction space to be explored, with the hope of significantly increasing the rate and productivity of the process. Alongside its robust nature, the commercial availability of Novozym-435 will aid in the reproducibility of the results.

The aim of this work is to assess and optimise the KR of the primary amine **70** in flow, by employing Novozym-435 in a packed bed. The approach is to utilise data-led DoE strategies to derive a set of reaction conditions that are kinetically aligned with the FTR strategy discovered in Section 3.2.

4.1. <u>Introduction</u>

4.1.1. <u>Novozym-435 Resolution in Batch</u>

The first examples of enzymatic kinetic resolution of the racemic amine **70** were reported independently by *Reetz* et al. and *Gotor* et al. (Table 31) in 1994.[94,123] *Reetz* et al. employed Novozym-435 for the first time, alongside ethyl acetate, **ii**, as the acyl donor (Entry 1), producing *R* - **135** with 43 % conversion and 98% e.e. in 60 hours, corresponding to a STY of 2.87 μmol mL^{-1} h^{-1}. Shortly afterwards *Gotor* et al. reported the same yield and selectivity by employing CALB alongside the ethyl acetoacetate, **iii**, as an acyl donor (Entry 2), to attain an improved, 2-fold increase in STY (5.97 μmol mL^{-1} h^{-1}).[123] The improved STY was possible due to the almost 3-fold increase in TOF of *Gotor*'s process, calculated through Equation 16. Unfortunately, the TOF of the KR processes could only be calculated for Novozym-435 as it was the only form of CALB where the number of active sites has been reported through a series of titration experiments.[124] However this pertains directly to the use of Novozym-435 in the later work described in this chapter.

$$\text{Batch TOF of KR (h}^{-1}) = \frac{\text{Conversion (\%) x Amine (mmol) x 60}}{\text{Number of Enzyme Active Sites (mmol) x Reaction Time (min)}} \qquad \text{Equation 16}$$

Hult and *Kanerva* both employed solvent free reaction conditions to improve the STY of the KR (Table 31, Entries 3 and 5).[125,126] *Hult* was able to achieve complete conversion and 95 % e.e. of *R* - **135** over 140 hours, aided by the use of reduced pressure to of 0.06 bar, driving the equilibrium controlled reaction, to elicit a 3-fold increase on *Gotor*'s work (Entry 2). While *Kanerva* achieved equivalent conversation and 97 % e.e. over 6 hours to deliver a huge leap forward in STY to 604 µmol mL^{-1} h^{-1}, representing a 33-fold increase compared to *Hult* et al. (Entry 3), alongside a 45-fold increase in TOF. The increased productivity of the reactions was due to the solvent free conditions that reduced the overall reaction volume. This also increased the substrate concentration which can increases the rate of the KR, as described by the Michaelis Menten Equation (Equation 17).

$$V_o = \frac{V_{max}[S]}{k_m + [S]} \qquad \text{Equation 17}$$

Initially, increasing concentration increases rate, following 1st order kinetics, which can be seen in *Kanerva*'s work.[127] However, too high a concentration can saturate the enzyme's active sites, and therefore further increases in substrate concentration will not result in further increases in rate, following 0 order kinetics. This could explain the significant increase in reaction time from 9 – 60 hours (Entries 1 and 2) to 140 hours (Entry 3) observed in *Hult*'s work.

Gil et al. employed higher temperatures (Table 31, Entry 4), attempting to exploit the high thermal stability of CALB to increase the rate of reaction and produced *R* – **135** with full conversion and > 99 % e.e.[93,122,128] Despite diluting the reaction through the reintroduction of solvent, *Gil* was able to achieve a STY of 12.5 µmol mL^{-1} h^{-1}, a 2-fold increase in STY and 1.5-fold increase in TOF, compared to the previous solvent containing reactions (Entries 1 and 2). The relatively high productivity achieved by *Gil* was surprisingly achieved while using a carbonylic acid, **v**, as the acyl donor. This is possible as the alcohol leaving group is not present during the enantioselective step, described in Section 1.5.3.. However, use of a carboxylic acid would create an equilibrium between the protonated and unprotonated form of the amine, impairing its nucleophilicity.

Acyl Donor, CALB

70   R - **135**   S - **70**

i   ii   iii   iv   v

vi   vii   viii   ix
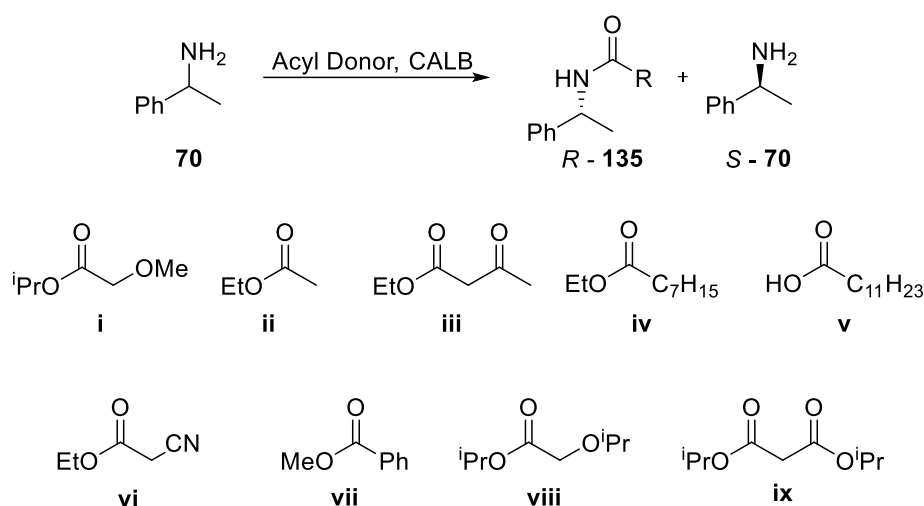
Table 31 A summary of the CALB mediated kinetic resolution of **70**.

Entry	Temp. (ºC)	Time (h)	Conc. (mM)	CALB (mg mmol^{-1})[a]	AD (Equiv.)	Conv (%)	Amine e.e. (%)	Amide e.e. (%)	STY (μmol mL^{-1} h^{-1})	TOF (h^{-1})	Reference
1	Room Temp.	60	400	50	**ii** (4)	43	74	98	2.87	102	[Reetz 1994][94]
2	30	9	125	120	**iii** (1)	43	75	> 98	5.97	284	[Gotor 1994][123]
3	39[b]	140	-[e]	25	**iv** (1)	51	99	95	18.2	104	[Hult 1996][126]
4	80	4	100	100	**v** (1)	50	> 99	> 99	12.5	446	[Gil 2007][128]
5	23	6	-[c]	12.5	**i** (1)	50	98	97	604	4762	[Kanerva 2012][125]
6	Room Temp.	4	205	244	**vi** (1)	48	90	99	24.4	176	[Hornyánszky 2015][129]
7	45	45	620	81	**vii** (1)	19	23	99	0.82	37	[Patti 2018][130]
8	30	1	778	19	**viii** (1)	29	>99	40	229	N/A[d]	[Poppe 2018][131]
9	40	4	2500	40	**ix** (2)	45	82	>99	281	N/A[d]	[Poppe 2022][132]

[a]mg of Novozym-435 per mmol of substrate. [b]Reduced pressure 0.06 bar. [c]Solvent free, volume of reaction for STY determined by volume of acyl donor. [d]Could not be determined due to lack of reporting of active sites of the CALB.

Hornyánszky, Patti and *Poppe* made more valuable contributions to the field (Table 31, Entries 6, 7 and 9) by employing acyl donors that install desirable functionality in the final molecule.[129,130,132] *Hornyánszky* notably used **vi** to allow for further functionalisation of the side chain through a Knoevenagel reaction (Scheme 27), with a suitably functionalised aryl aldehyde. This allows a family of Tyrphostins to be synthesised, **137**, which are used extensively in medicinal chemistry as inhibitors of protein tyrosine kinases.[129] Although the productivity (24.4 μmol mL^{-1} h^{-1}) suffered slightly, this reaction was able proceed with 48 % conversion and 99 % e.e. of the amide over 4 hours and allowed for key functionality to be installed in subsequent steps.
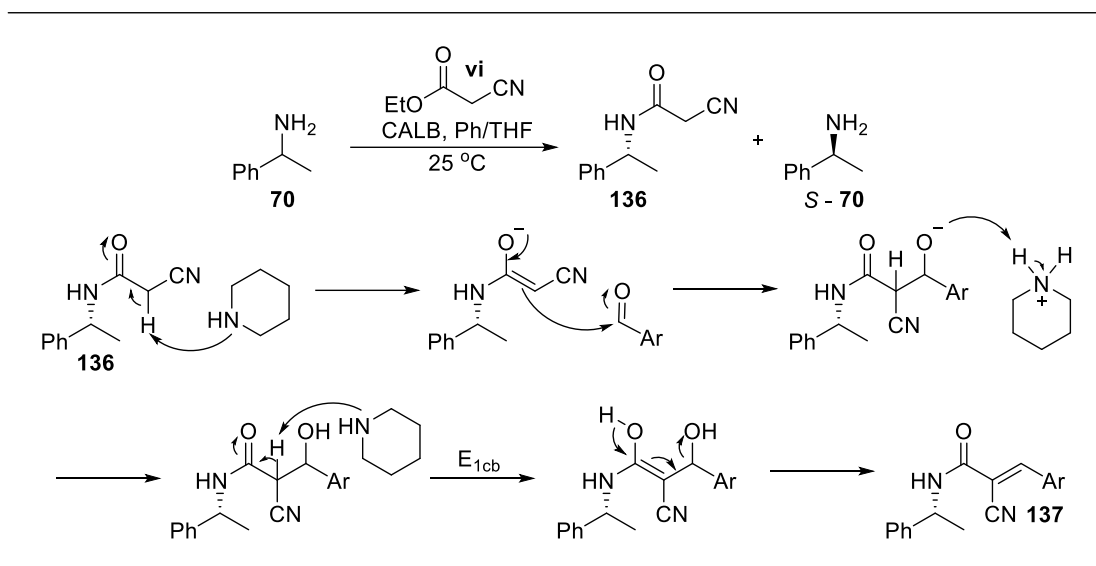
Scheme 27 Installing Michael donor functionality to chiral amines using a CALB mediated kinetic resolution to set up a Knoevenagel condensation reaction to produce Tyrphostins.[129]

Patti was able to perform a benzylic amide coupling, using acyl donor **vii** (Table 31, Entry 7), considered one of the hardest to perform with conventional amide coupling agents. The challenging benzylic amide coupling was observed to proceed much more slowly than other CALB KR reactions, with a 127-fold drop in TOF compared to *Kanerva* (Entry 5), achieving on 19 % conversion after 45 hours to give a STY of just 0.82 µmol mL^{-1} h^{-1}. Despite the reduced rate of reaction, this marks an extremely desirable transformation as it enables the direct synthesis of chiral benzyl amides with an e.e. of 99 %. This motif is widely found throughout natural products, medicinal chemistry and agrochemistry (Figure 40) in molecules such as *taxol*, *fezolinetant* and *Flamprop*.[8,133,134]
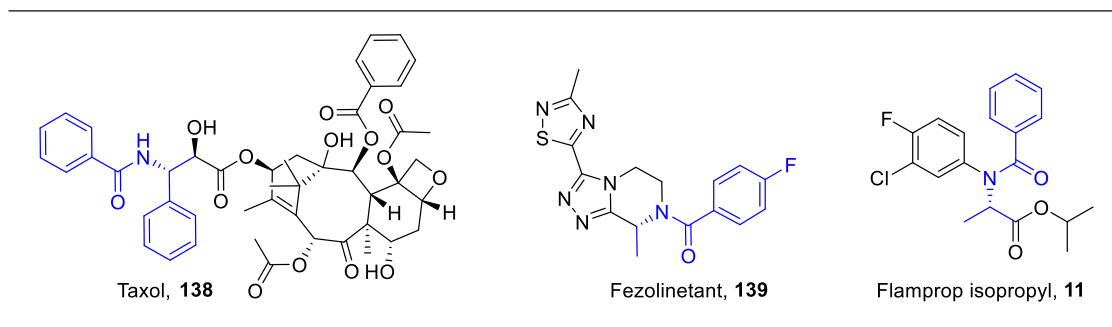
Figure 40 Chiral benzyl amides featuring in natural products, API's and Agrochemicals. [8,133,134]

4.1.2. The Effect of the Acyl Donor on Enzymatic Kinetic Resolution

Many variations in reaction conditions have been noted in the plethora of reported KR of **70** (Table 31). However, multiple reaction parameters are changed between each reported result making it difficult to fully understand the influence of an individual parameter on the outcome of the reaction. Although the effect of both the substrate concentration and enzyme loading can be predicted with Equation 17, the impact of the acyl donor on the enantioselectivity and rate of the reaction are harder to predict. To investigate the effect of the acyl donor on the reaction, a more methodical approach would need to be taken to allow an accurate comparison between reactions.

Patel and *Gil* both investigated a range of fatty acid acyl donors (Schemes 28) and their effect on the KR of **134** and **140**.[128,135] Both studies observed that the length of the lipophilic side chain could influence both the enantioselectivity and rate of the resolution (Figures 41 and 42). However, the optimal sidechain length appeared to be around C-8, with further homologation of the chain yielding no additional benefit to enantioselectivity or rate. The influence of lipophilicity on the reaction is thought to stem from the lipophilic nature of the CALB's large pocket. This means favourable lipophilic interactions can form with the side chain, however, there appears to be a limit to this effect when a side chain greater than C-8 is used.[128]
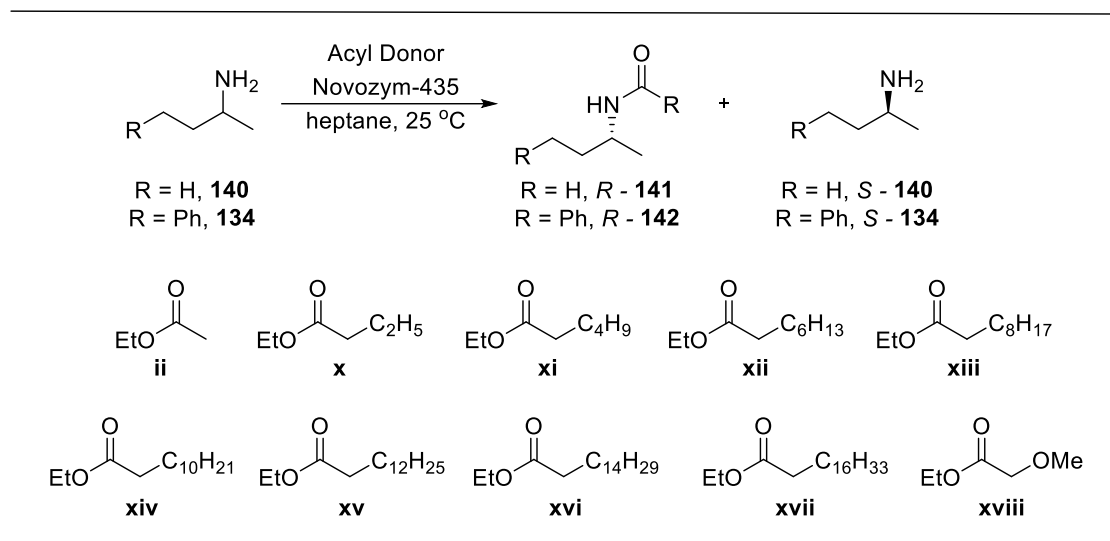
Scheme 28 Screening different acyl donors for the kinetic resolution of **134** and **140**. Reaction Conditions: *Patel*: Amine (0.5 mmol), 0.5 equiv. acyl donor, Novozym-435 (50 mg), heptane (1 mL), 25 °C, 7 days. *Gil*: Amine (1 mmol), 1 equiv. acyl donor, Novozym-435 (200 mg), heptane (10 mL), 80 °C, 1 – 8 hours [128,135]
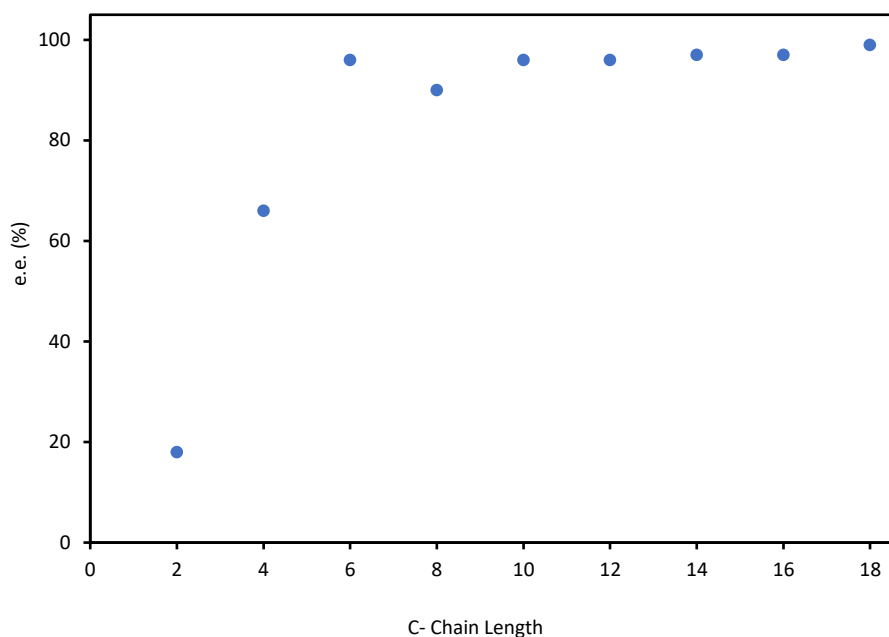
Figure 41 The effect of acyl donor side chain length (Scheme 28) on the enantioselectivity of **140** after 7 days. [135]
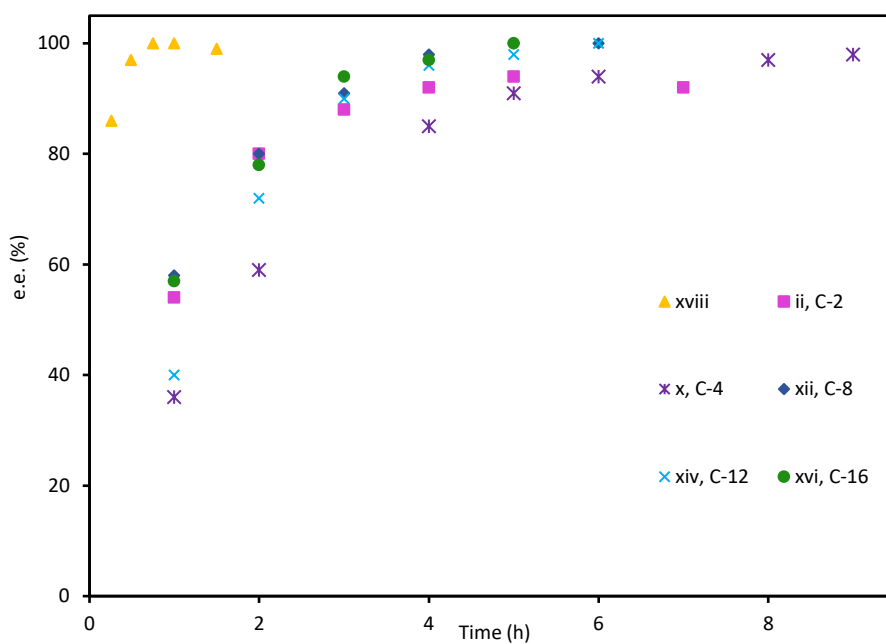
Figure 42 The effect of acyl donor on the kinetic resolution of **134** (Scheme 28).[128]

Gil et al. observed that **xviii** had a far greater rate of reaction compared to the lipophilic acyl donors, while delivering comparative enantioselectivity (Figure 42).[128] This phenomenon was explored by *Park* et al. (Scheme 29) using a related *Burkholderia cepacia* lipase (BCL), a related lipase enzyme. It was observed that reactions containing acyl donors with an ether side chain, such as **xix**, **xx** and **xxi**, proceeded at a far greater rate than acyl donors with alkyl side chain (Scheme 29), such as **xxii**.[136] Initially it was suspected that the O in the side chain

was affecting the resolution through an inductive effect.[136] However, the analogous experiments performed with

143 (Scheme 29) did not yield the same trend.
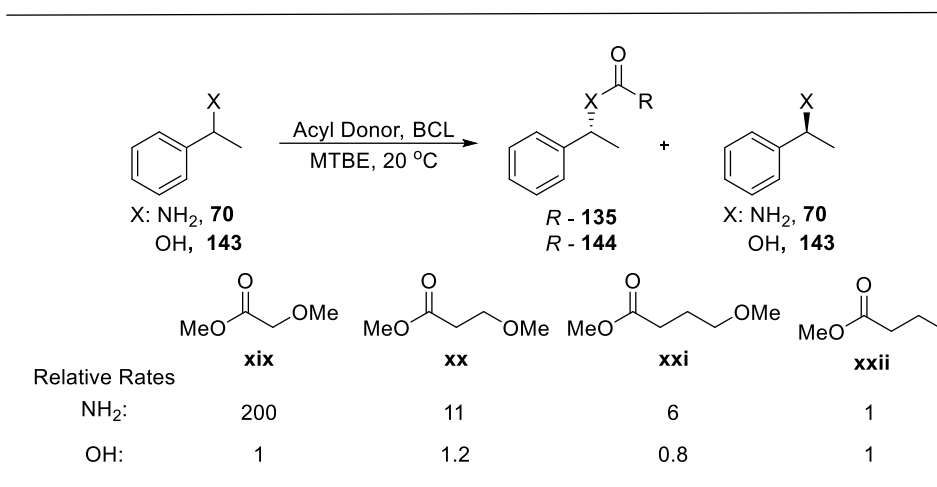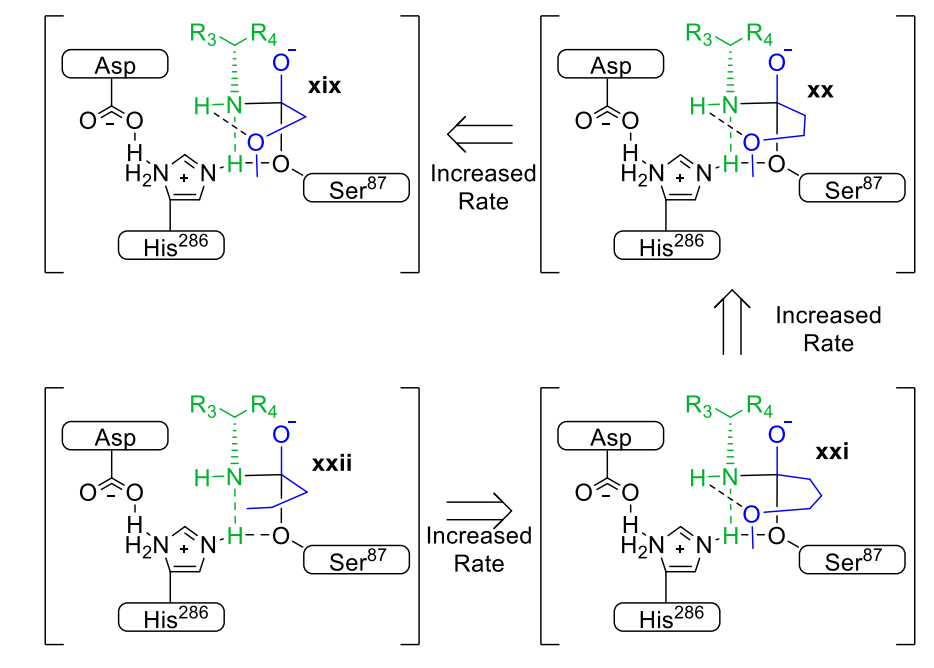
The BCL enzyme used by *Park* had the same Ser-His-Asp catalytic triad as CALB (Scheme 30) and it was

suggested that following the deprotonation of **70** by the His-286, the remaining N-H was forming a H-bond with

the ether side chain, of **xix**, **xx** and **xxi**, in the tetrahedral transition state thus helping to drive the rate of reaction.[137]

However, the increase in rate becomes less pronounced with homologation of the chain (Scheme 29 and 30),

increasing the ring size in the intermediate. This H-bond would not be observed with **143** as there would be no remaining O-H bond following the His-286 mediated deprotonation. The proposed H-bond formed during the tetrahedral intermediate was supported through molecular modelling.

Due to the desirable high rate of reaction and enantioselectivity of the **xix**, further investigation was conducted by *Poppe* into this class of acyl donor. This work focused on the impact that the size of the pendant alkoxy group on the rate of the KR of **70** (Scheme 31), comparing acyl donor **i**, **vii**, **xxiii** and **xxiv**.[131] It transpired that the order of reactivity was ^{i}PrO > EtO > BuO > MeO, with a steady increase in rate being observed. This trend correlated with the inductive power of the alkyl group, with the stronger inductive nature leading to a higher rate of reaction. The greater inductive power, the greater the electron density on the O atom to strengthen the H-bond in the tetrahedral intermediate (Scheme 30).
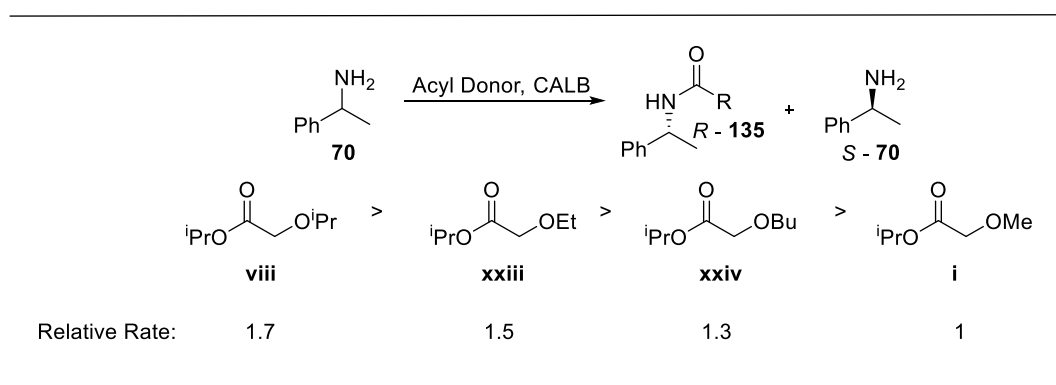
Scheme 31 Relative rate of alkoxy isopropyl ester acyl donors for the resolution of **70**.[138]

Bäckvall et al. provided some insight into the effect of the leaving group (Table 32) during the scale up of their CE-DKR of **70**.[86] It was observed that increasing the size of the alkyl group from Me < Et < ^{i}Pr, increased the yield of the reaction. However, this increase in yield is accompanied by a decrease in enantioselectivity. The stability of the leaving group can explain this trend, as the greater the stability of the leaving group the faster both the desired catalysed reaction and the competitive uncatalysed amidation reaction will occur. A compromise can be achieved with EtO donor (Entry 2) where both high e.e. and yield are achieved.
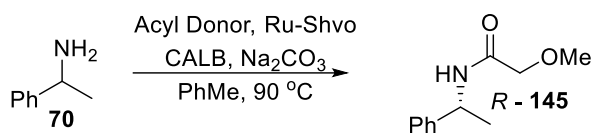
Table 32 The effect of acyl donor leaving groups on the CE-DKR of **70**.[86]

Entry	Acyl Donor (Leaving Group	e.e. (%)	Yield (%)
1	**xix** (MeO)	97	89
2	**xviii** (EtO)	95	96
3	**i** (iPrO)	88	97

Reaction Conditions: Amine (1 mmol), 1 equiv acyl donor, Rac. Cat. (1 mol %), CALB (10 mg), Na2CO3 (20 mg), 2.5 equiv diisopropylmethylalcohol, PhMe (5 mL), 90 °C, 72 hour.

4.1.3. <u>Novozym-435 Resolution in Flow</u>

Molinari et al. outline the many advantages of performing biocatalytic processes in flow, chief amongst which are the highly effective catalyst loading, good mass transfer and low mechanical stress.[139] Biocatalytic processes can proceed slowly in comparison to chemical transformations, therefore the higher effective concentration of enzyme to substrate that a PBR provides can be key to increasing the rate of reaction to industrially significant rates. Despite this, use of immobilised enzymes in flow is still economical as the overall loadings remain low when averaged out across the amount of product produced. Finally, because the mixing in the PBR system is no longer performed by mechanical stirring, the potential for the breakdown of the immobilised enzyme through mechanical sheering force (Figure 43) can be minimised.[122] This gives the enzyme a longer lifetime and allows it to be reused multiple times without any loss of activity. This further increases the cost efficiency of the catalyst as the overall loading of the enzyme relative to the material produced will be decreased with each reuse.

a) Before stirring b) After stirring
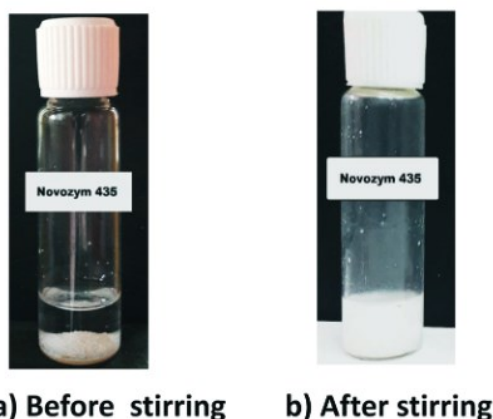
Figure 43 The effect of mechanical stirring on immobilised enzymes, specifically Novozym-435.[122]

Despite the clear advantages of performing the CALB mediated KR of amines in continuous flow, there remains very little published work in this area (Table 33). [89,90,138,140] *Miranda* et al. made the most significant early contributions to the field in 2013 (Entries 1 – 4), exploring the effects of different acyl donors and performing significant cost effective scale up to resolve 5 g of **70** (Entry 2). [140] *Poppe* successfully built on this work with two publications in 2018 (Entries 5 and 6), improving the STY of the processes and expanding the substrate scope to encompass wider amine functionality. [90,138] All three of these systems used similar, basic, flow systems (Figure 44), but notably none of them employed a recycle loop, restricting the system to long residences times to achieve full conversion in a single pass. Once again, TOF would be used to quantitatively compare each process and would be redefined in a flow setting by Equation 18.

$$\text{Flow TOF of KR. (h}^{-1}) = \frac{\text{Conversion (\%) x Volume of Reactor (mL) x [Amine]}_{\text{Initial}} \text{ x 60}}{\text{Number of Enzyme Active Sites (mmol) x } \tau \text{ (min)}} \qquad \text{Equation 18}$$

Miranda: Novozym-435   *Poppe*: CALB-TDP10   *Poppe*: CALB-CV-T2-150
25 - 70 °C   60 °C   60 °C
τ: 4 - 40 min   τ: 160 min   τ: 16 min
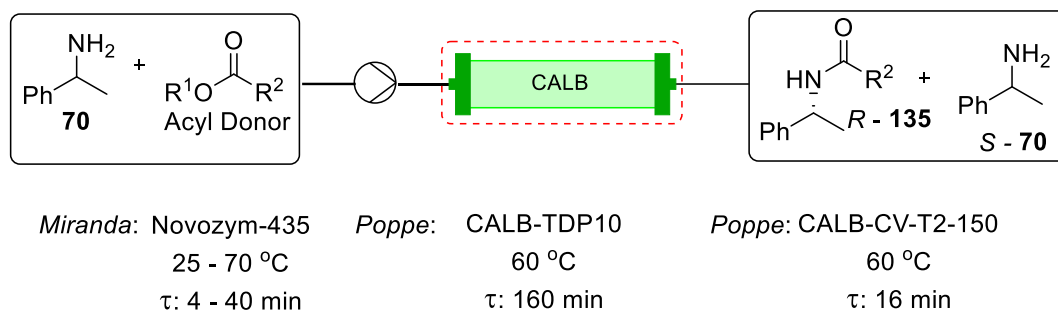
Figure 44 The KR continuous flow system used by *Miranda* and *Poppe*[138,140]

Miranda et al. first focused on transitioning the KR of **70** into continuous flow, using acyl donor **ii** due to its readily available nature (Table 33, Entry 1). Extremely encouraging results were obtained, achieving a STY of 58.6 µmol mL^{-1} h^{-1} while maintaining a selectivity factor of > 200. This illustrates the great advantage of performing KR in flow, as this reflects a 20-fold increase in STY compared to the equivalent batch process reported by *Reetz* et al. (Table 31, Entry 1). More generally the advantage of flow can be seen in that while using **ii**, an acyl donor renowned for slow reaction rates, *Miranda* was able to reported higher STY than 6 out of the 9 batch processes (Table 31,Entries 1 - 4, 6 and 7), by reducing the reaction time to 40 minutes.
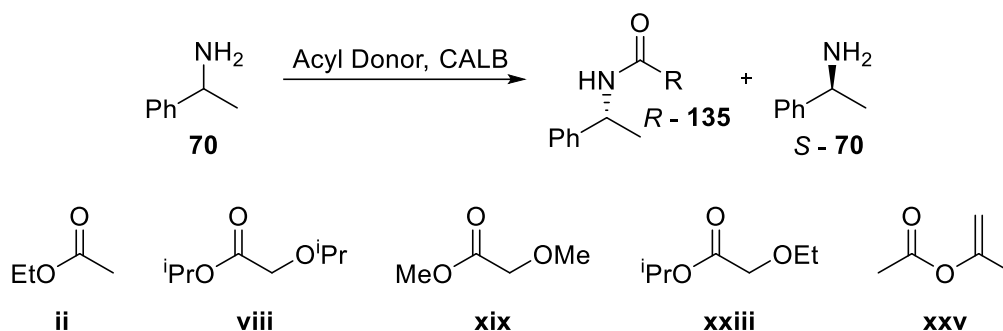
Table 33 A summary of the use of CALB in continuous flow to resolve **70**.

Entry	Temp. (°C)	τ (min)	Conc. (mM)	CALB (mg mmol^{-1})[a]	AD (Equiv.)	Conv (%)	Amine e.e. (%)	Amide e.e. (%)	STY (μmol mL^{-1} h^{-1})	TOF (h^{-1})	E	Reference
1	70	40	80	4456	**ii** (4)	48	94	99	58.7	115	> 200	[Miranda 2013][140]
2	70	40	900	396	**ii** (4)	42	72	99	578	1136	> 200	[Miranda 2013][140]
3	70	8	80	4456	**xix** (4)	50	99	98	306	601	> 200	[Miranda 2013][140]
4	25	40	80	4456	**xxv** (4)	54	91	79	66.0	130	28	[Miranda 2013][140]
5	60	160	136	1942	**xxiii** (2)	50	99	99.9	25.4	N/A[b]	> 200	[Poppe 2018][90]
6	60	16	650	407	**viii** (0.6)	46	85	99.7	1099	N/A[b]	> 200	[Poppe 2018][138]

[a]mg of Novozym-435 per mmol of substrate (in the PBR). [b]Couldn't be determined due to lack of reporting of active sites of the CALB.

The flow system also allowed for a straightforward scale up of this process (Table 33, Entry 2) by simply increasing the concentration of the reaction conditions. Although the STY and TOF were significantly increased by almost 10-fold to 578 μmol mL^{-1} h^{-1} and 1136 h^{-1} respectively, the conversion of the process dropped by 6 % while the selectivity of the process is maintained at > 200. It is likely that the residence time of the reaction is now too short to achieve full conversion over the same 40 minute residence time. This demonstrates how highly efficient biocatalytic flow processes can be on a multi gram scale, while achieving close to the highest STY reported for the KR of **70** to date (Table 31, Entry 5).

Miranda then switched the acyl donor to **xix** (Table 33, Entry 3),which increased the TOF of the reaction by >5-fold compared to acyl donor **ii** (Entry 1). This allowed the residence time to be further reduced from 40 to 8 minutes, resulting in a > 5-fold increase in STY compared to the analogous **ii** condition (Entry 1), while maintaining an excellent enantioselectivity. The greater efficiency of the KR afforded by **xix** means that the STY of the large scale process (Entry 2) is less than 2-fold more efficient, while increasing the concentration by 11-fold.

In contrast, less success was seen using acyl donor **xxv** (Table 33, Entry 4), where it was hoped that the increased stability of the leaving group, compared to **ii**, would increase the STY through a higher rate of reaction, allowing

shorter residence times to be used. Although the productivity of the reaction increased slightly compared to acyl donor **ii,** with a STY of 66.0 µmol mL^{-1} h^{-1} (Entry 1 and 4), a significant drop in the chemo and enantioselectivity of the reaction was observed. The selectivity factor fell from > 200 to 28, while a 9 % loss of material was also observed. This was also previously observed by *Bäckvall*, who associated the increased stability of the leaving group with the increase of competitive uncatalysed reactions occurring even at 25 °C.[86] The loss of material was a result of the amine, **70**, reacting with the acetone by product, **146**, to form imine, **147** (Scheme 32).
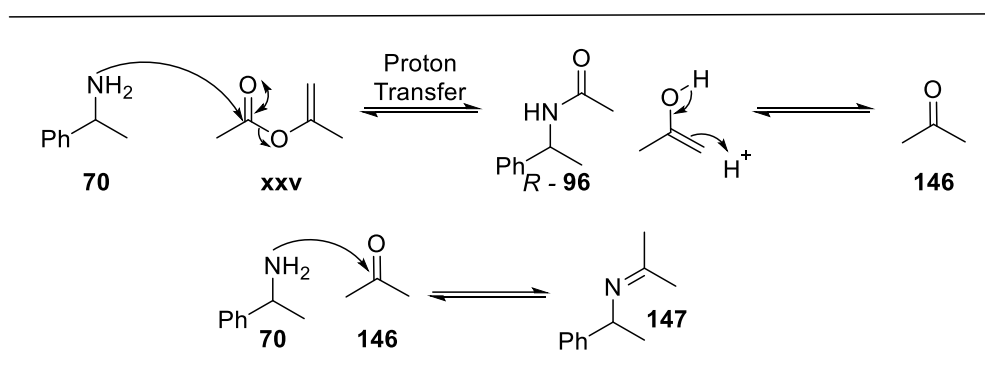
Scheme 32 By-product formation during the Novozym-435 resolution of **70** using isopropenyl acetate as an acyl donor.

Poppe et al. initially made great contributions to the field in 2018 by applying continuous flow KR to a wider selection of racemic amine substrates.[90] However, this work was hampered by lower STY due to the extremely long residence times of 160 minutes, required to achieve full conversion (Table 33, Entry 5). This shortcoming was addressed by the same group later that year with huge strides forward in the productivity and efficiency of the reaction (Entry 6), using a novel isopropyl ether acyl donor, **viii**.[138] During this work a conversion of 46 % was achieved at short residence times of just 16 minutes to deliver a STY of 1099 µmol mL^{-1} h^{-1}. This represents an almost 2-fold increase in STY compared to the scale up conducted by *Miranda* (Entry 2) with comparable selectivity factors. However, *Miranda* et al. were able to achieve their 578 µmol mL^{-1} h^{-1} STY using the less reactive **ii** as an acyl donor to afford a more cost effective transformation.

Interestingly *Poppe* et al. opted to use different forms of immobilised CALB enzymes, CALB-TDP10 (Entry 5) and CALB-CV-T2-150 (Entry 6).[90,138] Both of these catalysts were found to possess a lower thermal stability compared to Novzoym-435, with an upper limit of 60 °C, whereas Novozym-435 has extensively been used up to 100 °C.[86,90,91,140,141] This may have been inconsequential, however the upper limit of 60 °C is used in the both KR conditions, signifying that the productivity of the process may be limited by the inability to further increase the temperature. Having the ability to access high temperatures may have enabled a higher rate of reaction for the KR, thus allowing a shorter residence time to be used, and consequently increasing the STY. Furthermore, greater

thermal stability of the enzyme would allow greater compatibility with the racemisation catalyst in the mixed PBR discussed in Section 3.1.2.

Despite the greater productivity of these flow reactions (Table 33), as indicated by the increase STYs, the efficiency of the enzyme itself has not been notably increased compared to the batch processes (Table 31), as indicated by the similar TOF's reported. This is predominantly because of the longer reaction times permitted by batch processes, which allows significantly lower enzyme loading to be employed. However, it is important to recognise that the purpose of the use of flow for the KR of amines is to increase the throughput of material, which can be seen to have been very successful.

Furthermore, it can be seen that the TOF of the KR processes are approximately an order of magnitude greater than the racemisation reaction reported in Chapter 3. This is a product of how the values are calculated, since the racemisation TOFs are based on the total number of mols of the transition metal, whereas the KR TOF is calculated from the number of enzyme active sites available (based on the availability of information). In reality, the number of active sites on the heterogeneous racemisation catalysts would be significantly smaller, which would give a larger TOF, as demonstrated by *De Vos*[88]. With this in mind, direct comparisons between the racemisation and KR TOF values are not possible, although, they serve as a good quantitative comparison between reactions in the same class.

This work by *Poppe* and *Miranda* illustrates the advantages of performing KR processes in flow, compared to batch (Tables 31 and 33). Overall reaction times have now been reduced by 7.5-fold to 8 minutes (Table 33, Entry 3), compared to the fastest batch reaction of 1 hour (Table 31, Entry 8). The use of continuous flow also enabled the STY to be increased by almost 2-fold compared to the best batch process (Table 31, Entry 5) using an analogous acyl donor. Additionally, *Miranda* was able to demonstrate the scalability of the flow process (Table 33, Entry 2), to resolve **70** on a 40.5 mmol (4.91 g) scale.

4.2. <u>Results and Discussion</u>

Miranda and *Poppe* were able to demonstrate the ability to transition the KR of **70** into continuous flow.[90,140] During this work *Miranda* also reported a multigram scale resolution (Table 33, Entry 2), however the productivity was drastically reduced by the low reactivity of the acyl donor. This limited the reaction to the long, 40 minute, residence time that could not deliver full conversion. None-the-less this work delivered a STY of 578 μmol mL^{-1} h^{-1}, comparable to the 604 μmol mL^{-1} h^{-1} batch process reported by *Kanerva* (Table 31, Entry 5). Efforts by *Poppe*

to increase the productivity of the resolution were successful, achieving an STY of 1099 μmol mL^{-1} h^{-1} (Table 33, Entry 5), with a residence time of 16 minutes, however the scale of this process was limited to less than 1gram. Ultimately, it still remains for a process to demonstrate the ability to perform highly productive KR on a gram scale.

The overall FTR-CE-DKR system that we plan to develop will be created will utilise two sequential PBRs to perform the KR and FTR processes. For this to be achieved in a batch-recycle flow system, the two processes must operate on similar timescales. Although residence times can be manipulated by changing PBR volume and flow rates, this can only bridge moderate differences in reaction rates. The current residence times reported for the KR of **70** in flow of between 8 – 40 minutes are not compatible with the 9 second residence times established for FTR in Section 3.2.4.[138,140] Therefore, a new set of reaction conditions must be established that complement the FTR process.

Many key learnings could be taken from the prior work reported in this field with regards to the operating window, including the temperature ranges, concentrations, catalysts loadings, the number of acyl donor equivalents as well as the acyl donors themselves. In this work, data-led DoE optimisation of reaction will be utilised in an attempt to understand the interplay of the key reaction parameters and how they affect the conversion and selectivity of the process. This provides the best opportunity for the true potential of process to be realised.

4.2.1. Enzymatic Kinetic Resolution Flow System Development

It was decided that the customer KR flow system would be designed to maximise compatibility with the FTR system outlined in Section 3.2.1. (Figure 45) to enable the two systems to dovetail together easily during the construction of the full system.[118] Furthermore, even though a recycle loop was intended to be used, the KR would first simply be optimised for single pass conversion to achieve an acceptable residence time.

The literature precedent for the KR of **70** in flow gave an approximation of the order of magnitude expected for the residence time of the reaction to be between 4 – 40 minutes.[138,140] This is significantly longer than the 9 second residence time of the FTR. Therefore, in order to maximise the residence time of the KR a larger volume PBR would be required than used in the FTR process. In this proof of concept work an Omnifit glass column (10 x 100 mm), housed in a Uniqusis heating block was used as the KR PBR.[142] The new PBR could house a maximum of 1.7 g of Novozym-435 which equated to a void volume of 4.02 mL. This maximum volume equated to a 35 second

residence time using the 7 mL min^{-1} flow rate identified in the FTR process. This reflects a drastically shorter residence time compared to literature precedent.

The flow system previously constructed for the FTR work was reconfigured to accommodate the new heated PBR, followed by the Peltier heat exchanger and the BPR, used to maintain a consistent pressure of 8 bar in the system. The flow polarimeter was once again employed to establish when the breakthrough of the reactants and steady state had been achieved. Once this was confirmed, the product stream was switched from waste to the fraction collector (Figure 45).
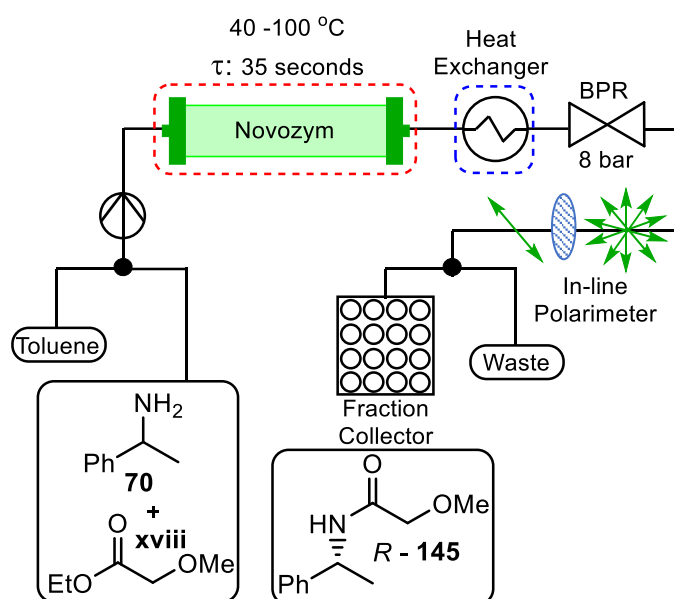
Figure 45 The flow system deployed for enzymatic KR of **70** in flow (single pass mode).[118]

4.2.2. Establishing Kinetic Resolution Reaction Conditions in Flow

Although DoE has previously been applied to the optimisation and understanding of Novozym-435 transformations, in batch and flow, the substrates have so far been limited to alcohols.[143–147] Therefore, available data from literature using OFAT optimisations were used to help identify the most suitable reaction space to be explored during the DoE. Furthermore, there were also certain parameters that are predefined by the FTR such as the flow rate which was fixed to 7 mL min^{-1}. With this in mind, the design of the DoE study of the KR process includes the following parameters: acyl donor, acyl donor equivalents, Novozym-435 loading, flow rate, temperature and solution concentration.

Prior literature has shown that the acyl donor is fundamental to permitting a highly efficient and selective KR process. [86,128,135,137,148] As the primary purpose for the development of the KR conditions was to maximise the rate of reaction in this proof-of-concept study (rather than cost efficiency), it was decided to employ a commercially available acyl donor. Although *Poppe* had demonstrate that **viii** was likely to be the most efficient acyl donor, its limited commercial availability led us to select **xviii** as the acyl donor (Scheme 28), which also had been shown to also be highly efficient for the KR of **70**.[86] The number of equivalents of acyl donor used varied considerably in the literature between 0.6 – 4 equivalents (Tables 31 and 33). Theoretically, only half an equivalent is necessary as only half of the racemic amine is acylated, therefore 0.5 equivalents was set as the lower limit. Increasing the number of equivalents was anticipated to increase the rate of reaction, and since increasing rate of reaction is the primary objective, the upper limit was increased to 10 equivalents, in the hope of identifying the ceiling where this parameter is no longer beneficial. Although loss of enantioselectivity was a concern with high acyl donor equivalents, it was hypothesised that the ability to adjust residence times effectively in flow would allow this to be optimised during the DoE.

The amount of Novozym-435 loaded into the column was determined by reference to the 3 previous examples, where CALB PBR have been used. These loadings had varied from approximately 200 mg up to 1.4 g of enzyme.[89,90,140] As the concentration of the amine solution would also be varied, an arbitrary 800 mg of enzyme was initially selected as a mid-point of the loadings reported previously. The range of solution concentration to be investigated was 20.6 – 82.5 mM as used in the FTR DoE, which also covers the 80 mM concentration investigated by *Miranda*, however it also permits the investigation of higher enzyme loadings which may increase conversion.[140]

However, it was found that 800 mg of enzyme did not use the full capacity of the Omnifit column. Given the flow rate of the amine is fixed at 7 mL min^{-1} by the previous FTR study, it was important that the full volume of the reactor was exploited to maximise the residence time and increase the single pass conversion. Therefore, the Novozym-435 was dispersed along the length of the column with crushed 5 Å molecular sieves. The small particle size of the molecular sieves and its porosity would allow effective distribution of the Novozym-435 along the length of the column while also maximising the pore space volume. Furthermore, in the future this would permit the loading to be easily adjusted with different amounts of Novozym-435 to molecular sieves, starting with 800 mg of Novozym-435.

The temperatures employed in studies using Novozym-435 enzymes vary from "room temperature" to 100 ℃ (Tables 31 and 33), owing to its attractive high thermal stability. [93] As "room temperature" is widely deemed an unhelpful reference point for temperature, due to the day-to-day and global variation, a commonly used 40 ℃ temperature was set as the low point for the DoE. While elongated use of Novozym-435 at temperatures between 70 – 90 ℃ has demonstrated high reproducibility, a top end temperature of 100 ℃ was chosen.[86,91,140]

As the racemisation of the amine is the greatest challenge in the overall CE-DKR process, some factors required for the KR were dictated by the FTR process. This was primarily the flow rate, which would be fixed to match the 7 mL min^{-1} used in the FTR, equating to a 35 second residence time for the KR. This would avoid the need for challenging chemical engineering solutions needed for complex changes in flow rate between each PBR. Due to the novelty of this approach to CE-DKR, it was felt that an initial proof of concept was required to validate the approach before subsequent refinement could be conducted. Furthermore, if the optimal concentration for the KR DoE was found to be different from the 82.5 mM optima for the FTR, the Novozym-435 loading would be adjusted within the column to recreate the same effective concentration of the substrate and enzyme.

4.2.3. Design of Experiments Optimisation

An I-optimal design DoE was once again created to screen the impact of the main effects, quadratic effects and second order interactions of temperature (40 – 100 ℃), solution concentration (20.6 – 82.5 mM) and number of acyl donor equivalents (0.5 – 10 equivalents) on the e.e. of **70** and **145**, as well as conversion.[118] This DoE consisted of 10 experiments, compared to the 18 experiments in the FTR DoE, as far greater prior knowledge was fed into the design. This meant that there was a higher degree of confidence that each set of conditions would provide an insightful result, therefore fewer experiments would be needed to create a detailed model. In this KR DoE, a decision was made not to include split plots since the convenience of not randomising one parameter comes at the cost of reduced precision in the estimates of the whole plot parameter, and the presence of split plots does add extra complexity to the analysis. We were able to negate the need for whole plots for two additional reasons. Firstly, far fewer experiments were to be performed therefore changing the reagent bottle was deemed less experimentally intensive. Secondly, the likelihood of catalyst deactivation was considered low due to the widely reported stability of Novozym-435 and its potential for prolonged, repeated use.[80,91,140]

ANOVA analysis would once again be used to establish which variables were deemed statistically significant, and subsequent analysis of the model would be carried out using actual by predicted plots, residuals by row and

studentised residuals. This would be followed by a validation of the model, before using the model to predict the optimal reaction conditions. Due to the DoE not having split plots, JMP allows you to fit the model to both responses at the same time. Therefore, a reaction parameter's statistical significance was determined relative to all outputs simultaneously, compared to the individual comparison made in the previous DoE. However, the F-ratio of each reaction parameter will be different for each response, therefore the strength of the contribution each reaction parameter has on each outcome can still be determined.

Table 34 I-optimal design screen effects summary.

Entry	Reaction Parameter	P-Value	F-Ratio (Amine e.e.)	F-Ratio (Amide e.e.)	F-Ratio (Conversion)
1	Acyl Donor	0.00073	87.6	5.98	0.305
2	Temp.	0.00662	26.8	0.09	0.006
3	Temp.*AD Equiv	0.00673	26.6	0.726	2.67
4	Temp.*Sol. Conc.	0.03200	10.4	2.93	0.562
5	Sol. Conc.	0.31744[a]	0.287	0.0485	1.30

[a]Included as it is part of a secondary interaction where α-value is < 0.05.

All of the reaction parameters (acyl donor equivalents, temperature and solution concentration) were deemed statistically significant (Table 34) alongside temperature*acyl donor equivalents and temperature*solution concentration secondary interactions. The number of acyl donor equivalents is the most significant reaction parameter (Entry 1), as it can be seen to contribute most to both **70** and **145**'s e.e.. As well as this, the number of acyl donor equivalents features in the only statistically significant reaction parameter for conversion, temperature*acyl donor equivalents (Entry 3) as it only parameter to have an F-ratio of > 1.

Using the interactive Predictor Profiler function, the number of acyl donor equivalents was seen to have a strong directly proportional relationship with the e.e. of **70**, whereby increasing the number of equivalents increased the e.e. of **70**. However, it was also observed to have a weakly negative effect on the e.e. of **145**. This suggests that increasing the acyl donor equivalents increases the rate of both the catalysed and uncatalysed reactions, however it appears to increase the rate of catalysed reaction to a greater extent than the uncatalysed reaction. This may be rationalised by the short 35 second residence time, largely permitting only the faster catalysed reaction and limiting the background reaction. If longer residence times were used the negative impact on the e.e. of **145** may be more pronounced.

Indeed, this can be observed in *Miranda*'s work where the increase in the number of acyl donor equivalents increases the e.e. of the amine without effecting the e.e. of *R* - **145** at 4 min residence time (Table 35, Entries 1 and 2).[140] However, at 40 minute residence times the e.e. of the amide can be seen to begin to drop with higher

121

acyl donor equivalents (Entries 3 and 4). This demonstrates how the increase in rate of reaction, permitted by using higher concentrations of acyl donor equivalents, can only be harnessed in flow reactions where the residence time can be used to remove the undesirable background reactions. This would not be permitted in a batch process as the reactions would be too long to prevent the reduction in e.e. of the amide. Although this trend was observed using an OFAT approach, this was part of a 9 experiment series to determine the effect of the acyl donor equivalents on the reaction. This represents almost the same number of reactions needed to understand one parameter in Miranda's work, as was needed to screen 3 reaction parameters in this work using DoE.
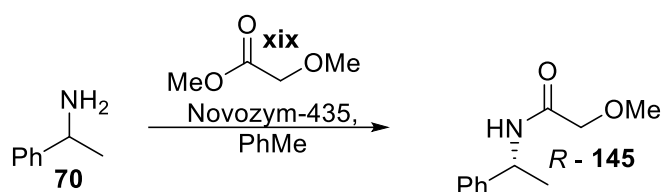

Table 35 The effect of acyl donor equivalents to the e.e. of the amine and amide product, as observed by *Miranda* et al.[140]

Entry	Acyl Donor (Equiv.)	τ (min)	Amine e.e. (%)	Amide e.e. (%)
1	1	4	62	99
2	5	4	88	>99
3	1	40	96	99
4	5	40	99	97

Temperature, as a main effect, can be seen to contribute to the e.e. of **70** (Table 34, Entry 2), but additional influence can be observed through a weaker temperature*acyl donor equivalents (Entry 3) and temperature*solution concentration (Entry 4) secondary effects. Although temperature does not directly affect the e.e. of **145** or conversion, it can also be observed to contribute to the **145**'s e.e. and conversion to a lesser extent through temperature*solution concentration (Entry 3) and temperature*acyl donor equivalents (Entry 4) secondary interactions. This is likely to be due to the small number of experiments used in the DoE, meaning the power of the model for each reaction parameter is relatively week. Only strong effects would be picked up but if they are missed as a main factor they can be picked up by the secondary interactions.

The temperature*solution concentration and temperature*acyl donor equivalents secondary interactions produce interesting relationships that are best visualised using the Predictor Profiler. When the solution concentration and acyl donor equivalents are at their midpoints and temperature is varied, a classical relationship can be seen where temperature only effects the e.e. of the amine, with higher temperatures reducing the e.e.. However, the secondary interactions mean that, if solution concentration is set too low, increasing temperature has a negative impact on the e.e. of **70** and **145**, alongside conversion. Whereas if solution concentration is too high, then higher temperature

positively impacts the e.e. of **70** and **145** and conversion. It is also found that when the solution concentration is kept at the mid-point, the inverse relationship is observed for the acyl donor equivalents.

The relationship between these factors becomes more complex as all the factors are linked through the secondary interactions. Consequently, varying all 3 simultaneously gives a plethora of different corelations. These relationships are extremely difficult, potentially impossible, to decipher by OFAT analysis. Furthermore, the visualisation of these interactions is extremely difficult, and it is therefore important to have computer aided tools, such as an interactive Profile Predictor, that enables them to be visualised and interpreted.
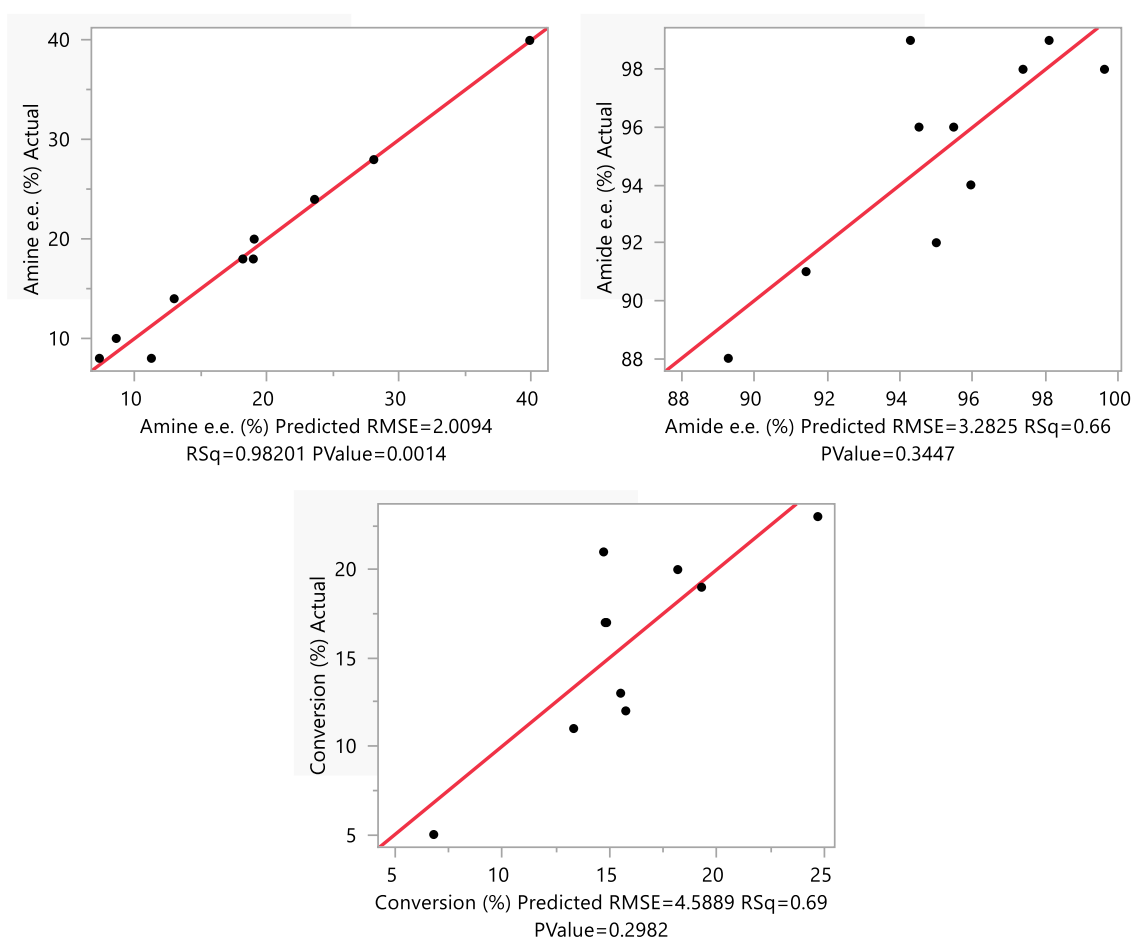
Figure 46 Actual by Predicted plots for the I-optimal design for the kinetic resolution of 1-phenyethylamine with respect to a) amine e.e. (left) and b) amide e.e. (right) and c) conversion (bottom).

Evaluating the actual by predicted plots for e.e. of both **70** (Figure 46a) and **145** (Figure 46b) along with conversion (Figure 46c) shows the excellent distribution of data across the full range of the response. This means that the data accurately described the whole reaction space for both responses, however once again the RMSE's were higher than typically desired. Furthermore, the R^2 values for both the e.e. of **145** (Figure 46b) and conversion (Figure 46c) are seen to be low. By interrogating the studentised residuals it can be seen that each reaction outcome

123

has 1 outlier: Experiment 9 for the e.e. of **70** (Figure 47a), experiment 7 for the e.e. of **145** (Figure 47b), experiment 4 for conversion (Figure 47c). The presence of outliers in smaller data sets, such as this one is concerning as they can have greater influence over the model, leading to poorer fits in the actual by predicted regressions. However, it is also harder to confirm that they are indeed outliers with fewer data points to compare against.
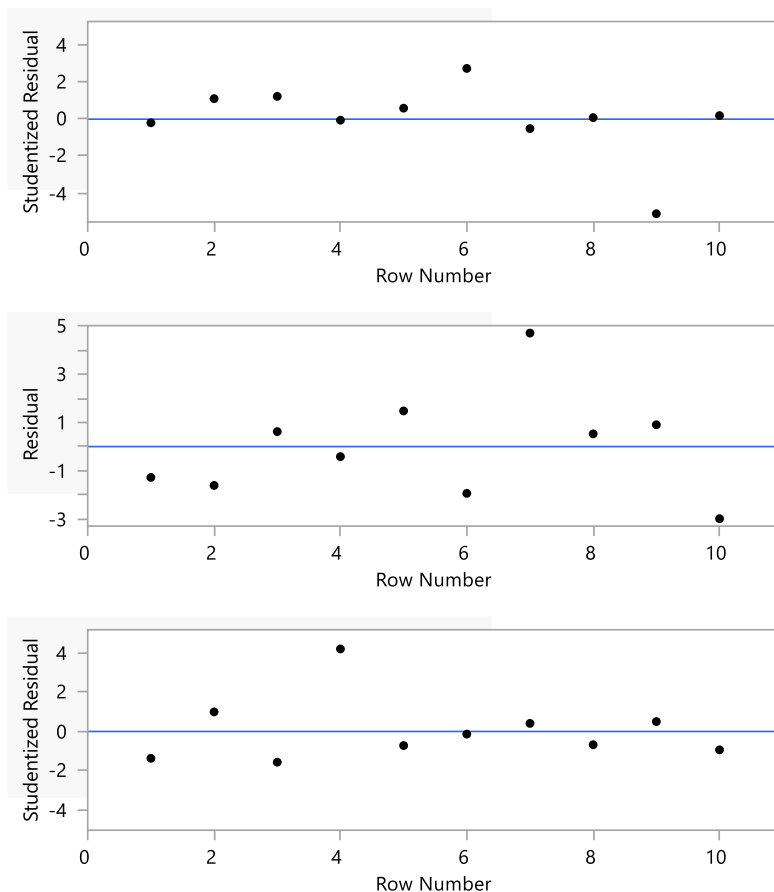
Figure 47 Studentised residual plots by row for a) amine e.e. (top), b) amide e.e. (middle) and c) conversion (bottom).

4.2.4. Design of Experiments Model Validation and Implementation

Despite the potential presence of outliers in the model, it was decided to assess the ability of the model to predict the outcome of reactions. If good predictability was shown, the influence of the potential outliers could be disregarded. It was hoped that this model would be able to sufficiently describe the reaction space with respect to the e.e. of **70** and **145** and conversion through Equations 19, 20 and 21. Randomly generated validation conditions were once again selected to assess the predictive power of the model (Table 36, Entry 1). The model was expected to predict the outcome of each parameter within +/- 7 % but the experimental values were found to fall slightly outside of the anticipated ranges (Entry 1). However overall, it was felt that the model had good predictability

124

from a small dataset as the predicted values fell within +/- 8 % on average. The validation data was fed back into the model to increase predictive power for the optimisation of reaction conditions.

$$\text{Amine e. e. }(\%) = 19.4 - 4.17\left(\frac{\text{Temp.} - 70}{30}\right) + 0.47\left(\frac{\text{Sol. Conc.} - 0.0516}{31}\right) \quad \text{Equation 19}$$

$$+ 8.18\left(\frac{\text{Acyl Donor} - 5.25}{4.75}\right) + 3.30\left(\frac{\text{Temp.} - 70}{30}\right)\left(\frac{\text{Sol. Conc.} - 0.0516}{31}\right)$$

$$- 5.27\left(\frac{\text{Temp.} - 70}{30}\right)\left(\frac{\text{Acyl Donor} - 5.25}{4.75}\right)$$

$$\text{Amide e. e. }(\%) = 94.6 - 0.40\left(\frac{\text{Temp.} - 70}{30}\right) + 0.31\left(\frac{\text{Sol. Conc.} - 51.6}{31}\right) \quad \text{Equation 20}$$

$$- 3.50\left(\frac{\text{Acyl Donor} - 5.25}{4.75}\right) + 2.86\left(\frac{\text{Temp.} - 70}{30}\right)\left(\frac{\text{Sol. Conc.} - 51.6}{31}\right)$$

$$- 1.42\left(\frac{\text{Temp.} - 70}{30}\right)\left(\frac{\text{Acyl Donor} - 5.25}{4.75}\right)$$

$$\text{Conversion }(\%) = 15.9 + 0.14\left(\frac{\text{Temp.} - 70}{30}\right) - 2.28\left(\frac{\text{Sol. Conc.} - 51.6}{31}\right) \quad \text{Equation 21}$$

$$+ 1.10\left(\frac{\text{Acyl Donor} - 5.25}{4.75}\right) + 1.75\left(\frac{\text{Temp.} - 70}{30}\right)\left(\frac{\text{Sol. Conc.} - 51.6}{31}\right)$$

Table 36 I-optimal design model prediction of reaction outcome.[a]

Entry	Temp. (°C)	Sol. Conc. (mM)	Acyl donor (Equiv.)	Pred. Amine. e.e. (%)[b]	Exp. Amine. e.e. (%)[b]	Pred. Amide e.e. (%)[c]	Exp. Amide e.e. (%)[c]	Pred. Conv. (%)[c]	Exp. Conv. (%)[c]
1	40	82.5	10	34	20	91	99	27	25
2	40	38.8	10	35	40	97	99	23	29

[a]Experiment started with a solution of optically inactive **70** in anhydrous PhMe. [b]Determined by chiral HPLC. [c]Determined by GC.

With our confidence in the model established, a set of desirability criteria were chosen (Table 37) from which the model aimed to generate optimal reaction parameters. These desired features were to maximise the e.e. of **70** and conversion with linear desirability between 0 – 100 %. While the desirability of the e.e. of **145** was set to have a lower limit of 90 % with the desirability exponentially increasing to 99 %. These criteria generated reaction

conditions of a temperature of 40 °C, 20.6 mM solution concentration and 10 equivalents of the acyl donor to theoretically deliver an e.e. of 39 % and 97 % for **70** and **145** respectively, alongside 23 % conversion.

Table 37 Desirability criteria for the optimal kinetic resolution conditions.

Entry	Amine e.e. (%)	Value	Desirability	Amide e.e. (%)	Value	Desirability	Conv. (%)	Value	Desirability
1	High	100	0.99	High	99.9	0.99	High	100	0.99
2	Middle	50	0.5	Middle	95	0.25	Middle	50	0.5
3	Low	0	0.01	Low	90	0.01	Low	0	0.01

To achieve further compatibility between the KR and FTR, the actual concentration of solution was to remain at 82.5 mM. It was therefore necessary to change the loading of the enzyme so that the effective loading within the PBR would replicate a solution concentration of 20.6 mM and 800 mg of Novozym-435. As the volume of the PBR is 4.02 mL, at 20.6 mM the effective Novozym-435 loading in the PBR would be 9660 mg mmol^{-1}. To maintain this loading at 82.5 mM, 3.2 g of Novozym-435 would be required in the column. However, 3.5 g of Novozym-435 could not fit into the available Omnifit column and .with no larger column, or heating block to accommodate it available, the maximum packing of the column was limited to be 1.7 g of Novozym-435. This meant that the system was limited to a loading of 5126 mg mmol^{-1}, which equated to an effective concentration of 38.8 mM.

Using this concentration as a limiting factor in the model, and the temperature set to 40 °C and acyl donor equivalents set to 10 (Table 36, Entry 2), the model predicted that e.e. of **70** and **145** would be 35 % and 97 % respectively, with 23 % conversion being achieved. These conditions were run experimentally to determine if the outcome of these conditions were as predicted by the model. An excellent overlap was observed with the predicted outcome of the reaction, achieving 40 % e.e. of **70**, 99 % e.e. of **145** and 29 % conversion (Table 36, Entry 2), with all of the experimental data falling comfortably within the +/- 7 % predictive power of the model.

By using DoE to develop the reaction, an effective KR process was developed that can achieve high levels of conversion in just 35 seconds. This was also achieved while making serval compromises in reaction conditions due to the limitations of the equipment available. The constraints from the FTR process that were fed into this reaction development mean that this process is also highly compatible with racemisation step of the CE-DKR, enabling the flow rate and concentration to be unchanged between the two PBR.

4.2.5. Scale Up of the Kinetic Resolution of 1-phenylethylamine, **70**

To further challenge the significance of the KR conditions that were developed, it was decided to apply them to a 1 gram scale KR of **70** (Figure 48). This would allow these conditions to be benchmarked against prior work in the field. To allow full conversion to be reached the flow system was modified to allow the partially resolved material to be recycled through a holding reservoir before subsequent additional passes through the KR PBR.
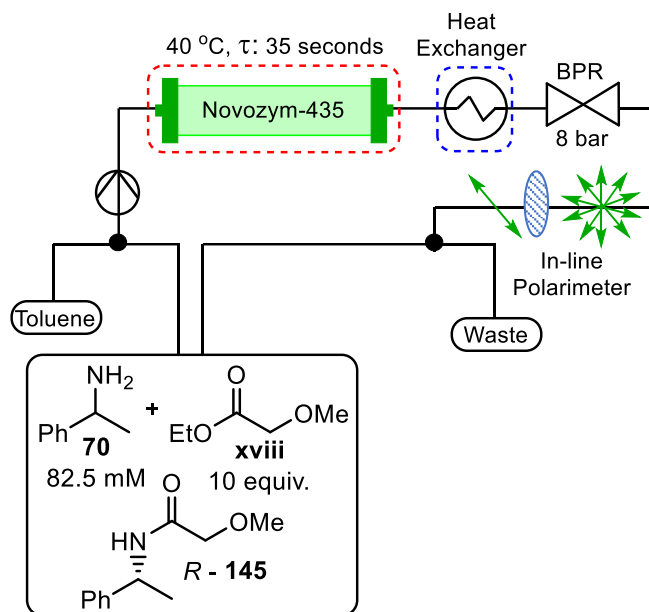
Figure 48 Modified kinetic resolution flow system including recycle reservoir.[118]

After 10 minutes the reaction had proceeded to 49 % conversion (Table 38, Entry 1), with *S* - **70** and *R* - **145** being delivered with 94 % and 99 % e.e. respectively. This resulted in a calculated STY of 6035 µmol mL^{-1} h^{-1} which represents the highest productivity of any reported kinetic resolution of **70**. This STY reflects a 5.5-fold increase compared to the previous highest STY of 1099 µmol mL^{-1} h^{-1} achieved by *Poppe* et al. (Entry 5).[140] Although it must be acknowledged that *Poppe* achieved this STY with a significantly lower CALB loading, albeit using a different form of the enzyme. Furthermore, the gram scale resolution developed in this work was able to deliver the highest TOF of a KR process with a value of 10191 h^{-1}, reflecting an almost 2-fold improvement compared to the previous highest TOF reported by *Kanerva* et al. (Entry 2), where extremely low loadings were employed.

Table 38 A comparison of CALB mediated kinetic resolutions of **70**.

Entry	Batch /Flow	Temp. (ºC)	Time (min)	Conc. (mM)	CALB (mg mmol⁻¹)ᵃ	AD (Equiv.)	Conv. (%)	Amine e.e. (%)	Amide e.e. (%)	STY (μmol mL⁻¹ h⁻¹)	TOF (h⁻¹)	Reference
1	Flow	40	10	82.5	5127	**xviii** (10)	49	94	99	6035	10191	This Work[118]
2	Batch	23	360	-ᵈ	12.5	**i** (1)	50	98	97	604	4762	[Kanerva 2012][125]
3	Flow	70	40	900	396	**ii** (4)	42	72	99	578	1136	[Miranda 2013][140]
4	Batch	30	60	778	19	**viii** (1)	29	>99	40	229	N/Aᵃ	[Poppe 2018][138]
5	Flow	60	200	650	407	**viii** (0.6)	46	85	99.7	1099	N/Aᵉ	[Poppe 2018][138]
6	Batch	40	240	2500	40	**ix** (2)	45	82	>99	281	N/Aᵉ	[Poppe 2022][132]

ᵃmg of Novozym-435 per mmol of substrate ᵇCalculated from e.e. of amide and conversion. ᶜReduced pressure 0.06 bar. ᵈSolvent free, volume of reaction for STY determined by volume of acyl donor. ᵉ ᵇCouldn't be determined due to lack of reporting of active sites of the CALB.

Interestingly, it can be seen that the flow processes were able to achieve higher STY than their batch counterparts, particularly when taking the acyl donor into consideration. The difference in productivity appears to stem from the greater effective concentration that can be achieved in the PBR of flow systems helping to drive higher rates of reaction. Although this may appear undesirable, it has to be taken in the context of how much material is converted over the catalyst's lifetime. The longer the catalyst is used, the lower its actual loading will become, making it more cost effective. Alongside this, the use of enzymes in flow naturally elongates their lifetime due to the lack of degradation caused by mechanical stirring.[149] This helps further reduce the loading of the catalyst during its lifetime. Furthermore, the higher acyl donor loading can be offset through recovery and reuse though simple distillation.

Despite these potential drawbacks, the primary purpose of this work was not to minimise enzyme loading or acyl donor equivalents. Rather, the objective was to create a set of KR conditions for **70** that was sufficiently fast to allow for their combination with the FTR protocol designed previously. This objective was met, and an attractive by-product of this was developing a process which compares extremely favourably with regard to STY to previously reported KR conditions (Table 38).

4.3. Conclusion

During the development of a suitable set of KR conditions, a flow system was designed that was compatible with the FTR system. Following this, DoE has once again been used to efficiently screen the reaction parameters to develop a higher level of understanding of the reaction than would be possible using a OFAT approach. The DoE accurately predicted the outcome of reactions and designed optimal reaction conditions. This approach also showed good adaptability to the practical limitations of laboratory equipment. With these limitations fed into the

model, an alternative set of conditions were generated that were able to mitigate any loss in efficiency due to the practical constraints.

These conditions were able to effectively resolve **70** on a gram scale to deliver the highest STY achieved by a CALB resolution reaction (Table 38). Previously, the racemisation step limited the CE-DKR process. With the advent of FTR, the rate limiting step is now the KR of the amine. With the KR conditions having been demonstrated to be highly efficient on a gram scale, it was expected that this would translate well into the fully developed CE-DKR system to deliver a highly productive process.

Chapter 5. <u>Chemoenzymatic Dynamic Kinetic Resolution</u>

In Chapter 2 an HTS methodology was established that facilitated the identification of a series of thermally induced racemisation catalysts that showed very promising levels of activity for the racemisation of **70**. In Chapter 3, this work was successfully translated into a novel FTR process in flow and further enhanced with data-led DoE optimisation to enable the rate of the amine racemisation process to be increased to an unprecedented level (TOF: 218 h^{-1}). In Chapter 4, the development of a set of KR conditions for chiral amines was described that were able to match the level of productivity of the FTR process.

This Chapter aims to bring the work of the previous chapters together, to achieved the first fully compartmentalised CE-DKR flow system that does not require extraneous additives, such as H-donors or a base. It is hoped the new design will represent a significant improvement in process efficiency and productivity that is also more scalable and more environmentally sustainable.

To fully assess this approach, the system will once again be applied to the chosen model substrate **70** on a gram scale. This will allow us to benchmark this work against literature precedent, whilst simultaneously overcoming the established challenges that CE-DKR faces in terms of productivity and selectivity. Finally, this FTR-CE-DKR strategy will be applied to the resolution of a pharmaceutically active amine intermediate, to highlight its relevance to industry.

5.1. <u>Introduction</u>

5.1.1. <u>Traditional 'One-Pot' Batch Reactors</u>

As previously discussed in Section 2.1, the first CE-DKR process was reported by *Reetz* et al. in 1996 (Table 39, Entry 1). This was quickly built upon by *Kim* et al. in 2001 (Entry 2), with both processes employing Pd/C as the racemisation catalyst and CALB as the lipase, in 'one-pot', using a batch reactor.[81,84] Although *Kim*'s process was found to proceed in 5 days (rather than 8 days) and higher levels of conversion were achieved, no discernible increase in productivity was observed with very similar STY's of 0.8 μmol mL^{-1} h^{-1}. This was largely due to the 2-fold drop in concentration used and ultimately only half the amount of material was processed.
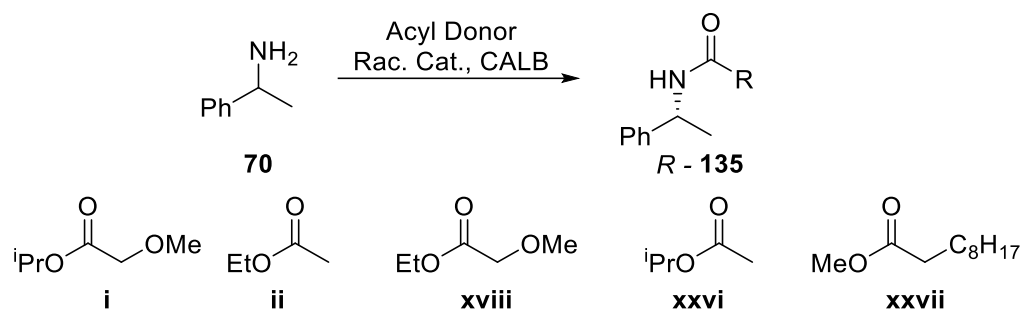
NH₂ → Acyl Donor / Rac. Cat., CALB → amide

70 → *R* - **135**

^{i}PrO...OMe **i** EtO... **ii** EtO...OMe **xviii** ^{i}PrO... **xxvi** MeO...C$_8$H$_{17}$ **xxvii**

Table 39 A summary of the CE-DKR of **70** performed in 'one-pot' using a batch reactor.

Entry	Catalyst	Temp. (°C)	Time (h)	Conc. (mM)	AD (Equiv.)	Additives	Conv. (%)	Amide e.e. (%)	STY (µmol mL⁻¹ h⁻¹)	Reference
1	Pd/C	52.5	192	200	**ii** (4)	Et₃N /H₂	77	99	0.802	[Reetz 1996][81]
2	Pd/C	60	120	100	**ii** (2)	DIPEA/H₂	98	98	0.816	[Kim 2001][84]
3	Ru-Shvo	90	72	62.5	**xxvi** (7)	Na₂CO₃/IPA	90	98	0.781	[Bäckvall 2005][80]
4	Pd/BaSO₄	70	24	82.5	**xxvi** (1)	H₂	91	>99	3.13	[De Vos 2005][101]
5	Pd/AlO(OH)	70	72	100	**ii** (3)	-	97	98	1.35	[Kim 2007][83]
6	Ru-Shvo	100	26	62.5	**i** (1)	Na₂CO₃/DIPMA	100	98	2.40	[Meijer 2007][150]
7	Raney Ni	80	120	82.5	**xvii** (1)	H₂	62	94	0.426	[De Vos 2008][87]
8	Raney Co	70	72	82.5	**xxvi** (1)	H₂	63	> 99	0.722	[De Vos 2008][87]
9	Pd/AlO(OH)	70	6	37.5	**i** (1.7)	Na₂CO₃	97	99	6.06	[Kim 2010][82]
10	Ru-Shvo	100	72	200	**xviii** (1)	Na₂CO3/DIPMA	93	97	2.58	[Bäckvall 2010][86]

A significant increase in STY was reported by *De Vos* in 2005 (Table 39, Entry 4), a near 4-fold increase compared to the system reported by *Kim* (Entry 2). At 70 °C, the reaction time was reduced to just 1 day without significant dilution of the reaction mixture. This was made possible through the switch to the alkaline earth metal catalyst Pd/BaSO₄. Pd/BaSO₄ was shown to be a significantly more efficient racemisation catalyst compared to Pd/C and Ru-Shvo catalyst, with a TOF of 3.00 h⁻¹ (Section 2.1.1, Table 6, Entry 8) compared to 0.33 and 0.47 h⁻¹ respectively (Section 2.1.1, Table 6, Entry 11, Section 2.1 Table 5 Entry 1). With the approximate 10-fold increase in the rate of racemisation, a significantly higher STY for the CE-DKR could be achieved.

Although Raney Ni and Co were found to be effective racemisation catalysts (Section 2.1.1.), achieving full racemisation with high selectivity, this did not translate well into CE-DKR (Table 39, Entries 7 and 8) with neither system achieving a STY > 1 µmol mL⁻¹ h⁻¹. *De Vos* discovered that there was a lack of compatibility between the Raney Ni racemisation catalyst and the Novozmy-435 (Table 40), leading to a 2-fold drop off in activity of the racemisation catalyst rendering the processes extremely ineffective (Table 39, Entries 7 and 8), resulting in STY of < 1 µmol mL⁻¹ h⁻¹. Similarly, *Blacker* et al. noticed deactivation of their homogeneous Ir SCRAM catalyst, **106**, in combination with Novozym-435, due to suspected leaching of unknown material from the immobilised enzyme.[151]
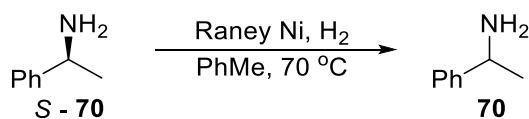
Table 40 The deactivation of Raney Ni caused by Novozym-435 for the racemisation of **70**.

Entry	Additive	e.e. (%)	Rac. TOF (h^{-1})	Sel. (%)
1	-	0	0.0202	92
2^a	Novozym-435	43	0.0115	100

Reaction Conditions: Ni (40 mg), 0.33 mmol amine, PhMe (4 mL), 0.1 bar H$_2$, 70 °C. Co (80 mg), 0.33 mmol amine, PhMe (4 mL), 0.2 bar H$_2$, 70 °C. [87]

Kim followed up on the seminal work in 2001 with two further publications in the field (Entries 5 and 9).[82,83] The second iteration of this work transitioned from a Pd/C racemisation catalyst to Pd/AlO(OH) while eliminating both previously used additives, DIPEA and H$_2$, (Entry 5) however this resulted in only a moderate increase in STY. Significant improvements were made 2010 (Entry 9), through a combination of reducing of the particle size of the Pd and introducing Na$_2$CO$_3$. Reducing the Pd particle size was found to greatly improve the efficiency of the catalyst, with an almost 5.5-fold increase in TOF (Section 2.1.1.) while maintaining the same mild temperatures. Switching the acyl donor from the slow reacting donor **ii** to the highly reactive and selective acyl donor **i** further helped develop the reaction. The culmination of these modifications resulted in 4.5-fold increase in STY relative to their previous effort (Entries 5 and 9), and the highest STY of the classical batch reactions of 6.06 µmol mL^{-1} h^{-1}.

Bäckvall et al. reported the use of a homogeneous racemisation catalyst in a CE-DKR process, employing the Ru-Shvo catalyst **105** (Table 39, Entries 3 and 10).[80,86] Initially this system was able to reduce the reaction time and increase conversion relative to the previous publications (Entries 1 and 2), however there was no significant improvement in the productivity of the reaction, due to the high dilution condition required. However, these efforts were followed up with an important contribution to the field by establishing the only recorded multi-gram scale CE-DKR resolution of **70** while demonstrating the ability of **xviii** to deliver high levels of conversion and enantioselectivity. The group was able to perform a 10 and 45 mmol scale CE-DKR (1.21 g and 5.45 g) achieving high conversions in both cases (90% and 83 % respectively), over the course of 24 hours. An STY of 2.58 µmol mL^{-1} h^{-1} was achieved in the 10 mmol reaction, which represents a much greater efficiency than many of the sub mmol scale reactions.

5.1.2. Alternative Reactor Systems

There have been several attempts to increase the productivity of the CE-DKR process by exploring alternatives to traditional batch reactor systems where the racemisation and enzyme-catalysed steps are not compartmentalised (Table 41). The first example of this was described by *Parrett* et al. in 2007, where a pump was used to transfer the reaction mixture between a KR continuous stir tank reactor (CSTR) and a racemisation CSTR (Figure 49), where in-line filtration of the enzyme negates the need for intensive manual works ups.[152] This allowed two different sets of conditions to be applied to the reaction mixture at different stages of the reaction. The volume of the KR CSTR was 83 mL and heated to 30 °C whereas the racemisation CSTR was 60 mL and heated to 100 °C. This meant the residence time could be 38 % longer in the KR CSTR with a 70 °C lower temperature, reflecting the milder temperatures and longer reaction times that the enzymatic reaction requires.
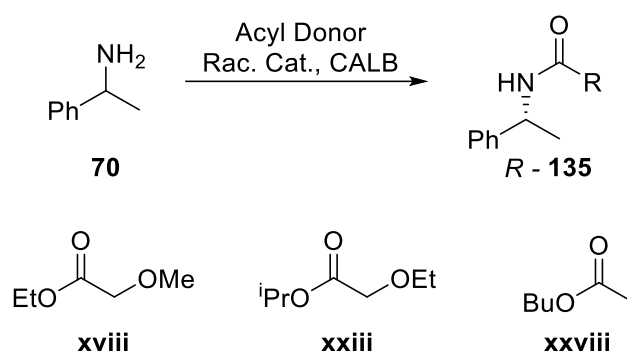

Table 41 A summary of the CE-DKR of **70** performed in alternative reactor systems.

Entry	Reactor	Catalyst	Temp. (°C)	Time (h)	Conc. (mM)	AD	Additives	Conv. (%)	Amide e.e. (%)	STY (μmol mL^{-1} h^{-1})	Reference
1	Dual CSTR	Ru-Shvo	100/30	72	65	**xxviii**	-	91	99	0.213	[Parrett 2007][152]
2	Microwave	Pd/CaCO$_3$	100[a]	50 min	82.5	**xviii**	H$_2$	73	99	72.3	[De Vos 2008][74]
3	Microwave	Pd/CaCO$_3$	100[b]	50 min	82.5	**xviii**	H$_2$	88	97	87.1	[De Vos 2008][74]
4	Flow	Pd/AMP-KG	60	16	138	**xxiii**	NH$_4$HCO$_2$	99	> 99	25.1	[Poppe 2018][90]

[a] Thermally active reaction. [b] Microwave activated reaction.

This reactor was able to achieve 91 % conversion, over a 72 hour reaction time to deliver *R* – **145** with 99 % e.e. (Table 41, Entry 1). Despite the attempt to employ optimised reaction conditions to the KR and racemisation steps, a STY of just 0.213 μmol mL^{-1} h^{-1} was achieved, representing the least productive CE-DKR system. It was not possible to rationalise the reason for this poor performance due to the vague description of the results.

Although 91 % conversion was reported, the author also observed a 55 % mass balance at the end of the reaction. *Parrett* et al. claimed that the loss of material was due to the deactivation of the Novozym-435, caused by instability of the enzyme under the KR reaction conditions. However, considering the multiple accounts of the

long-term stability of Novozym-435 under similar conditions, an alternative explanation seems more likely. [86,91,93,140] Any deactivation of the enzyme is more likely due to the homogeneous nature of the racemisation catalyst, meaning it is present throughout the reactor and therefore could cause deactivation of the Novozym-435, in a similar manner observed by *De Vos*.[87]
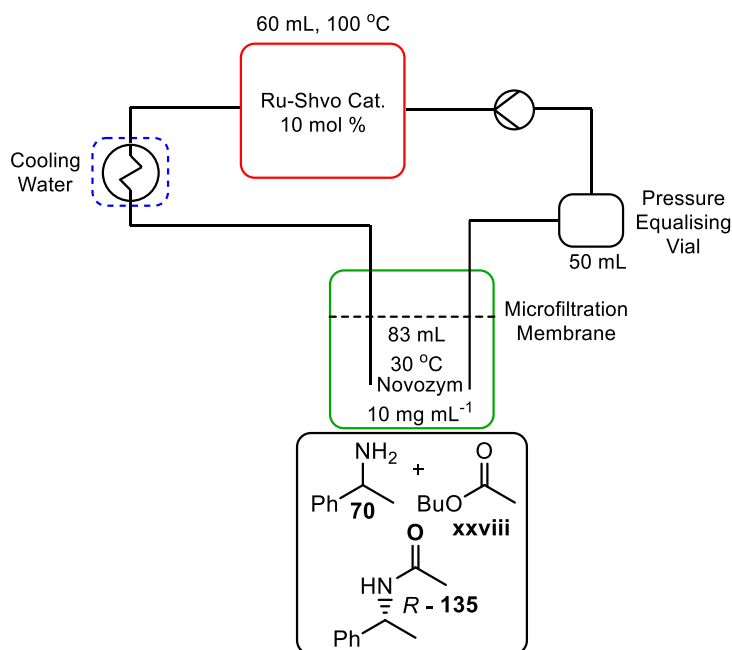

Figure 49 Parrett et al.'s dual CSTR flow system.[152]

The low mass balance could also be linked to deactivation of the racemisation catalyst through by-product formation during the racemisation step. Previously *Bäckvall* had reported 82 % selectivity with the same Ru-Shvo catalyst at 2 mol % catalyst loading. Therefore, at the elevated 10 mol % loading used in this process, the rate of by-product formation could be considerably increased, leading to low mass balance and the deactivation of the racemisation catalyst which in turn would inhibit further product formation.

De Vos et al., applied the high temperature and short reaction time conditions that were shown to deliver extremely high TOF for the racemisation of $S - 70$, (Section 3.1.1.), to the CE-DKR process. [74] The conditions were slightly modified, using a lower 100 °C reaction temperature and longer 50 minute reaction time, alongside Novozym-435 and the highly active acyl donor **xviii**. Both the microwave and thermally activated reactions were shown to deliver extremely high STY's of > 72 μmol mL^{-1} h^{-1} (Table 41, Entries 2 and 3). This marked a 23-fold and 28-fold increase on the same group's previous work in 2005 (Table 39, Entry 4) and the highest recorded STY of any CE-DK process. Although this work was pioneering, the difficulties around scalability of this approach was previously discussed in Section 3.1.1.

Poppe et al. have reported the only previous successful racemisation of primary amines in continuous flow, discussed in Section 3.12.[90] This work was coupled to the KR in continuous flow, reported in the same paper, as discussed in Section 4.1.2., to form the first fully continuous CE-DKR system (Figure 50) in 2018. Despite the use of a standalone KR PBR, this system is not compartmentalised due to the mixed nature of the second PBR, therefore continuing the compromise of the racemisation conditions. However, this system was able to deliver *R* - **122** with > 99 % e.e. and a STY of 25.1 µmol mL^{-1} h^{-1} (Table 41, Entry 4), the highest of any CE-DKR flow system; however, it has only been demonstrated on a 0.66 mmol (80 mg) scale. The productivity of this system could be hugely increased by fully compartmentalising the racemisation step and employing a recycle loop which would permit higher flow rates to be used. Furthermore, elimination of NH_4CO_2, suspected of deactivating CALB, could also increase the operating time of the system.
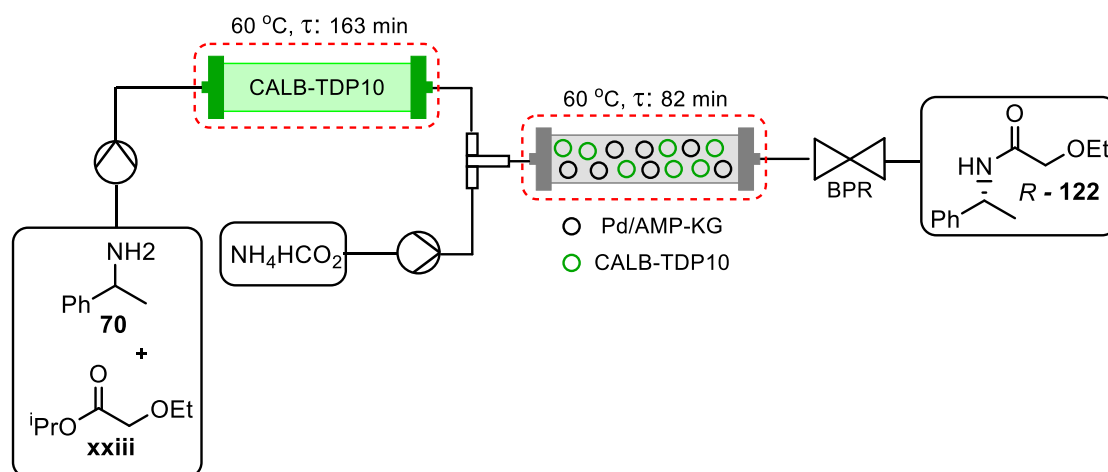

Figure 50 The first fully continuous CE-DKR system for the resolution of amines by *Poppe* et al..[90]

5.1.3. Compartmentalised Reactor Systems

One of the key limitations of implementing a dual catalyst system is the lack of compatibility between the reaction conditions required for each step and the stability of the catalysts, especially the biocatalyst. The lack of compatibility between the two optimal sets of conditions has led to one-pot methodologies being conducted under milder, more enzyme-friendly conditions. Such a compromise ultimately limits the productivity, as prolonged reaction times of over 24 hours are often required for < 1 mmol scale reactions. These long reaction times, in turn, exacerbates catalyst deactivation and limits the scalability. Compartmentalisation of the two catalytic processes into separate reactors can enable both catalysts to perform under optimal conditions. Several attempts have been made to implement this approach (Table 42), however, as yet this has not been achieved in a manner that fully utilises both the effective compartmentalisation of the reaction and continuous flow capabilities.
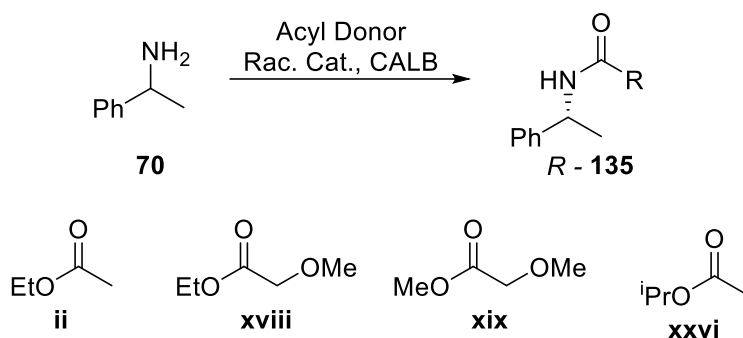
135

$$\text{70} \xrightarrow[\text{Rac. Cat., CALB}]{\text{Acyl Donor}} R\text{ - }\textbf{135}$$

EtO (O) Me **ii** EtO (O) OMe **xviii** MeO (O) OMe **xix** ^{i}PrO (O) Me **xxvi**

Table 42 A summary of the CE-DKR of **70** in compartmentalised reactors.

Entry	Reactor	Catalyst	Temp. (°C)	Time (h)	Conc. (mM)	AD (Equiv.)	Additives	Conv. (%)	Amide e.e. (%)	STY (μmol mL⁻¹ h⁻¹)	Reference
1	Batch	Ru-Shvo	110/40	304	125	**ii** (4)	DIPMA	75	> 98	0.308	[Bäckvall 2002][85]
2	Batch	Raney Ni	80	52	82.5	**xviii** (1.5)	H_2	100	91	1.59	[De Vos 2008][74]
3	Batch	Raney Co	70	26	82.5	**xxvi** (1.8)	H_2	70	99	2.22	[De Vos 2008][74]
4	Batch-Flow	Pd/BaSO₄	70	10	213	**xix** (2)	NH₄HCO₂/Na₂CO₃	77	95	14.5	[Miranda 2014][89]

The first attempt at compartmentalisation of a CE-DKR system was reported by *Bäckvall* et al. in 2002 (Table 42, Entry 1).[85,126] In this work, the racemisation and KR were performed in separate manual steps – starting with a KR of the amine, followed by a workup to remove the amide, acyl donor and enzyme, before the racemisation was performed. A second work up was used to remove the racemisation catalyst before the KR processes were repeated to afford the chiral amide (Figure 51). Although this allowed bespoke optimal conditions to be applied to each step, with the KR being performed at 40 °C and the racemisation at 110 °C, the manual process is not only laborious but also highly inefficient (Entry 1), giving an extremely low STY of 0.308 μmol mL⁻¹ h⁻¹. Furthermore, the 304 hours of operating time, does not include the time needed for work up and transfer material between each reactor.

De Vos looked to take a similar compartmentalisation approach to *Bäckvall* to improve the productivity of Raney Ni and Co in a CE-DKR process (Table 42, Entry 2 and 3).[87] After the discovery that the Novozym-435 was deactivating the Raney catalysts the two processes were separated to improve the productivity of the CE-DKR. This was performed in a very similar, manual process, employed by *Bäckvall* (Figure 51).[85] However, in this instance the compartmentalisation of the two steps showed significant improvement in the CE-DKR process due to the extreme lack of compatibility of the two catalysts (Table 40). The STY of both the Raney Ni and Raney Co processes were improved by between 3 to 4 -fold (Table 42, Entries 2 and 3) using a two-pot compartmentalised system, compared to the one-pot system (Table 39, Entries 7 and 8). Interestingly, the Raney Co processes

delivered a higher STY than the Raney Ni, despite the Raney Nickel using a much more efficient ethoxy ester acyl donor, **xviii** This is even more surprising since Raney Ni was shown to have a > 6.5-fold great TOF than Raney Co.
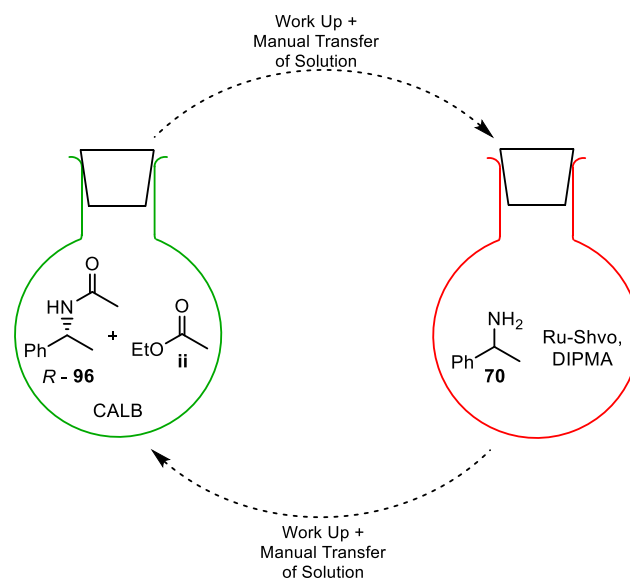

Figure 51 Performing the CE-DKR as two compartmentalised batch reactions.[85,87]

Miranda created a batch-flow system, building on their seminal work on the transition of KR of amine **70** in continuous flow, as discussed in Section 4.1.3.[89,140] By using a heterogeneous Pd/BaSO$_4$ racemisation catalyst in a CSTR, and the immobilised Novozym-435 in a PBR, connected by a continuous flow of reactants between them (Figure 52), the catalysts can be totally isolated and prevented from exposure to the reaction conditions in each reactor. This allowed for the racemisation to have a much longer residence time in the batch process at an elevated, 70 °C temperature, while allowing the KR to be performed at a much lower room temperature reaction. Conversely, *De Vos* employed the same reagents in a one-pot strategy which restricted both catalysts to being subject to 70 °C.[88] The effectiveness of the compartmentalisation allowed the high productivity to be achieved, with the system reaching 77 % conversion over 10 hours to deliver *R* – **145** with 95 % e.e., to achieve a STY of 14.5 μmol mL^{-1} h^{-1} (Table 42, Entry 4), a > 4.5-fold increase in STY compared to the *De Vos* one-pot system.[88,89,101]

This significant contribution was found to outperform any of the other previous CE-DKR processes, bar the microwave irradiated system, more than doubling the previous highest STY achieved by *Kim* in 2010 (Table 39, Entry 9) and producing a 7-fold increase compared to the previous best compartmentalised system reported by *De Vos* (Table 42, Entry 3).[87] This impressive productivity was achieved on a 3.2 mmol (388 mg) scale, the second largest scale CE-DKR reported in literature.[86]
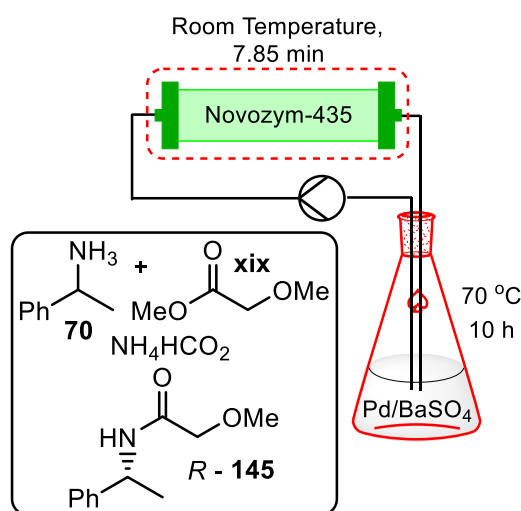
137

Figure 52 The first batch-flow CE-DKR system for the resolution of amines developed by Miranda. [89]

Despite these impressive reports, the STY could be further improved by transitioning the racemisation step into continuous flow as well, although the 2.5 hour reaction times are not conducive to flow methodologies. The increase in STY observed in this system highlights the great increase in efficiency that effective compartmentalisation can bring, however the author noted that more developmental work is needed as steady deactivation of one, or both, of the catalysts can be observed. Over time the rate of production of the R – **145** and its e.e. drops (Table 43) and full conversion is never reached, with only 77 % product formation. The author postulated that this could be due to poisoning of the Novozym-435 by the NH_4CO_2 and the subsequent liberation of NH_3 or CO_2, meaning that the elimination of the NH_4CO_2 or switching to a cleaner H_2 source could improve the process. Although the productivity and scale of the reaction are extremely impressive, this process remains unscalable until catalyst deactivation can be overcome.

Table 43 Production of R – **145** over time in *Miranda*'s et al's. batch-flow system.[89]

Entry	Time (h)	Amide (%)	Amide e.e. (%)
1	2.5	53	99
2	4.5	64	97
3	7	68	96
4	8	76	96
5	10	77	95

138

5.2. Results and Discussion

Over the past few decades many attempts have been made to increase the productivity of CE-DKR processes (Figure 53), however for the most part progress has been limited. There have been some notable exceptions that have breathed new life into the field and demonstrated where the future progress of the field lies. The high temperature, short reaction times used by *De Vos* et al. in 2008 clearly showed that this strategy was key to eliciting high productivity from CE-DKR processes. Further innovation was demonstrated by *Miranda* et through separation of the dual catalyst system into compartmentalised reactors, with transfer of the material through the batch-flow system by continuous flow which greatly improves the STY. Finally, *Poppe* et al. demonstrated that the use of a fully continuous flow system, could also provide great advantage in terms of productivity.
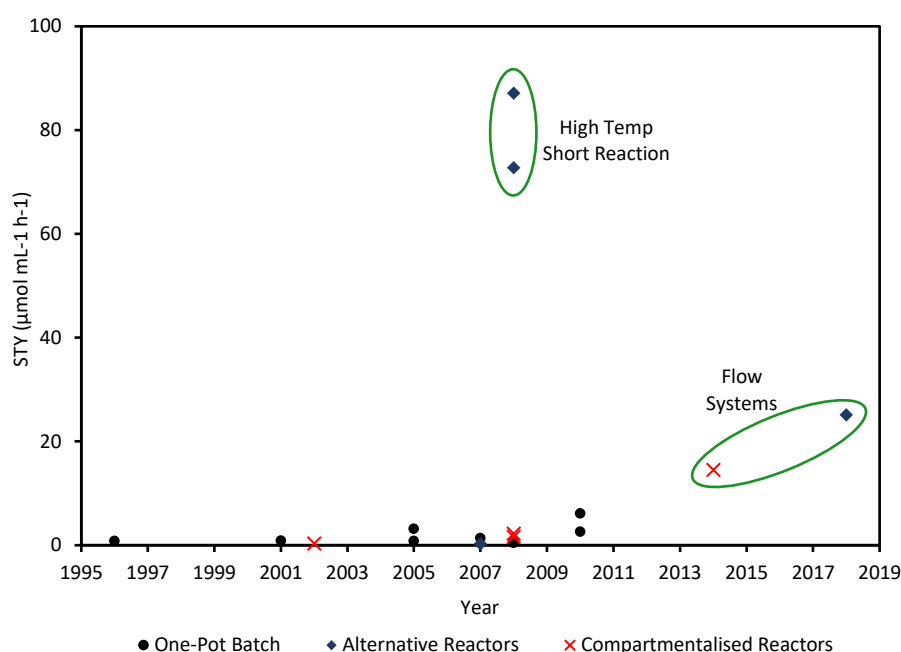

Figure 53 The progress of STY of CE-DKR over time.

Each of these strategies shows great ingenuity to progress the field but fell short in another aspect. Although, *Poppe* et al. were able to transition the racemisation of amines into batch, the productivity of the system was limited by the mixed PBR and single pass nature of the system. The scalability of the system was also limited by the stability of the Novozym-435 catalyst due to the mixed PBR and presence of deactivating $NHCHO_2$, limiting the runtime of the process. *Miranda* et al. was able to physically decouple the two processes effectively, however the use of a batch-based racemisation strategy increased reaction times and limited productivity. Furthermore, the two reactors remained chemically linked through the need for NH_4CHO_2 to maintain selectivity of the racemisation. This deactivated the Novozym-435 and prevented complete conversion and longer run times being

achieved, limiting both the productivity and scalability. Finally, although *De Vos* was able to develop an extremely effective racemisation strategy, which transition well into CE-DKR on a small scale. Short reaction times were key to driving the high selectivity to go alongside the high racemisation rate, which was not achievable on a larger scale in a batch reactor.

5.2.1. The Development of the CE-DKR System

As the FTR methodology and the KR of amines have already been optimised in their respective PBR and the compatibility of the flow systems built into the designs (Chapters 3 and 4, respectively), assembly of the CE-DKR flow system can be achieved by simply connecting the two reactors *via* a short piece of tubing.[118] The recycle loop had previously been employed as part of the gram scale KR in Section 4.2.5 and consisted of the product stream being connected back to the stock solution reservoir. The in-line polarimeter would continue to be employed in the system, to give an indication of reaction progress and to support the data collected from off-line analytical samples. The heat exchanger would play a valuable role in this set up, cooling the high 140 °C temperature FTR product stream back down to room temperature to allow the accurate measurements of optical activity, and to maintain the temperature of the reservoir at ambient temperature (Figure 54).

The final developmental step of the FTR-CE-DKR process was to confirm that the kinetically-resolved chiral amide *R* – **145** is not racemised by the Pd catalyst under the hard FTR conditions. Using the DSPR to simulate the high temperature and pressure flow conditions in batch over longer reaction times, an optically pure sample of *R* – **145** was exposed to Pd/γ-Al$_2$O$_3$ at 145 °C for 1 hour. It was confirmed that the amide remained configurationally stable with no change of mass balance, indicating the chiral amide is safe to be recycled through the system without decomposition or compromise in optical activity.
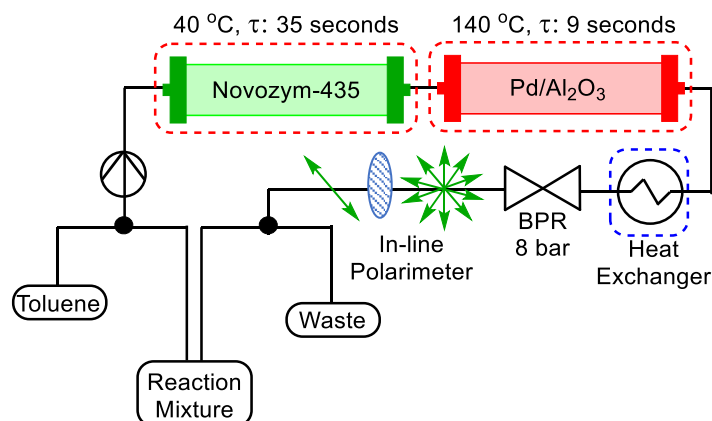

Figure 54 The fully compartmentalised FTR-CE-DKR flow system for the resolution of racemic amines.[118]

5.2.2. The CE-DKR of 1-phenylethylamine, **70**

With the flow system assembled, a CE-DKR process was performed with 1 gram of **70**, in order to benchmark this approach against previously reported processes. This would simultaneously attempt to address two limitations of CE-DKR, with regard to both productivity and scalability. The CE-DKR of **70** has been consistently limited to small scale reactions across all processes, the only exception being *Bäckvall's* successful gram scale synthesis in 2010.[86]
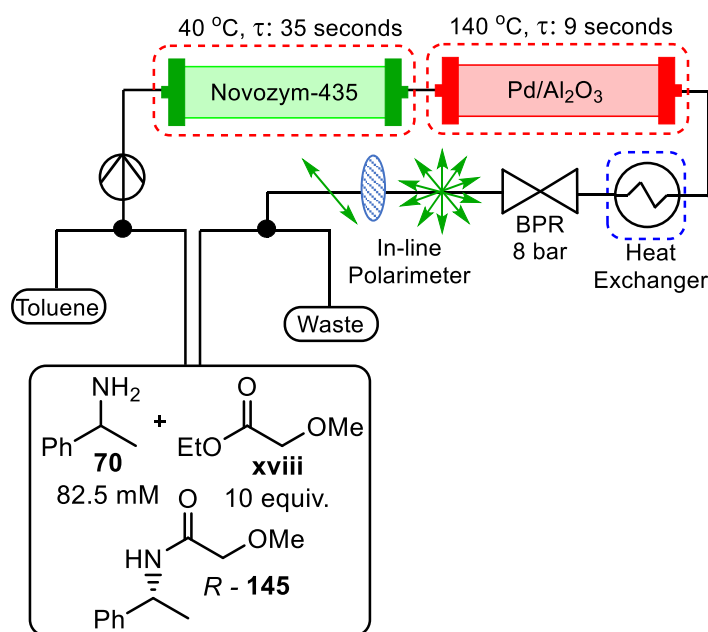

Figure 55 The fully compartmentalised FTR-CE-DKR flow system for the resolution of **70**.[118]

An 82.5 mM stock solution of **70** was prepared in anhydrous toluene, to which 10 equivalents of the acyl donor **xviii** and 25 g of molecular sieve was added, in order to ensure the stock solution maintained anhydrous and the EtOH by-product was removed from solution (Figure 55). The system was primed with anhydrous toluene, while the temperatures of the reactors was brought to the set points. Once the temperatures had stabilised, the flow rate of the mobile phase was increased to the 7 mL min^{-1}. The inlet was switched to the stock solution. Once breakthrough of the substrate was observed by the polarimeter, the outlet was diverted from waste to the stock solution reservoir. Aliquots of the reaction mixture were taken every 15 minutes, for off-line GC analysis to quantify the progress of the reaction, and chiral HPLC to establish the e.e. of *R* – **145**. The reaction progressed steadily over the 1 hour reaction time with good retention of chemo-and enantio-selectivities (Figure 56). After 1 hour, the reaction was observed to proceed to 90 % conversion, to afford the *R* – **145** with an overall 95 % e.e. and 96 % selectivity. The selectivity of a CE-DKR process is defined as the sum of the final concentrations of the amine and amide, relative to the initial amine concentration (Equation 22).

141

$$CE - DKR \text{ Selectivity (\%)} = \frac{[\text{Amine}]_{\text{Final}} + [\text{Amide}]_{\text{Final}}}{[\text{Amine}]_{\text{Initial}}} \times 100 \quad \text{Equation 22}$$

The productivity and scalability of this reaction stem from the physical and chemical compartmentalisation that this system achieves. The two individually optimised processes are shown to perform best at temperatures 100 °C apart. This shows the substantial compromises that have to be taken when they are not decoupled. Furthermore, the absence of any additives in this process prevents deactivation of either catalyst, as well as greatly reducing waste.
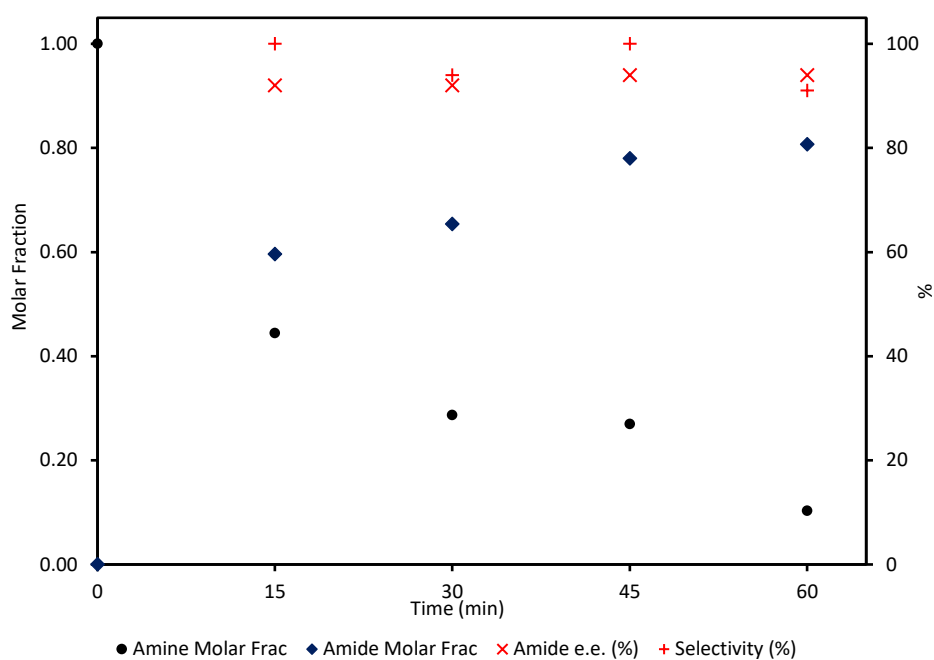

Figure 56 Reaction progression of the CE-DKR of **70**.[118]

This result was hugely encouraging, not only was the reaction able to deliver high e.e. and selectivity, but it was also able to deliver a STY of 1465 µmol mL^{-1} h^{-1} (Table 44, Entry 1). This represents a > 600-fold increase in productivity compared to the only other previously reported gram scale CE-DKR by *Bäckvall* (Entry 8).[86] Furthermore, it was also able to out-perform flow systems developed by *Miranda* and *Poppe* (Entries 9 and 10) by > 100-fold and 58-fold respectively.[90,140]

Table 44 A summary of the green chemistry metrics for the most productive CE-DKR of **70**.

Entry	Reactor	Conc. (mM)	Conv. (%)	e.e. (%)	STY (μmol mL^{-1} h^{-1})	AE	RME	PMI	Reference
1	Flow	82.5	90	95	1465	80.8	13.4	69.2	This Work[118]
2	Batch	62.5	91	> 99	3.13	73.1	66.5	75.1	[De Vos 2005][101]
3	Batch	82.5	100	91	1.59	80.8	79.6	57.8	[De Vos 2008][87]
4	Batch	82.5	70	99	2.22	73.1	50.5	97.7	[De Vos 2008][87]
5	Microwave	82.5	73	99	72.3	80.8	57.2	79.2	[De Vos 2008][74]
6	Microwave[a]	82.5	88	97	87.1	80.8	69.0	65.7	[De Vos 2008][74]
7	Batch	37.5	97	99	6.06	76.3	54.2	96.2	[Kim 2010][82]
8	Batch	200	93	97	2.38	80.8	75.1	27.3	[Bäckvall 2010][86]
9	Flow	213	77	95	14.5	85.8	45.2	33.3	[Miranda 2014][89]
10	Flow	138	99	> 99	25.1	76.3	49.6	37.0	[Poppe 2018][90]

[a]Microwave irradiated.

Although this work was developed to maximise the productivity of the reaction, it is also important to evaluate the sustainability of the process. To conduct a quantitative analysis the Chem21 Toolbox, a holistic evaluation of the green metric of a reaction, was used (Table 44).[153] It can be observed that the Atom Economy (AE) (Equation 23), where a score closer to 100 is more desirable, of all processes was high, due to the relatively small mass of the acyl donor leaving group. However, our work was able feature towards the upper end of this metric due to the use of a EtO which has a lower molecular weight compared to an ^{i}PrO group (Section 4.1.2.).

$$\text{AE} = \frac{\text{Molecular Weight of Product}}{\text{Total Molecualar Weight of Reactants}} \times 100 \quad \text{Equation 23}$$

This process was shown to perform badly with regard to Reaction Mass Efficiency (RME) (Equation 24), where the higher the value reflects a more desirable process as less reagents are wasted (Entry 1). This is exclusively due to the extremely high number of acyl donor equivalents, 10, used in this work. This was necessary to drive high rates of productivity, observed in the STY, but is extremely wasteful compared to many of the alternative process that use close to 1 equivalent. If the FTR-CE-DKR was further optimised to decrease the number of acyl donors to just 1equivalent, the RME would be significantly improved to 72.7, making it competitive with the best performing processes developed by *De Vos* and *Bäckvall* (Entries 3 and 8).

$$\text{RME} = \frac{\text{Mass of Product}}{\text{Total Mass of Reactants}} \times 100 \quad \text{Equation 24}$$

143

The final green chemistry metric that was evaluated was the Process Mass Intensity (PMI) (Equation 25), where all chemicals involved in the process are considered. However, unfortunately, during the reporting of the prior literature there is insufficient detail to include the chemicals and solvents involved in the PMI calculations. By this metric the FTR-CE-DKR process (Entry 1) performed well due to the absence of any additional additives, outperforming many of the other processes (Entries 2 – 7). The exceptions to this were the Raney Co two-pot system (Entry 3), which is an extremely unproductive process due to the need for manual intervention, and the microwave irradiated process (Entry 6) which performed very similarly. The PMI can be seen to decrease drastically for Entries 8 – 10, this is largely due to a significant increase in substrate concentration, which greatly reduces the mass of the solvent involved. This suggests further development of the FTR-CE-DKR process to operate at higher concentrations could be considered to increase this desirability metric, since doubling the concentration of the reaction to 165 mM would decrease the PMI from 69.2 to 32.9, making it extremely competitive. Increasing the concentration of the process would also further increase the productivity.

$$\text{PMI} = \frac{\text{Total Mass in Process}}{\text{Mass of Product}} \times 100 \quad \text{Equation 25}$$

Overall, it can be seen that although the FTR-CE-DKR process falls short of other CE-DKR processes with regard to RME, it remains competitive with many of the literature precedents with regard to AE and PMI whilst also delivering greatly improved productivity (Table 44). Furthermore, the alternative processes discussed in this work are not scalable, therefore reuse of the racemisation and KR catalysts in the FTR-CE-DKR further increase the green characteristic of this process. A final significant advantage that the FTR-CE-DKR process brings over the other approaches, and which would decrease the PMI relative to the other strategies, is that the reaction has been found to be an extremely clean, requiring no formal work up. The solvent and any excess acyl donor are simply removed by rotary evaporation to leave an extremely pure crude product by NMR (Figure 57).
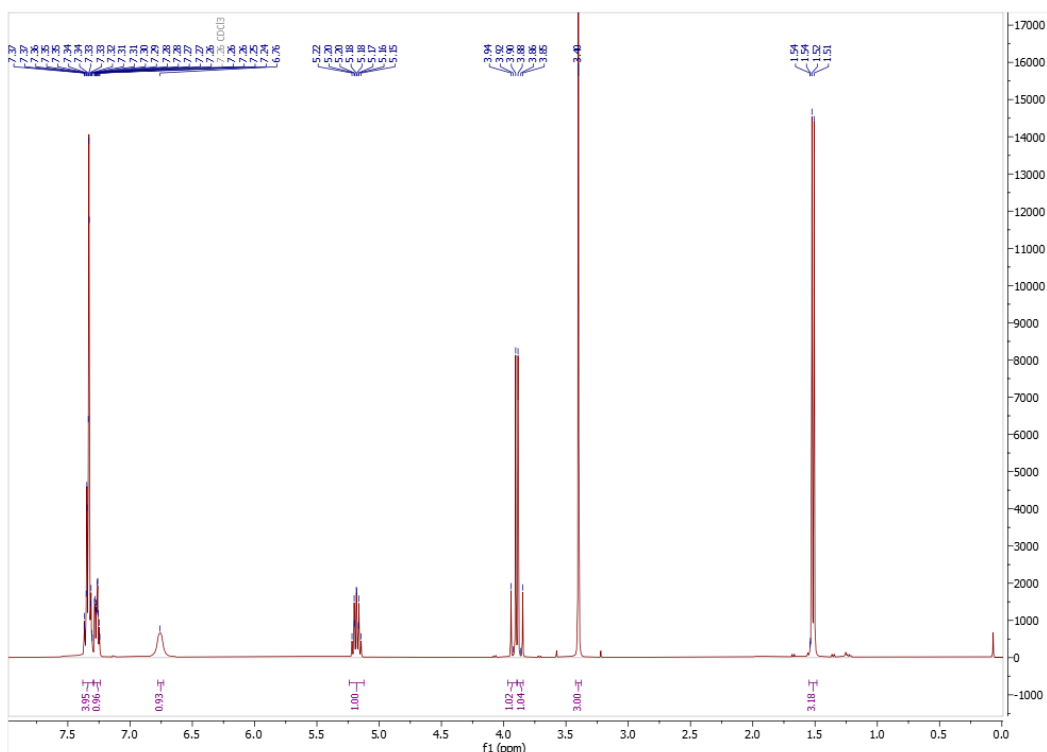
Figure 57 The crude NMR of *R* - **145**.[118]

5.2.3. The CE-DKR of 1-aminoindan, **94**

With extremely encouraging results being achieved with the model substrate, **70**, it was decided to apply FTR-CE-DKR to a substrate that is of commercial interest. To this end, 1-aminoindan, **94**, a key building block for the anti-Parkinson's disease drug Rasagiline was selected (Scheme 33).[118] There were few literature precedents for the CE-DKR for **94** (Table 45). The first reported resolution was by *Kim* et al. who employed Pd/C as the racemisation catalyst to achieved 98 % conversion over 120 hour to deliver *R* – **95** with 95 % e.e. (Entry 1.)[84] Subsequently, *Bäckvall* used the homogeneous Ru-Shvo catalyst **105**, to achieved 92 % conversion over 72 hours (Entry 2) to attain the same enantioselectivity and productivity reported by *Kim* (Entry 1).[80]
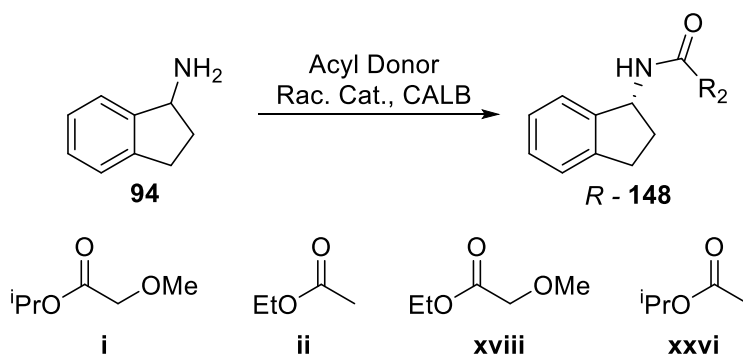
Scheme 33 The generic scheme for the CE-DKR of **94**.

Table 45 A summary of the CE-DKR of **94**.

Entry	Catalyst	Temp. (°C)	Time (h)	Conc. (mM)	AD (Equiv.)	Additives	Conv. (%)	Amide e.e. (%)	STY (μmol mL^{-1} h^{-1})	Reference
1	Pd/C	60	120	100	**ii** (2)	DIPEA	98	95	0.817	[Kim 2001][84]
2	Ru-Shvo	90	72	62.5	**xxvi** (7)	Na$_2$CO$_3$/IPA	92	95	0.799	[Bäckvall 2005][80]
3	Pd/AlO(OH)	70	72	100	**ii** (3)	-	88	99	1.22	[Kim 2007][83]
4	Pd/AlO(OH)	70	12	50	**i** (1.7)	-	93	96	3.88	[Kim 2010][82]
5	Pd/AlO(OH)	50	12	1500	**i** (1.5)	Na$_2$CO$_3$	88	97	110	[Jia 2014][91]
6	Pd/Al$_2$O$_3$	40/140	1	82.5	**xviii** (10)	-	92	99	1362	This Work[118]
7	Pd/Al$_2$O$_3$	40/140	1.5	82.5	**xviii** (2)	-	85	98	839	This Work[118]

The CE-DKR of the substrate was revisited by *Kim* et al. twice more over the next decade (Entries 3 and 4), continuing to employ Pd based heterogeneous catalysts, in doing so the STY was improved by 5-fold compared to Entry 1.[80,82,83] However, the most significant breakthrough was achieved by *Jia* et al. in 2014 (Entry 5) with a multigram scale one-pot synthesis, as discussed in Section 1.5.3.[91] This work employed Pd/AlO(OH) to achieve an the resolution of 73.2 g (550 mmol) of **94** in 12 hours with 88 % conversion and 97 % e.e. of *R* – **95**, delivering an impressive STY of 110 μmol mL^{-1} h^{-1}, a 28-fold increase compared to *Kim* et al. (Entry 4).[82] This catalytic system was reported to be stable for up to 6 cycles. Despite the impressive results, *Jia* re-iterated the compromise that was struck between the ideal racemisation and KR conditions.

Using the same conditions optimised for **70**, the CE-DKR of **94** was performed with an 82.5 mM solution of the racemic amine in anhydrous toluene, with 10 equivalents of acyl donor **xviii**, and 25 g of molecular sieves (Figure 58). Even under these unoptimised conditions, the reaction proceeded with steady production of the desired amide and maintained high chemo and enantioselectivity throughout (Figure 59). After just 1 hour 92 % conversion to *R* - **95** can be achieved with 99% e.e. and 99 % selectivity (Table 45, Entry 6). These conditions delivered an extremely high STY of 1362 μmol mL^{-1} h^{-1}, significantly outperforming all previous attempts to resolve **94** using CE-DKR. In particular. FTR-CE-DKR achieved a > 12-fold increase in STY when compared to the synthesis by *Jia* et al. (Entry 5), whilst delivering slightly improved enantioselectivity.
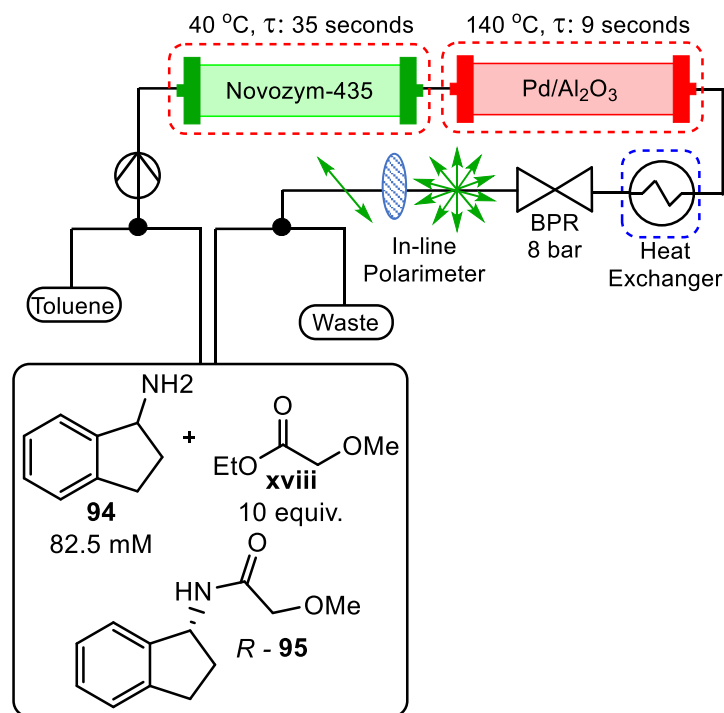
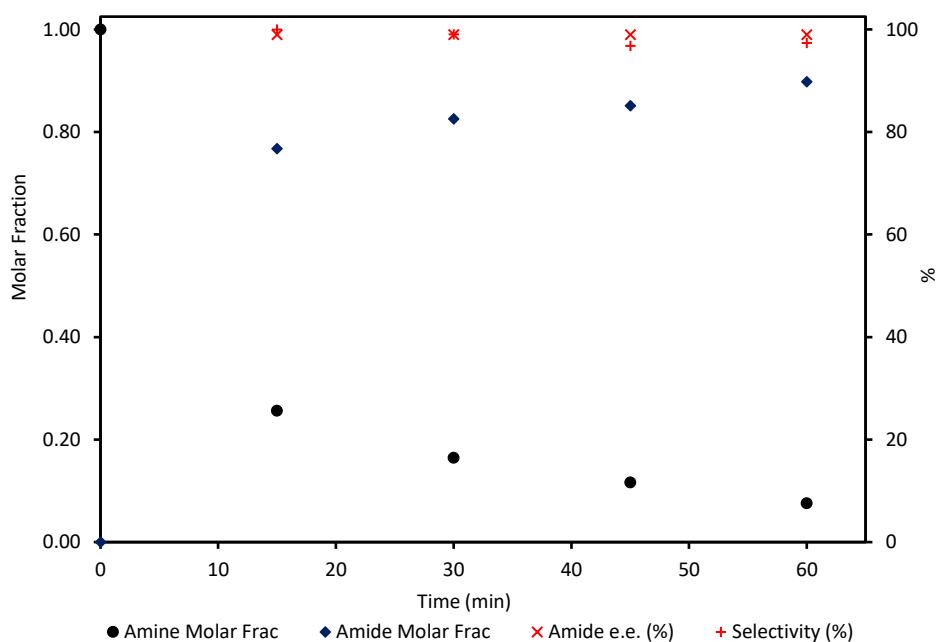*Figure 58* The FTR-CE-DKR flow system used for the resolution of **94**.[118]

Figure 59 The progression of the CE-DKR of 94, 10 equivalents.[118]

Although the STY was increased with the FTR-CE-DKR process compared to the large scale batch reaction reported by *Jia*, there were further significant improvements with respect to Process Mass Intensity and Green Chemistry Metrics (Table 46).[44] *Jia* et al.'s process requires 27.5 g of 5 % Pd/AlO(OH) (Entry 3), equating to 12900 μmol of Pd (Entry 4). Whereas the FTR-CE-DKR process only required the use of 200 mg of 5 % Pd/Al$_2$O$_3$

(Entry 3) equating to 94.0 mmol of Pd (Entry 4). If the STY of each process is normalised to the amount of Pd used, to give units of $\mu mol\ \mu mol(Pd)^{-1}\ mL^{-1}\ h^{-1}$ (Entry 5), then the FTR-CE-DKR process becomes >1700-fold more efficient than *Jia* et al.'s process. This can result in a hugely more cost effective process if carried out on an industrial scale, which as previously outlined in Section 1.3. can be the difference in the financial viability of an industrial process. Furthermore, since FRT-CE-DKR is a continuous manufacturing processes the longer the process is allowed to run, the lower the effective loading of the catalyst also becomes over the total amount of material produced, making it increasingly attractive.

Table 46 A comparison of productivity of FTR-CE-DKR and batch CE-DKR of **94**.[118]

Entry	Product	This Work	*Jia* et al.
1	Conv. (%)	92	88
2	**95** e.e. (%)	99	96
3	Catalyst (g)	0.2	27.5
4	Pd (μmol)	94.0	12900
5	STY ($\mu mol\ mL^{-1}\ h^{-1}$)	1362	109.6
6	STY ($\mu mol\ \mu mol(Pd)^{-1}\ mL^{-1}\ h^{-1}$)	14.5	0.008

Although the productivity of the FTR-CE-DKR processes was significantly improved, a comparison of the environmental factors was once more conducted using the Chem21 Toolkit (Table 47). A comparison of the AE of two processes showed a marginal advantage towards to FTR-CE-DKR (Entry 1) as the EtO ester of the 2-methoxyacetate acyl donor was used in comparison to the ^{i}PrO used by *Jia* (Entry 2). Although this could easily be modified in the batch process, the STY of the process may be found to decrease due to the greater rate of reaction that the ^{i}PrO derivative affords (Section 4.1.2).

Turning the attention of the analysis of the process to the PMI (Table 47) it can be seen that *Jia* et al. (Entry 2) greatly outperforms the FTR-CE-DKR process (Entry 1) by an almost 10-fold decrease, despite the use of significant amounts of catalyst (27.5 g), Novozym-435 (18.3 g) and additives in the form of Na_2CO_3 (18.3 g). This is, once again, almost exclusively down to the 18-fold increase in concentration that is used in the large scale reaction. This once again signifies that the concentration of this proof-of-concept FTR-CE-DKR would have to be significantly increased to compete with the *Jia* process in terms of PMI. Performing the FTR-CE-DKR on the equivalent concentration to *Jia* would reduce the PMI to just 12.1, accounting for almost all of this disparity between the two processes, the remainder once again stemming from the high acyl donor equivalents.

Finally, comparing the RME results (Table 47), it can be clearly seen that *Jia* et al. (Entry 2) once again outperformed the FTR-CE-DKR approach (Entry 1), using just 1.5 equivalents of the acyl donor and significantly reducing the amount of reactant mass. Although it was felt that the acyl donor could be easily recovered and reused *via* simple distillation, it was seen as a fair criticism that such a large excess was employed. To combat this, a compromise was made and the resolution of **94** was repeated with reduced acyl donor loadings of 2 equivalents. The KR DoE created in Section 4.2.3. for **70** suggested that the conversion per pass of the KR PBR would drop from 23 % to 15 %, with no change to the amide e.e.. This was predicted to increase the reaction time to approximately 80 minutes, however that DoE was created for a different substrate, **70**, and therefore this only served as an approximation of this new substrate system.

Table 47 A comparison of the green chemistry metrics FTR-CE-DKR and traditional CE-DKR for the resolution of **94.**

Entry	Conc. (mM)	Acyl Donor Equiv	Conv. (%)	e.e. (%)	STY (μmol mL^{-1} h^{-1})	AE	RME	PMI	Reference
1	82.5	10	92	99	1362	76.9	13.5	67.9	This Work[118]
2	1500	1.5	88	97	110	72.7	51.3	6.0	[Jia 2014][91]

The FTR-CE-DKR of **94** was repeated with 2 equivalents of the acyl donor (Table 48, Entry 2) and was found, once again, to proceed in a timely manner. Although there was a drop in productivity, as expected, 85 % conversion was achieved in 90 minutes (Figure 60) to deliver a STY of 839 μmol mL^{-1} h^{-1}, which remained greater than the *Jia* et al.'s synthesis by > 7.5-fold (Table 45, Entries 5 and 7). Despite the e.e. of *R* – **95** being observed to mildly decrease over the course of the reactions, overall, the reaction was able to achieve high enantio and chemical purity, 98 % e.e. and 99 % selectivity.
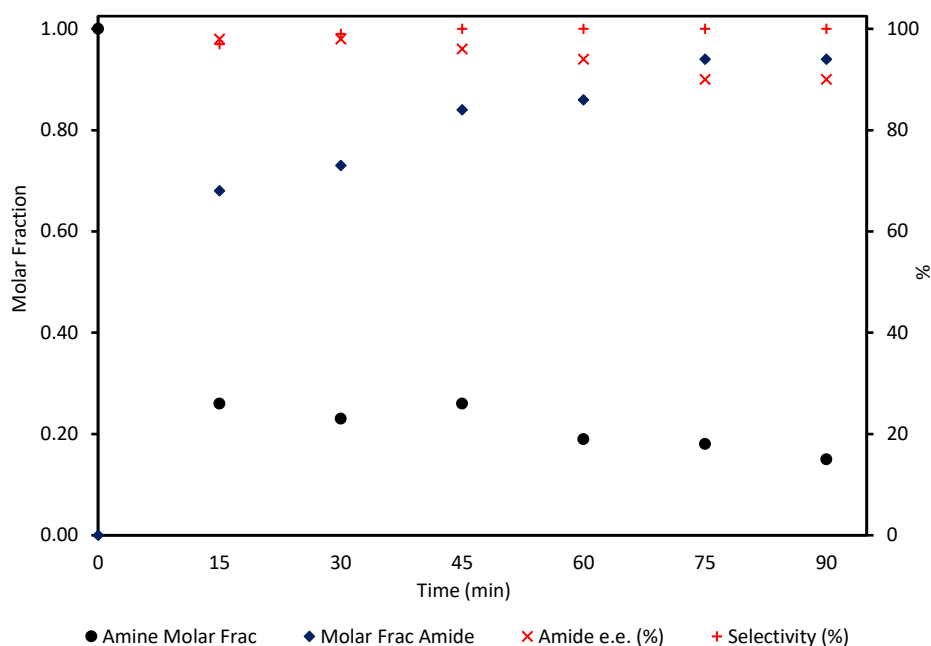
149

Figure 60 The progression of the CE-DKR of **94**, 2 equivalents.[118]

Revisiting the analysis of the Green Chemistry metrics (Table 48), it can be seen that the RME of the two processes are now very comparable (Entries 2 and 3). Further reduction of the acyl donor equivalents would enable the FTR-CE-DKR process to rank above *Jia* et al. in this metric, however it appears likely that under the current reaction conditions the conversion and integrity of *R* – **95**'s optical purity would begin to suffer. Therefore, more fundamental redevelopment may be needed to facilitate further changes to the system.

Table 48 A comparison of green chemistry metrics of the revised FTR-CE-DKR process compared to traditional the CE-DKR for the resolution of **94**.

Entry	Conc. (mM)	Acyl Donor Equiv	Conv. (%)	e.e. (%)	STY ($\mu mol\ mL^{-1}\ h^{-1}$)	AE	RME	PMI	Reference
1	82.5	10	92	99	1362	76.9	13.5	67.9	This Work[118]
2	82.5	2	85	98	839	76.9	44.5	67.8	This Work[118]
3	1500	1.5	88	97	110	72.7	51.3	6.0	[Jia 2014][91]

Despite the reduction in acyl donor equivalents, the PMI remains unchanged. This emphasises how weighted this metric is by the concentration of the substrate. The DoE of the KR process suggests that increasing the concentration of this system without redevelopment would significantly limit the productivity of the KR process (Section 4.2.4.) and therefore greatly reduce the STY. To increase the reaction concentration and maintain the high STY afforded by the FTR-CE-DKR in this example, there would have to be additional reaction engineering of the Novozym-435 PBR. Despite the slight drop in conversion of FTR-CE-DKR process with just 2 equivalents of acyl donor, an extremely clean reaction was once again achieved. The decreased conversion to 85 % warranted a simple acid wash to deliver a highly pure NMR of the crude *R* – **95** (Figure 61).
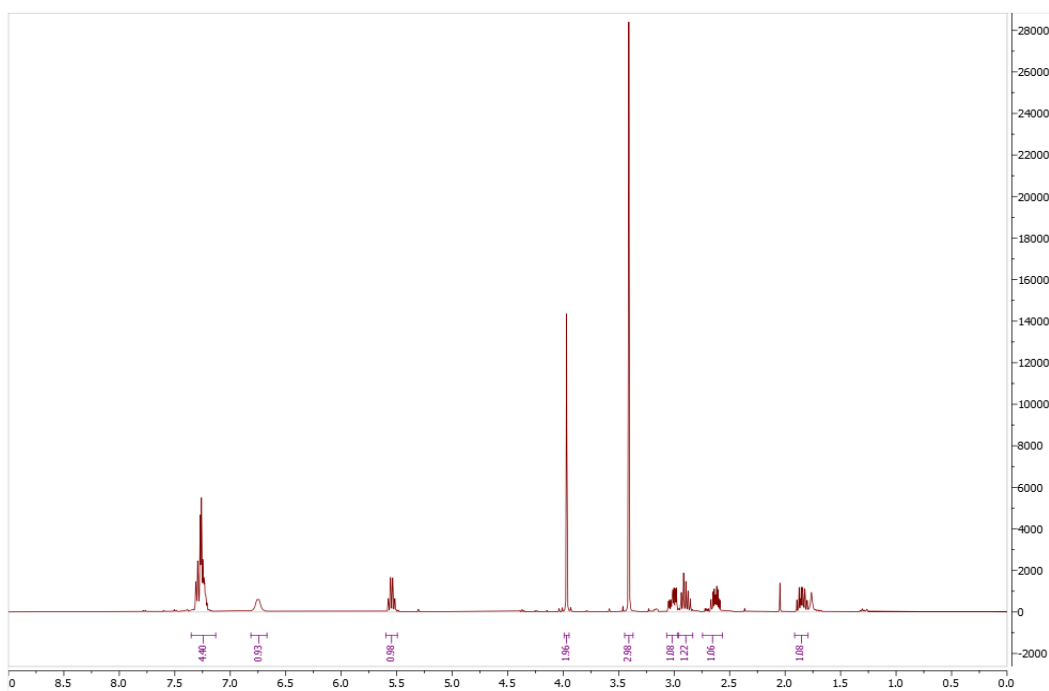
Figure 61 The crude NMR of the FTR-CE-DKR of **94** using 2 equivalents of acyl donor.[118]

5.2.4. <u>Catalytic Deactivation</u>

During the development of the FTR-CE-DKR strategy it became apparent that the presence of molecular sieves prevented the deactivation of the racemisation catalyst. A comparison of the reaction profiles obtained from experiments with and without the desiccants (Figures 62 and 63) revealed that the plateauing in conversion and drop in selectivity of the reaction was observed in the absence of the molecular sieves. It is suspected that this was due to the EtOH by-product produced during the KR reaction. This is rationalised on the basis that palladium catalysts are known to abstract H_2 from the EtOH, **149**, to form ethanal, **150** (Scheme 34), as part of a hydrogen transfer hydrogenation reaction mechanism.[154] This can result in a competitive reaction with the oxidation of the amine substrates, **70**. If the oxidation of **149** is faster than the oxidation of **70**, racemisation will be slowed or stopped completely, depending on the concentration of **149**, leading to a plateauing in conversion (Figure 62) as the feedstock of $R - $ **70** is no longer being maintained. The decrease in selectivity of the reaction is also proposed to stem from the same alcohol oxidation reaction. The presence of the reactive aldehyde could sequester **70**, *via* imine **151** to form the secondary amine, **152** (Scheme 34). This would lead to the consumption of **70** without the production of $R - $ **145**, reflected in the reduced selectivity (Figure 63). Furthermore **150** could then start a competitive reaction with the reduction of **90**, and in doing so prolonging the lifetime of **90** and increase the likelihood of reaction with **70** and the formation of diastereomeric by-products.
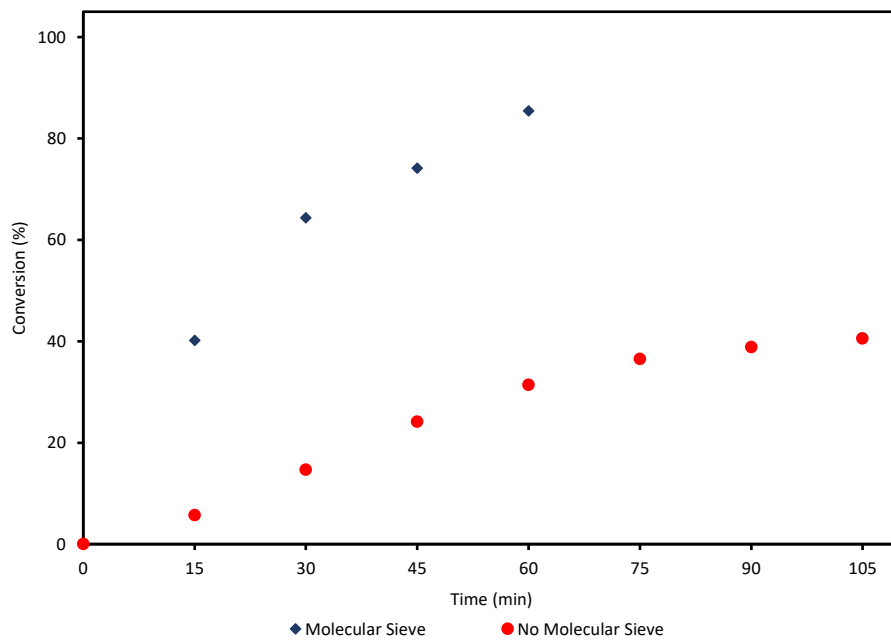
151

Figure 62 The effect of molecular sieves on conversion for the CE-DKR of **70**, 10 equivalents.[118]
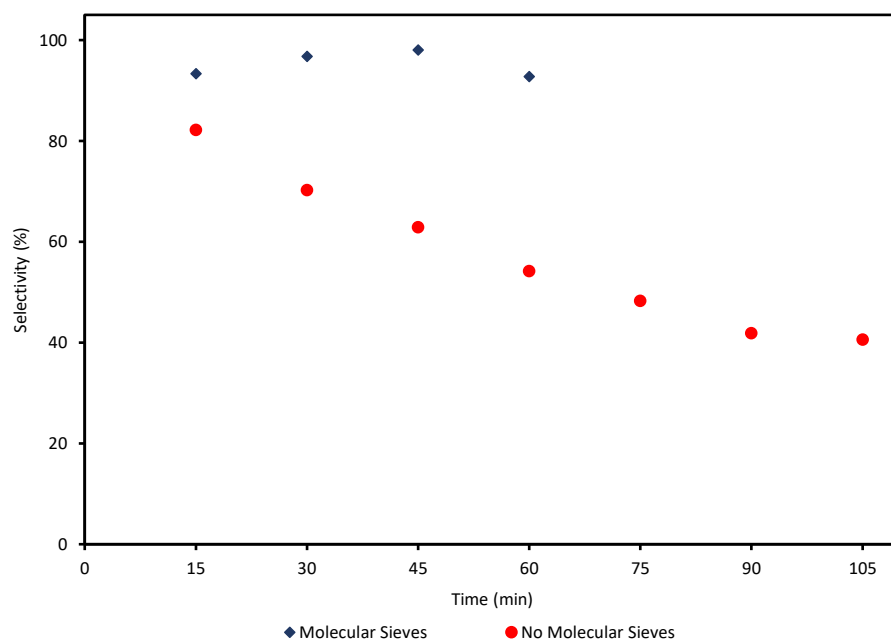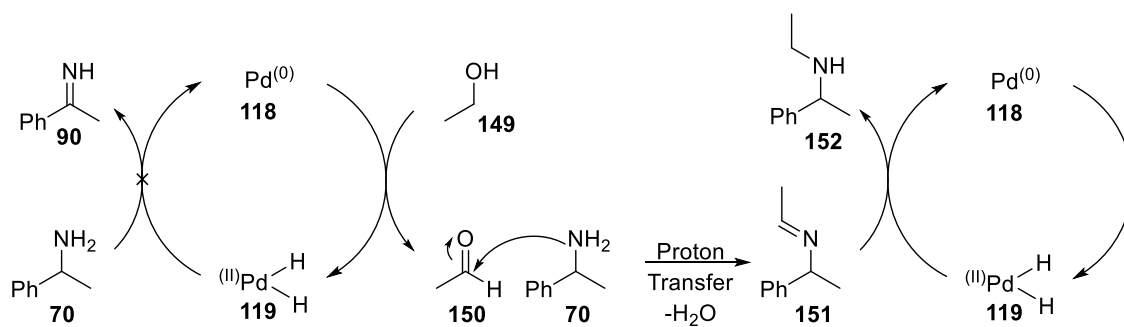

Figure 63 The effect of molecular sieves on selectivity for the CE-DKR of **70**, 10 equivalents.[118]

152

*Scheme 34* The Pd catalysed oxidation and reduction mechanism of EtOH.

The presence of molecular sieves in the reaction is proposed to absorb the EtOH produced during the KR reaction and thus prevent these competitive reactions occurring. This hypothesis is supported by the 5 Å pore size of the molecular sieves being larger than the diastereomer of EtOH molecules, 4.4 Å. This theory could be further investigated by doping of the starting reaction solution with different quantities of EtOH to monitor the conversion and selectivity of the subsequent reactions.

5.2.5. Stereocentre Inversion

Starting the synthesis of molecules containing chiral amines can be significantly more economic if starting from a chirally pure substrate, such as the chiral pool. As discussed in Section 1.1, harnessing the chiral pool for chiral amines starting materials has played a significant role in the field for over 100 years. However, using naturally occurring chiral amines as a starting point for asymmetric synthesis can be extremely restrictive as oftentimes nature only produces a single enantiomer of the desired material, such a L-amino acids and D-sugars. Purchasing the unnatural versions of these molecules is often several fold more expensive, and the materials are much less widely available. Therefore, it would be extremely desirable to have an effective method to invert the stereochemistry of these molecules without significant synthetic effort.

The most prominent example of this is the Mitsunobu reaction (Scheme 35), where an alcohol, $S-$ **143** can undergo an inversion reaction to produce $R-$ **162**, often in high yield and high stereochemical purity.[155,156] This is achieved through triphenylphosphine, **153**, attacking diethylazodicarboxylate (DEAD), **154**, to produce intermediate **153**. **153** can then deprotonate the alcohol coupling partner **156**, to produce the electrophilic species, **157**. The alcohol substrate $S-$ **143** then attacks the positively charged P atom of **157**, to form **158** which decomposes to give **159** and **160**, driven by the formation of a strong P=O bond. Attack of **160** by **156**, in an SN2 manner leads to

stereoinversion of the chiral centre to yield the inverted product $R - 162$. However, this approach is limited exclusively alcohols, relies on the coupling acid to have a pKa of < 15 and produces stoichiometric waste products.
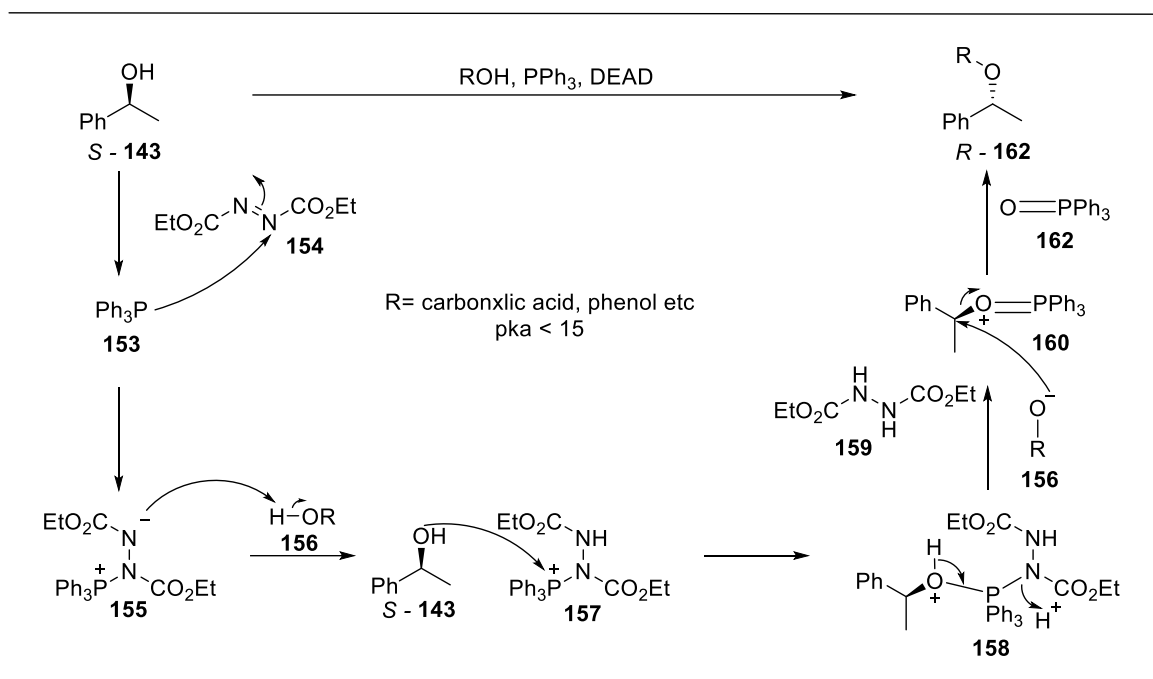
Scheme 35 The mechanism for the inversion of stereochemistry during the Mitsunobu reactions.[155,156]

It was proposed that CE-DKR could be used to perform a similar inversion of the stereochemistry of chiral amines (Scheme 36). To investigate this approach, it was decided to revert back to the model substrate and start the process with a chirally pure sample, $S - 70$.[118] From here the FTR-CE-DKR flow system could be modified by reversing the order of the PBR in the flow system (Figure 64), allowing for the FTR process to occur first. Due to the high level of racemisation that can be achieved by the FTR, after a single pass through the racemisation PBR the CE-DKR would then be able to proceed in the same way as a conventional CE-DKR reaction. At the end of the reaction $S - 70$ should be fully converted to the $R - 145$, thus fully inverting the stereochemistry.
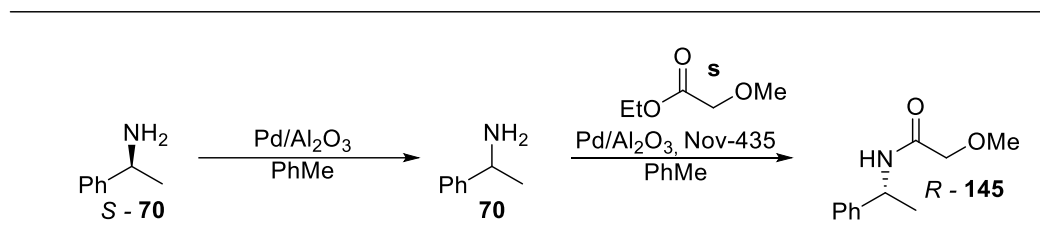
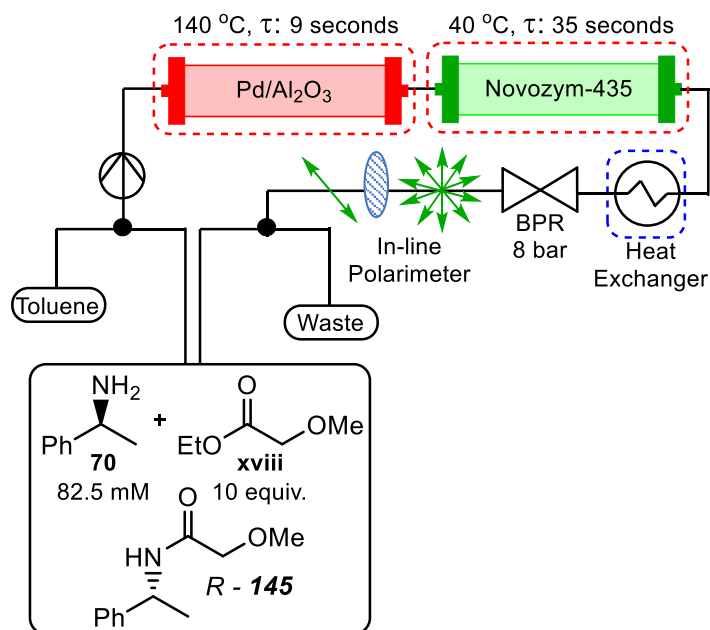Scheme 36 Using CE-DKR to invert the stereochemistry of 70.

Figure 64 The reconfigured FTR-CE-DKR flow system for the inversion of the *S* – **70** stereocentre.[118]

The inversion reaction was to be performed once again on a gram scale and using 10 equivalents of the acyl donor to maximise productivity and protect the integrity of the *R* – **145** stereocentre. It was expected that the reaction time would increase compared to the conventional FTR-CE-DKR as more mols of amine would need to be racemised, therefore more passes of the FTR PBR would be required. However, the stereoinversion reaction was found to proceed with the same efficiency as the resolution reaction (Figure 65), with 93 % conversion being achieved within 1 hour, delivering *R* – **145** with an overall e.e. of 97 % and 95 % selectivity.
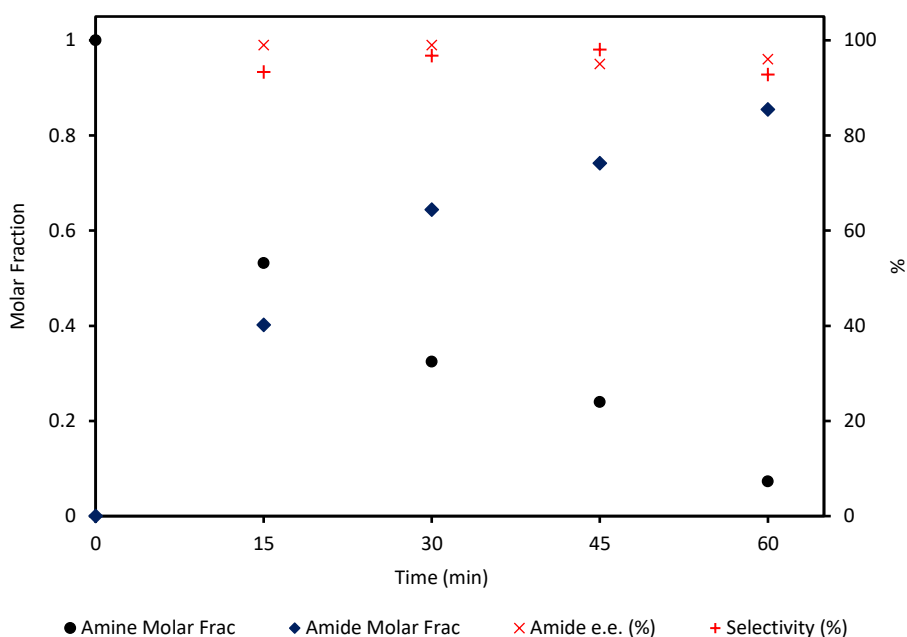

Figure 65 The progression of the FTR-CE-DKR stereocentre inversion reaction for *S*-**70**.[118]

This highly effective stereocentre inversion was able to yield a STY of 1514 μmol mL^{-1} h^{-1}, moderately outperforming the conventional FTR-CE-DKR process due to the increased conversion. This showed that the inversion reaction could be equally as productive as the resolution reactions. This is testament to the highly efficient FTR conditions, whereby the e.e. of the amine can be reduced from 100 to 41 % in the first pass. This means the reaction stream leaving the FTR PBR is 71 % of S – **70** and 29 % R – **70**, which matched the 29 % conversion that is seen during the first pass of the KR PBR. Therefore, there is no drop in productivity as the KR PBR is able to resolve the same proportion of the amine with the first pass as it would with the classical FTR-CE-DKR process. To the best of our knowledge, there has never been any reported use of CE-DKR to invert the stereochemistry of chiral amines, therefore making this productivity incomparable and a truly innovative approach.

This approach could be considered a form of molecular editing, where only a single aspect of a molecule is altered while the rest of the structure remains untouched. This is most commonly seen in the insertion, deletion or exchange of atoms in a molecule (Figure 66); however, this could be expanded into the inversion of a stereocentre.[157]

The inversion of amine stereocentres in this way could have huge implications in generating the unnatural enantiomers of amino acids. A cost-effective inversion of the stereocentre that greatly increases the value of the material would be of great interest to industry, and could no doubt be applied to other naturally occurring chiral sources. Furthermore, the easy access to unnaturally occurring amino acids may unlock easier synthesis of them for wider used in peptide drugs, where the unnatural configuration of the chiral centres may help reduce metabolism. Additionally, as previously alluded to, the cost of a multistep synthesis could be greatly reduced if a chirally pure starting material of the desired stereochemistry was readily accessible A simple inversion of the stereochemistry of a chiral pool starting material in a cost effective way, could greatly reduce cost through more direct synthesis while also cutting the cost of raw materials. Lastly, it could have an extremely interesting role in mid-stage divergent synthetic routes in natural product or medicinal chemistry, where it would be desirable to explore the properties of the opposite enantiomer of a molecule of interest, but redevelopment of the whole synthetic route is not an effective strategy.
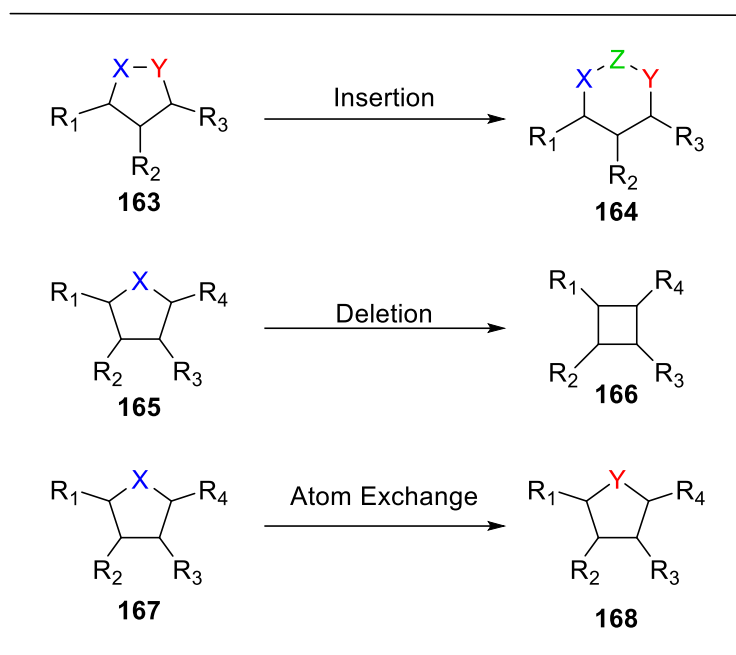
Figure 66 Examples of 'molecular editing' reactions.[157]

5.3. Conclusion

Previously CE-DKR processes suffered from both long reaction times and largely limited scalability. Although progress had been made to improve both of these limitations, efforts to compartmentalise each step of the process and transition into continuous flow had been met with limited effectiveness. In this work the FTR and KR methodologies developed in Sections 3.2. and 4.2. have successfully been brought together to create an integrated FTR-CE-DKR flow system. This has been shown to be an extremely effective methodology to produce highly enantiopure chiral amides primarily through the exponential increase in the rate of racemisation, which has largely evaded previous attempts, using FTR and deploying it as part of a compartmentalised reactor. This has allowed the overall efficiency of the system to be vastly improved, allowing the true potential of the CE-DKR transformation to be realised. As well as being shown to be much more productive than traditional CE-DKR methodologies, it has been able to achieve these improved results whilst not sacrificing Green Chemistry Principles.[44] The combination of these factors has allowed this work to take great strides towards validating this approach as an industrially viable route for the resolution of chiral amines on scale through the use of continuous manufacturing principles.

This novel system has been demonstrated to be a highly efficient strategy for the resolution of both the model substrate **70**, as well as an industrially relevant API building block **94**. Both of these substrates were resolved on a gram scale over the course of just 1 hour with both selectivity and the e.e. of the product amide being in excess of 95 %. These impressive demonstrations of efficiency were achieved with a flow system that was deemed fit for

proof-of-concept but further significant increases in productivity are anticipated with additional development. Furthermore, this system has given rise to the inventive use of CE-DKR to invert the stereochemistry of amines in a newly explored branch of molecular editing. This has great potential for use across a wide range of synthetic organic chemistry pertaining to both R&D as well as production scale usage.

Moving forward, while the productivity of the reaction has been greatly improved, the FTR-CE-DKR process must be further developed to improve the green chemistry metrics measured during the Chem21 Toolbox analysis. Continued development of the KR reactor system is hoped to permit the number acyl donor equivalents to be reduced further, to fall in-line with competitive literature and increase the RME, whilst negating the fall in conversion and the potential for the loss of enantioselectivity during the process. Furthermore, this will allow the concentration of substrate used in the process to be increased. This will not only further increase the STY of the system, but also greatly reduce the currently high PMI of the system. Addressing these shortcomings of the current system will further increase the viability of this process as a complimentary tool for the synthesis of chiral amines in an industrial setting.

Chapter 6: <u>Future Works</u>

Currently the FTR-CE-DKR process developed in this work has demonstrated that it is capable of highly productive resolutions of both **70** and **94** on a gram scale. However, much of the reported work has been of a proof-of-concept nature, therefore providing many areas of potential improvement. As part of this future work, development of the flow system would be conducted whereby the capacity of the KR PBR would be increased to permit a greater residence time and Novozym-435 loading to be achieved. This would enable greater single pass conversions as well as higher concentrations of the substrate to be used, further increasing the STY of the system. The increase in concentration achieved would greatly improve the PMI of the process, an area that is currently found to be underdeveloped (Section 5.2.3.). Additional chemical engineering modifications would include the refinement of the recycle loop system to formally produce a fully continuous system including automation of the switching of the inlet and outlet valves.

Although the substrates explored in the FTR-CE-DKR process to date covered the ubiquitous **70** and the industrially relevant API, **94**, further expansion of the substrate scope is of high priority. Demonstrating the high productivity of this methodology across a larger range of widely used substrates would lend greater weight to support the push for such a strategy to be adopted into industrial processes. This could include utilising more of the substrates already explored during the FTR substrate scoping exercise detailed in Section 3.2.5. which have already been shown to be amenable to the FTR strategy. More generally, this could also be applied to alcohol substrates that are extensively explored in the CE-DKR space, owing to their more facile racemisation, to further challenge the FTR-CE-DKR process against the established methodologies.

The development of the flow system and the diversification of the substrate scope could be brought together to permit an effective scale up of industrially relevant compounds on the 10 g – 100 g scale. Subsequently a techno-economic analysis could be performed, alongside the Chem21 toolbox analysis, to benchmark this work against existing manufacturing processes. This would provide a quantitative comparison of a scientific, economic and environmental metrics which would be able to determine whether this process is truly viable for industrial use.

Chapter 7: <u>Experimental</u>

7.1. <u>Materials and Characterisation</u>

Unless otherwise stated, materials were purchased from commercial sources and used as received. All anhydrous solvents were dried over molecular sieves using solvent purification systems. 5 wt% Pd/Al_2O_3 was purchased from Sigma and silicon carbide (SiC) was purchased from Fischer; both were sieved to afford samples with particle sizes of between 60–108 micron (Pd/Al_2O_3) and 140-180 micron (SiC), respectively, before they were deployed in the packed bed. ^1H and ^{13}C NMR spectra were recorded on a 400 MHz Bruker AVANCE III HD spectrometer. Unless otherwise stated, ^1H and ^{13}C NMR chemical shifts are reported in $CDCl_3$, relative to residual protic solvent peaks: $\delta_H = 7.26$ ppm and $\delta_C = 77$ ppm, respectively. Multiplicity is denoted as follows: s = singlet, b = broad, d = doublet, t = triplet, q = quartet, p = pentet, m = multiplet and coupling constants (J values) are given in Hz. Infrared spectra (solid sample or thin film) were recorded on an Agilent Cary 630 FTIR fitted with a diamond ATR crystal. Melting points were recorded using a Gallenkamp melting point apparatus. GC-MS analysis was performed using a HP 6890 gas chromatograph equipped with a H_2 flame ionisation detector and an HP5 (5% phenyl methyl siloxane) Agilent column (30 m × 0.32 mm × 0.25 μm). The temperature ramp used was: 50 °C (hold 0.5 min), 50 – 150 °C (50 °C min^{-1}), 150 - 300 °C (75 °C min^{-1}), 300 °C (Hold 2 min). Chiral LC analysis was performed using an Agilent 1290 Infinity II instrument, fitted with an InfinityLab Poroshell 120 Chiral CF column (100 mm x 2.1 mm x 2.7 μm) using an isocratic solvent system of 80/20/0.3/0.2 MeCN/MeOH/acetic acid/triethylamine at 0.25 mL min^{-1}, or an OD-H Chiralpak column using an isocratic cyclohexane/IPA/Et$_2$NH (95/5/0.1) solvent system at 0.8 mL min^{-1}. Chromatograms were recorded by a diode array UV-Vis detector, using 254 and 210 nm absorbances for quantification.

Specific terminologies (Conversion, Selectivity, Space-Time Yield and TOF) are used in the thesis according to conventional usage of these terms in the field of dynamic kinetic resolution:

1. Conversion (%) refers to the amount of the amine precursor consumed during the (dynamic) kinetic resolution:

2.

$$\text{Conversion (\%)} = \frac{[\text{Amine}]_{\text{Initial}} - [\text{Amine}]_{\text{Final}}}{[\text{Amine}]_{\text{Initial}}} \times 100$$

3. Selectivity (%) refers to the amount of the desired product in the product mixture.

a. For the FTR:

$$\text{Selectivity (\%)} = \frac{[\text{Amine}]_{\text{Final}}}{[\text{Amine}]_{\text{Intial}}} \times 100$$

b. For the DKR:

$$\text{Selectivity (\%)} = \frac{[\text{Amine}]_{\text{Final}} + [\text{Amide}]_{\text{Final}}}{[\text{Amine}]_{\text{Initial}}} \times 100$$

4. Enantioselectivity (e.e.) refers to the optical purity of the chiral amine or chiral amide:

$$\text{ee (\%)} = \frac{\text{ee}_{\text{S}} - \text{ee}_{\text{R}}}{\text{ee}_{\text{S}} + \text{ee}_{\text{R}}} \times 100$$

5. Space-Time-Yield (STY):

$$\text{STY (\textmu mol mL}^{-1}\text{h}^{-1}) = \frac{\text{Amine (\textmu mol)}}{\text{Volume (mL)x Time (h)}}$$

6. Turnover Frequency

a. Batch:

$$\text{TOF (h}^{-1}) = \frac{\text{Frac. Racemised x Amine (mmol) x 60}}{\text{Cat. (mmol) x Reaction Time (min)}}$$

b. Continuous Flow

$$\text{TOF (h}^{-1}) = \frac{\text{Frac. Racemised x Volume of Reactor (mL) x [Amine]}_{\text{Initial}} \text{ x 60}}{\text{Cat. (mmol) x } \tau \text{ (min)}}$$

7.2. Racemisation of **70** in Batch

A 0.5 – 2 mL Biotage microwave vial was charged with 5 % Pd/γ-Al$_2$O$_3$ (84 mg, 12 mol %; 42 mg, 6 mol %; 21 mg, 3 mol %; or 7 mg, 1 mol %) and appropriate stirrer bar under N$_2$. To this a solution of *S* - **70** (42.6 µL, 0.330 mmol) in anhydrous toluene (4 mL) was added. The inert atmosphere was then exchanged for H$_2$ *via* a vacuum line and H$_2$ balloon before the balloon was removed to leave a sealed system. The reaction mixture was heated to 70 or 100 ºC under stirring in a thermostatically controlled oil bath for 1 hour. The e.e. of the product was determined by chiral LC.

7.3. DPSR HTS Protocol 3 – Reproductivity Screen

46 x 2 mL HPLC vials were loaded into the DSPR 48-well plate, and the reactor placed in the Unchained Junior Solid Dispensing Robot. The robot dispensed 46 x 5 % Pd/γ-Al$_2$O$_3$ (1.75 mg, 1 mol %) into each of the HPLC vials, before a 0.5 – 2 mL Biotage stirrer bars was manually placed into each vial. The Handystepper Repetitive Pipette was fitted with the 50 mL reservoir, which was charged with a previously prepared stock solution of 82.5

mM of *S* - **70** in anhydrous toluene. The pipette "steps" were set to 50 x 1 mL, and 1 mL of the solution was subsequently dispensed into each of the HPLC vials. Two further HPLC vials were randomly distributed across the plate, one containing 1 mL of the stock solution and the other completely empty. The vials were then covered by a Telon cover sheet, followed by a Silicon Rubber vial cushion before a metal plate was gently screwed into position to secure the vials. The top plate of the DSPR was then fitted and screwed into place, ensuring each screw was tightened to its full extent. The atmosphere in the DSPR was then exchanged by pressurising to 3.5 bar with N_2 before releasing the inert atmosphere. This was repeated three times, leaving the system under a N_2 atmosphere. The N_2 atmosphere was displaced *via* the same method using H_2 at 3.5 bar before increasing to 5 bar with H_2. The DSPR was heated *via* the Junior Reactor to 100 °C, while under monitoring by the internal thermocouple. Once the desired temperature had been reached stirring at 200 RPM was initiated. After 1 hour the reactor was actively cooled to 15 °C *via* the Junior Reactors Recirculatory Chiller Unit, the pressure released, and the top plate and vial covers removed. The DSPR was then transferred to the Opentron OT-2 Pipetting Robot for analytical sample preparation, fitted with both 20 µL and a 1 mL pipette tips. The robot took a 20 µL aliquot of each reaction and dispensed it into a new HPLC vial. After each reaction had been sampled, the robot performed a 50-fold dilution by dispensing 1 mL of a 10 mM anisole in MeOH stock solution into the new vials. Each sample was analysed by chiral LC to determine e.e. and achiral GC to determine selectivity.

7.4. Catalyst Cartridge Preparation

7.4.1. Pd/Al$_2$O$_3$

The end of a ¼-inch OD SS column was sealed with a plug of glass wool, on top of which 200 mg of sand was loaded. 200 mg of 5 wt% Pd/Al$_2$O$_3$ (60 - 108 micron) was mixed with 1 g of SiC (180 micron) thoroughly before loading. The packed bed was topped with 200 mg of sand and sealed using glass wool. Residence time was calculated from taking the difference between dry and wet weight of the column, to give a void volume of 1.05 mL (toluene $\rho = 0.867$ mg/mL)[158]. This results in residence times of 63 seconds, 16 seconds and 9 seconds at 1 mL min^{-1}, 4 mL min^{-1} and 7 mL min^{-1} respectively.

7.4.2. Novozym-435

A packed bed reactor was created by loosely packing an Omnifit glass column (10 mm ID. x 100 mm) with Novozym-435 (800 mg) and crushed 5 Å molecular sieves (1.90 g, for the DoE work, Figure 69) or exclusively Novozym-435 (1.70 g, for the CE-DKR, Figure 70). The column was mounted in a heating jacket and fitted in the Custom Flow Reactor where anhydrous toluene was passed through the packed bed at 1 mL min^{-1}. The packed

bed column was then left for 0.5 hours to allow the resin to swell, before it was compressed by depressing the plunger manually to give the working reactor unit. Residence time was calculated from taking the difference between dry and wet weight of the column, to give a void volume of 4.02 mL (toluene $\rho = 0.867$ mg/mL[1]). This corresponds to a residence time of 35 seconds at a flow rate of 7 mL min^{-1}.

7.5. Continuous Flow Reactors

The Gilson 305 HPLC pump used in the flow systems described below was fitted with a 10 mL WSC pump head. The pump was maintained by regularly cleaning of the check values and pump components by sonication in MeOH and checking flow rate of the reassembled system at different flow rates and temperatures.

The detection range of the Jasco 2090 Flow Polarimeter was set to 5, Response set to Slow, and Gain set to x 1.
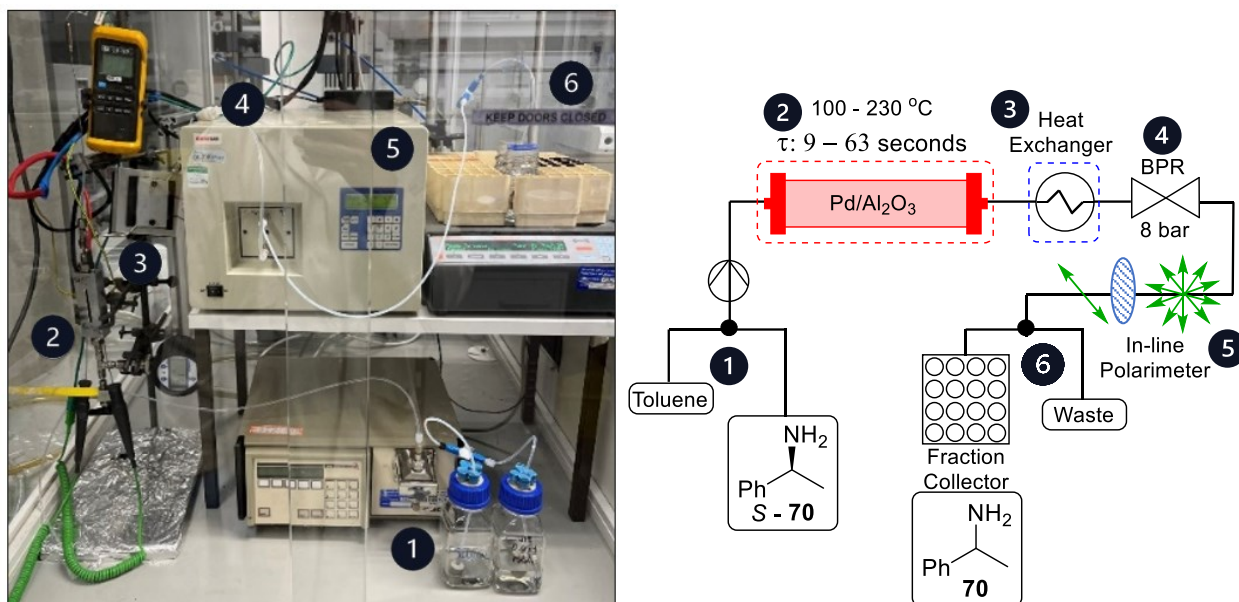
7.5.1. Flow reactor for Amine Racemisation

Figure 67 Schematic of a custom-built FTR reactor: 1. HPLC pumps; 2. Packed-bed reactor (PBR); 3. Heat Exchanger; 4. Back pressure regulator (BPR); 5. In-line polarimeter; 6. Fraction collector, or waste.

A flow reactor system was constructed for the thermal flash racemisation of chiral amines (Figure 67) :

1. Solvents and amine solutions are delivered from Duran bottles **70** fitted with a 4-port screw cap containing inlet tubing and a nitrogen-filled balloon to keep the content under dry conditions (not shown). The inlet PFA tubing lines (1/8" OD, 1.59 mm ID, 24 cm) are connected to a three-way ball valve, which is connected to a Gilson 305 HPLC pump (1/8" PFA tubing, 24 cm).

2. Using PFA tubing (1/8" OD, 35 cm), the outlet of the pump is connected to a Swagelok T-piece, fitted with an in-line Omega digital pressure gauge, and the SS heating block containing the packed bed reactor (PBR), which

163

was previous described in earlier work from the Hii Group.[159] The heating block containing the PBR was heated by cartridges with PID temperature control, with a separate thermocouple fitted at the exit of the heating block to monitor the temperature of the exiting solution.

3. The exit of the heating block was connected to 10 cm of SS tubing (1/8" OD, 1.59 mm ID) which passes through a custom-built custom cooling block milled to fit 1/8" OD SS tubing, powered by a 60 W Peltier thermo-electric cooling module and heatsink assembly (PiHut).

4. The exit of the cooling module is connected to PFA tubing (1/8" OD, 10 cm) to a back pressure regular (BPR), manually adjusted to 8 bar.

5. The outlet of the PBR is directed into a JASCO-2090 Polarimeter. Finally, PFA tubing (1/8" OD, 65 cm) connects the exit of the polarimeter to a two-way valve, which diverts the flowing solution either to a fraction collector (Spectrum Lab CD-2), or waste.

The total reactor volume is approximately 4.43 mL, comprising of 3.38 mL tubing and 1.05 mL void volume in the PBR. The residence time distribution (RTD) of the reactor system was established by pumping an 82.5 mM solution of **70** in toluene at 7 mL min^{-1} through the system, samples were collected every 30 seconds and analysed by achiral GC and chiral HPLC. A full breakthrough is obtained after 2 minutes (Figure 68a). This equates to approximately 3.25 reactor volumes to achieve steady state.
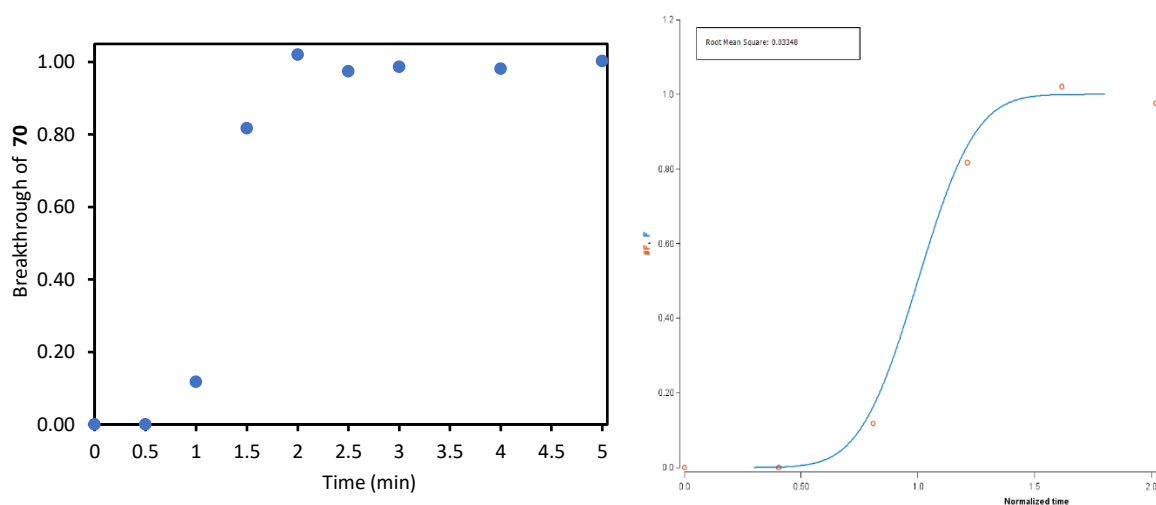

Figure 68 a)*:* A breakthrough plot of the concentration of **1** through the reactor system against time (left). B) Fitting Equation 1 (using Berkeley Madonna) to the experimental data (right).

The Péclet number (Pe) for the reactor system can be obtained by fitting a dispersion function to the sigmoidal change in the concentration of **70** (Equation 26, Figure 68b), to obtain a description of the extent of the deviation of the system from a Plug Flow Reactor (PFR).[160]

$$\frac{dF}{dt} = \frac{e^{-\frac{(1-t)^2}{4\,X}}}{\sqrt{12.566\,X}} \quad \text{Equation 26}$$

where

$$X = \frac{1}{Pe} \quad \text{Equation 27}$$

The Péclet number was experimentally determined to be 53, indicating average plug flow behaviour over the entire rector system.

7.5.1.1. <u>Typical Procedure for FTR of Amines</u>

The packed bed reactor was prepared as described in Section 7.4.1. and mounted in the heating block. The flow reaction system primed by anhydrous toluene at 1 mL min^{-1} for 10 minutes. The flow was then adjusted to 0.5 mL min^{-1} during heating. When the desired temperature was reached, the flow was then set to the desired rate (Table 49), until the in-line polarimeter showed a stable reading and set to zero. The inlet was then switched to the reagent line, containing S - **70**. The reaction was monitored by the polarimeter, which was used to established when steady state had been achieved (a stable reading). The flow of the reactant was maintained for a further 5 minutes at steady state, during which time 5 samples were collected (1 sample/min). The volume of sample collected will therefore depend on the flow rate i.e., 1/0.7/0.3 mL min^{-1} = 5 x 1/0.7/0.3 mL samples, respectively. The collected sample were diluted and subject to GC and (chiral) HPLC analysis to determine the product distribution.

1-Phenylethylamine, **70**: ^{1}H NMR (400 MHz, CDCl$_3$) δ 7.41 – 7.33 (m, 4H), 7.30 – 7.21 (m, 1H), 4.14 (q, J = 6.6 Hz, 1H), 1.50 (NH, s, 2H), 1.42 (d, J = 6.6 Hz, 3H). ^{13}C NMR (101 MHz, CDCl3) δ 147.7, 128.3, 126.6, 125.5, 51.1, 25.56. IR: ν$_{max}$/cm^{-1} 3373 (N-H stretch), 2961 (Ar C-H), 1449 (C-H bend), 1367 (C-N stretch). Chiral HPLC conditions: InfinityLab Poroshell 120 Chiral CF, t_s = 5.38 min, t_R = 5.77 min. S/R- 1-phenyl-N-(1-phenylethyl)ethan-1-imine, **91**: ^{1}H NMR (400 MHz, CDCl3) δ 7.90 – 7.83 (m, 2H), 7.49 (d, J = 7.6 Hz, 2H), 7.40 – 7.33 (m, 5H), 7.28 – 7.20 (m, 1H), 4.86 (q, J = 6.5 Hz, 1H), 2.28 (s, 3H), 1.57 (d, J = 6.5 Hz, 3H). ^{13}C NMR (101 MHz, CDCl3) δ 163.6, 146.3, 141.6, 129.5, 128.6, 128.5, 128.3, 126.9, 126.8, 126.7, 125.9, 59.9, 25.2, 15.7. IR: ν$_{max}$/cm^{-1} 3025 (Ar C-H stretch), 2968 (Ar C-H stretch), 1682 (C=N stretch), 1263 (C-N stretch). Bis(1-phenylethyl)amine, **92**: S/R-isomer: ^{1}H NMR (400 MHz, CDCl$_3$) δ 7.39 – 7.32 (m, 4H), 7.32 – 7.23 (m, 6H), 3.54 (q, J = 6.7Hz, 2H), 1.32 (d, J = 6.7 Hz, 6H). ^{13}C NMR (101 MHz, CDCl$_3$) δ 145.6, 128.5, 126.9, 126.8, 55.3, 24.9.

IR: v_{max}/cm^{-1} 3240 (2° N-H stretch), 3060 (Ar C-H stretch), 3026 (Ar C-H stretch), 1562 (N-H bend), 1449 (C-H bend), 1075 (C-N stretch). *meso*-isomer: ^{1}H NMR (400 MHz, CDCl$_3$) δ 7.39 – 7.32 (m, 4H), 7.32 – 7.23 (m, 6H), 3.80 (q, J = 6.6 Hz, 2H), 1.38 (d, J = 6.6 Hz, 6H). ^{13}C NMR (101 MHz, CDCl$_3$) δ 145.6, 128.5, 126.9, 126.8, 54.9, 23.2. Ethylbenzene, **93**: ^{1}H NMR (400 MHz, CDCl$_3$) δ 7.43 – 7.38 (m, 2H), 7.35 – 7.27 (m, 3H), 2.78 (q, J = 7.6 Hz, 2H), 1.37 (t, J = 7.6 Hz, 3H).^{13}C NMR (101 MHz, CDCl$_3$) δ 144.4, 128.4, 127.9, 125.7, 29.0, 15.8. IR: v_{max}/cm^{-1} 3025 (Ar C-H stretch), 2964 (Ar C-H stretch), 1494 (C-H bend), 1453 (C-H bend).

Table 49 DoE study on the racemisation of *S* – **70** in flow catalysed by Pd/γ-Al$_2$O$_3$.

Entry	Whole Plots	Temp. (°C)	Flow rate (mL min^{-1})	Sol. Conc. (mM)	Amine e.e. (%)[a]	Sel. (%)[b]
1	1	100	1	20.6	100	94
2	1	165	4	20.6	10	48
3	1	230	1	20.6	15	6
4	2	100	7	20.6	100	94
5	2	165	4	20.6	7	54
6	2	230	7	20.6	8	40
7	3	100	1	51.6	100	96
8	3	165	4	51.6	10	65
9	4	230	4	51.6	3	25
10	4	165	7	51.6	37	77
11	5	100	7	82.5	100	97
12	5	230	1	82.5	8	16
13	6	100	1	82.5	100	98
14	6	230	7	82.5	5	12
15	7	165	4	51.6	8	76
16	7	230	7	51.6	3	56
17	8	100	4	51.6	100	97
18	8	165	1	51.6	9	44
19	9	145	6.4	51.6	23	70
20	9	135	5	51.6	28	73
21	9	110	5.8	51.6	100	88
22	9	150	2.4	51.6	8	61
23	9	125	1.7	51.6	19	72
24	9	115	3.2	51.6	90	79
25	10	140	7	82.5	42	91
26	10	165	4	51.6	5	65
27	10	200	2	51.6	5	26
28	10	125	5.5	51.6	90	100

[a]Determined by chiral HPLC. [b]Determined by GC.

7.5.2. Reactor System for Kinetic Resolution.

A flow reactor system was constructed for the kinetic resolution of **70**. Solvents and amine solutions are delivered from Duran bottles fitted with a 4-port screw cap containing inlet tubing, a nitrogen-filled balloon and 25g of 5 Å molecular sieves, to keep the content under dry conditions. PFA tubing (1/8" OD, 1.59 mm ID, 24 cm) connect the solutions to a three-way ball valve, which is connected to a Gilson 305 HPLC pump (1/8" PFA tubing, 24 cm). The outlet of the pump is connected by PFA tubing to an Omnifit glass column (10 mm OD x 100 mm) containing a packed bed of Novozym-435. The column is mounted in a column heater module of a Uniqsis FlowSyn reactor.[142] PFA tubing is used to connect the outlet of the PBR to a BPR (set at 8 bar), followed by a JASCO-2090 Polarimeter, and to waste or fraction collector, as described in steps 4 and 5 in Section 7.5.1. The void volume of the reactor is 4.02 mL.
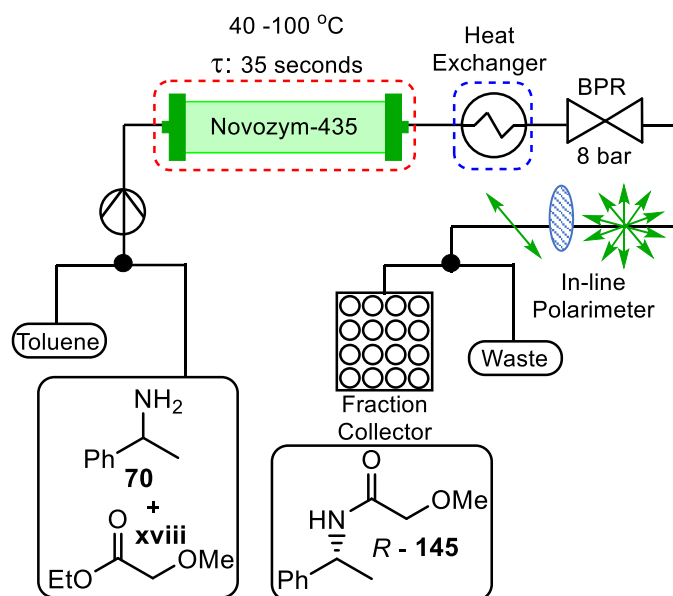
Figure 69 Schematic of a custom-built enzymatic KR reactor.

7.5.2.1. Typical Procedure for Enzymatic Kinetic Resolution in Flow

The flow reactor system was fitted with a packed bed of Novozym-435, prepared as described in Section 7.4.2. before it was primed by anhydrous toluene at 1 mL min^{-1} for 10 minutes. The flow rate was adjusted to 0.5 mL min^{-1} as heating commenced and that the desired temperature was reached. The flow rate was then adjusted to the desired value. Once the in-line polarimeter showed a stable reading and set to zero, the inlet was switched to the reagent line containing a mixture of **70** and ethyl 2-methoxyacetate at the desired concentrations and equivalents. When steady state had been achieved (indicated by a stable reading on the polarimeter), the reaction mixture was

passed through the system for a further 5 minutes, during which time, 5 samples were collected every 1 minute (see above). 1-Phenylethylamine, **70**: ^{1}H NMR (400 MHz, CDCl$_3$) δ 7.41 – 7.33 (m, 4H), 7.26 (td, J = 6.4, 3.0 Hz, 1H), 4.14 (q, J = 6.6 Hz, 1H), 1.50 (NH, s, 2H), 1.42 (dd, J = 6.7, 1.2 Hz, 3H). ^{13}C NMR (101 MHz, CDCl3) δ 147.7, 128.3, 126.6, 125.5, 51.1, 25.6. IR: ν_{max}/cm^{-1} 3373 (1° N-H stretch), 2961 (Ar C-H), 1449 (C-H bend), 1367 (C-N stretch). Chiral HPLC conditions: InfinityLab Poroshell 120 Chiral CF, t_s = 5.38 min, t_R = 5.77 min.

2-methoxy-N-(1-phenylethyl)acetamide, **145**. ^{1}H NMR (400 MHz, CDCl$_3$) δ 7.38 – 7.30 (m, 4H), 7.29 – 7.24 (m, 1H), 6.76 (NH, d, J = 7.5 Hz, 1H), 5.18 (dq, J = 8.1, 7.0 Hz, 1H), 3.92 (d, J = 14.9 Hz, 1H), 3.87 (d, J = 15.0 Hz, 1H), 3.40 (s, 3H), 1.52 (d, J = 6.9 Hz, 3H). ^{13}C NMR (101 MHz, CDCl$_3$) δ 168.6, 143.1, 128.8, 127.5, 126.3, 72.1, 59.2, 48.1, 22.0. IR: ν_{max}/cm^{-1} 3341 (N-H stretch), 2972 (Ar C-H stretch), 1648 (2° C=O stretch), 1520 (C-H bend). Chiral HPLC: OD-H Chiralpak: t_R =8.26 min, t_S = 9.82 min.

Table 50 A small DoE study on the kinetic resolution of **70**.

Entry	Temp. (ºC)	Sol. Conc. (mM)	Acyl Donor (Equiv.)	Amine e.e. (%)[a]	Amide e.e. %[b]	Conversion (%)[c]	E [d]
1	100	51.6	10	20	88	11	19
2	40	20.6	0.5	14	98	17	114
3	100	82.5	5.25	20	98	13	120
4	70	82.5	10	28	92	21	32
5	40	82.5	0.5	8	96	5	53
6	100	20.6	0.5	10	94	19	36
7	70	20.6	5.25	18	99	20	>200
8	40	20.6	10	40	96	23	73
9	70	51.6	0.5	8	99	17	>200
10	40	51.6	5.25	24	92	12	30
11	40	82.5	10	20	99	25	>200
12	40	38.7	10	40	99	29	>200

[a]Determined by chiral LC. [b]Determined by chiral LC. [c]With respect to rac-1. Determined by GC. [d]Selectivity factor for the kinetic resolution = $\ln[(1-c)(1-e.e._S)]/\ln[(1-c)(1+e.e._S)]$; where c = conversion = $e.e._S/(e.e._S+e.e._P)$; e.e.$_S$ = e.e. of recovered *S*-**70** in the reaction mixture and e.e.$_P$ = e.e. of recovered *R* - **145** in the reaction mixture.

7.5.3. Reactor system for the CE-DKR of Racemic Amines
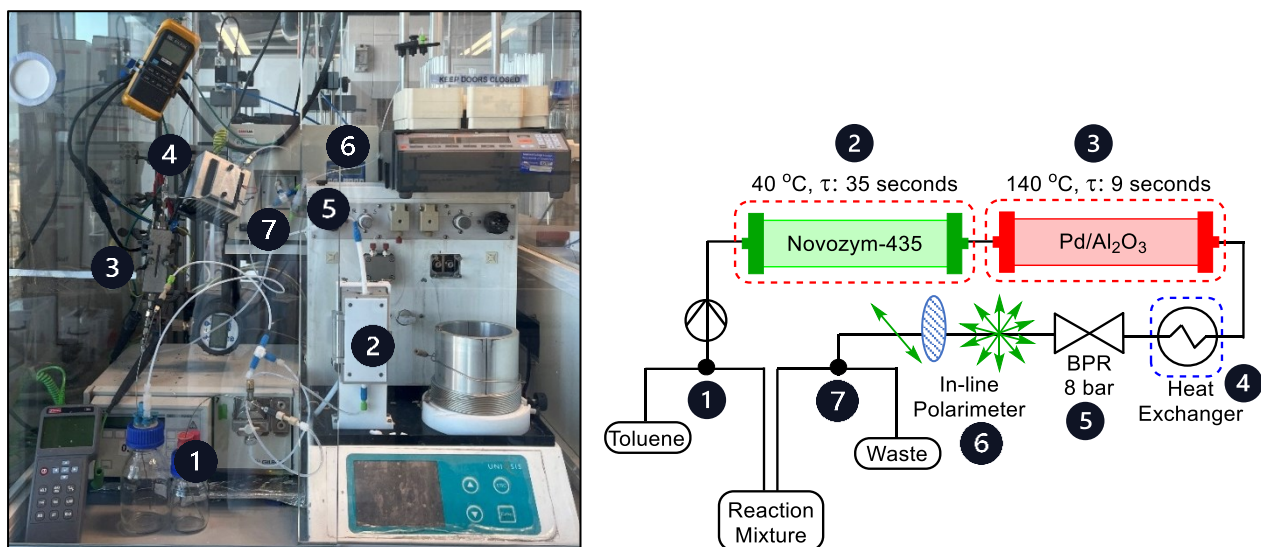

Figure 70 The custom-built FTR-CE-DKR reactor: 1. HPLC pumps; 2. Kinetic resolution packed-bed reactor (PBR); 3. Racemisation packed-bed reactor (PBR); 4. Heat Exchanger; 5. Back pressure regulator (BPR); 6. In-line polarimeter; 7. Recycle loop or waste.

The two reactor systems described in Sections 7.5.1. and 7.5.2. are combined to provide a tandem PBR system for the CE-DKR of racemic amines (Figure 70). The outlet of the enzymatic PBR described in Section 7.2 is connected *via* PFA tubing to the inlet of the PBR containing the racemisation catalyst, the cooling device, the BPR and the polarimeter as described earlier. The outlet of the polarimeter is connected either to waste, or back into the Duran bottle containing the racemic amine, which acts as a reservoir that contains 25g of molecular sieves 5 Å (not under stirring) for the update of the EtOH formed during the KR.

7.5.3.1. Typical procedure for CE-DKR of **70** or **94**

The flow reactor system was fitted with the Novozym-435 and Pd/γ-Al$_2$O$_3$ packed bed reactors, both prepared as described in Section 7.2. The reactor was primed by anhydrous toluene at 1 mL min^{-1} for 10 minutes. The flow rate was adjusted to 0.5 mL min^{-1} while the enzymatic and racemisation PBR's were heated to 40 °C and 140 °C, respectively. The flow rate was then increased to 7 mL min^{-1}, once the system has reached a steady state, the polarimeter was set to zero, before the inlet was switched to the delivery a solution of **70** (1 g, 82.5 mM in toluene) and ethyl 2-methoxyaceate (10 equiv.), kept over 25 g of 5 Å molecular sieves without stirring. The polarimeter was used to monitor the progression of the reaction, while samples (1 mL each) were collected every 15 minutes. After 1 h the reaction reached 90% conversion with 96% selectivity (GC), affording $R-$**145** with 99% e.e. (chiral HPLC), $[\alpha]^{23.7}$ +67.5 (c=0.5, CHCl$_3$) in accordance with those previously reported for this compound.[83] The

procedure was also used to transform **94** (1 g, 82.5 mM in toluene) to *R* – **95**. After 1 h, the reaction was found to reach 92% conversion with 99% selectivity and 99% e.e.(chiral HPLC), $[\alpha]^{23.7}$ +43.9 (c=0.5, CHCl$_3$) in accordance with those previously reported for this compound.[83] The reaction was subsequently repeated with 2 equivalents of the acylating agent to afford 85% conversion to *R* – **95** in 1.5 h with 99% selectivity and 98% e.e. (chiral HPLC), $[\alpha]^{23.7}$ +43.8 (c=0.5, CHCl$_3$) in accordance with those previously reported for this compound.[83] At the end of the reaction, the reaction mixture was recovered by switching the feed to toluene for 3 min. Product *R* – **145** was obtained by evaporation of the combined content of the reservoir under reduced pressure. Product *R* – **95** was obtained through washing of the content of the reservoir with saturated aqueous NH$_4$Cl (3 x 10 mL), before drying with MgSO$_4$, filtering and evaporation under reduced pressure.

7.5.4. Stereocentre Inversion

The positions of the two PBR's were swapped, such that the outlet of the cooling module after the racemisation reactor is connected to the inlet of the Omnifit column (10 mm ID x 100 mm) housed in the Uniqsis heating module as shown in Figure 71. The same procedure described in S2.2 was followed to convert an 82.5 mM solution of *S* - **70** to *R* - **145** in 1 h with 93% conversion, 95% selectivity and 99% e.e. (chiral HPLC), $[\alpha]^{23.7}$ +43.9 (c=0.5, CHCl$_3$) in accordance with those previously reported for this compound.[83]
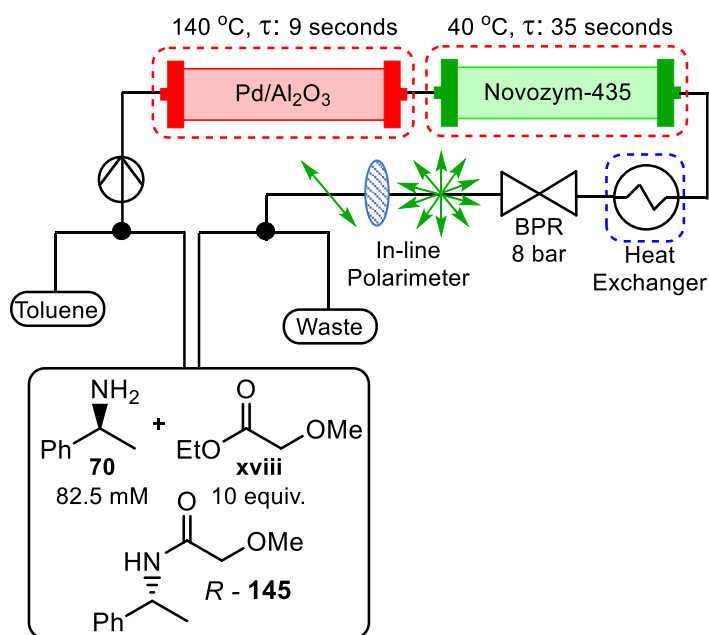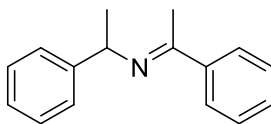

Figure 71 The custom built FTR-CE-DKR reactor for the stereoinversion of chirally pure amines.

## 7.6. Independent Synthesis of Authentic Samples

7.6.1. Synthesis of *S/R*- 1-phenyl-N-(1-phenylethyl)ethan-1-imine, **91**

In a round bottom flask fitted with a Dean-Stark apparatus, a solution of **70** (2.12 mL, 16.5 mmol) and acetophenone (2.41 mL, 20.7 mmol) in toluene (40 mL) was prepared under an inert atmosphere. To this acetic acid (94 µL, 10 mol %) was added. The reaction mixture was heated to reflux for 2 h, during which water was continuously removed. After cooling to ambient temperature, the reaction mixture was washed with saturated $NH_4Cl_{(aq)}$ (5 x 10 mL), dried over $MgSO_4$, filtered and reduced *in vacuo* to yield the desired product, **91**, as a yellow oil (2.64 g, 72 %). ^{1}H NMR (400 MHz, CDCl3) δ 7.90 – 7.83 (m, 2H), 7.49 (d, J = 7.6 Hz, 2H), 7.40 – 7.33 (m, 5H), 7.28 – 7.20 (m, 1H), 4.86 (q, J = 6.5 Hz, 1H), 2.28 (s, 3H), 1.57 (d, J = 6.5 Hz, 3H). ^{13}C NMR (101 MHz, CDCl3) δ 163.6, 146.3, 141.6, 129.5, 128.6, 128.5, 128.3, 126.9, 126.8, 126.7, 125.9, 59.9, 25.2, 15.7. IR: v_{max}/cm[-1] 3025 (Ar C-H stretch), 2968 (Ar C-H stretch), 1682 (C=N stretch), 1263 (C-N stretch). Data obtained was consistent with existing literature.[161]

7.6.2. Synthesis of *S,S/R,R/meso*- *bis*(1-phenylethyl)amine, **92**
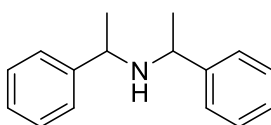
A solution of **91** (490 mg, 2.2 mmol) in MeOH (40 mL) was prepared under an inert atmosphere cooled to 0 ºC under stirring. Separately, a solution of $NaBH_4$ (166 mg, 4.4 mmol) in MeOH (5 mL) was prepared under an inert atmosphere and added dropwise to the imine solution. Once the addition was complete, the reaction mixture was left to stir at 0 ºC for 10 minutes, before being allowed to warm to room temperature for a further 20 minutes. The reaction was quenched with the addition of 1 M H_2SO_4 (5 mL), and MeOH was removed under reduced pressure. The resulting suspension was diluted with ethyl acetate (30 mL) and washed with 1 M NaOH (3 x 15 mL), before drying with $MgSO_4$, filtered and reduced *in vacuo* to yield the desired product, **92**, a white solid (915 mg, 91 %). B*is*(1-phenylethyl)amine, **92**: *S/R*-isomer: ^{1}H NMR (400 MHz, CDCl₃) δ 7.39 – 7.32 (m, 4H), 7.32 – 7.23 (m, 6H), 3.54 (q, J = 6.7Hz, 2H), 1.32 (d, J = 6.7 Hz, 6H). ^{13}C NMR (101 MHz, CDCl₃) δ 145.6, 128.5, 126.9, 126.8, 55.3, 25.0. IR: v_{max}/cm[-1] 3240 (2º N-H stretch), 3060 (Ar C-H stretch), 3026 (Ar C-H stretch), 1562 (N-H bend),

1449 (C-H bend), 1075 (C-N stretch). *meso*-isomer: [^1]H NMR (400 MHz, CDCl$_3$) δ 7.39 – 7.32 (m, 4H), 7.32 – 7.23 (m, 6H), 3.80 (q, J = 6.6 Hz, 2H), 1.38 (d, J = 6.6 Hz, 6H). [^13]C NMR (101 MHz, CDCl$_3$) δ 145.6, 128.54 126.9, 126.8, 54.9, 23.2. Data obtained was consistent with existing literature.[162]

7.6.3. Synthesis of 2-methoxy-N-(1-phenylethyl)acetamide, 145
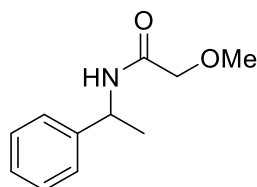
A solution of **70** (2.12 mL, 16.5 mmol) and ethyl 2-methoxyacetate (2.44 mL, 20.7 mmol) in toluene (50 mL) was prepared under an inert atmosphere, to which acetic acid (94 µL, 10 mol %) was added. The reaction was heated to reflux under stirring for 16 h. After cooling to ambient temperature, the organic solution was washed with saturated NH$_4$Cl(aq) (3 x 10 mL) followed by 1 M NaOH(aq) (3 x 10 mL). The organic layer was dried with MgSO$_4$, filtered, and reduced *in vacuo* to yield the desired product, **145**, as a white solid (3.20 g, quantitative). [^1]H NMR (400 MHz, CDCl$_3$) δ 7.38 – 7.30 (m, 4H), 7.29 – 7.24 (m, 1H), 6.76 (NH, d, J = 7.5 Hz, 1H), 5.18 (dq, J = 8.1, 7.0 Hz, 1H), 3.92 (d, J = 14.9 Hz, 1H), 3.87 (d, J = 15.0 Hz, 1H), 3.40 (s, 3H), 1.52 (d, J = 6.9 Hz, 3H). [^13]C NMR (101 MHz, CDCl$_3$) δ 168.6, 143.1, 128.8, 127.5, 126.3, 72.1, 59.2, 48.1, 22.0. IR: ν$_{max}$/cm^{-1} 3341 (N-H stretch), 2972 (Ar C-H stretch), 1648 (2° C=O stretch), 1520 (C-H bend). Chiral HPLC: OD-H Chiralpak: t_R =8.26 min, t_S = 9.82 min. Data obtained was consistent with existing literature.[86]

7.6.4. Synthesis of 2-methoxy-N-(1-aminoindan)acetamide, 95
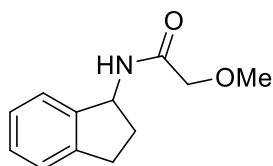
A solution of **94** (193 µL, 1.5 mmol) and ethyl 2-methoxyacetate (400 µL, 3.75 mmol) in toluene (3 mL) was prepared under an inert atmosphere, to which acetic acid (9 µL, 10 mol %) was added. The reaction was heated to reflux under stirring for 16 h. After cooling to ambient temperature, the organic solution was washed with 1 M NaOH(aq) (3 x 10 mL). The organic layer was dried with MgSO4, filtered, and reduced *in vacuo* to yield the desired product, **95**, as a white solid (233 mg, 74 %). [^1]H NMR (400 MHz, CDCl$_3$) δ 7.35 – 7.13 (m, 4H), 6.75 (s, 1H), 5.55 (q, J = 7.9 Hz, 1H), 3.97 (s, 2H), 3.41 (s, 3H), 3.07 – 2.97 (m, 1H), 2.96 – 2.83 (m, 1H), 2.74 – 2.56 (m,

1H), 1.91 – 1.79 (m, 1H). ^{13}C NMR (101 MHz, CDCl$_3$) δ 169.3, 143.5, 142.9, 128.0, 126.8, 124.9, 124.1, 72.0, 59.2, 53.9, 34.1, 30.3. IR: v_{max}/cm^{-1} 3280 (N-H stretch), 2932 (Ar-H, stretch, 1646 (C=O stretch), 1521 (C-H bench), 1478 (C-H bend). Chiral HPLC: OD-H Chiralpak: t_R =10.30 min, t_S = 16.74 min. Data obtained was consistent with existing literature.[91]
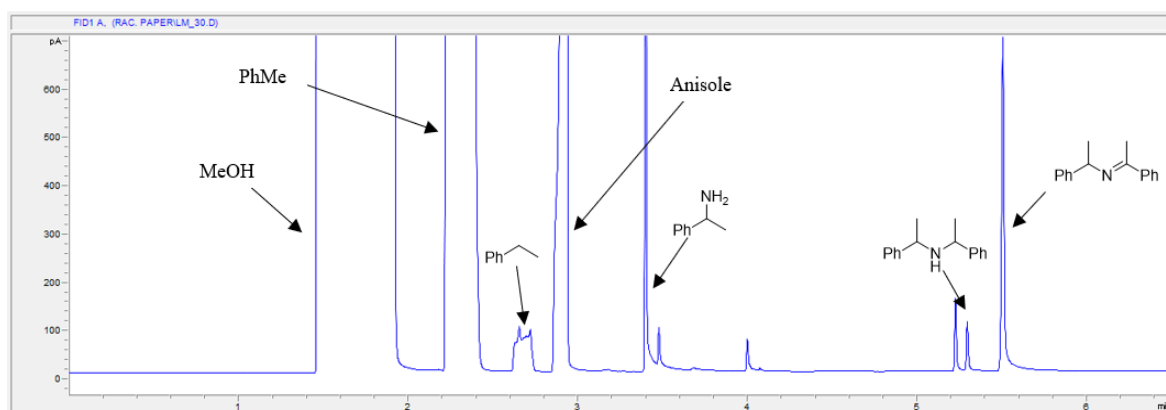
7.7. Analytical Data

7.7.1. Gas Chromatography

Figure 72 GC chromatograph of a reaction mixture obtained from a typical racemisation experiment, showing the side-products. Anisole was added as an internal standard.
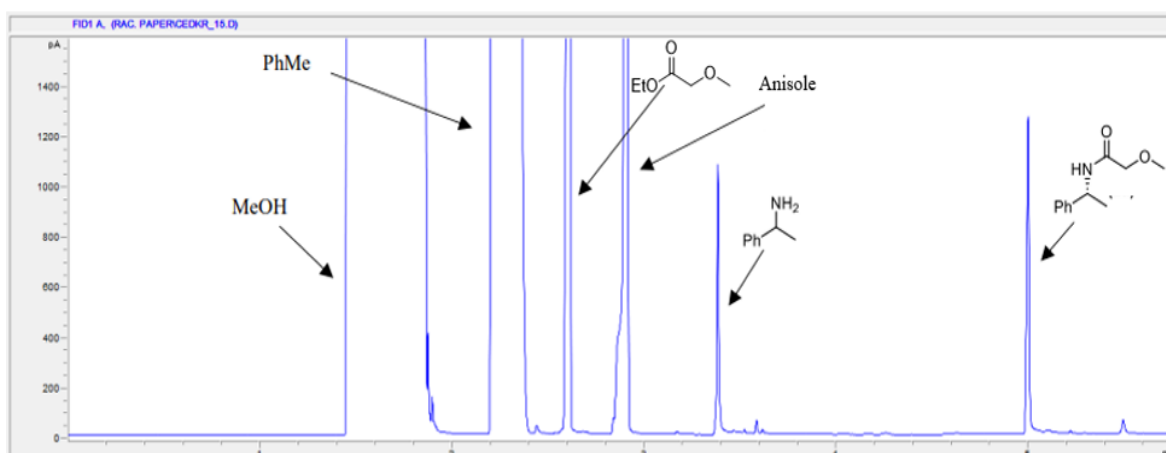

Figure 73 GC chromatograph obtained for the reaction mixture of the CE-FTR-DKR of **70** to *R* - **145**, highlighting the selectivity of the process. Anisole was added as the internal standard.
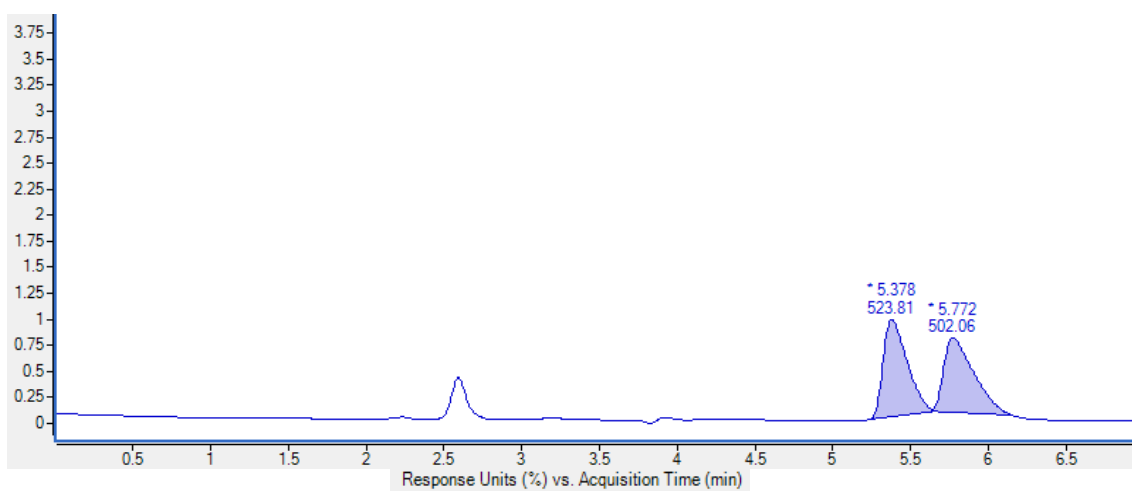
7.7.2. Chiral LC

Peak	RT	Area	Area Sum %	Height
1	5.378	523.81	51.06	48.71
2	5.772	502.06	48.94	37.26

Figure 74 Chiral HPLC chromatograph of **70** (InfinityLab Poroshell 120 Chiral CF column).

Peak	RT	Area	Area Sum %	Height
1	5.291	1231.04	100	88.62
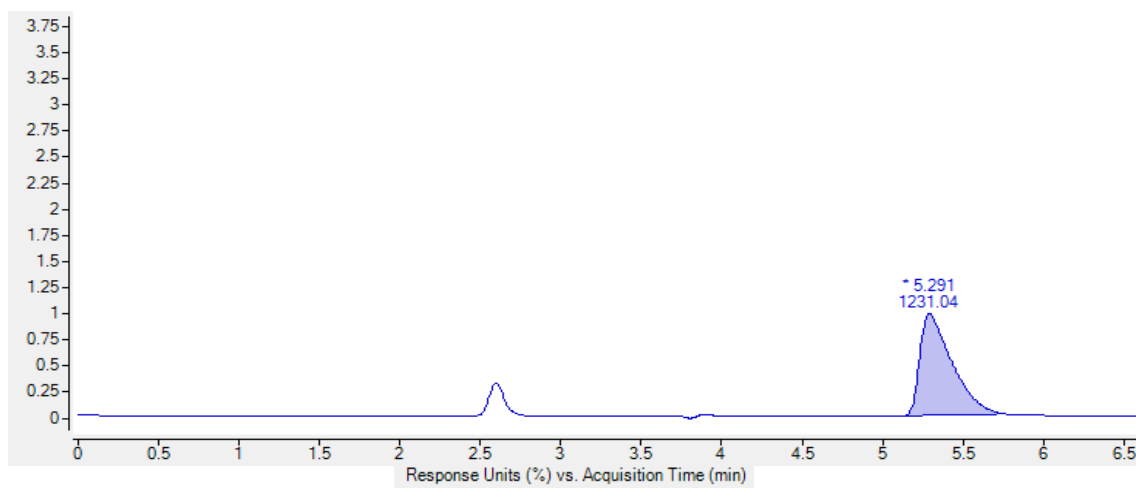
Figure 75 Chiral HPLC chromatograph of *S* - **70** (InfinityLab Poroshell 120 Chiral CF column).
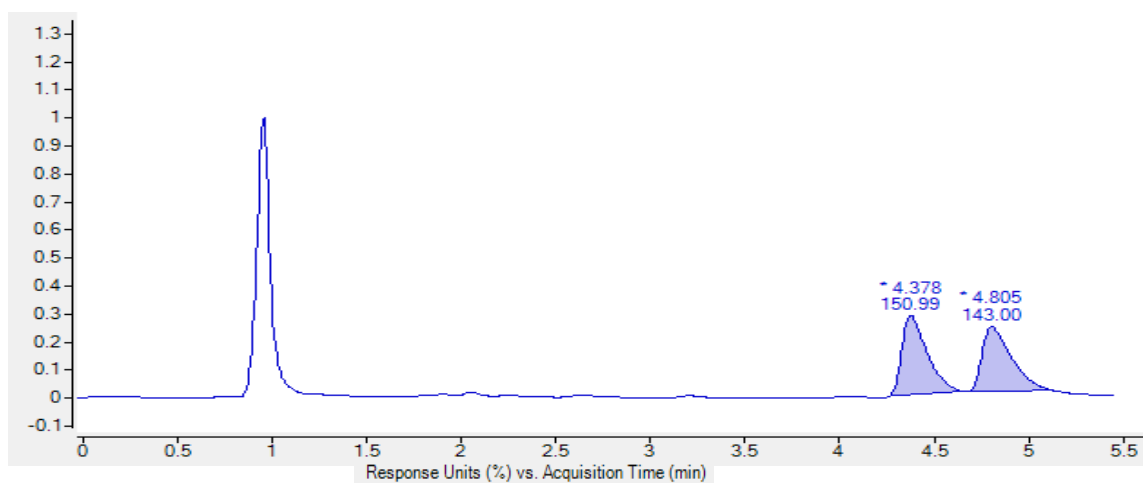
Peak	RT	Area	Area Sum %	Height
1	4.378	150.99	51.36	16.29
2	4.805	143	48.64	13.41

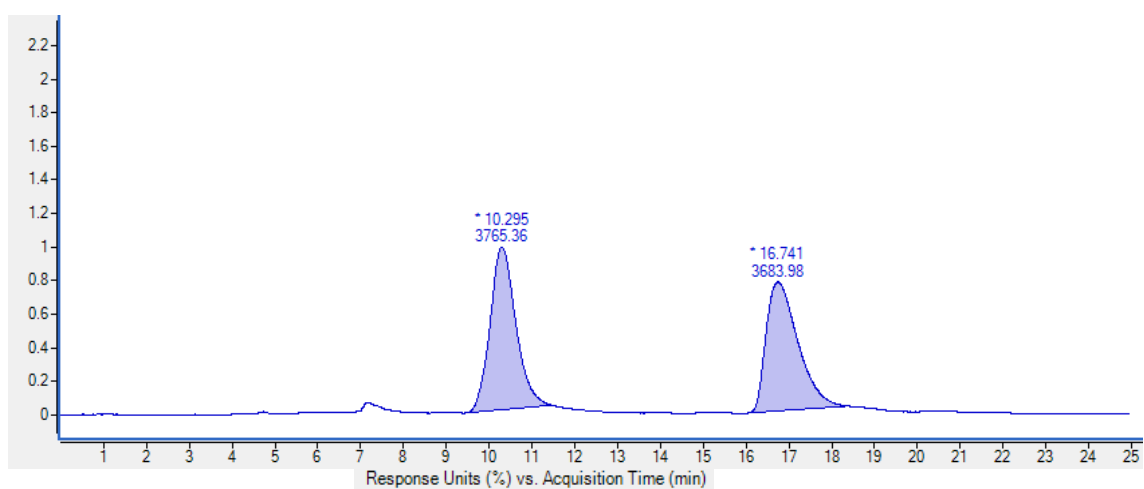*Figure 76* Chiral HPLC chromatograph of **94** (InfinityLab Poroshell 120 Chiral CF column).
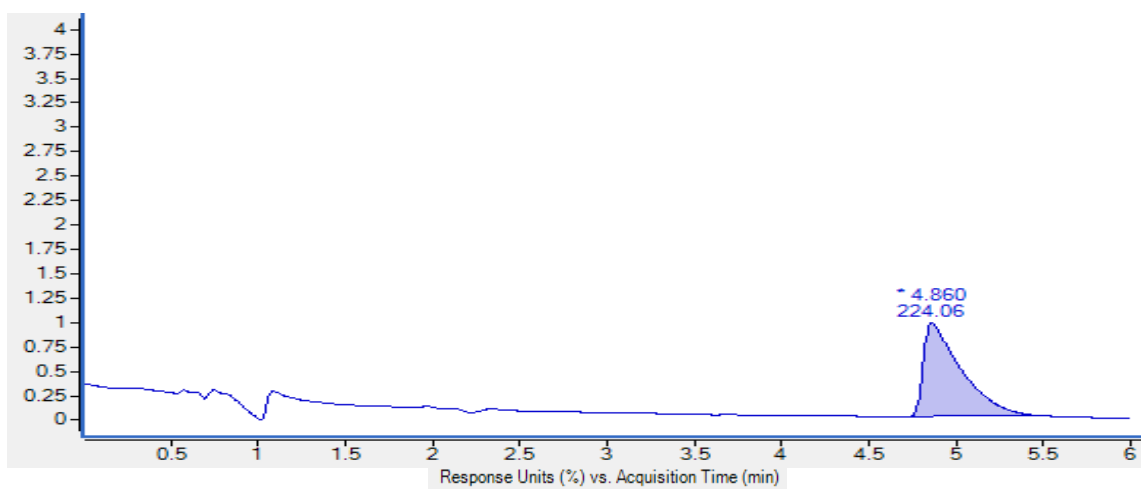
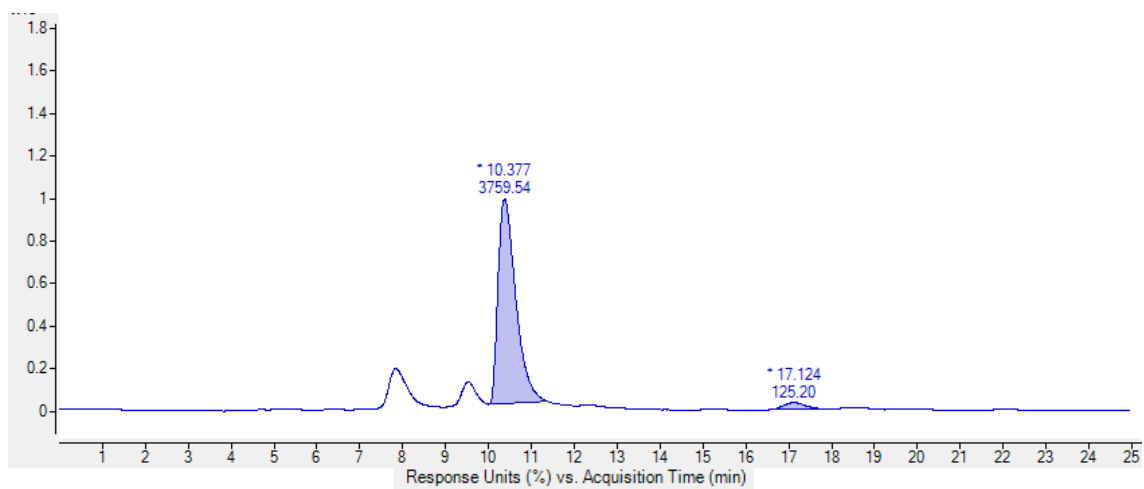| Peak	RT	Area	Area Sum %	Height
1	4.86	224.06	100	15.05

Figure 77 Chiral HPLC chromatograph of *S* - **94** (InfinityLab Poroshell 120 Chiral CF column).

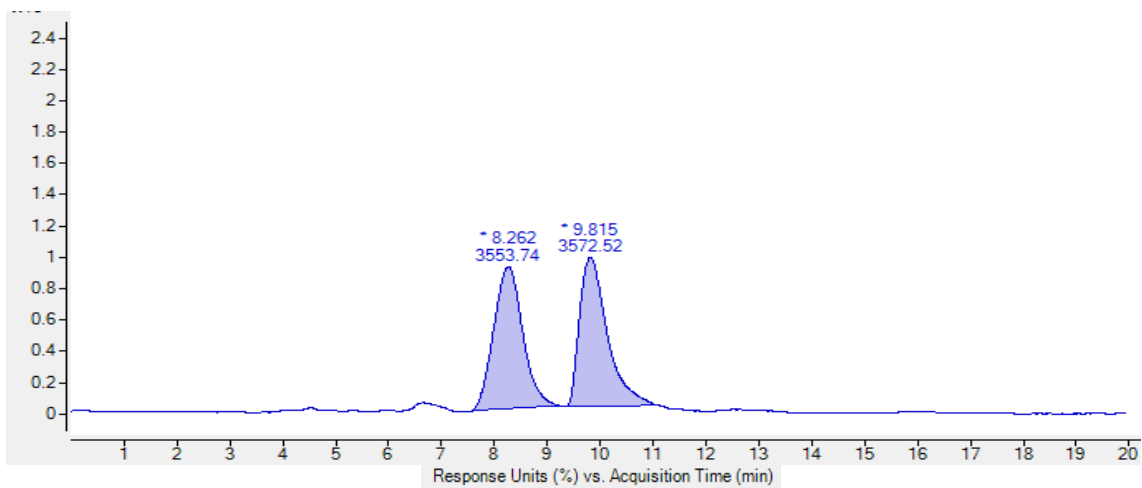| Peak	RT	Area	Area Sum %	Height
1	10.294	3765.36	50.55	89.99
2	16.741	3683.98	49.45	71.31

Figure 78 Chiral HPLC chromatograph of **95** (Chiralpak OD-H column).

Peak	RT	Area	Area Sum %	Height
1	10.377	3759.54	96.78	131.04
2	17.124	125.2	3.22	3.87

Figure 79 Chiral HPLC chromatograph of *R* – **95** (Chiralpak OD-H column).

Peak	RT	Area	Area Sum %	Height
1	8.262	3553.74	49.87	93.38
2	9.815	3572.52	50.13	97.88

Figure 80 Chiral HPLC chromatograph of **145** (Chiralpak OD-H column).
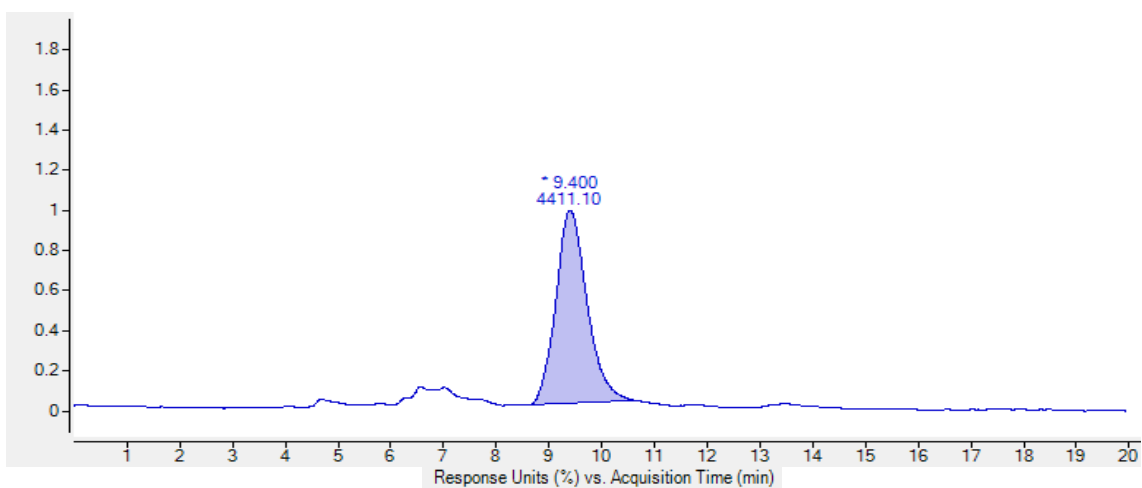
Peak	RT	Area	Area Sum %	Height
1	9.4	4411.1	100	107.21

Figure 81 Chiral HPLC chromatograph of *R* - **145** (Chiralpak OD-H column).
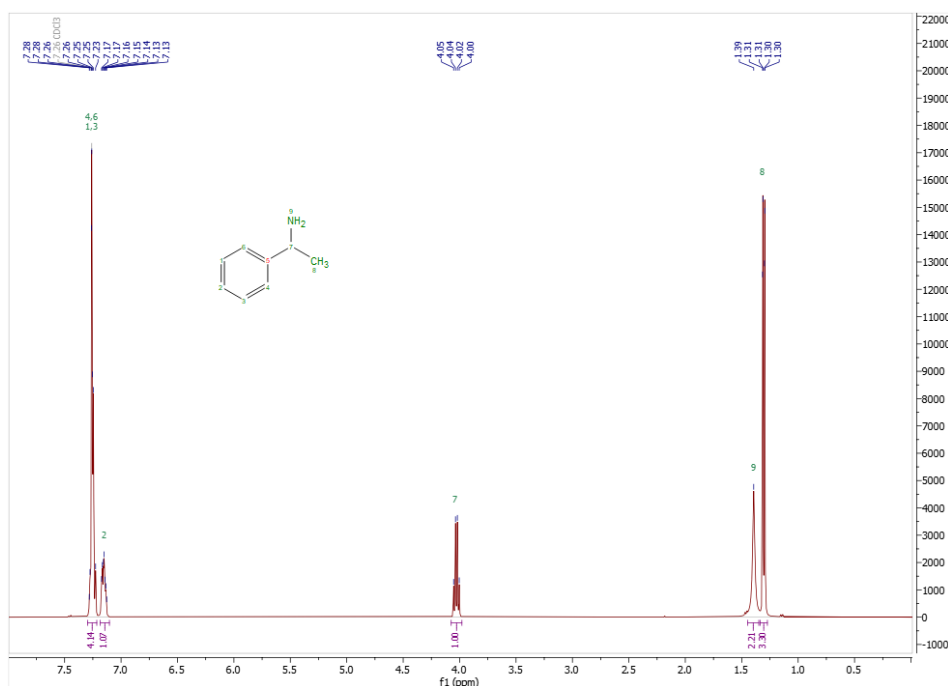
177

7.7.3. ^{1}H and ^{13}C NMR Spectra

Figure 82 ^{1}H NMR of **70**.
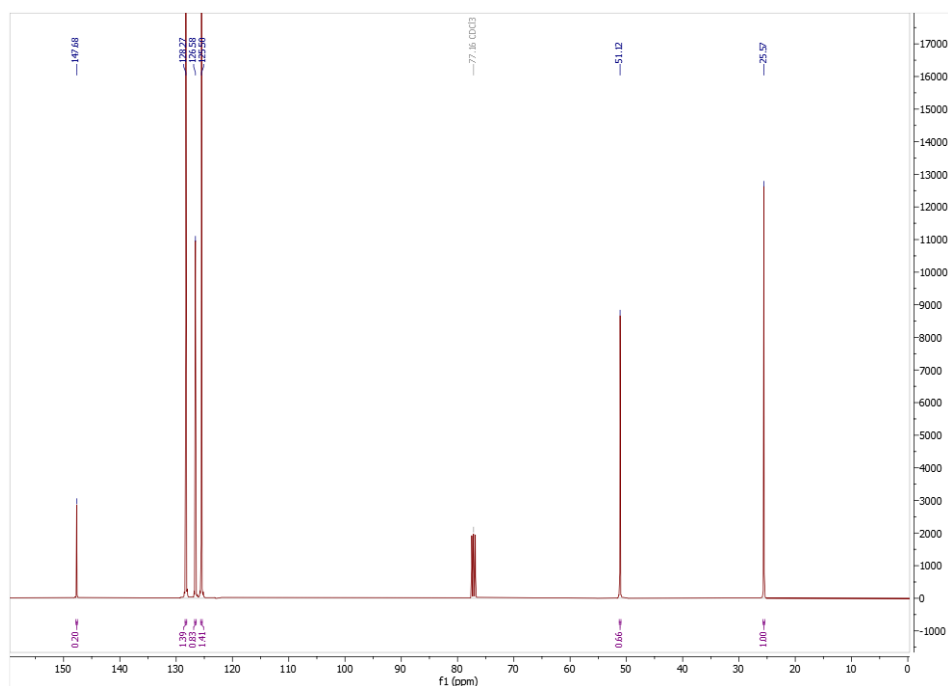
Figure 83 ^{13}C NMR of **70.**
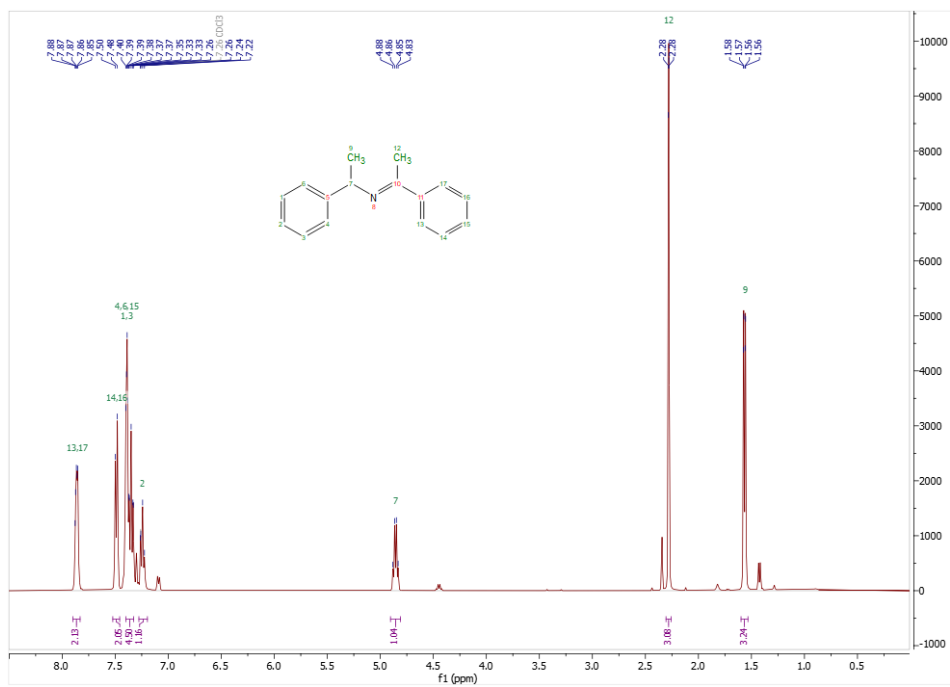
Figure 84 ¹H NMR of **91**.
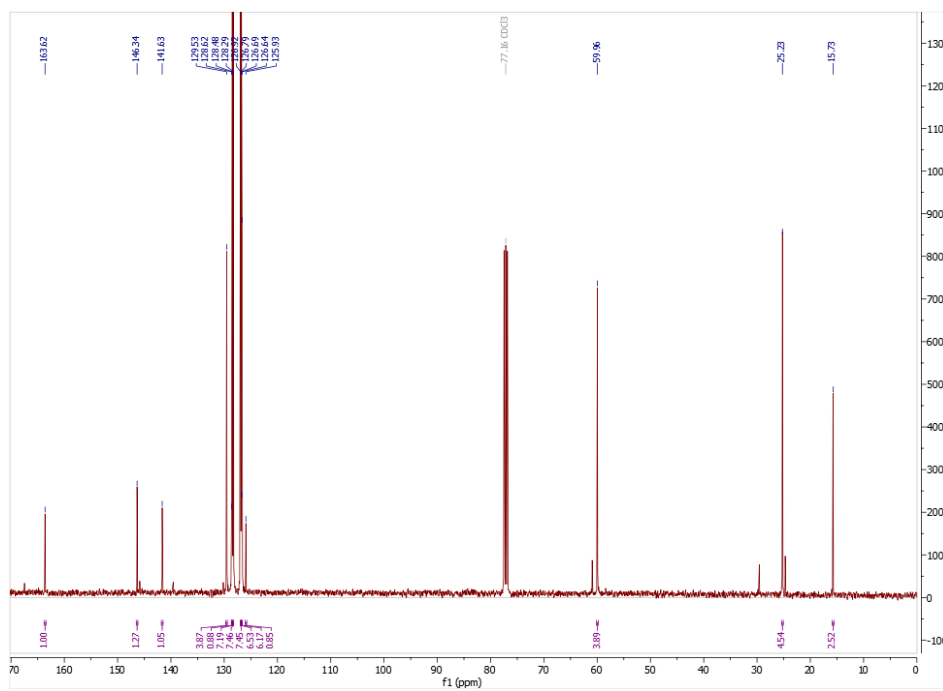
Figure 85 ¹³C NMR of **91**.
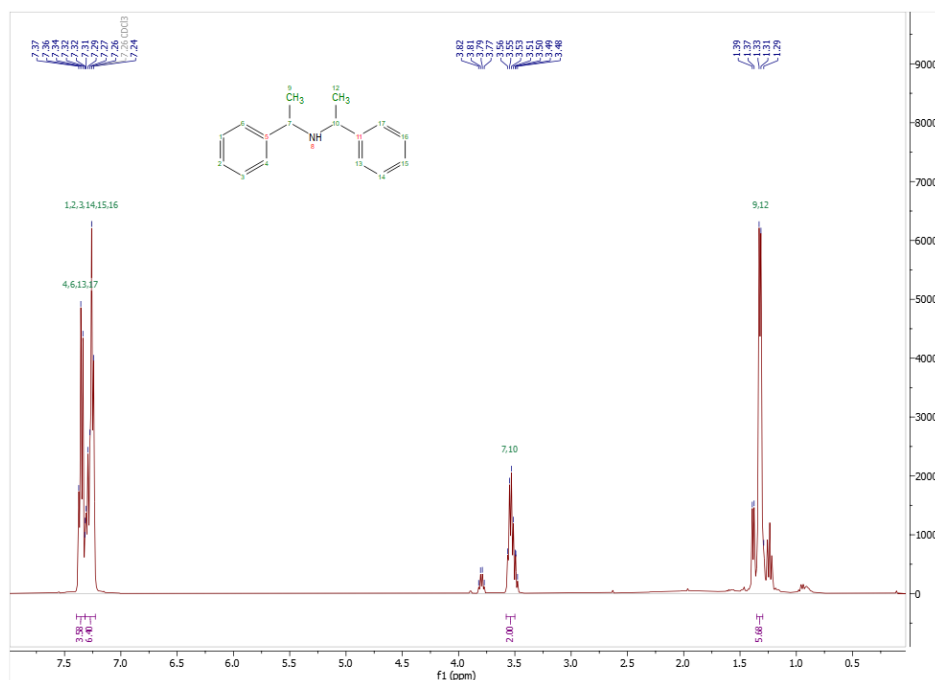
Figure 86 ^{1}H NMR of **92**.
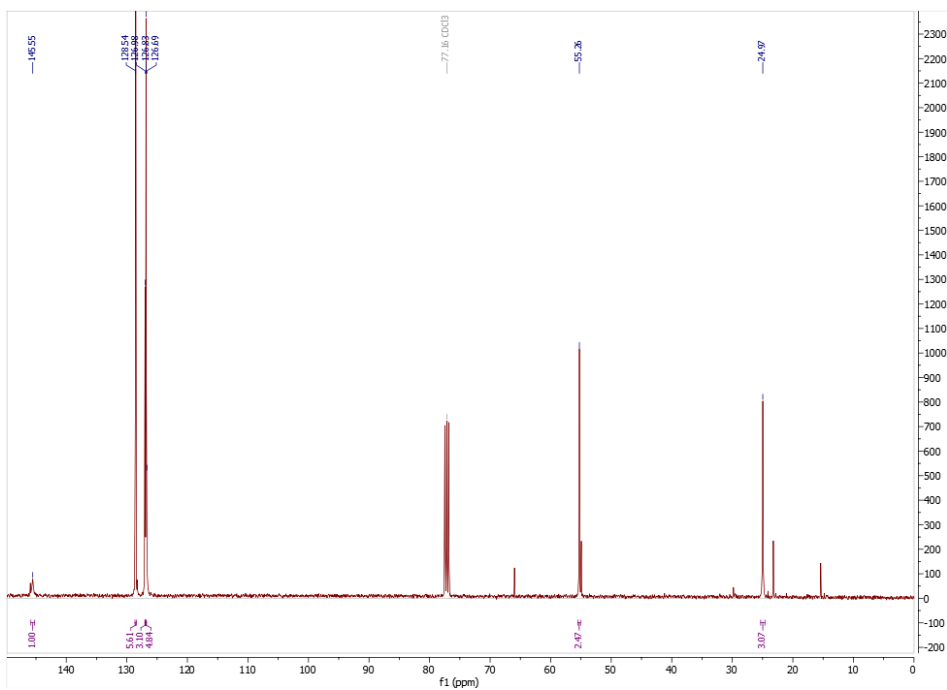
Figure 87 ^{13}C NMR of **92**.

180
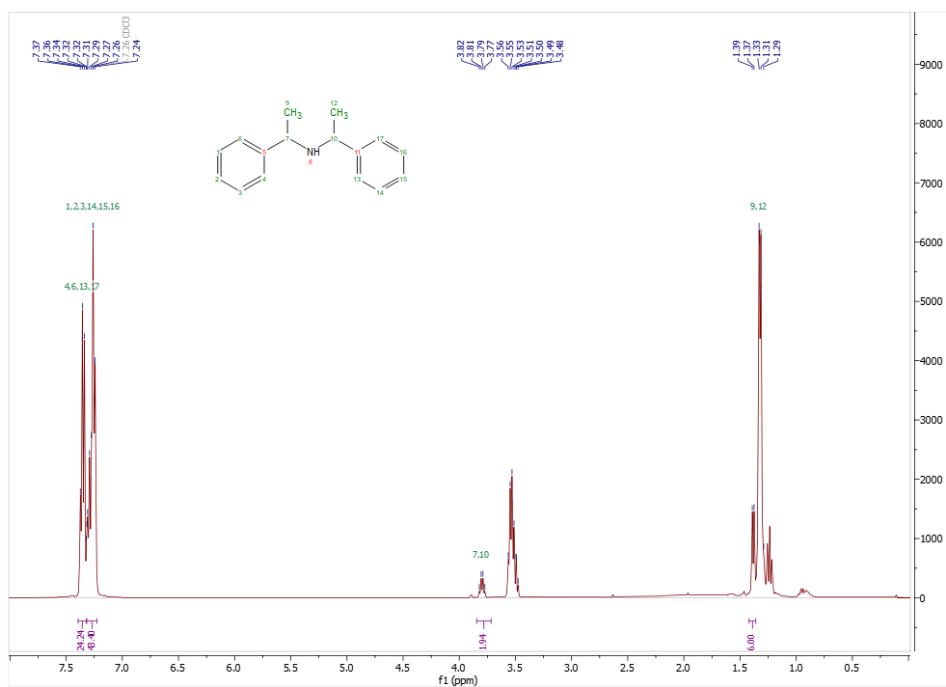
Figure 88 ¹H NMR of **92**.
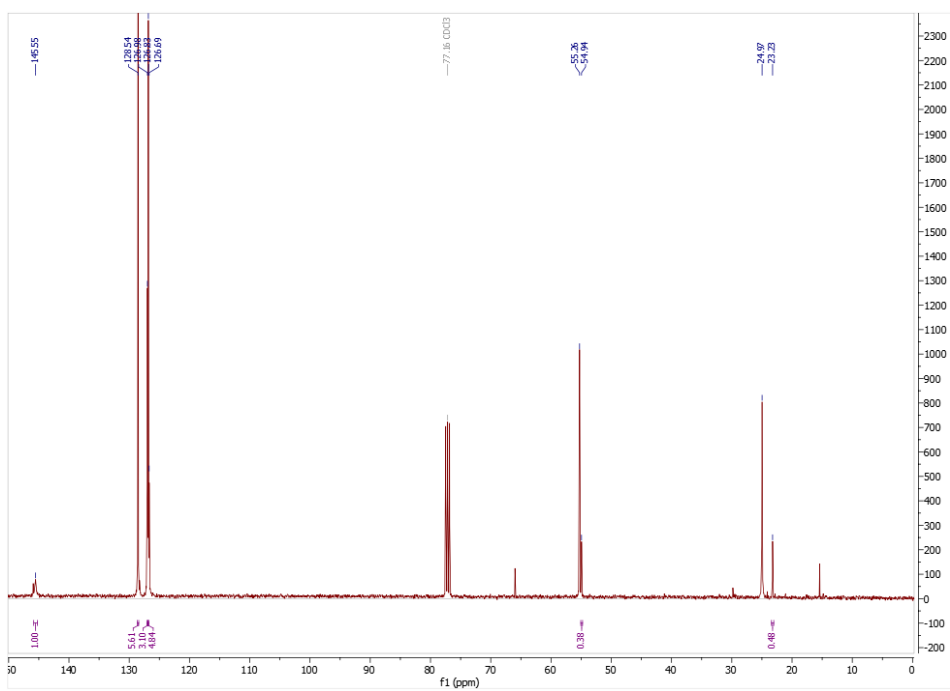
Figure 89 ¹³C NMR of **92**.
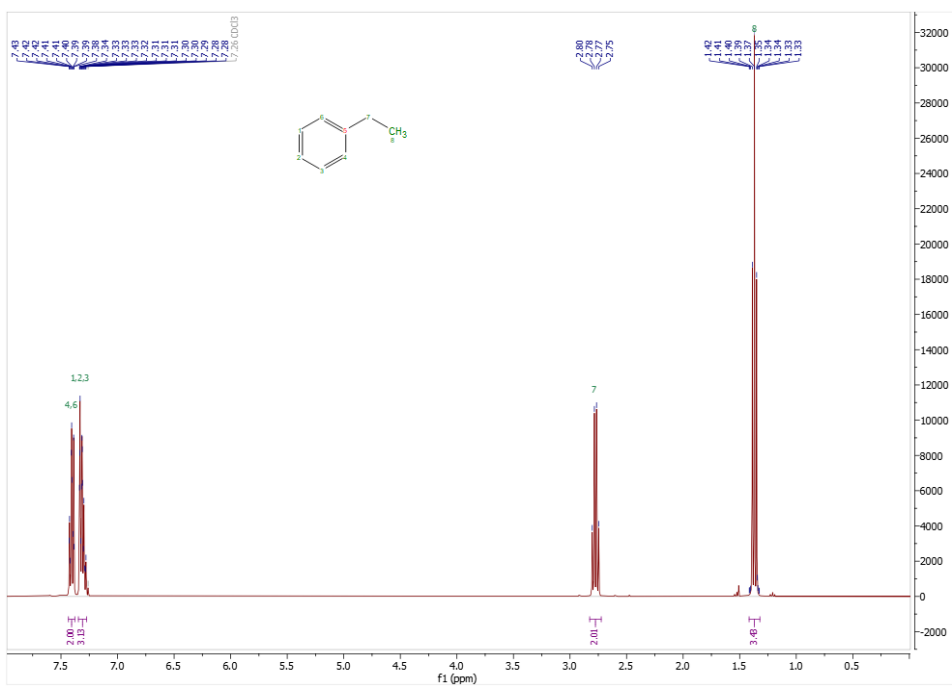
Figure 90 ^{1}H NMR of **93**.
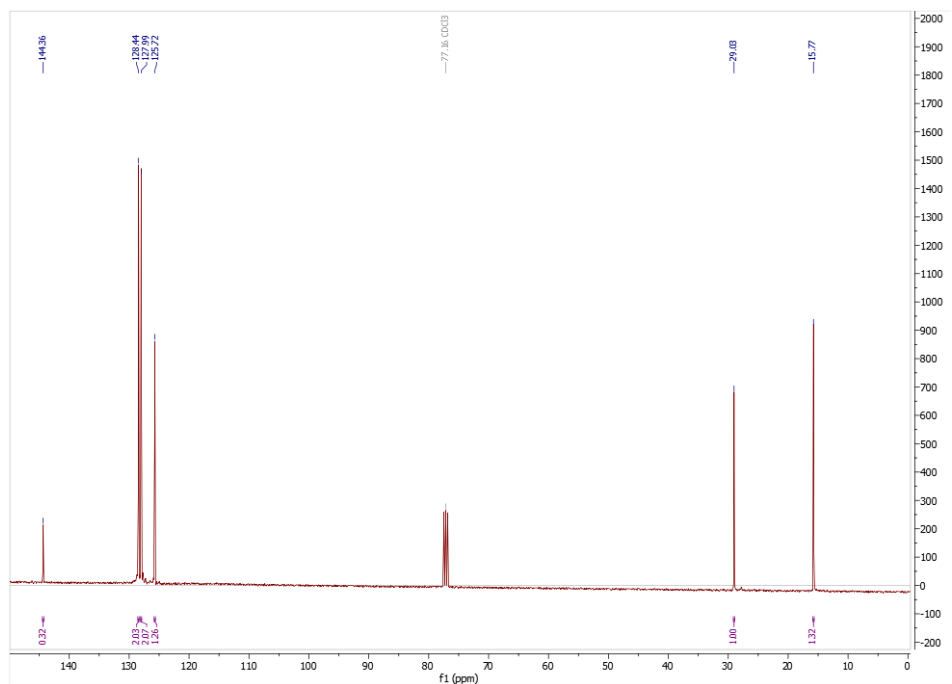
Figure 91 ^{13}C NMR of **93**.
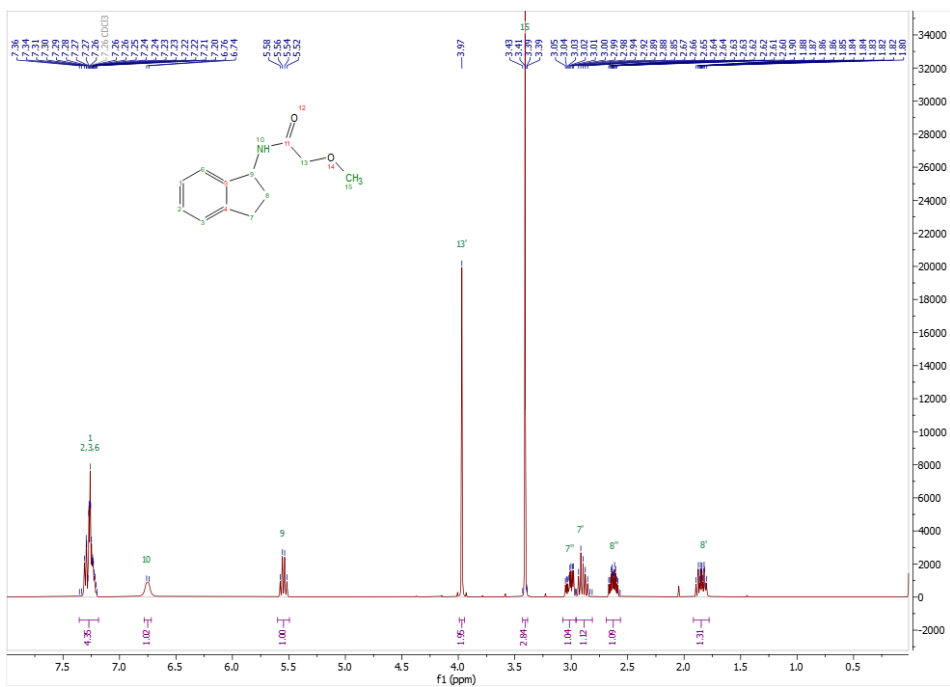
Figure 92 ^{1}H NMR of **95**.

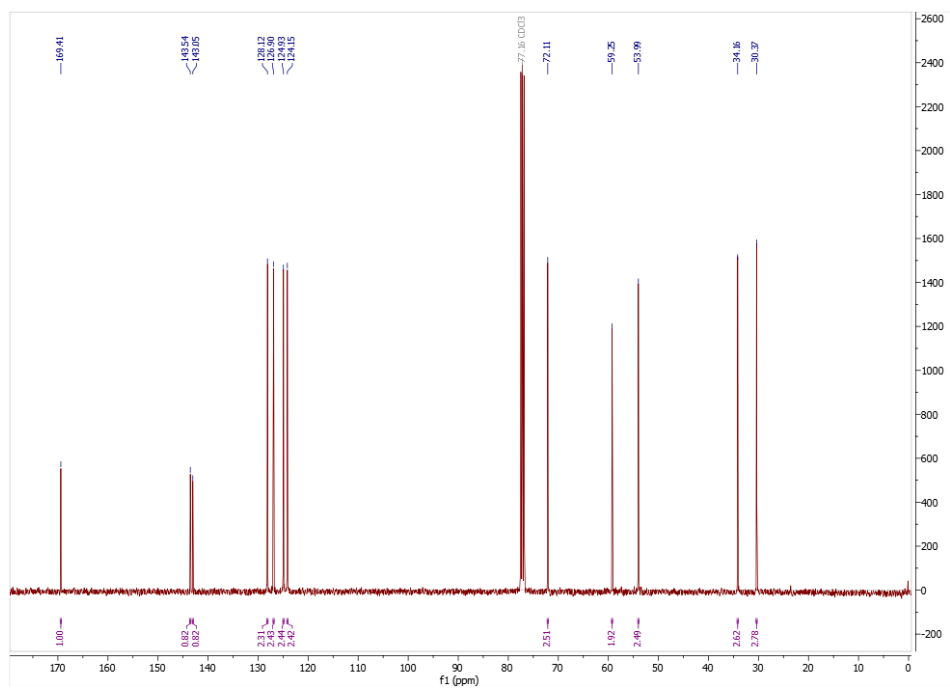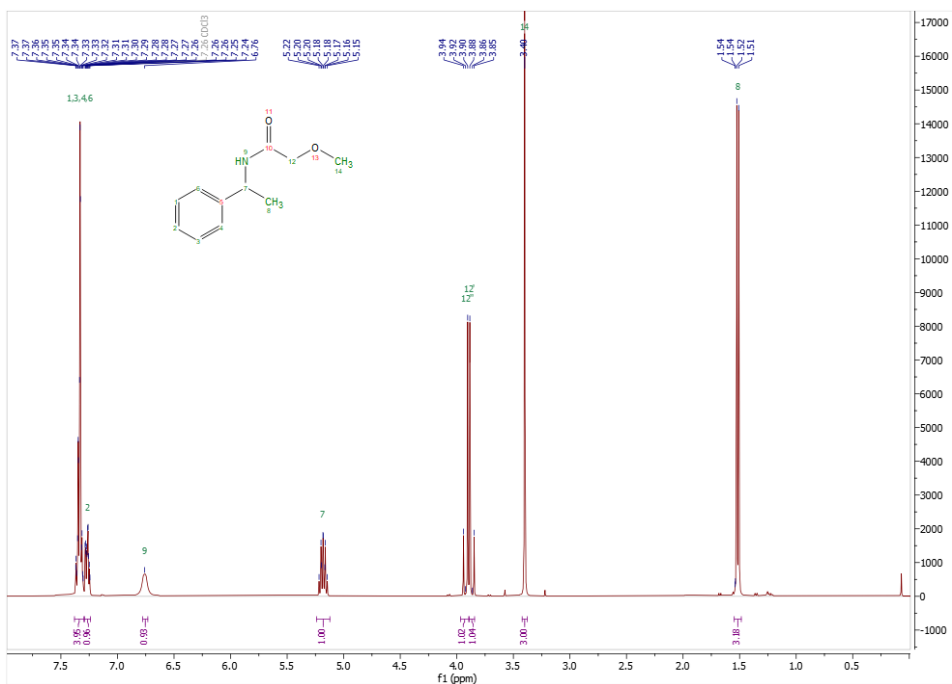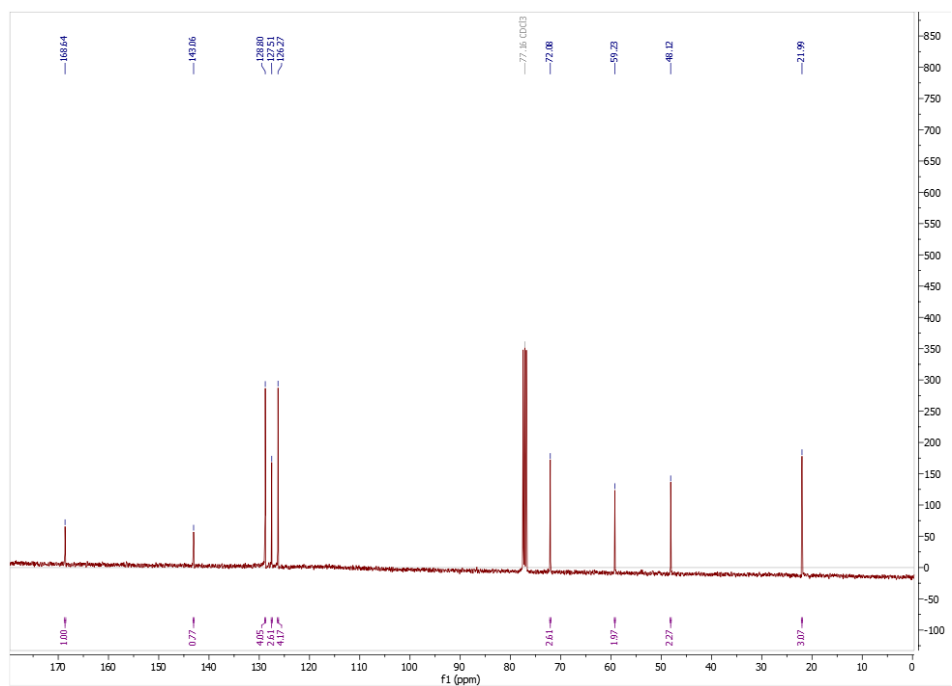*Figure 93* ^{13}C NMR of **95**.

183

Figure 94 ^{1}H NMR of **145**.

Figure 95 ^{13}C NMR of 2-methoxy-N-(1-phenylethyl)acetamide, **145**.

184

8. References

(1)   *Rivastigmine | C14H22N2O2 | CID 77991 - PubChem*.
       https://pubchem.ncbi.nlm.nih.gov/compound/77991 (accessed 2023-07-11).

(2)   *Repaglinide | C27H36N2O4 | CID 65981 - PubChem*.
       https://pubchem.ncbi.nlm.nih.gov/compound/65981 (accessed 2023-07-11).

(3)   *Solifenacin | C23H26N2O2 | CID 154059 - PubChem*.
       https://pubchem.ncbi.nlm.nih.gov/compound/154059 (accessed 2023-07-11).

(4)   *Cinacalcet | C22H22F3N | CID 156419 - PubChem*.
       https://pubchem.ncbi.nlm.nih.gov/compound/156419 (accessed 2023-07-11).

(5)   *Rasagiline | C12H13N | CID 3052776 - PubChem*.
       https://pubchem.ncbi.nlm.nih.gov/compound/3052776 (accessed 2023-07-11).

(6)   *Tamsulosin hydrochloride | C20H29ClN2O5S | CID 5362376 - PubChem*.
       https://pubchem.ncbi.nlm.nih.gov/compound/5362376 (accessed 2023-07-11).

(7)   *S-Metolachlor | C15H22ClNO2 | CID 11140605 - PubChem*.
       https://pubchem.ncbi.nlm.nih.gov/compound/S-Metolachlor (accessed 2023-07-11).

(8)   *Flamprop-isopropyl | C19H19ClFNO3 | CID 40520 - PubChem*.
       https://pubchem.ncbi.nlm.nih.gov/compound/40520 (accessed 2023-07-11).

(9)   *Tolprocarb | C16H21F3N2O3 | CID 57957886 - PubChem*.
       https://pubchem.ncbi.nlm.nih.gov/compound/57957886 (accessed 2023-07-11).

(10)   *Dapoxetine | C21H23NO | CID 71353 - PubChem*.
       https://pubchem.ncbi.nlm.nih.gov/compound/71353 (accessed 2023-07-19).

(11)   *Sertraline | C17H17Cl2N | CID 68617 - PubChem*.
       https://pubchem.ncbi.nlm.nih.gov/compound/68617 (accessed 2023-07-19).

(12)   *Tecalcet | C18H22ClNO | CID 158797 - PubChem*.
       https://pubchem.ncbi.nlm.nih.gov/compound/158797 (accessed 2023-07-19).

(13)   Yang, J.; Buekenhoudt, A.; Dael, M. Van; Luis, P.; Satyawali, Y.; Malina, R.; Lizin, S. A Techno-
       Economic Assessment of a Biocatalytic Chiral Amine Production Process Integrated with in
       Situ Membrane Extraction. *Org Process Res Dev* **2022**, *26* (7), 2052–2066.
       https://doi.org/10.1021/ACS.OPRD.1C00464/SUPPL_FILE/OP1C00464_SI_001.PDF.

(14)   Jeschke, P. Current Status of Chirality in Agrochemicals. *Pest Manag. Sci.* **2018**, *74* (11), 2389–
       2404. https://doi.org/10.1002/ps.5052.

(15)   Pugin, B.; Blaser, H. U. Immobilized Complexes for Enantioselective Catalysis: When Will They
       Be Used in Industry? *Top Catal* **2010**, *53* (13–14), 953–962. https://doi.org/10.1007/s11244-
       010-9514-8.

(16)   Cabré, A.; Verdaguer, X.; Riera, A. Recent Advances in the Enantioselective Synthesis of Chiral
       Amines via Transition Metal-Catalyzed Asymmetric Hydrogenation. *Chem Rev* **2021**, *122*, 269–
       339. https://doi.org/10.1021/acs.chemrev.1c00496.

(17)   Kelly, S. A.; Pohle, S.; Wharry, S.; Mix, S.; Allen, C. C. R.; Moody, T. S.; Gilmore, B. F. Application of ω-Transaminases in the Pharmaceutical Industry. *Chem. Rev.* **2018**, *118*, 349–367. https://doi.org/10.1021/acs.chemrev.7b00437.

(18)   Petty, F.; Maul, A. *Sertraline*; StatPearls Publishing, 2023. https://doi.org/10.1016/B978-008055232-3.62614-5.

(19)   Murala, S.; Bollu, P. C. *Norepinephrine*; StatPearls Publishing, 2023. https://doi.org/10.1007/978-3-031-07897-2_9.

(20)   *Sertraline HCl Market Size, Trends and Forecast to 2030*. https://www.coherentmarketinsights.com/market-insight/sertraline-hcl-market-5355 (accessed 2023-08-15).

(21)   Junaid, S. Z. S.; Patel, J. B. *Cinacalcet*; StatPearls Publishing, 2022. https://doi.org/10.1016/B978-008055232-3.63963-7.

(22)   Yeh, M. W.; Ituarte, P. H. G.; Zhou, H. C.; Nishimoto, S.; In-Lu Amy Liu; Harari, A.; Haigh, P. I.; Adams, A. L. Incidence and Prevalence of Primary Hyperparathyroidism in a Racially Mixed Population. *J Clin Endocrinol Metab* **2013**, *98* (3), 1122. https://doi.org/10.1210/JC.2012-4022.

(23)   EPA Office of Pesticide Programs, U. *US EPA - Pesticides - Fact Sheet for Metolachlor*; 1995.

(24)   *Top corn producing countries worldwide 2022/23 | Statista*. https://www.statista.com/statistics/254292/global-corn-production-by-country/ (accessed 2023-08-15).

(25)   *Metolachlor Market Report Size, 2022-2027*. https://www.industryarc.com/Report/16168/metolachlor-market.html (accessed 2023-08-15).

(26)   Brill, Z. G.; Condakes, M. L.; Ting, C. P.; Maimone, T. J. Navigating the Chiral Pool in the Total Synthesis of Complex Terpene Natural Products. *Chem Rev* **2017**, *117* (18), 11753–11795. https://doi.org/10.1021/ACS.CHEMREV.6B00834.

(27)   Stöckigt, J.; Antonchick, A. P.; Wu, F.; Waldmann, H. The Pictet-Spengler Reaction in Nature and in Organic Chemistry. *Angew. Chem., Int. Ed.* **2011**, *50* (37), 8538–8564. https://doi.org/10.1002/ANIE.201008071.

(28)   *Pinoline | C12H14N2O | CID 1868 - PubChem*. https://pubchem.ncbi.nlm.nih.gov/compound/1868 (accessed 2023-08-16).

(29)   *Harmaline | C13H14N2O | CID 3564 - PubChem*. https://pubchem.ncbi.nlm.nih.gov/compound/3564 (accessed 2023-08-16).

(30)   *Eudistomin C | C14H16BrN3O2S | CID 184887 - PubChem*. https://pubchem.ncbi.nlm.nih.gov/compound/Eudistomin-C (accessed 2023-08-16).

(31)   Cox, E. D.; Cook, J. M. The Pictet-Spengler Condensation: A New Direction for an Old Reaction. *Chem Rev* **1995**, *95* (6), 1797–1842. https://doi.org/10.1021/CR00038A004/ASSET/CR00038A004.FP.PNG_V03.

(32) Ungemach, F.; Soerens, D.; Weber, R.; DiPierro, M.; Campos, O.; Mokry, P.; Cook, J. M.; Silverton, J. V. General Method for the Assignment of Stereochemistry of 1,3-Disubstituted 1,2,3,4-Tetrahydro-β-Carbolines by Carbon-13 Spectroscopy. *J Am Chem Soc* **1980**, *102* (23), 6976–6984. https://doi.org/10.1021/JA00543A012/SUPPL_FILE/JA00543A012_SI_001.PDF.

(33) Curran, M. P.; Keating, G. M. Tadalafil. *Drugs* **2003**, *63*, 2203–2212.

(34) Shi, X. X.; Liu, S. L.; Xu, W.; Xu, Y. L. Highly Stereoselective Pictet–Spengler Reaction of d-Tryptophan Methyl Ester with Piperonal: Convenient Syntheses of Cialis (Tadalafil), 12a-Epi-Cialis, and Their Deuterated Analogues. *Tetrahedron Asymmetry* **2008**, *19* (4), 435–442. https://doi.org/10.1016/J.TETASY.2007.12.017.

(35) Bardsley-Elliot, A.; Noble, S. Oseltamivir. *Drugs* **1999**, *58* (5), 851–860.

(36) Ghosh, S.; Chisti, Y.; Banerjee, U. C. Production of Shikimic Acid. **2012**. https://doi.org/10.1016/j.biotechadv.2012.03.001.

(37) Ize-Ludlow, D.; Ragone, S.; Bernstein, J. N.; Bruck, I. S.; Duchowny, M.; Garcia Pena, B. M. Chemical Composition of Chinese Star Anise (Illicium Verum) and Neurotoxicity in Infants. *JAMA* **2004**, *291* (5), 562–563.

(38) Diaz-Muñoz, G.; Miranda, I. L.; Sartori, S. K.; de Rezende, D. C.; Alves Nogueira Diaz, M. Use of Chiral Auxiliaries in the Asymmetric Synthesis of Biologically Active Compounds: A Review. *Chirality* **2019**, *31* (10), 776–812. https://doi.org/10.1002/CHIR.23103.

(39) Tanuwidjaja, J.; Peltier, Hillary. M.; Ellman, Jonathan. A. One-Pot Asymmetric Synthesis of Either Diastereomer of Tert-Butanesulfinyl-Protected Amines from Ketones. *J. Org. Chem.* **2007**, *72*, 626–629. https://doi.org/10.1021/jo0616512.

(40) Robak, M. T.; Herbage, M. A.; Ellman, J. A. Synthesis and Applications of Tert -Butanesulfinamide. *Chem Rev* **2010**, *110* (6), 3600–3740. https://doi.org/10.1021/cr900382t.

(41) Narode, H.; Gayke, M.; Eppa, G.; Singh Yadav, J. A Review on Synthetic Advances toward the Synthesis of Apremilast, an Anti-Inflammatory Drug. *Cite This: Org. Process Res. Dev* **2021**, *25*, 1512–1523. https://doi.org/10.1021/acs.oprd.1c00107.

(42) Keating, G. M. Apremilast: A Review in Psoriasis and Psoriatic Arthritis. *Drugs* **2017**, *77* (4), 459–472. https://doi.org/10.1007/S40265-017-0709-1/FIGURES/3.

(43) Fei, Z.; Wu, Q.; Zhang, F.; Cao, Y.; Liu, C.; Shieh, W. C.; Xue, S.; McKenna, J.; Prasad, K.; Prashad, M.; Baeschlin, D.; Namoto, K. A Scalable Synthesis of an Azabicyclooctanyl Derivative, a Novel DPP-4 Inhibitor. *Journal of Organic Chemistry* **2008**, *73* (22), 9016–9021. https://doi.org/10.1021/JO801830X.

(44) Sheldon, R. A. Metrics of Green Chemistry and Sustainability: Past, Present, and Future. *ACS Sustain Chem Eng* **2018**, *6* (1), 32–48. https://doi.org/10.1021/ACSSUSCHEMENG.7B03505.

(45) Diéguez, M.; Claver, C.; Margalef, J. Asymmetric Hydrogenation of Imines. *Advances in Catalysis* **2021**, *68*, 205–289. https://doi.org/10.1016/BS.ACAT.2021.08.003.

(46) Tang, W.; Johnston, S.; Li, C.; Iggo, J. A.; Bacsa, J.; Xiao, J. Cooperative Catalysis: Combining an Achiral Metal Catalyst with a Chiral Brønsted Acid Enables Highly Enantioselective Hydrogenation of Imines. *Chemistry - A European Journal* **2013**, *19* (42), 14187–14193. https://doi.org/10.1002/CHEM.201302437.

(47)   Zhou, X.-M.; Huang, J.-D.; Luo, L.-B.; Zhang, C.-L.; Zheng, Z.; Hu, X.-P. Readily Available Chiral Phosphine-Aminophosphine Ligands Derived from 1-Phenylethylamine for Rh-Catalyzed Enantioselective Hydrogenations. **2010**. https://doi.org/10.1016/j.tetasy.2010.03.008.

(48)   Hansen, K. B.; Hsiao, Y.; Xu, F.; Rivera, N.; Clausen, A.; Kubryk, M.; Krska, S.; Rosner, T.; Simmons, B.; Balsells, J.; Ikemoto, N.; Sun, Y.; Spindler, F.; Malan, C.; Grabowski, E. J. J.; Armstrong, J. D. Highly Efficient Asymmetric Synthesis of Sitagliptin. *J Am Chem Soc* **2009**, *131* (25), 8798–8804. https://doi.org/10.1021/JA902462Q.

(49)   *Merck Announces Fourth-Quarter and Full-Year 2021 Financial Results - Merck.com*. https://www.merck.com/news/merck-announces-fourth-quarter-and-full-year-2021-financial-results/ (accessed 2023-08-17).

(50)   *Metals prices | Umicore Precious Metals Management*. https://pmm.umicore.com/en/prices/ (accessed 2023-07-11).

(51)   *Industrial Enzymes Market Size, Share & Growth Report*. https://www.grandviewresearch.com/industry-analysis/industrial-enzymes-market (accessed 2023-07-13).

(52)   Kroutil, W.; Fischereder, E. M.; Fuchs, C. S.; Lechner, H.; Mutti, F. G.; Pressnitz, D.; Rajagopalan, A.; Sattler, J. H.; Simon, R. C.; Siirola, E. Asymmetric Preparation of Prim -, Sec -, and Tert-Amines Employing Selected Biocatalysts. *Org Process Res Dev* **2013**, *17* (5), 751–759. https://doi.org/10.1021/op4000237.

(53)   Sayer, C.; Martinez-Torres, R. J.; Richter, N.; Isupov, M. N.; Hailes, H. C.; Littlechild, J. A.; Ward, J. M. The Substrate Specificity, Enantioselectivity and Structure of the (R)-Selective Amine: Pyruvate Transaminase from Nectria Haematococca. *FEBS Journal* **2014**, *281* (9), 2240–2253. https://doi.org/10.1111/FEBS.12778.

(54)   Shin, Y. C.; Yun, H.; Park, H. H. Structural Dynamics of the Transaminase Active Site Revealed by the Crystal Structure of a Co-Factor Free Omega-Transaminase from Vibrio Fluvialis JS17. *Scientific Reports 2018 8:1* **2018**, *8* (1), 1–9. https://doi.org/10.1038/s41598-018-29846-0.

(55)   C. K. Saville; J. M. Janey; E. C. Mundorff; J. C. Moore; S. Tam; W. R. Jarvis; J. C. Colbeck; A. Krebber; F. J. Fleitz; J. Brands; P. N. Devine; G. W. Huisman; G. J. Hughes. Biocatalytic Asymmetric Synthesis of Chiral Amines from Ketones Applied to Sitagliptin Manufacture. *Science (1979)* **2010**, *329*, 305–308. https://doi.org/10.1126/science.1189106.

(56)   Fuchs, M.; Koszelewski, D.; Tauber, K.; Sattler, J.; Banko, W.; Holzer, A. K.; Pickl, M.; Kroutil, W.; Faber, K. Improved Chemoenzymatic Asymmetric Synthesis of (S)-Rivastigmine. **2012**. https://doi.org/10.1016/j.tet.2012.06.031.

(57)   Koszelewski, D.; Lavandera, I.; Clay, D.; Rozzell, D.; Kroutil, W. Asymmetric Synthesis of Optically Pure Pharmacologically Relevant Amines Employing ω-Transaminases. *Adv Synth Catal* **2008**, *350* (17), 2761–2766. https://doi.org/10.1002/ADSC.200800496.

(58)   Koszelewski, D.; Clay, D.; Rozzell, D.; Kroutil, W. Deracemisation of α-Chiral Primary Amines by a One-Pot, Two-Step Cascade Reaction Catalysed by ω-Transaminases. *European J Org Chem* **2009**, No. 14, 2289–2292. https://doi.org/10.1002/EJOC.200801265.

(59)   *Presidential Green Chemistry Challenge: 2010 Greener Reaction Conditions Award | US EPA*.
         https://www.epa.gov/greenchemistry/presidential-green-chemistry-challenge-2010-greener-
         reaction-conditions-award (accessed 2023-08-18).

(60)   Blaser, H. U.; Spindler, F.; Studer, M. Enantioselective Catalysis in Fine Chemicals Production.
         Appl Catal A Gen **2001**, *221*, 119–143.

(61)   Levit, G. L.; Gruzdev, D. A.; Krasnov, V. P. *Kinetic Resolution Using Diastereoselective Acylating
         Agents as a Synthetic Approach to Enantiopure Amines*; 2018; Vol. 12.

(62)   Binanzer, M.; Hsieh, S. Y.; Bode, J. W. Catalytic Kinetic Resolution of Cyclic Secondary Amines. *J
         Am Chem Soc* **2011**, *133* (49), 19698–19701. https://doi.org/10.1021/JA209472H.

(63)   Azamatov, A. A.; Zhurakulov, S. N.; Vinogradova, V. I.; Tursunkhodzhaeva, F.; Khinkar, R. M.;
         Malatani, R. T.; Aldurdunji, M. M.; Tiezzi, A.; Mamadalieva, N. Z. Evaluation of the Local
         Anesthetic Activity, Acute Toxicity, and Structure–Toxicity Relationship in Series of Synthesized
         1-Aryltetrahydroisoquinoline Alkaloid Derivatives In Vivo and In Silico. *Molecules* **2023**, *28* (2).
         https://doi.org/10.3390/molecules28020477.

(64)   *Norreticuline | C18H21NO4 | CID 443766 - PubChem*.
         https://pubchem.ncbi.nlm.nih.gov/compound/Norreticuline (accessed 2023-10-19).

(65)   Teng, Y.; Gu, C.; Chen, Z.; Jiang, H.; Xiong, Y.; Liu, D.; Xiao, D. Advances and Applications of
         Chiral Resolution in Pharmaceutical Field. *Chirality* **2022**, *34* (8), 1094–1119.
         https://doi.org/10.1002/CHIR.23453.

(66)   Pandey, B.; Lohray, V.; Bhushan, L.; Bhushan, B. Process for Pre-Paring Clopidogrel Patent.
         WO02/059128 A3. https://doi.org/WO02/059128 A3.

(67)   Wang, L.; Shen, J.; Tang, Y.; Chen, Y.; Wang, W.; Cai, Z.; Du, Z. Synthetic Improvements in the
         Preparation of Clopidogrel. **2007**. https://doi.org/10.1021/op700025d.

(68)   *Clopidogrel: an antiplatelet medicine to prevent blood clots - NHS*.
         https://www.nhs.uk/medicines/clopidogrel/ (accessed 2023-07-17).

(69)   Topol, E. J.; Schork, N. J. Catapulting Clopidogrel Pharmacogenomics Forward. *Nat Med* **2011**,
         17 (1), 40–41. https://doi.org/10.1038/nm0111-40.

(70)   Thompson, L. A. Chemo-and Bio-Catalysis for the Synthesis of Chiral Amines in Continuous
         Flow Reactors, University of Leeds, 2017.

(71)   Lee, J. H.; Han, K.; Kim, M. J.; Park, J. Chemoenzymatic Dynamic Kinetic Resolution of Alcohols
         and Amines. *European J Org Chem* **2010**, No. 6, 999–1015.
         https://doi.org/10.1002/ejoc.200900935.

(72)   Pàmies, O.; Bäckvall, J. E. Combination of Enzymes and Metal Catalysts. A Powerful Approach
         in Asymmetric Catalysis. *Chem Rev* **2003**, *103* (8), 3247–3261.
         https://doi.org/10.1021/CR020029G.

(73)   Verho, O.; Bäckvall, J. E. Chemoenzymatic Dynamic Kinetic Resolution: A Powerful Tool for the
         Preparation of Enantiomerically Pure Alcohols and Amines. *J Am Chem Soc* **2015**, *137* (12),
         3996–4009. https://doi.org/10.1021/jacs.5b01031.

(74)   Parvulescu, A. N.; Van der Eycken, E.; Jacobs, P. A.; De Vos, D. E. Microwave-Promoted Racemization and Dynamic Kinetic Resolution of Chiral Amines over Pd on Alkaline Earth Supports and Lipases. *J Catal* **2008**, *255* (2), 206–212. https://doi.org/10.1016/j.jcat.2008.02.005.

(75)   Parvulescu, A. N.; Jacobs, P. A.; De Vos, D. E. Palladium Catalysts on Alkaline-Earth Supports for Racemization and Dynamic Kinetic Resolution of Benzylic Amines. *Chemistry - A European Journal* **2007**, *13* (7), 2034–2043. https://doi.org/10.1002/CHEM.200600899.

(76)   Parvulescu, A. N.; Jacobs, P. A.; De Vos, D. E. Heterogeneous Raney Nickel and Cobalt Catalysts for Racemization and Dynamic Kinetic Resolution of Amines. *Adv Synth Catal* **2008**, *350* (1), 113–121. https://doi.org/10.1002/ADSC.200700336.

(77)   Parvulescu, A.; Janssens, J.; Vanderleyden, J.; De Vos, D. Heterogeneous Catalysts for Racemization and Dynamic Kinetic Resolution of Amines and Secondary Alcohols. *Top Catal* **2010**, *53* (13–14), 931–941. https://doi.org/10.1007/s11244-010-9512-x.

(78)   Apps, J. F. S.; Livingston, A. G.; Parrett, M. R.; Pounder, R. J.; Taylor, P. C.; Turner, A. R. Racemisation of 1-Arylethylamines with Shvo-Type Organoruthenium Catalysts Racemisation of 1-Arylethylamines. *Synlett* **2014**, *25*, 1391–1394. https://doi.org/10.1055/s-0033-1341228.

(79)   Blacker, A. J.; Stirling, M. J.; Page, M. I. Catalytic Racemisation of Chiral Amines and Application in Dynamic Kinetic Resolution. *Org Process Res Dev* **2007**, *11* (3), 642–648. https://doi.org/10.1021/op060233w.

(80)   Paetzold, J.; Bäckvall, J. E. Chemoenzymatic Dynamic Kinetic Resolution of Primary Amines. *J Am Chem Soc* **2005**, *127* (50), 17620–17621. https://doi.org/10.1021/ja056306t.

(81)   Reetz, M. T.; Schimossek, K. Lipase-Catalyzed Dynamic Kinetic Resolution of Chiral Amines: Use of Palladium as the Racemization Catalyst. *NOTES Chimia* **1996**, *50*, 668–669.

(82)   Kim, Y.; Park, J.; Kim, M. J. Fast Racemization and Dynamic Kinetic Resolution of Primary Benzyl Amines. *Tetrahedron Lett* **2010**, *51* (42), 5581–5584. https://doi.org/10.1016/J.TETLET.2010.08.050.

(83)   Kim, M. J.; Kim, W. H.; Han, K.; Yoon, K. C.; Park, J. Dynamic Kinetic Resolution of Primary Amines with a Recyclable Pd Nanocatalyst for Racemization. *Org Lett* **2007**, *9* (6), 1157–1159. https://doi.org/10.1021/ol070130d.

(84)   Kyung Choi, Y.; Jung Kim, M.; Ahn, Y.; Kim, M.-J.; Org Lett, J. W. Lipase/Palladium-Catalyzed Asymmetric Transformations of Ketoximes to Optically Active Amines. *Org Lett* **2001**, *3* (25), 4099–4101. https://doi.org/10.1021/ol0168622.

(85)   Pàmies, O.; E, A. H.; M Samec, J. S.; Hermanns, N.; Bäckvall, J.-E. *An Efficient and Mild Ruthenium-Catalyzed Racemization of Amines: Application to the Synthesis of Enantiomerically Pure Amines*; 2002; Vol. 43.

(86)   Thalén, L. K.; Bäckvall, J. E. Development of Dynamic Kinetic Resolution on Large Scale for (±)-1-Phenylethylamine. *Beilstein Journal of Organic Chemistry* **2010**, *6*, 823–829. https://doi.org/10.3762/bjoc.6.97.

(87)   Parvulescu, A. N.; Jacobs, P. A.; De Vos, D. E. Heterogeneous Raney Nickel and Cobalt Catalysts for Racemization and Dynamic Kinetic Resolution of Amines. *Adv Synth Catal* **2008**, *350* (1), 113–121. https://doi.org/10.1002/ADSC.200700336.

(88)   Parvulescu, A. N.; Jacobs, P. A.; De Vos, D. E. Support Influences in the Pd-Catalyzed Racemization and Dynamic Kinetic Resolution of Chiral Benzylic Amines. *Appl Catal A Gen* **2009**, *368* (1–2), 9–16. https://doi.org/10.1016/j.apcata.2009.07.042.

(89)   De Miranda, A. S.; De Souza, R. O. M. A.; Miranda, L. S. M. Ammonium Formate as a Green Hydrogen Source for Clean Semi-Continuous Enzymatic Dynamic Kinetic Resolution of (+/-)-1-Methylbenzylamine. **2014**. https://doi.org/10.1039/c4ra00462k.

(90)   Farkas, E.; Oláh, M.; Földi, A.; Kóti, J.; Éles, J.; Nagy, J.; Gal, C. A.; Paizs, C.; Hornyánszky, G.; Poppe, L. Chemoenzymatic Dynamic Kinetic Resolution of Amines in Fully Continuous-Flow Mode. *Org Lett* **2018**, *20* (24), 8052–8056. https://doi.org/10.1021/acs.orglett.8b03676.

(91)   Ma, G.; Xu, Z.; Zhang, P.; Liu, J.; Hao, X.; Ouyang, J.; Liang, P.; You, S.; Jia, X. A Novel Synthesis of Rasagiline via a Chemoenzymatic Dynamic Kinetic Resolution. **2014**. https://doi.org/10.1021/op500152g.

(92)   Murahashi, S.-I.; Yoshimura, N.; Tsumiyama, T.; Kojima, T. Catalytic Alkyl Group Exchange Reaction of Primary and Secondary Amines. *J. Am. Chem. Soc.* **1982**, *105*, 5002–5011.

(93)   Poojari, Y.; Clarson, S. J. Thermal Stability of Candida Antarctica Lipase B Immobilized on Macroporous Acrylic Resin Particles in Organic Media. **2012**. https://doi.org/10.1016/j.bcab.2012.10.002.

(94)   Reetz, M. T.; Dreisbach, C. Highly Efficient Lipase-Catalyzed Kinetic Resolution of Chiral Amines. *Chima* **1994**, *12*, 570.

(95)   Jerphagnon, T.; Gayet, A. J. A.; Berthiol, F.; Ritleng, V.; Mršić, N.; Meetsma, A.; Pfeffer, M.; Minnaard, A. J.; Feringa, B. L.; De Vries, J. G. Fast Racemisation of Chiral Amines and Alcohols by Using Cationic Half-Sandwich Ruthena- and Iridacycle Catalysts. *Chemistry - A European Journal* **2009**, *15* (46), 12780–12790. https://doi.org/10.1002/chem.200902103.

(96)   Pàmies, O.; Bäckvall, J. E. Enzymatic Kinetic Resolution and Chemoenzymatic Dynamic Kinetic Resolution of δ-Hydroxy Esters. An Efficient Route to Chiral δ-Lactones. *Journal of Organic Chemistry* **2002**, *67* (4), 1261–1265. https://doi.org/10.1021/jo016096c.

(97)   Kwan, M. H. T.; Breen, J.; Bowden, M.; Conway, L.; Crossley, B.; Jones, M. F.; Munday, R.; Pokar, N. P. B.; Screen, T.; Blacker, A. J. Continuous Flow Chiral Amine Racemization Applied to Continuously Recirculating Dynamic Diastereomeric Crystallizations. *Journal of Organic Chemistry* **2021**, *86* (3), 2458–2473. https://doi.org/10.1021/acs.joc.0c02617.

(98)   Vaz, B. G.; Milagre, C. D. F.; Eberlin, M. N.; Milagre, H. M. S. Shvo's Catalyst in Chemoenzymatic Dynamic Kinetic Resolution of Amines-Inner or Outer Sphere Mechanism? *Org. Biomol. Chem* **2013**, *6695* (11), 46. https://doi.org/10.1039/c3ob41318g.

(99)   Stirling, M. J.; Mwansa, J. M.; Sweeney, G.; Blacker, A. J.; Page, M. I. The Kinetics and Mechanism of the Organo-Iridium Catalysed Racemisation of Amines. *Org Biomol Chem* **2016**, *14*, 7092. https://doi.org/10.1039/c6ob00884d.

(100) Ferreira, M. M. M.; Cabreira, C. R.; Chaves, P. H. K.; Labussiére, G. M.; Zimpeck, R. C.; De Lima, S. M.; De Siqueira, F. A. Preparation, Characterization and Catalytic Activity of Palladium Catalyst Supported on MgCO 3 for Dynamic Kinetic Resolution of Amines. *Article J. Braz. Chem. Soc* **2018**, *29* (10), 2144–2149. https://doi.org/10.21577/0103-5053.20180089.

(101) Parvulescu, A.; De Vos, D.; Jacobs, P. Efficient Dynamic Kinetic Resolution of Secondary Amines with Pd on Alkaline Earth Salts and a Lipase. *Chemical Communications* **2005**, No. 42, 5307–5309. https://doi.org/10.1039/b509747a.

(102) *Junior - Benchtop Automation Solution | Unchained Labs*. https://www.unchainedlabs.com/junior/ (accessed 2023-08-30).

(103) *HandyStep® Repetitive pipette | VWR*. https://uk.vwr.com/store/product/26710046/null (accessed 2023-08-30).

(104) *OT-2 Liquid Handler | Opentrons Lab Automation*. https://opentrons.com/products/robots/ot-2/ (accessed 2023-08-30).

(105) Tallon, L. Heterogeneous Catalysts for the Alkylation of Amines Using Alcohols, 2015.

(106) Ma, R.; He, L.-N.; Song, Q.-W.; Zhou, Y.-B.; Liu, K.-X. Efficient Hydrogenation of Imines over Fe and ZnO Powder in a Self-Neutralizing Acidic CO 2-H 2 O System †. **2014**. https://doi.org/10.1039/c4ra00026a.

(107) Etayo, P.; Vidal-Ferran, A. Rhodium-Catalysed Asymmetric Hydrogenation as a Valuable Synthetic Tool for the Preparation of Chiral Drugs. *Chem Soc Rev* **2013**, *42* (2), 728–754. https://doi.org/10.1039/c2cs35410a.

(108) Li, W.; Cui, X.; Junge, K.; Surkus, A. E.; Kreyenschulte, C.; Bartling, S.; Beller, M. General and Chemoselective Copper Oxide Catalysts for Hydrogenation Reactions. *ACS Catal* **2019**, *9* (5), 4302–4307. https://doi.org/10.1021/ACSCATAL.8B04807/SUPPL_FILE/CS8B04807_SI_001.PDF.

(109) Santoro, F.; Psaro, R.; Ravasio, N.; Zaccheria, F. N-Alkylation of Amines through Hydrogen Borrowing over a Heterogeneous Cu Catalyst †. **2014**. https://doi.org/10.1039/c3ra44364g.

(110) Anisimova, T. B.; Kinzhalov, M. A.; Guedes Da Silva, M. F. C.; Novikov, A. S.; Kukushkin, V. Y.; Pombeiro, A. J. L.; Luzyanin, K. V. Addition of: N -Nucleophiles to Gold(III)-Bound Isocyanides Leading to Short-Lived Gold(III) Acyclic Diaminocarbene Complexes. *New Journal of Chemistry* **2017**, *41* (9), 3246–3250. https://doi.org/10.1039/c7nj00529f.

(111) González-Arellano, C.; Corma, A.; Iglesias, M.; Sánchez, F. Enantioselective Hydrogenation of Alkenes and Imines by a Gold Catalyst. **2005**. https://doi.org/10.1039/b505271h.

(112) Yoshida, J. *Flash Chemistry: Fast Organic Synthesis in Microsystems*; Wiley: Chichester, UK, 2008. https://doi.org/10.1002/9780470723425.

(113) Stadler, A.; Yousefi, B. H.; Dallinger, D.; Walla, P.; Van Der Eycken, E.; Kaval, N.; Kappe, C. O. Scalability of Microwave-Assisted Organic Synthesis. From Single-Mode to Multimode Parallel Batch Reactors. **2003**. https://doi.org/10.1021/OP034075.

(114) Martina, K.; Cravotto, G.; Varma, R. S. Impact of Microwaves on Organic Synthesis and Strategies toward Flow Processes and Scaling Up. *Journal of Organic Chemistry* **2021**, *86* (20), 13857–13872. https://doi.org/10.1021/ACS.JOC.1C00865.

(115) Plutschack, M. B.; Pieber, B.; Gilmore, K.; Seeberger, P. H. The Hitchhiker's Guide to Flow Chemistry. *Chem Rev* **2017**, *117* (18), 11796–11893. https://doi.org/10.1021/acs.chemrev.7b00183.

(116) Hone, C. A.; Kappe, C. O. Towards the Standardization of Flow Chemistry Protocols for Organic Reactions. *Chemistry–Methods* **2021**, *1* (11), 454–467. https://doi.org/10.1002/CMTD.202100059.

(117) Yoshida, J.-I.; Takahashi, Y.; Nagaki, A. Flash Chemistry: Flow Chemistry That Cannot Be Done in Batch. *Chem. Commun* **2013**, *49*, 9896. https://doi.org/10.1039/c3cc44709j.

(118) Takle, M. J.; Deadman, B. J.; Hellgardt, K.; Dickhaut, J.; Wieja, A.; Kuok, K.; Hii, M. A Flash Thermal Racemization Protocol for the Chemoenzymatic Dynamic Kinetic Resolution and Stereoinversion of Chiral Amines. **2023**, *13*, 10541–10546. https://doi.org/10.1021/acscatal.3c02859.

(119) Bowden, G. D.; Pichler, B. J.; Maurer, A. A Design of Experiments (DoE) Approach Accelerates the Optimization of Copper-Mediated 18F-Fluorination Reactions of Arylstannanes. *Sci Rep* **2019**, *9* (11370). https://doi.org/10.1038/s41598-019-47846-6.

(120) Taylor, C. J.; Baker, A.; Chapman, M. R.; Reynolds, W. R.; Jolley, K. E.; Clemens, G.; Smith, G. E.; Blacker, & A. J.; Chamberlain, T. W.; Christie, S. D. R.; Taylor, B. A.; Bourne, R. A. Flow Chemistry for Process Optimisation Using Design of Experiments. *J Flow Chem* **2021**, *11*, 75–86. https://doi.org/10.1007/s41981-020.

(121) *(S)-Salsolidine - PubChem*. https://pubchem.ncbi.nlm.nih.gov/compound/164752 (accessed 2023-09-07).

(122) Ortiz, C.; Ferreira, M. L.; Barbosa, O.; Dos Santos, J. C. S.; Rodrigues, R. C.; Berenguer-Murcia, Á.; Briand, L. E.; Fernandez-Lafuente, R. Novozym 435: The "Perfect" Lipase Immobilized Biocatalyst? *Catal Sci Technol* **2019**, *9* (10), 2380–2420. https://doi.org/10.1039/c9cy00415g.

(123) Garcia, M. J.; Rebolledo, F.; Gotor, V. Lipase-Catalyzed Aminolysis and Ammonolysis of β-Ketoesters. Synthesis of Optically Active β-Ketoamides. *Tetrahedron* **1994**, *50* (23), 6935–6940.

(124) Joubioux, F. Le; Bridiau, N.; Henda, Y. Ben; Achour, O.; Graber, M.; Maugard, T. The Control of Novozym® 435 Chemoselectivity and Specificity by the Solvents in Acylation Reactions of Amino-Alcohols. *J Mol Catal B Enzym* **2013**, *95*, 99–110. https://doi.org/10.1016/J.MOLCATB.2013.06.002.

(125) Päiviö, M.; Perkiö, P.; Kanerva, L. T. Solvent-Free Kinetic Resolution of Primary Amines Catalyzed by Candida Antarctica Lipase B: Effect of Immobilization and Recycling Stability. **2012**. https://doi.org/10.1016/j.tetasy.2012.02.008.

(126) Öhrner, N.; Orrenius, C.; Mattson, A.; Norin, T.; Hult, K. Kinetic Resolutions of Amine and Thiol Analogues of Secondary Alcohols Catalyzed by the Candida Antarctica Lipase B. *Enzyme Microb Technol* **1996**, *19* (5), 328–331. https://doi.org/10.1016/S0141-0229(96)00031-2.

(127) Johnson, K. A.; Goody, R. S. The Original Michaelis Constant: Translation of the 1913 Michaelis-Menten Paper. *Biochemistry* **2011**, *50* (39), 8264–8269. https://doi.org/10.1021/BI201284U.

(128) Nechab, M.; Azzi, N.; Vanthuyne, N.; Bertrand, M.; Gastaldi, S.; Gil, G. Highly Selective Enzymatic Kinetic Resolution of Primary Amines at 80°C: A Comparative Study of Carboxylic Acids and Their Ethyl Esters as Acyl Donors. *Journal of Organic Chemistry* **2007**, *72* (18), 6918–6923. https://doi.org/10.1021/JO071069T.

(129) Csuka, P.; Boros, Z.; Orfi, L.; Dobos, J.; Poppe, L.; Hornyánszky, G. Chemoenzymatic Route to Tyrphostins Involving Lipase-Catalyzed Kinetic Resolution of 1-Phenylethanamine with Alkyl Cyanoacetates as Novel Acylating Agents. *Tetrahedron Asymmetry* **2015**, *26* (12–13), 644–649. https://doi.org/10.1016/J.TETASY.2015.04.013.

(130) Sanfilippo, C.; Paternò, A. A.; Patti, A. Resolution of Racemic Amines via Lipase-Catalyzed Benzoylation: Chemoenzymatic Synthesis of the Pharmacologically Active Isomers of Labetalol. *Molecular Catalysis* **2018**, *449*, 79–84. https://doi.org/10.1016/J.MCAT.2018.02.017.

(131) Ark Ol Ah, M.; Acs, K.; Katona, G.; Abor Horny Anszky, G.; Aszl O Poppe, L. Optimization of 2-Alkoxyacetates as Acylating Agent for Enzymatic Kinetic Resolution of Chiral Amines. **2018**. https://doi.org/10.1016/j.tet.2018.05.032.

(132) Szemes, J.; Malta-Lakó, Á.; Tóth, R. E.; Poppe, L. Diisopropyl Malonate as Acylating Agent in Kinetic Resolution of Chiral Amines with Lipase B from Candida Antarctica. *Periodica Polytechnica Chemical Engineering* **2022**, *66* (3), 458–464. https://doi.org/10.3311/PPch.19521.

(133) *Taxol | C47H51NO14 | CID 36314 - PubChem*. https://pubchem.ncbi.nlm.nih.gov/compound/36314 (accessed 2023-10-09).

(134) *Fezolinetant | C16H15FN6OS | CID 117604931 - PubChem*. https://pubchem.ncbi.nlm.nih.gov/compound/Fezolinetant (accessed 2023-10-09).

(135) Goswami, A.; Guo, Z.; Parker, W. L.; Patel, R. N. Enzymatic Resolution of Sec-Butylamine. *Tetrahedron Asymmetry* **2005**, *16* (9), 1715–1719. https://doi.org/10.1016/J.TETASY.2005.03.012.

(136) Cammenberg, M.; Hult, K.; Park, S. Molecular Basis for the Enhanced Lipase-Catalyzed N-Acylation of 1-Phenylethanamine with Methoxyacetate. *ChemBioChem* **2006**, *7* (11), 1745–1749. https://doi.org/10.1002/cbic.200600245.

(137) Cammenberg, M.; Hult, K.; Park, S. Molecular Basis for the Enhanced Lipase-Catalyzed N-Acylation of 1-Phenylethanamine with Methoxyacetate. *ChemBioChem* **2006**, *7* (11), 1745–1749. https://doi.org/10.1002/CBIC.200600245.

(138) Oláh, M.; Kovács, D.; Katona, G.; Hornyánszky, G.; Poppe, L. Optimization of 2-Alkoxyacetates as Acylating Agent for Enzymatic Kinetic Resolution of Chiral Amines. *Tetrahedron* **2018**, *74* (27), 3663–3670. https://doi.org/10.1016/J.TET.2018.05.032.

(139) Tamborini, L.; Fernandes, P.; Paradisi, F.; Molinari, F. Flow Bioreactors as Complementary Tools for Biocatalytic Process Intensification. *Trends Biotechnol* **2018**, *36* (1), 73–88. https://doi.org/10.1016/j.tibtech.2017.09.005.

(140) De Miranda, A. S.; Miranda, L. S. M.; De Souza, R. O. M. A. Ethyl Acetate as an Acyl Donor in the Continuous Flow Kinetic Resolution of (±)-1-Phenylethylamine Catalyzed by Lipases. *Org Biomol Chem* **2013**, *11* (20), 3332–3336. https://doi.org/10.1039/c3ob40437d.

(141) Weiser, D.; Nagy, F.; Bánóczi, G.; Oláh, M.; Farkas, A.; Szilágyi, A.; László, K.; Gellért, Á.; Marosi, G.; Kemény, S.; Poppe, L. Immobilization Engineering – How to Design Advanced Sol–Gel Systems for Biocatalysis? **2017**, *19*, 3927. https://doi.org/10.1039/c7gc00896a.

(142) *Uniqsis Ltd - FlowSyn Maxi*. https://www.uniqsis.com/paProductsDetail.aspx?ID=FLW_MAXI (accessed 2023-04-17).

(143) Sayuri Shiki, P.; Nayana Perreira, G.; Cristina de Meneses, A.; de Oliveira, D.; Alberto Lerin, L. Novozym ® 435 and Lipozyme ® RM IM as Biocatalysts for Benzyl Benzoate Synthesis. **2022**, *12* (6), 8271–8284. https://doi.org/10.33263/BRIAC126.82718284.

(144) Sontakke, J. B.; Yadav, G. D. Optimization and Kinetic Modeling of Lipase Mediated Enantioselective Kinetic Resolution of (±)-2-Octanol. **2013**, *5* (9), 1025–1033. https://doi.org/10.4236/ns.2013.59127.

(145) Soyer, A.; Bayraktar, E.; Mehmetoglu, U. Optimization of Lipase-Catalyzed Enantioselective Production of 1-Phenyl 1-Propanol Using Response Surface Methodology. *Prep Biochem Biotechnol* **2010**, *40* (4), 389–404. https://doi.org/10.1080/10826068.2010.525433.

(146) Lerin, L. A.; Feiten, M. C.; Richetti, A.; Toniazzo, G.; Treichel, H.; Mazutti, M. A.; Vladimir Oliveira, J.; Oestreicher, E. G.; De Oliveira, D. Enzymatic Synthesis of Ascorbyl Palmitate in Ultrasound-Assisted System: Process Optimization and Kinetic Evaluation. *Ultrason Sonochem* **2011**, *18* (5), 988–996. https://doi.org/10.1016/J.ULTSONCH.2010.12.013.

(147) Moreira, K. S.; Moura Júnior, L. S.; Monteiro, R. R. C.; De Oliveira, A. L. B.; Valle, C. P.; Freire, T. M.; Fechine, P. B. A.; De Souza, M. C. M.; Fernandez-Lorente, G.; Guisan, J. M.; Dos Santos, J. C. S. Optimization of the Production of Enzymatic Biodiesel from Residual Babassu Oil (Orbignya Sp.) via RSM. *Catalysts* **2020**, *10* (414), 1–20. https://doi.org/10.3390/catal10040414.

(148) Oláh, M.; Kovács, D.; Katona, G.; Hornyánszky, G.; Poppe, L. Optimization of 2-Alkoxyacetates as Acylating Agent for Enzymatic Kinetic Resolution of Chiral Amines. *Tetrahedron* **2018**, *74* (27), 3663–3670. https://doi.org/10.1016/J.TET.2018.05.032.

(149) Tamborini, L.; Fernandes, P.; Paradisi, F.; Molinari, F. Flow Bioreactors as Complementary Tools for Biocatalytic Process Intensification. *Trends Biotechnol* **2018**, *36* (1), 73–88. https://doi.org/10.1016/j.tibtech.2017.09.005.

(150) Veld, M. A. J.; Hult, K.; Palmans, A. R. A.; Meijer, E. W. Fast DKR of Amines Using Isopropyl 2-Methoxyacetate as Acyl Donor. *European J Org Chem* **2007**, No. 32, 5416–5421. https://doi.org/10.1002/EJOC.200700568.

(151) Clayton, A. D.; Labes, R.; Blacker, A. J. Combination of Chemocatalysis and Biocatalysis in Flow. *Curr. Opin. Green Sustain. Chem.* **2020**, *26*. https://doi.org/10.1016/j.cogsc.2020.100378.

(152) Roengpithya, C.; Patterson, D. A.; Livingston, A. G.; Taylor, P. C.; Irwin, J. L.; Parrett, M. R. Towards a Continuous Dynamic Kinetic Resolution of 1-Phenylethylamine Using a Membrane Assisted, Two Vessel Process. **2007**. https://doi.org/10.1039/b709035h.

(153) Mcelroy, C. R.; Constantinou, A.; Jones, L. C.; Summerton, L.; Clark, J. H. Towards a Holistic Approach to Metrics for the 21st Century Pharmaceutical Industry. **2015**, *17*, 3111. https://doi.org/10.1039/c5gc00340g.

(154) Baráth, E. Hydrogen Transfer Reactions of Carbonyls, Alkynes, and Alkenes with Noble Metals in the Presence of Alcohols/Ethers and Amines as Hydrogen Donors. *Catalysts* **2018**, *8* (12). https://doi.org/10.3390/catal8120671.

(155) Munawar, S.; Zahoor, A. F.; Ali, S.; Javed, S.; Irfan, M.; Irfan, A.; Kotwica-Mojzych, K.; Mojzych, M. Mitsunobu Reaction: A Powerful Tool for the Synthesis of Natural Products: A Review. *Molecules* **2022**, *27* (20). https://doi.org/10.3390/molecules27206953.

(156) Fletcher, S. The Mitsunobu Reaction in the 21 St Century. *Org. Chem. Front* **2015**, *2*, 739–752. https://doi.org/10.1039/c5qo00016e.

(157) Hui, C.; Wang, Z.; Wang, S.; Xu, C. Molecular Editing in Natural Product Synthesis. *Organic Chemistry Frontiers* **2022**, *9* (5), 1451–1457. https://doi.org/10.1039/d2qo00043a.

(158) *TOLUENE | CAMEO Chemicals | NOAA*. https://cameochemicals.noaa.gov/chemical/4654 (accessed 2022-10-27).

(159) Brazier, J. B.; Nguyen, B. N.; Adrio, L. A.; Barreiro, E. M.; Leong, W. P.; Newton, M. A.; Figueroa, S. J. A.; Hellgardt, K.; Hii, K. K. M. Catalysis in Flow: Operando Study of Pd Catalyst Speciation and Leaching. *Catal Today* **2014**, *229*, 95–103. https://doi.org/10.1016/J.CATTOD.2013.10.079.

(160) Levenspiel, O. *Chemical Reaction Engineering, 3rd Edition*; Wiley: New York, 1998.

(161) Park, J. H.; Ko, K. C.; Kim, E.; Park, N.; Ko, J. H.; Ryu, D. H.; Ahn, T. K.; Lee, J. Y.; Son, S. U. Photocatalysis by Phenothiazine Dyes: Visible-Light-Driven Oxidative Coupling of Primary Amines at Ambient Temperature. *Org Lett* **2012**, *14* (21), 5502–5505. https://doi.org/10.1021/ol302584y.

(162) Muratov, K.; Afanasyev, O. I.; Kuchuk, E.; Runikhina, S.; Chusov, D. One-Pot Synthesis of Symmetrical Tertiary and Secondary Amines from Carbonyl Compounds, Ammonium Carbonate and Carbon Monoxide as a Reductant. **2019**. https://doi.org/10.1002/ejoc.201901175.